The Development of a Drug Delivery System Using Brain Endothelial Non-Antibody Binding Domains as Transport Carriers

Thesis

The development of a drug delivery system using brain endothelial non-antibody binding domains as transport carriers.

Mohammad Daas, M.Sc

Faculty of STEM
Department of Life, Health and Chemical Sciences
The Open University

A thesis submitted to The Open University for the degree of
Doctor of Philosophy

Submitted March 31st 2017

Declaration

The work in this thesis is entirely my own and is the result of my own academic and experimental enquiry. Contributions to the work by colleagues are fully acknowledged in the manuscript.

I further assert that this thesis does not exceed 79,000 words, including headers and references.

Abstract

The highly specialised brain capillary endothelial cells (BCEC) that constitute the blood brain barrier (BBB) exhibit high resilience to the penetration of xenobiotic and biologic therapeutics, making drug delivery to the central nervous system (CNS) a challenging feat. Endogenous BCEC receptors such as transferrin receptor (TfR) have been proposed as exploitable targets for therapeutic payload transport into the CNS, and have been successfully targeted using monoclonal antibodies to deliver therapeutic molecules into the brains of rodents and non-human primates via receptor mediated transcytosis (RMT).

The overall aim of this study was to develop a BCEC drug delivery system using alternative domains to antibodies e.g. peptides and ssDNA aptamers, as a means of exploiting endogenous receptor transport mechanisms to deliver macromolecular drugs into the CNS via RMT.

The expression of three receptor candidates, TfR, low-density lipoprotein receptor (LDLR) and low-density lipoprotein-related receptor protein 1 (LRP1) were characterised for use as selectable targets on the cell surface of Immortalised human brain endothelial cells (hCMEC/D3) by flow cytometric analysis. Aptamers and cyclic peptide domains were then selected via *in vitro* selection techniques.

The present findings highlight the selection of 13 peptides that demonstrate species cross-reactivity to human, mouse and rat TfR as determined by phage ELISA. Moreover, the lead candidate Pep1 was identified to share homology with a conserved ‘DCSGNFCLF’ motif found on transferrin. When expressed as a bivalent peptide-Fc fusion molecule, Pep1 was shown to internalise within the mouse and human brain endothelial cell lines, bEnd.3, and hCMEC/D3. Additionally, the overall enrichment of hTFR specific aptamers was demonstrated following twelve rounds of selection and high throughput sequencing of selected pools, data that warrants further investigation.

Table of Contents

DECLARATION ..... **I**

ABSTRACT ..... **II**

TABLE OF CONTENTS ..... **III**

ACKNOWLEDGEMENTS ..... **VIII**

ABBREVIATIONS ..... **IX**

LIST OF FIGURES ..... **XV**

LIST OF TABLES ..... **XVII**

CHAPTER 1: GENERAL INTRODUCTION ..... **I**

1.1. Burden of Neurological Diseases 2

1.2. Blood-Brain Barrier Historical Aspects 2

1.3. Blood-Brain Barrier Structure and Function 3

1.4. Transport mechanisms present at the Blood-Brain Barrier 9

1.5. Cellular trafficking at the BBB 11

1.5.1. Macropinocytosis 12

1.5.2. Caveolae-dependant endocytosis 13

1.5.3. Clathrin-dependant endocytosis 13

1.5.4. Intracellular trafficking 16

1.6. Receptor mediated transcytosis at the BBB 19

1.6.1. Insulin receptor 20

1.6.2. Lipoprotein receptor family 21

1.7. Transferrin receptor (TfR) 23

1.7.1. Iron transport at the BBB 26

1.8. Targeting the BBB for drug delivery 29

1.8.1. TfR targeted drug delivery 29

1.9. Biopharmaceuticals 33

1.10. Peptide therapeutics 35

1.10.1. Peptides targeting TfR 37

1.11. Aptamers as novel targeting biologics 39

1.11.1. Aptamers targeting TfR 42

1.12. *In vitro* enrichment selection techniques for the identification of target binding biologics 45

1.12.1. Phage display 45

1.12.2. Systematic evolution of ligands by exponential enrichment (SELEX) 48

1.13. Aims and Objectives 50

CHAPTER 2: CHARACTERISATION OF CANDIDATE RECEPTOR TARGETS THAT FUNCTION VIA RMT AT THE BBB. 52

2.1. INTRODUCTION 53
2.2. MATERIALS AND METHODS 56
2.2.1. Pre-coating culture flasks and plates with collagen type I 56
2.2.2. Cell culture of the hCMEC/D3 cell line 56
2.2.2.1. Thawing cells from cryostorage and initial culture 57
2.2.2.2. Sub-culture of adherent hCMEC/D3 cells 57
2.2.3. Cell culture of CHO cell lines (TRVb and TRVb-1) 58
2.2.4. Assessment of cell-surface protein expression using Flow cytometry 59
2.2.5. Western Blotting 61
2.2.6. Immunocytochemistry CHO-TRVb cell line internalisation assays 63
2.2.7. Statistical analysis 64
2.3. RESULTS 64
2.3.1. Expression of candidate receptor targets by hCMEC/D3 cells 64
2.3.1.1. Cell surface expression of TfR, LDLR and LRP1 on hCMEC/D3 cells 64
2.3.1.2. Expression of TfR, LDLR and LRP1 with long-term hCMEC/D3 culture 66
2.3.1.3. Effect of cell detachment protocol on surface TfR expression 69
2.3.2. Characterising the expression of human TfR by CHO-TRVb cell lines. 71
2.3.2.1. Expression of hTfR on CHO-TRVb cell lines 71
2.3.2.2. Immunoblotting of CHO-TRVb cell lysates 73
2.3.2.3. Assessing the uptake of hTfR on CHO-TRVb and CHO-TRVb1 cell lines 74
2.4. DISCUSSION 75
2.4.1. TfR, LDLR and LRP1 receptors are expressed on the cell surface of hCMEC/D3 cells 75
2.4.2. The CHO-TRVb-1 cell line expresses similar surface protein levels of TfR to hCMEC/D3 cells. 82

CHAPTER 3: SELECTION OF TFR BINDING PEPTIDES FOR USE AS BBB DRUG DELIVERY VECTORS. 86

3.1. INTRODUCTION 87
3.2. MATERIALS AND METHODS 89
3.2.1. Preparation of TfR antigens for phage display selections 89
3.2.1.1. Biotinylation of recombinant transferrin receptor 89
3.2.1.2. Antigen presentation ELISA 89
3.2.2. Cyclic peptide library growth. 90
3.2.3. Phage purification via PEG precipitation 91
3.2.4. Soluble phage display selection 91
3.2.4.1. Inoculation of *E. coli* TG1 culture 92
3.2.4.2. Pre-blocking of phage library and streptavidin coated magnetic agarose beads 92
3.2.4.3. De-selection of phage library against streptavidin coated magnetic agarose beads 93
3.2.4.4. Incubating de-selected phage library or rescued phage with biotinylated antigen 93

3.2.4.5. Capturing binding phage particles 94
3.2.4.6. Infecting TG1 cells with eluted phage 94
3.2.5. Phage selection rescue 94
3.2.5.1. Harvesting cells from bioassay plates and freezing of glycerol selection outputs 94
3.2.6. Live cell surface phage display selection 95
3.2.6.1. Cell culture and harvesting of bEnd.3 cells 95
3.2.6.2. Pre-blocking phage and bEnd.3 cells 96
3.2.6.3. Elution of internalised phage particles 96
3.2.7. Phage ELISA screening for cross-species TfR binding peptide hits 96
3.2.8. Sequencing and identification of unique cross-species binding peptides. 98
3.2.9. Sequence analysis of fdDOG positive hit sequencing data 98
3.2.10. Multiple sequence alignment using ClustalW 99
3.2.11. Predicting the molecular interaction of Pep1 with TfR 99
3.3. RESULTS 99
3.3.1. Biotinylation of recombinant mouse TfR 99
3.3.2. Cyclic peptide phage display selection summary and input/ output titres. 102
3.3.3. Identification of species cross-reactive TfR binding cyclic peptides by phage ELISA 105
3.3.4. Summary of fdDOG sequence analysis and lead peptide identification. 106
3.3.5. Sequence homology of the 16 unique peptides 108
3.3.6. Re-evaluation of the 16 sequence validated cross-species TfR binding cyclic peptides 109
3.3.7. Pep1 demonstrates homology with highly conserved residues on transferrin C-lobe. 111
3.4. DISCUSSION 114
3.4.1. Biotinylated mTfR maintains anti-mouse specific 8D3 antibody binding activity. 114
3.4.2. Sequence analysis resulted in the identification of thirteen cross-species binding sequences 115
3.4.3. Pep1 demonstrates sequence homology with a conserved motif on transferrin C1-lobe 122
CHAPTER 4: EXPRESSION AND CHARACTERISATION OF LEAD TFR BINDING PEPTIDES 124
4.1. INTRODUCTION 125
4.2. MATERIALS AND METHODS 127
4.2.1. Sub-cloning of cyclic peptides into pCANTAB6-D1/FLAGHIS expression vector 127
4.2.1.1. Modification of pC6-D1 expression vector to introduce a NotI and FLAG tag coding region 127
4.2.1.2. Purification of pC6-D1/FLAGHIS plasmid DNA 128
4.2.1.3. Restriction digestion of pC6-D1/FLAGHIS and CPep DNA vector 129
4.2.1.4. Ligation reaction and transformation into E.coli Z' TG1 competent cells 130
4.2.2. E.coli periplasmic expression and affinity purification of CPep-D1 fusion domains. 130
4.2.2.1. Buffer preparation 130
4.2.2.2. Expression, culture harvest, periplasm extraction and His capture affinity purification. 131
4.2.3. SDS-PAGE purity analysis of expressed CPep-D1 fusion domains 132
4.2.4. Soluble CPep-D1 fusion TfR binding ELISA 132

4.2.5. Immunocytochemistry based cell binding, internalisation and intracellular co-localisation assays 133

4.2.5.1. Cell culture 133

4.2.5.2. Cell binding assays 134

4.2.5.3. Cell internalisation and intracellular co-localisation assays 135

4.2.6. Statistical analysis 135

4.3. RESULTS 136

4.3.1. Flag and His_{10} coding region successfully inserted into pC6-D1 expression vector 136

4.3.2. Periplasmic expression of the CPep-D1 fusion domains resulted in variable yields of the uniquely identified peptides. 140

4.3.3. Four lead peptides identified to exhibit recombinant mouse and human TfR specific binding over the control antigen. 142

4.3.4. Lead peptide candidates bind to immortalised mouse and human brain endothelial cell lines, bEnd.3 and hCMEC/D3. 145

4.2.7. Pep1-Fc/IL1RA fusion molecule demonstrates mouse and human brain endothelial cell internalisation. 148

4.4. DISCUSSION 152

4.4.1. Construction of pC6-D1/FLAGHIS expression vector and sub-cloning of CPep sequences. 152

4.4.2. Periplasmic expression of monovalent CPep-D1 domains. 155

4.4.3. Four CPep candidates bind specifically to recombinant mouse and human TfR expressed as CPep-D1 fusion domains. 158

4.4.4. Lead cyclic peptide candidates bind bEnd.3 and hCMEC/D3 cells 161

4.4.5. Pep1-Fc/IL1RA internalises within bEnd.3 and hCMEC/D3 cells 162

CHAPTER 5: SELECTION OF HTFR BINDING DNA APTAMERS FOR USE AS ALTERNATIVE BBB SHUTTLES. 169

5.1. INTRODUCTION 170

5.2. MATERIALS AND METHODS 172

5.2.1. Western blotting 172

5.2.2. ssDNA aptamer SELEX 173

5.2.2.1. Recombinant hTfR aptamer SELEX 174

5.2.2.2. CHO-TRVB-1 cell SELEX 176

5.2.3. PCR amplification of selected aptamer pool outputs 177

5.2.3.1. Initial PCR amplification of Round 1 selected pool 177

5.2.3.2. Optimisation PCR 178

5.2.3.3. Preparative PCR 179

5.2.4. Purification of ssDNA from PCR product 180

5.2.5. Desalting, quantification and lyophilisation of purified ssDNA 180

5.2.6. Next-generation sequencing of aptamer selected pools 181

5.2.6.1. DNA pool preparation for Illumina MiSeq sequencing 181
5.2.6.2. Enrichment analysis of NGS sequencing Data 181
5.3. RESULTS 182
5.3.1. Assaying recombinant hTfR immobilisation onto Ni-NTA agarose beads 182
5.3.2. Adapted SELEX protocol for the selection of hTfR binding ssDNA aptamers immobilised on Ni-NTA beads. 184
5.3.3. Enrichment observed following 12 rounds of SELEX 186
5.4. DISCUSSION 188
5.4.1. hTfR-His6 efficiently immobilised to Ni-NTA magnetic agarose beads 188
5.4.2. Analysis of PCR amplification steps 189
5.4.3. Significant enrichment observed following 12 rounds of hTfR SELEX 191
CHAPTER 6: GENERAL DISCUSSION 193
6.1. ASSESSMENT OF RECEPTOR TARGETS THAT FUNCTION VIA RMT AT THE BBB 194
6.2. SELECTION AND IDENTIFICATION OF TFR BINDING CYCLIC PEPTIDES 197
6.3. CHARACTERISATION OF BINDING AND INTERNALISATION OF LEAD PEPTIDES 201
6.4. SELECTION AND ENRICHMENT ANALYSIS OF APTAMER SELECTED POOLS 205
6.5. CONCLUSION AND PERSONAL REFLECTIONS 207
BIBLIOGRAPHY 209
APPENDIX 254

Acknowledgements

First and foremost, I wish to extend my sincere gratitude to Prof. Nacho Romero for his continued support and encouragement, throughout the course of the PhD. I would also like to thank Dr. George Thom for his companionship, guidance and support within the lab during the course of my placement at MedImmune. Similarly, I would also like to thank Prof. David Male, Dr. Carol Midgley and Dr. Carl Webster. I am very grateful to have had such extensive theoretical and technical knowledge afforded to me in the form of a large supervision team.

I wish to thank my colleagues within the BBB research teams at The Open University and MedImmune for their advice, support and friendship during the course of this project. Additionally, I would also like to extend my gratitude to the multitude of lab managers and technical staff at both organisations, for aiding and maintaining the efficient running of the labs.

I wish to thank Prof. Joan Abbott for organising and inviting me to attend multiple sessions of the Blood-Brain Barrier Consortium Club (King's College London). I would like to extend my gratitude to the rest of the blood-brain barrier research community that I have had the pleasure of interacting with over the years.

Finally, I would like to extend my heartfelt thanks to family and friends for their encouragement, support and patience during the course of this PhD.

This project was supported by a studentship funded by MedImmune and The Open University.

Abbreviations

2xTYTET	2x Trypton yeast tetracycline
AA	Amino acid
ABCA1	ATP binding cassette transporter A1
AMT	Adsorptive mediated transcytosis
ANOVA	Analysis of variance
apoTf	Apotransferrin
APPL1	Adaptor protein containing PH domain and leucine zipper motif 1
APS	Ammonium persulphate
ATP	Adenosine triphosphate
BBB	Blood-brain barrier
BCA	Bicinchoninic acid assay
BCEC	Brain capillary endothelial cells
BDNF	brain-derived neurotropic factor
bEnd.3	immortalised mouse brain endothelial cell line
bp	base pairs
BRCP	Breast cancer resistance protein
BSA	Bovine serum albumin
CAM	Cell adhesion molecule
CD98hc	CD98 heavy chain
cfu	Colony forming units
CHO	Chinese hamster ovary

CHO-TRVb	Chinese hamster ovary-transferrin receptor variant (deficient)
CHO-TRVb1	Chinese hamster ovary-transferrin receptor variant (hTfR transfected)
CLASPs	Clathrin-associated sorting proteins
CNS	Central nervous system
CPep	Cyclic peptide
Cpep-D1	Cyclic peptide-domain 1
CSF	Cerebro-spinal fluid
DARPin	Designed ankyrin repeat proteins
DMEM	Dulbecco's modified Eagle's medium
DMSO	Dimethyl sulfoxide
DMT1	Divalent metal transporter 1
DNA	Deoxyribonucleic acid
DPBS	Dulbecco's phosphate buffered saline
E.coli	*Escherichia coli*
EBM-2	Endothelial basal medium-2
EDTA	Ethylenediaminetetraacetic acid
EEA1	Early endosomal antigen 1
EGF	Epidermal growth factor
EPS15	Epidermal growth factor receptor pathway substrate 15
EGM-2	Endothelial growth medium-2
ELISA	Enzyme-linked immunosorbent assay

EM	Electron microscopy
EpCAM	Epithelial cell adhesion molecule
FACS	Flow cytometry
FBS	Foetal bovine serum
Fc	Fragment crystallisable
FCHo	F-BAR domain-containing Fer/Cip4 homology domain-only
FITC	Fluorescein isothiocyanate
FluMag	Fluorescence monitored *in vitro* selection
Fn3	Fibronectin type-III
g3p	Gene 3 major coat protein
GAPDH	glyceraldehyde-3-phosphate dehydrogenase
HBSS	Hank's balanced salt solution
hCMEC/D3	Human cerebral microvascular endothelial cells/D3
hEGF	Human endothelial growth factor
hFGF	Human fibroblast growth factor
His	Histidine
HIV	Human Immunodeficiency virus
hTfR	Human transferrin receptor
HTS	High throughput sequencing
HUVEC	Human Umbilical Vein Endothelial Cells
ICC	Immunocytochemistry
IgG	Immunoglobulin G

IL1	Interleukin 1
IL1R	Interleukin 1 receptor
IL1RA	Interleukin 1 receptor antagonist
IR	Insulin receptor
IRE	Iron regulatory element
IRP	Iron regulatory protein
JAMs	Junctional adhesion molecules
Kd	Dissociation constant
kDa	Kilo Daltons
LA	LDLR type A
LAMP1	Lysosomal-associated membrane protein 1
LDL	Low-density lipoprotein
LDLR	Low-density lipoprotein receptor
LRP1	Low-density lipoprotein receptor-related protein 1
LXR	Liver-X receptor
MAb	Monoclonal antibody
MPBS	Milk phosphate buffered saline
MRP	Multidrug resistant associated protein
mTfR	Mouse transferrin receptor
Mw	Molecular weight
PAMAM	Polyamidoamine
PBS	Phosphate buffered saline

PBST	Phosphate buffered saline with tween
pC6	pCANTAB6
PCR	Polymerase chain reaction
PEG	Polyethylenglycol
Pep	Peptide
Pgp	P-glycoprotein
PIP_2	Phosphatidylinositol 4,5-bisphosphate
PPAR	Peroxisome-proliferator activated receptor
RAGE	Receptor for advanced glycation end-products
RAB	Ras-related protein
RMT	Receptor mediated transcytosis
RNA	Ribonucleic acid
rpm	Revolutions per minute
ScFv	Single-chain variable fragment
SDS	Sodium dodecyl sulfate
SDS-PAGE	Sodium dodecyl sulphate-polyacrylamide gel electrophoresis
SELEX	Systematic evolution of ligands by exponential enrichment
SEM	Standard error of mean
SNARE	Soluble N-ethylmaleimide sensitive factor attachment protein receptor
SR-BI	Scavenger receptor class B type 1
ssDNA	Single stranded deoxyribonucleic acid

TAR	Transactivation response element
TEA	Triethylamine
TEER	Trans-endothelial electrical resistance
TEM	Transmission electron microscopy
TEMED	Tetramethyl-ethlenediamine
Tf	Transferrin
TfR	Transferrin receptor
TGF-β1	Transforming growth factor – β1
TJ	Tight junctions
TMB	3,3',5,5'-Tetramethylbenzidine
TRV	Transferrin receptor variant
TTF	Thyroid transcription factor
TUP	Target-unrelated peptides
TYAG	Tryptone yeast ampicillin glucose
VEGF	Vascular endothelial growth factor
vLDL	Very low-density lipoprotein
ZO-1	Zonula occludens

List of Figures

Figure 1.3.1: Barriers of the brain (adapted from Abbott, *et al*. 2010). 4

Figure 1.3.2: Schematic representation of the neurovascular unit (Adapted from Abbott, *et al*. 2010) 5

Figure 1.3.3: Structural tight junctions at the BBB (adapted from Abbott, *et al*. 2010) 6

Figure 1.4.1: Schematic representation of endogenous transport mechanisms present on the cell surface of BCEC (Adapted from Abbott, *et al*. 2010) 9

Figure 1.5.1: Formation of clathrin-coated pits and vesicle internalisation 14

Figure 1.5.2: Vesicular trafficking at the BBB. 17

Figure 1.7.1: Extracellular structure of hTfR as determined by X-ray crystallography at 3.2 Å resolution. 24

Figure 1.7.2: TfR mediated transcytosis and endocytosis of Tf/TfR complexes at the BBB. 26

Figure 1.12.1: Schematic representation of soluble phage display selection. 47

Figure 1.12.2: Schematic representation of typical aptamer SELEX procedure. 48

Figure 2.3.1: Facs detection of transport receptor proteins TfR, LDLR and LRP1 on hCMEC/D3 cells (p35) 65

Figure 2.3.2: FACS detection of indirect antibody labelled, TfR, LDLR and LRP1 with long-term culture on the cell surface of hCMEC/D3 cells. 67

Figure 2.3.3: Summarised results of TfR, LDLR and LRP1 hCMEC/D3 cell surface expression with long-term culture. 68

Figure 2.3.4: FACS detection of TfR on cell surface of hCMEC/D3 cells after Trypsin / EDTA or Accutase detachment. 70

Figure 2.3.5: Characterisation of TfR expression on the cell surface of hCMEC/D3, TRVb and TRVb-1 cells. 72

Figure 2.3.6: Immunoblot of hTfR in TRVb and TRVb-1 cell lysates. 73

Figure 2.3.7: Uptake of anti-hTfR and anti-mTfR (8D3) antibodies in CHO-TRVb and -TRVb-1 cell lines. 74

Figure 2.3.8: Summarised results of CHO-TRVb and -TRVb-1 cell line uptake study using anti-mTfR and anti-hTfR antibodies. 75

Figure 3.2.1: Schematic representation of soluble phage display selections conducted using cyclic peptide libraries. 92

Figure 3.3.1: Amino acid sequence of the extracellular domain of mouse TfR. 100

Figure 3.3.2: Validating the biotinylation of mTfR-His6 using anti-mouse TFR (8D3) antibody. 101

Figure 3.3.3: Phage ELISA initial screen hit output summary. 106

Figure 3.3.4: Sequence homology of 16 unique peptide sequences. 108

Figure 3.3.5: Phage ELISA screening summary of uniquely identified hits against mouse, human and rat TfR. 109

Figure 3.3.6: Binding re-evaluation of Pep-g3p clones towards biotinylated TfR by phage ELISA. 110

Figure 3.3.7: Sequence homology of Pep1 towards human, mouse and rat transferrin. 112

Figure 3.3.8: Predicted interaction of Pep1 with transferrin receptor monomer. 113

Figure 4.3.1: Circular vector map of stock pCANTAB6 expression vector. 137

FIGURE 4.3.2: VALIDATION OF PC6-D1 FLAG MODIFIED INSERT DNA PRODUCT AND DIGESTED PCANTAB6 STOCK EXPRESSION VECTOR FRAGMENTS VIA AGAROSE GEL ELECTROPHORESIS. 139
FIGURE 4.3.3: SEQUENCE VALIDATION OF THE MODIFIED INSERT REGION OF PC6-D1/FLAGHIS EXPRESSION VECTOR. 139
FIGURE 4.3.4: VALIDATION OF EXPRESSED HIS_{10} TAGGED MONOVALENT CPEP-D1 FUSION MOLECULES BY SDS-PAGE. 141
FIGURE 4.3.5: SUMMARY OF SOLUBLE CPEP-D1 ANTIGEN BINDING ELISA AND LEAD IDENTIFICATION. 144
FIGURE 4.3.6: TITRATION SUMMARY OF LEAD CPEP-D1 SOLUBLE PEPTIDE BINDING TO MOUSE AND HUMAN TFR. 145
FIGURE 4.3.7: CPEP-D1 BEND.3 AND HCMEC/D3 CELL BINDING ASSAY AS DETERMINED BY IMMUNOCYTOCHEMISTRY. 147
FIGURE 4.3.8: CPEP-FC/IL1RA BEND.3 CELL INTERNALISATION TIME COURSE AT 5, 15, 30, 60 AND 120 MIN TIME POINTS. 149
FIGURE 4.3.9: QUANTIFIED AVERAGE MEAN GREY VALUES OF CPEP-FC/IL1RA BEND.3 INTERNALISATION ASSAY. 150
FIGURE 4.3.10: PEP1-FC/IL1RA HCMEC/D3 CELL INTERNALISATION AND INTRACELLULAR CO-LOCALISATION ASSAYS. 151
FIGURE 4.4.1: SCHEMATIC REPRESENTATION OF CPEP-FC/IL1RA STRUCTURE. 164
FIGURE 5.2.1: SCHEMATIC REPRESENTATION OF DNA APTAMER SELECTION USING RECOMBINANT PROTEIN IMMOBILISED ON NI-NTA COATED MAGNETIC AGAROSE BEADS. 175
FIGURE 5.3.1: ASSESSING IMMOBILISATION OF RECOMBINANT HTFR TO NI-NTA MAGNETIC AGAROSE BEADS. 183
FIGURE 5.3.2: OPTIMISATION PCR AMPLIFICATION RESULTS. 185
FIGURE 5.3.3: SUMMARY OF NGS COUNT ANALYSIS AS AN OVERALL ASSESSMENT OF APTAMER ENRICHMENT. 187

List of Tables

TABLE 1.8.1: RECENT OX26 NANO-CARRIER DRUG DELIVERY APPROACHES AT THE BBB. 32

TABLE 2.2.1: PREPARING COMPLETE EGM-2 GROWTH MEDIUM. 56

TABLE 2.2.2: CHO-TRVB AND TRVB-1 CELL CULTURE MEDIA. 58

TABLE 2.2.3: RECEPTOR PROTEIN SPECIFIC ANTIBODIES UTILISED IN FACS ANALYSIS. 59

TABLE 2.2.4: TABLE SHOWING RECIPES FOR POLYACRYLAMIDE GELS AND WESTERN BLOTTING BUFFERS. 61

TABLE 3.2.1: SEQUENCING PRIMERS USED FOR AMPLIFYING INSERT REGION OF FDDOG PHAGE DISPLAY VECTOR. 98

TABLE 3.3.1: CYCLIC PEPTIDE PHAGE DISPLAY SELECTION ROUND CONDITIONS. 103

TABLE 3.3.2: CPEP LIBRARY PHAGE INPUT AND OUTPUT TITRES, AND ENRICHMENT FACTOR WITH TFR SELECTION PROGRESSION.. 104

TABLE 3.3.3: SEQUENCE ANALYSIS SUMMARY OF IDENTIFIED CROSS-SPECIES TFR BINDING PEPTIDE HITS. 107

TABLE 4.2.1: PRIMERS USED FOR TWO-STEP PC6-D1 VECTOR MODIFICATION PROCESS. 127

TABLE 4.2.2. AMPLIFICATION OF PC6-D1 VECTOR INSERT. 128

TABLE 4.2.3: PCR REACTION FOR AMPLIFICATION OF CPEP INSERT DNA FROM FDDOG PHAGE VECTOR. 129

TABLE 4.2.4: LIGATION OF INSERT INTO PC6-D1/FLAGHIS EXPRESSION VECTOR 130

TABLE 4.2.5: ASPEC PURIFICATION BUFFER COMPOSITIONS. 131

TABLE 4.4.1: MOST COMMONLY REPORTED MINOR CODONS AND THEIR FREQUENCY REPRESENTATION BY *E.COLI* (ADAPTED FROM: KANE *ET AL*. 1995). 156

TABLE 4.4.2: MINOR CODON USAGE WITHIN THE VARIABLE PEPTIDE ENCODING REGION OF POORLY EXPRESSING CPEP-D1 DOMAINS. 156

TABLE 5.2.1 : COMPOSITION OF BUFFERS USED FOR NI-NTA MAGNETIC AGAROSE BEAD APTAMER SELECTIONS. 172

TABLE 5.2.2: TABLE SHOWING AN OVERVIEW OF SELECTION CONDITIONS FOR RECOMBINANT HTFR-HIS6 SELEX. 176

TABLE 5.2.3: INITIAL PCR AMPLIFICATION OF ENTIRE FIRST ROUND SELECTED POOL. 177

TABLE 5.2.4: PCR AMPLIFICATION PROGRAMME REACTION CONDITIONS. 178

TABLE 5.2.5: OPTIMISATION PCR REACTION SETUP. 179

TABLE 5.2.6: PREPARATIVE PCR AMPLIFICATION REACTION SETUP. 180

Chapter 1: General introduction

Chapter 1:

1.1. Burden of Neurological Diseases

Given today's globally aging population we are witnessing high rates of morbidity due to debilitating neurological conditions. According to the global burden of disease study 2010, neurological and cerebrovascular diseases are estimated to represent 7.1% of the overall global disease burden for all age groups (Murray et al., 2012). Recently, it has been suggested that these figures are largely underestimated due to the categorisation of mental illnesses, with true figures estimated to be 13% (Vigo et al., 2016). In the UK alone, it is regarded that the economic burden of dementia is equivalent to 23.5 billion pounds per year. This estimated financial burden is expected to more than double by 2051 due to the growing aging population in the UK (Pool, 2015).

Despite the development of many drugs with therapeutic potential, very few treatments are clinically approved for treating disorders of the central nervous system (CNS), and this is primarily due to the impermeable nature of the blood brain barrier (BBB) (Gribkoff and Kaczmarek, 2017). The BBB excludes the majority of large and small molecule drugs from reaching the CNS at therapeutically relevant concentrations, and this poses major limitations for the systemic delivery of neuro-therapeutics to the CNS via non-invasive delivery methods. The impermeability of the BBB to therapeutics has meant that even with today's advancements in medicine and targeted drug delivery, an efficient transport mechanism for delivering macromolecular drugs into the CNS at pharmacologically relevant concentrations remains to be established (Stanimirovic et al., 2015).

1.2. Blood-Brain Barrier Historical Aspects

Pioneering experiments carried out in 1885 by the German physician Paul Ehrlich demonstrated that intravenously injecting dyes into an animal's circulation caused staining of all peripheral organs with the exception of tissues of the CNS (Serlin et al., 2015). This finding was initially attributed to a low affinity of the alkaline dye to CNS tissues. However, this initial assumption was later discredited in 1913 with successive studies carried out by Edwin Goldmann. Goldmann found that injecting trypan blue into the cerebro-spinal fluid (CSF) of rats caused exclusive

staining of the CNS and not the peripheral organs. This study enabled Goldmann to conclude that the exclusive staining of the CNS was due to the presence of a barrier between the circulatory system and the CNS (Abbott et al., 2010).

The introduction of electron microscopy (EM) techniques further enhanced our understanding of the BBB, by allowing the differentiation of intercellular regions between endothelial cells and the surrounding perivascular region. Seminal work by Reese and Karnovsky (1967) demonstrated that intravenous injection of horseradish peroxidase (an electron dense marker) did not cause permeation of endothelial cells. Through the use of transmission electron microscopy (TEM) at magnifications greater than 135,000x, the authors also documented the cause of reduced solute permeability to the CNS as being due to tight junctions located within the intercellular clefts of cerebrovascular endothelial cells.

1.3. Blood-Brain Barrier Structure and Function

The CNS is a highly delicate system that is susceptible to damage by a wide variety of blood-borne and exogenous substances. A highly regulated neuronal extracellular microenvironment is therefore necessary for effective neuronal and glial function. Three principle barriers exist between the blood and brain tissue; the blood-brain barrier, the blood-CSF barrier, and the arachnoid barrier, these are shown in Figure 1.3.1.

The BBB constitutes the largest surface area for exchange between the blood and the brain interfaces. Functionally, the BBB maintains CNS homeostasis by regulating the movement of ions, solutes, proteins and migrating immune cells (Abbott et al., 2010). This mechanism protects the CNS from entry of potentially neurotoxic agents and provides a highly regulated transport system that facilitates the supply of necessary nutrients to the brain parenchyma, whilst simultaneously sustaining the ionic concentration gradient within the CNS for optimal neuronal function (Abbott, 2013).

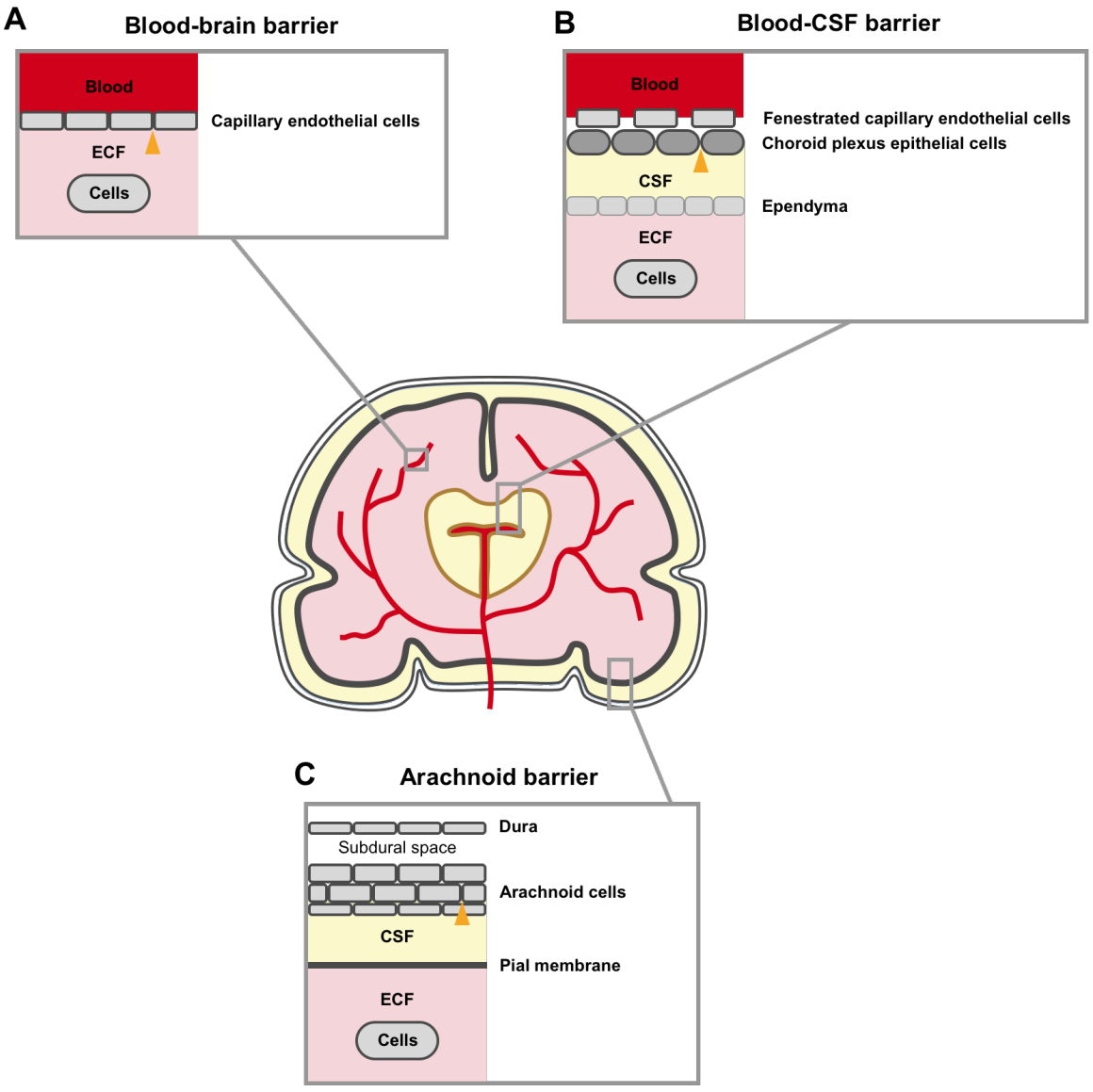

Figure 1.3.1: Barriers of the brain (adapted from Abbott, *et al*. 2010).

Schematic representation of the three principle barriers found between the blood and brain interfaces. The blood-brain barrier (**A**) is formed via specialised tight junctions between brain capillary endothelial cells and is the largest surface for exchange of solutes and drugs. The blood-cerebrospinal fluid barrier (**B**) is located at the lateral third and fourth ventricles of the brain and tight junctions are found at the CSF apical surface of epithelial cells. The arachnoid barrier (**C**) is located below the dura at the multilayered arachnoid cells. Tight junctions are located between the arachnoid cells of the inner layer. Although this region is avascular, the CSF can exchange with the blood via arachnoid villi, that project into the nearest source of blood located at the sagittal sinus.

BBB integrity is mediated and maintained through a number of structural and cellular components, which are shown in Figure 1.3.2. Alterations in these components through various mechanisms results in BBB disruption, which has been associated with several CNS pathological conditions, including Alzheimer's and

Parkinson's diseases, multiple sclerosis and stroke (Chung et al.,2013; Haarmann et al., 2015; Halliday et al., 2016; Liu et al., 2012, Wan et al., 2015).

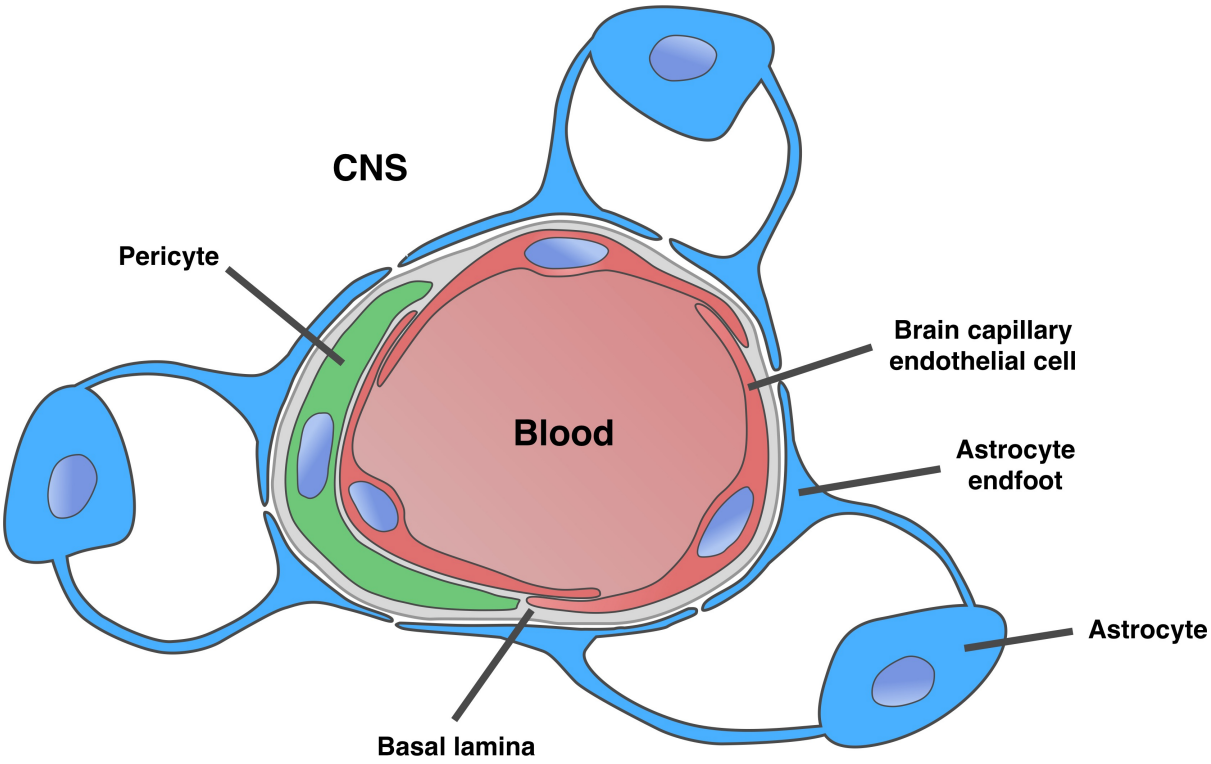

Figure 1.3.2: Schematic representation of the neurovascular unit (Adapted from Abbott, *et al.* 2010)

Figure showing cellular interactions of the BBB functional unit. Pericytes form part of the perivascular basal lamina. Astrocytic endfeet processes surround the basal lamina and provide structural integrity to the vascular unit.

The BBB primarily consists of single cell thick layer of brain capillary endothelial cells (BCEC). These highly polarised microvascular endothelial cells are anatomically flat and possess oval nuclei that form the thickest region of the capillary wall. A luminal or apical endothelial membrane interacts with the blood interface, while the opposing abluminal or basolateral endothelial membrane interacts with the CNS. Adjacent BCEC are connected via a belt like region of specialised intercellular tight junctions (TJ) and adherens junctions, which form a physical barrier through interaction of several intercellular anchoring proteins (Bauer et al., 2014). In addition to sealing the paracellular space, tight junctions alongside multi-protein complexes based on the proteins Par, Crumbs and Scribble, play a role in establishing apico-basal polarity and the specific distribution of membrane components at distinct sites

of the plasma membrane (Artus et al., 2014; Lee and Streuli, 2014). Polarisation of cells is vital for correct functioning of endosomal trafficking pathways and the transport of proteins to the correct membrane surfaces (Apodaca et al., 2012; Cramm-Behrens et al., 2008). The tight junctional proteins expressed in BCEC are outlined in Figure 1.3.3.

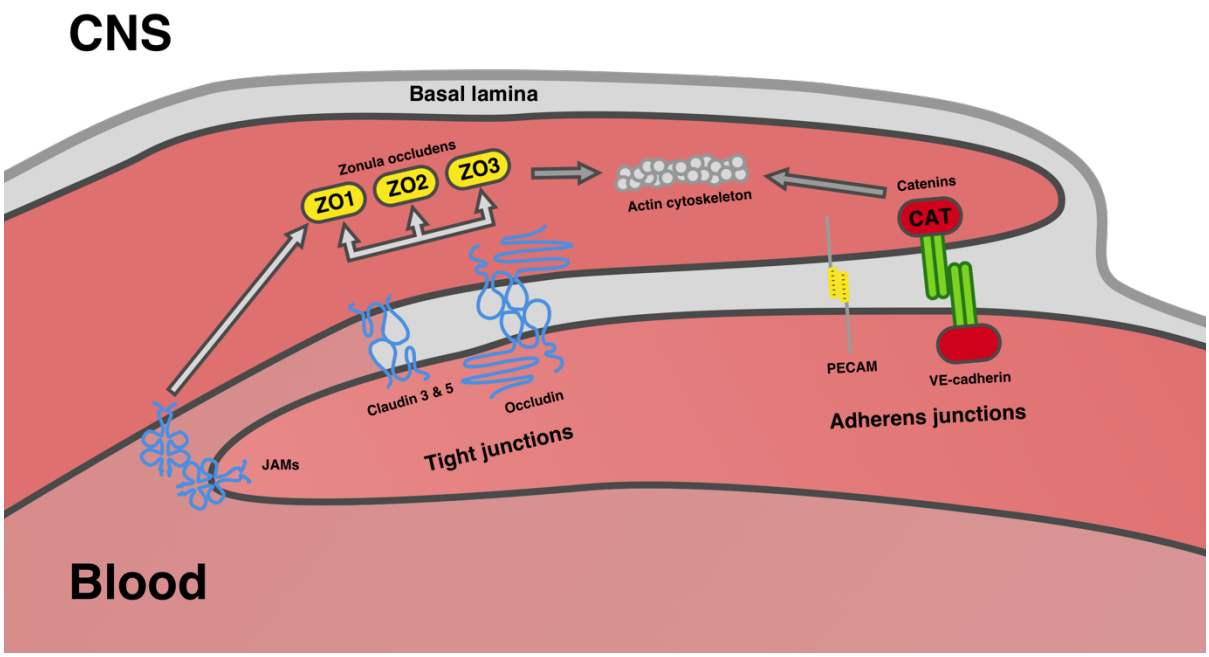

Figure 1.3.3: Structural tight junctions at the BBB (adapted from Abbott, *et al*. 2010)

Figure outlining the tight junctional protein complex between adjacent BCEC. Claudins 3 and 5 are primarily responsible for barrier impermeability to paracellular diffusion, through direct association across the intercellular cleft. Occludin also forms self-associations across the intercellular cleft, however these are less tight. Claudins and occludin both form intracellular linkages to cellular scaffolding proteins (ZO-1, 2, and 3). ZO scaffolding proteins form further interactions with actin-associated proteins such as cingulin. VE cadherin anchors adjacent cells and provides structural integrity. JAMs are thought to interact with leukocytes during leukocyte adhesion.

As observed with epithelial cells in other tissues, the TJs between BCEC consist of the transmembrane proteins, occludin, claudins and junctional adhesion molecules (JAMs) (Morita et al., 2003). The tight junctional protein complexes formed produce phenotypically unique endothelial cells that restrict paracellular permeability of solutes. Claudins 3 and 5 are primarily responsible for barrier impermeability to paracellular diffusion, by forming homophilic and/or heterophilic tight interactions with each other across the inter-cellular cleft (Yamamoto et al.,

2008). Claudins and occludin form additional intracellular associations with the cytoplasmic scaffolding proteins zonula occludens (ZO-1, ZO-2 and ZO-3), these successively form linkages with actin cytoskeletal associated proteins such as cingulin (Luissint et al., 2012). It has been shown that calcium influx can modulate the efficacy of tight junctional barriers by promoting cross-bridge movement of actin and myosin filaments (De Bock et al., 2012). This generates a contractile force, which pulls adjacent cells apart resulting in a reduced trans-endothelial electrical resistance (TEER) and increased paracellular permeability (Schnittler et al., 1990).

The BBB exhibits highly dynamic barrier properties (variable regulation of TJ and receptor protein expression). This feature is due to close interactions of the endothelial cells with several other cell types. Indeed, BCEC alongside pericytes, perivascular neurons, and astrocytic end feet projections constitute the functional neurovascular unit as shown in Figure 1.3.2. This intimate relationship allows for biochemical modulation and regulation of endothelial cell permeability according to various pathological and physiological situations (Persidsky et al., 2006).

BCEC are surrounded by the basal lamina, a three-dimensional basement membrane, 20 – 200 nm in thickness, that provides a support for attachment and interaction of all cellular components of the neurovascular unit. It is composed of the structural proteins collagen and elastin as well as fibronectin, laminin, proteoglycans and cell adhesion molecules (CAM) (Thomsen et al., 2017)

The basement membrane is essential for maintenance of BBB integrity. Deletion of laminin α2 derived from astrocytes causes impaired vascular smooth muscle cells and haemorrhage within the brain (Chen et al., 2013). Basement membrane digestion by matrix metalloproteinases, has been shown to disrupt cytoskeletal anchoring of BCEC, causing a reduced tight junctional integrity and increased barrier permeability (Cardoso et al., 2010). Upregulation of matrix metalloproteinases and the plasminogen activator system following stroke has been shown to lead to degradation of the vascular basement membrane, compromising the BBB, and leading to infiltration of the brain parenchyma by neutrophils, macrophages and monocytes (Katsu et al., 2010; Fukuda et al., 2004). Additionally, amyloid beta (Aβ) peptide deposition in the basement membrane during cerebral

amyloid angiopathy, has be associated with basement membrane thickening and changes in its protein composition (Held et al., 2017; Hawkes et al., 2013). Similarly, basement membrane remodelling and thickening has been reported with multiple sclerosis and this is thought to play a role in the further recruitment of inflammatory cells via the transforming growth factor- β1 (TGF- β1) (van Horssen et al., 2006; 2005).

Surrounding up to 32% of the abluminal side of BCEC in microvessels, pericytes are embedded within the para-cellular basal lamina. Pericytes provide structural support to BCEC, via integrin mediated endothelial cell-pericyte and pericyte-extracellular matrix adhesive interactions. Pericytes have also been identified to regulate capillary blood flow (via contractile activity of cytoskeletal filaments), angiogenesis and immunogenic responses to the brain (Kamouchi et al., 2011). Additionally, pericytes are also responsible for the synthesis of most components of the basal lamina and play an essential role in endothelial cell differentiation, migration and proliferation (Kamouchi et al., 2011).

Astrocytic end feet projections surround 95% of BCEC and their associated basal lamina. Alongside pericytes, astrocytes have been shown to regulate the synthesis of proteoglycans that maintain the charge selectivity of the BCEC. *In vivo* studies have identified that selected loci removal of astrocytes leads to a delayed loss of vascular function, with subsequent vascular repair processes remaining effective even in the absence of astrocytic contact (Willis et al., 2004). Furthermore, astrocytes have been demonstrated to play an important role in controlling the active and passive uptake of K^+ from the interstitial space. Studies have shown that K^+ concentration is maintained at a consistent 3 mM, irrespective of fluctuations in plasma K^+. Additionally, K^+ concentrations return to the aforementioned 3 mM concentration following acute elevations induced by neuronal activity and seizures (Schielke et al., 1990). Astrocytic endfeet are enriched in the gap junctional proteins connexins 30 and 43 (Cx30 and Cx43) which are responsible for the trafficking of ions within the perivascular space. Knockout of these connexins in mice has been shown to lead to astrocytic endfeet oedema (via the loss of the water channel

aquaporin-4) and reduced anchorage of astrocytic endfeet to the basal lamina (via the loss of the transmembrane protein β-dystroglycan) (Ezan et al., 2012).

1.4. Transport mechanisms present at the Blood-Brain Barrier

Several active and passive transport mechanisms are present on the cell surface of brain endothelial cells that are essential for transport of nutrients to the CNS and removal of cellular metabolic waste products. These transport mechanisms vary in their transport capabilities and are outlined in Figure 1.4.1.

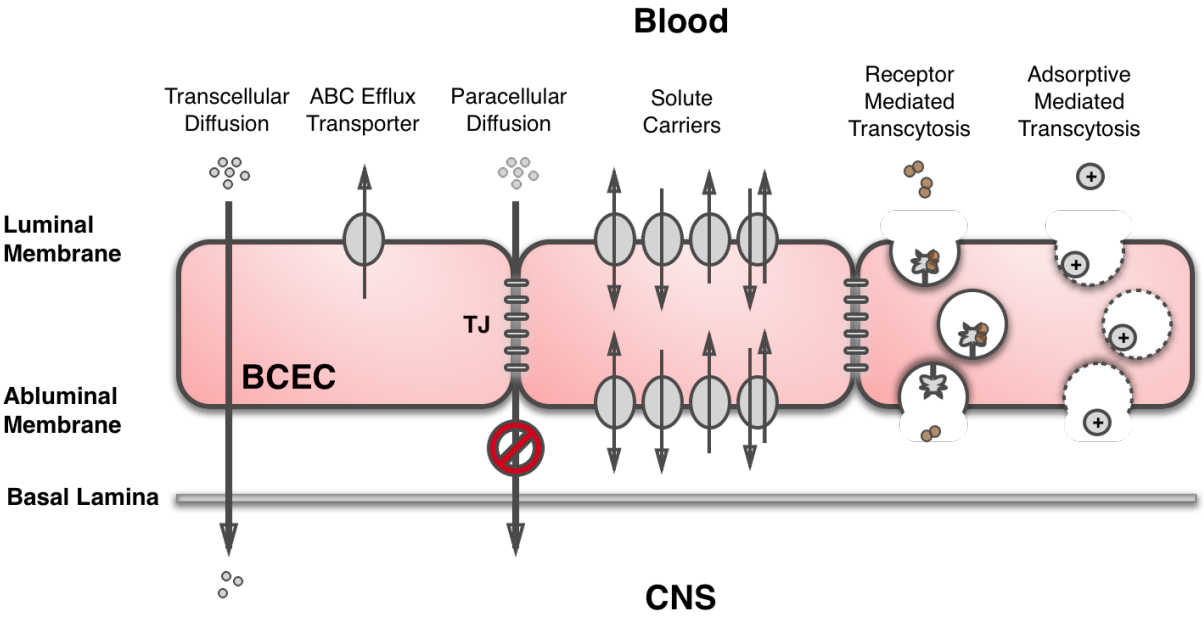

Figure 1.4.1: Schematic representation of endogenous transport mechanisms present on the cell surface of BCEC (Adapted from Abbott, *et al.* 2010)

Figure outlining potentially exploitable transport mechanisms for CNS drug delivery at the cell surface of brain capillary endothelial cells. The paracellular diffusion pathway is effectively sealed due to the presence of tight junctional complexes. Transcellular diffusion is limited to small lipophilic molecules no larger than 500 Da. Efflux transporters actively expel passively diffusing substrates. Solute carriers allow the active bi-directional transport of solutes and nutrients across a concentration gradient. Transcytosis mechanisms rely on vesicular cargo transport across the BCEC. Receptor mediated transcytosis relies on receptor specific binding and transport of a ligand, whereas adsorptive mediated transcytosis relies on the non-specific binding of a positively charged molecule to the negatively charged plasma membrane. Both mechanisms subsequently undergo endocytic internalisation and subsequent trafficking through the cell to the abluminal membrane where they may be released and made available to the CNS.

The simplest form of transport across the BBB is passive diffusion. Para-cellular diffusion of hydrophilic compounds is highly prohibited due the unique tight junctional protein complexes anchoring neighbouring BCEC in close proximity. Transcellular diffusion is possible, however limited to lipophilic compounds no larger than 400-500 Da in size (Airan et al., 2017). Transcellular diffusion is further complicated by the capability of a given compound to form hydrogen bonds at the BCEC cell membrane. Molecules that can form greater than six hydrogen bonds and have a polar surface area greater than 80 $Å^2$ are less likely to transition from aqueous phase into the lipid phase of the plasma membrane due to increased free energy requirement (Clark, 2003; Mahar Doan et al., 2002).

Carrier-mediated transport involves the active transport of compounds in a direction opposing to the concentration gradient. The activity of these transporters is adenosine triphosphate (ATP)-driven and sensitive to fluctuations in temperature. Moreover, these carriers may function either as influx transporters, efflux transporters or a combination of both (Ohtsuki and Terasaki, 2007). Several active efflux carriers are present at the BBB. These transporters are responsible for the elimination of hydrophilic metabolic substrates from the brain into the circulation (Terasaki and Hosoya, 1999). Alongside their natural ligands, many efflux transporters also bind and eliminate CNS drugs preventing their accumulation within the CNS (Groenendaal et al., 2007; Leggas et al., 2004; Yang and Liu., 2008). Examples include the ABC efflux unidirectional transporters, P-Glycoprotein (Pgp) and breast cancer resistance protein (BRCP), and the bi-directional multi drug resistance associated protein family (MRP 1-5) (Begley, 2004). The most characterised of these efflux transporters, Pgp, is localised to the apical membrane and eliminates large, cationic, hydrophobic molecules (de Lange, 2013; Urquhart and Kim, 2009). Solute carriers facilitate the bi-directional transport of nutrients such as amino acids, glucose, nucleosides, and monocarboxylic acids (Ohtsuki and Terasaki, 2007). The rate of transport of these carriers is dependent on the concentration of ligand present, and can also be modulated by competitive and non-competitive inhibitors (de Lange, 2013). As a targeted drug delivery approach carrier mediated transport has a large transport capacity but is restricted by cargo size, stereo-selective (only binding endogenous substrates), and plasma concentration

which can reach saturation and faces significant competition with endogenous substrates (Ohtsuki and Terasaki, 2007).

Two vesicular transcytosis mechanisms are also responsible for the transport of large macromolecules, adsorptive-mediated transcytosis (AMT) and receptor-mediated transcytosis (RMT). AMT involves the non-specific endocytosis and subsequent transcytosis of polycationic compounds through binding to electrostatically generated anionic regions on the plasma membrane within the glycocalyx, a lattice of glycoproteins, glycosaminoglycans and proteoglycans which line the vascular endothelium (Zhu et al., 2017). RMT allows for the transport of large, polar macromolecular proteins and peptides via receptor specific ligand binding and subsequent endocytosis, intracellular trafficking and exocytosis at the abluminal cell membrane (Demeule, Currie, et al., 2008; Haqqani et al., 2017). The detailed cellular trafficking mechanisms are discussed in section 1.5. The most prevalent ligands that have been shown to endocytose at BCEC are transferrin (Manich et al., 2013), insulin (Gray et al., 2017) and low-density lipoprotein (LDL) (Demeule, Currie, et al., 2008). RMT mostly occurs at clathrin-coated pits, which are primarily localised at the luminal membrane suggesting that transcytosis occurs predominantly in the blood to brain direction (Simionescu et al., 1988).

The large network of capillaries within the brain make the exploitation of vascular delivery mechanisms highly favourable. The average inter-capillary distance is 40 μm and therefore the body of a neuron is never more than 10 – 20 μm from the nearest capillary (Duvernoy et al., 1983; Schlageter et al., 1999; Wong et al., 2013). Established transport mechanisms provide potentially exploitable means of targeted drug delivery to the brain (Gaillard et al., 2012). The present study will focus on RMT as an exploitable mechanism of crossing BCEC and overcoming the transport restrictions of the BBB. In order to comprehend RMT we must explore the cellular trafficking mechanisms present at the BBB.

1.5. Cellular trafficking at the BBB

The cellular plasma membrane is impervious to many biological components within the blood. Endocytosis is a vital mechanism by which all mammalian cells can

acquire nutrients, proteins and solutes from their extracellular environment (De Bock et al., 2016). In addition to nutrient uptake, endocytosis is vital for activation of cellular signalling pathways, membrane component recycling and degradation (Kurgonaite et al., 2015; Fletcher et al., 2014) . Furthermore, these established endocytic mechanisms have been exploited by viruses, bacteria and parasites in order to gain access to the intra-cellular environment of the cell (Abraham et al., 2010; Ahmad et al., 2017; Asmat et al., 2014; Bonazzi et al., 2012; Botero-Kleiven et al., 2001; Romero et al., 2000).

Macromolecules that are too large or polar to traverse the hydrophobic phospholipid bilayer can be taken up by cells from the extracellular environment via several pinocytotic pathways that are subdivided into clathrin-dependent and clathrin-independent endocytosis mechanisms, and macropinocytosis (De Bock et al., 2016).

These highly regulated pathways begin at specific regions in the plasma membrane (clathrin coated pits, non-coated lipid rafts and caveolae) and lead to the formation of endocytic vesicles, distinguishable via their size and vesicular markers (Xu et al.,2017). The trafficking fate of internalised vesicles and their content is further determined according to the subcellular endosomal compartments with which they fuse, i.e. early or recycling endosomes, late endosome or lysosome (Kalaidzidis et al., 2015).

1.5.1. Macropinocytosis

Macropinocytosis, is a non-specific, fluid phase endocytosis process that occurs via rearrangement of cytoskeletal components that lead to the formation of membrane protrusions. These subsequently fold back to the plasma membrane to encapsulate extracellular fluid (Müller-Greven et al., 2017). Unlike clathrin-coated and caveolae internalised vesicles, macropinosomes are distinguishable via their large size (0.2 – 5 μm) and lack of vesicular coating (Preston et al., 2014). Whilst in theory macropinocytosis can mediate transcytosis across cells, it faces significant hurdles as a drug delivery mechanism at the BBB, primarily due to lack of specificity

and reduced pinocytotic uptake at healthy BCEC (Lim and Gleeson, 2011; Reese and Karnovsky, 1967).

1.5.2. Caveolae-dependant endocytosis

Caveolae are morphologically and functionally distinct from clathrin-coated vesicles. They consist of flask-shaped invaginations within the plasma membrane and once internalised their vesicles are 50-100 nm in size and have a neutral pH. The plasma membrane regions that form caveolae are enriched in saturated phospholipids, sphingolipids, cholesterol and ethanolamine plasmalogens (Andreone et al., 2017). Caveolae vesicles are formed through interaction of the cavin family of cytosolic proteins and caveolin coat proteins (Cav1, Cav2 and Cav3) (De Bock et al., 2016).

Typically, BCEC possess few caveolae (Soares et al., 2016). However, several receptors have been identified at the BBB that function via this mechanism. Low-density lipoprotein receptor (LDLR) has been shown to function via this mechanism at the BBB and more recently on human umbilical vein endothelial cells (HUVEC) (Candela et al., 2008; Bian et al., 2017). Another receptor which mediates the transport of Aβ, receptor for advanced glycation end-products (RAGE), has also been shown to function via caveolae-mediated transport (Candela et al., 2010; D. Zhu et al., 2018). More recently, a novel BBB receptor, CD98 heavy chain (CD98hc), has also been suggested to function via caveolae-mediated transport at the BBB since it was identified to co-localise with caveolin-1 (Zuchero et al., 2016).

1.5.3. Clathrin-dependant endocytosis

The most defined mechanism, clathrin-dependant endocytosis, occurs at clathrin-coated invaginations within the plasma membrane termed clathrin-coated pits. These pits are enriched in extracellular receptor proteins that mediate the transport of their constitutive ligands via endocytosis (Neutra et al., 1985).

The formation of clathrin-coated vesicles consists of five steps; initiation, cargo selection, cargo vesicle budding, vesicle scission, and uncoating. The process is outlined in Figure 1.5.1.

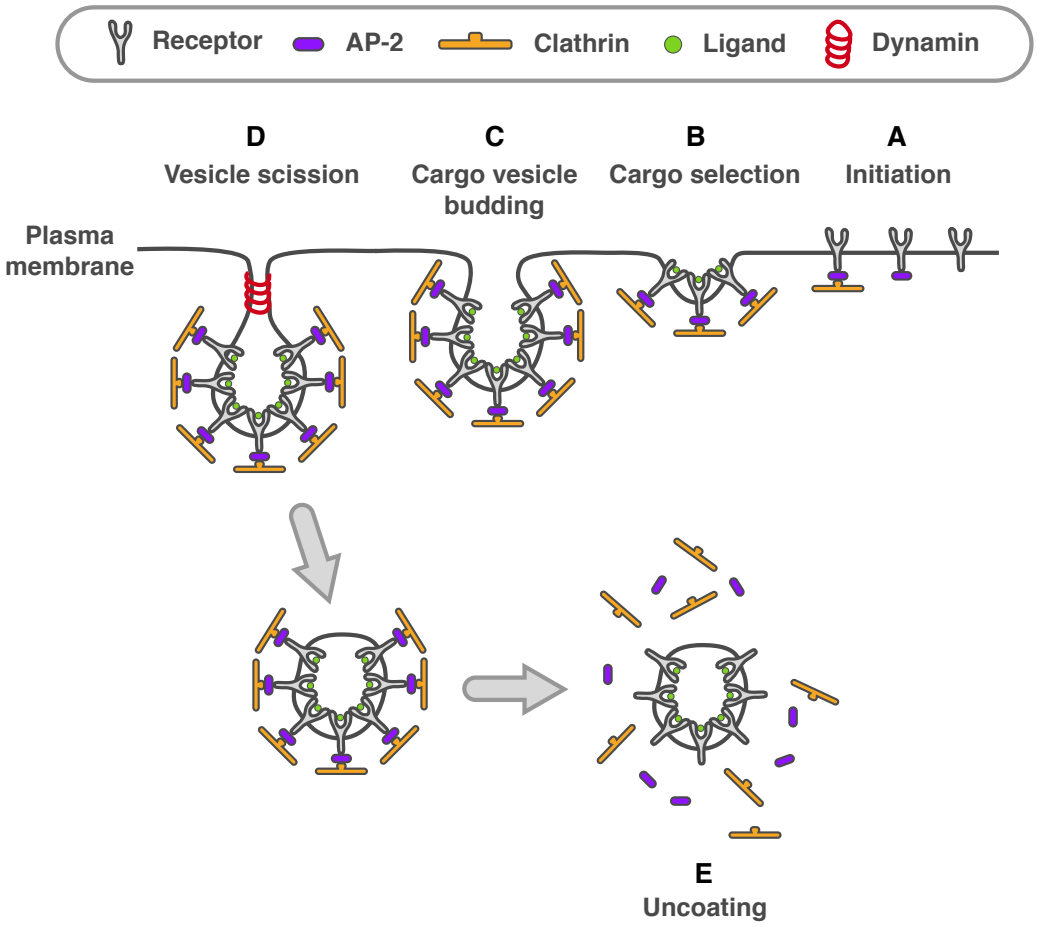

Figure 1.5.1: Formation of clathrin-coated pits and vesicle internalisation

Schematic representation of the process clathrin-coated pit formation and clathrin-mediated cargo internalisation at the plasma membrane. During the initiation and cargo selection stages (**A** and **B**), adapter proteins such as AP-2 are recruited to nucleation regions within the plasma membrane which contain uncoated pits produced through membrane bending effectors. AP-2 then associates with endocytic signaling motifs within the cytoplasmic domains of transmembrane proteins. Clathrin triskelions are recruited and can bind adaptor proteins which initiates lattice assembly. During cargo vesicle budding (**C**), additional adaptor proteins are recruited for polymerisation and assembly of the clathrin coat. (**D**) The process of vesicle scission is mediated via the large GTPase dynamin resulting in an internalised clathrin-coated vesicle. (**E**) The clathrin coat is uncoupled from the vesicle allowing it to fuse with the early endosomal compartments.

The initiation stage involves nucleation modules which determine the loci on the plasma membrane where vesicles will bud. The process involves the binding of F-BAR domain-containing Fer/Cip4 homology domain-only (FCHo) proteins to regions in the plasma membrane that are rich in phosphatidylinositol 4,5-bisphosphate (PIP_2). Epidermal growth factor receptor pathway substrate 15 (EPS15) and intersectins are recruited to FCHo and this initiates formation of a pit via the introduction of membrane bending forces (Ma et al., 2016). Previous studies, have shown that depletion of FCHo 1 and 2 results in reduced membrane clathrin-

coated vesicle budding and endocytosis events (Henne et al., 2010). However, a more recent study by Wang *et al*. (2016) has also demonstrated that EPS15 and FCHo function in a partially redundant manner.

Clathrin cannot directly bind to the membrane or cargo, instead it relies on a set of adaptor proteins known as clathrin-associated sorting proteins (CLASPs) and their complexes for recruitment. CLASPs mediate intracellular sorting and are recruited to the plasma membrane through interactions with sorting signals within the intracellular domains of transmembrane cargos and via specific interaction GTPases, phosphoinositide lipids and other CLASPs (Traub and Bonifacino, 2013). Following initiation, the cargo selection stage involves the recruitment of the heterotetrameric adapter protein 2 (AP-2) complex. AP-2 is the primary adapter protein that clathrin engages at the plasma membrane (Boucrot et al., 2010). AP-2 recognises endocytic signalling motifs such as the simple tyrosine motif (YXXØ, where Ø represents a hydrophobic residue) or the di-leucine motif [DE]XXXL[LI] within the cytoplasmic regions of transmembrane cargo destined for endocytic internalisation (Byland et al., 2007; Collawn et al., 1990; Owen and Evans, 1998). The tyrosine motif was shown to bind to the μ2 subunit of AP-2 at an affinity between 10 – 70 μM, and this binding was reported to be strongest when AP-2 formed complexes with clathrin (Rapoport et al., 1997). Structural interaction studies have also shown that the tyrosine motif adopts a linear conformation and binding occurs via the hydrophobic pockets within the μ2 subunit that interact with tyrosine and leucine in the peptide (Owen and Evans, 1998).

AP-2 may also directly or indirectly form interactions with other adaptors, which are themselves directly associated with particular cargo proteins. Some of these adaptor proteins (e.g. AP180/CALM, ARH, Epsin, β-arrestin) have also been shown to directly bind to PIP_2 and clathrin, and may function in mediating clathrin recruitment, via a mechanism independent of AP-2 (Motley et al., 2003). Depletion of AP2 prevents clathrin recruitment but does not stop the formation of the nucleation complex (Motley et al., 2003). Signal adapter interaction with AP-2 leads to the concentration of endocytic cargo proteins within clathrin-coated pits. Early studies

have shown that multiple species of receptor cargo bound to their respective ligands could occupy a single clathrin coated pit (Carpentier et al., 1982; Neutra et al., 1985).

The clathrin structure consists of three heavy chains associated with three light chains, forming a 'three-legged structure' termed *triskelion*. During the vesicle budding stage, the triskelia of clathrin polymerise into hexagonal and pentagonal lattice assemblies around the AP-2 complex forming the coat assembly. The polymerisation stabilises the curvature of the forming vesicle, whilst curvature effectors such as EPS15 and epsin develop the budding vesicle (Avinoam et al., 2015; McMahon and Boucrot, 2011). A recent study by Kukulski *et al*. (2016) has highlighted that in addition to facilitating in vesicle budding, clathrin is also involved in the timing of the scission event and hence regulating the overall size of the endocytic vesicles that are formed. Clathrin-coated vesicles are typically 70 – 150 nm in size, and can be as large as 200 nm (De Bock et al., 2016).

Vesicle scission is mediated via the large GTPase dynamin, which in itself is recruited by BAR domain-containing proteins, where it polymerises around neck of the vesicle and induces scission following GTP hydrolysis. Mutational studies of dynamin results in halted vesicle formation following clathrin polymerisation (van der Bliek et al., 1993). Once internalised, the clathrin lattice surrounding the vesicle is dismantled via ATPase, heat shock cognate 70 (HSC70) and auxilin (Morgan et al., 2013; Yim et al., 2010).

1.5.4. Intracellular trafficking

Internalised vesicles undergo a complex process of intracellular trafficking and delivery to various endocytic compartments, (e.g. early endosomal, late endosomal and lysosomal compartments). The process is summarised in figure 1.5.2.

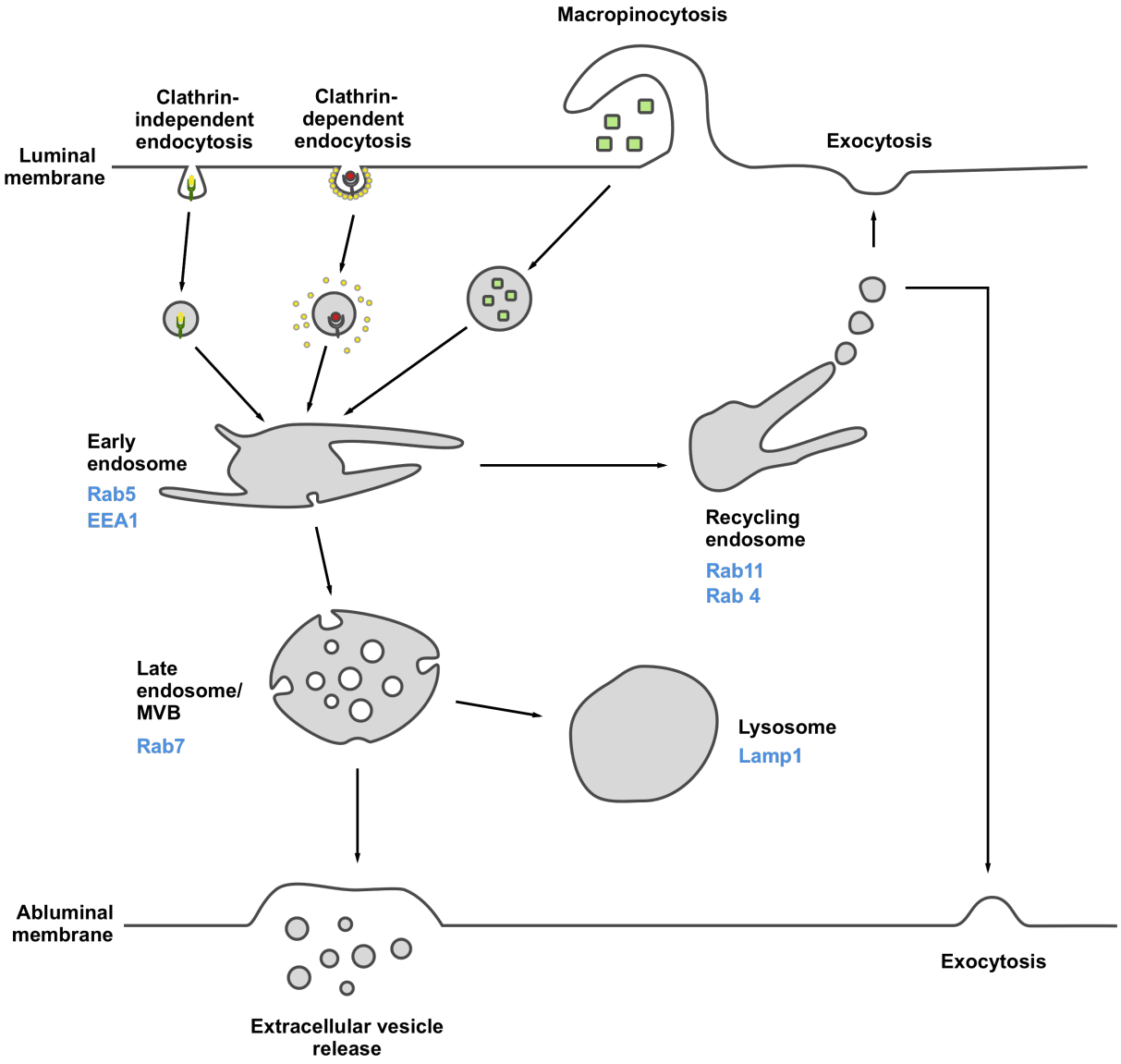

Figure 1.5.2: Vesicular trafficking at the BBB.

Cellular uptake of molecules occurs via clathrin-dependent endocytosis and clathrin-independent endocytosis (macropinocytosis and caveolae-mediated endocytosis) mechanisms. Internalised vesicles fuse with early endosomes, where they are sorted and destined for recycling/ transcytosis or degradation. This process is mediated through various Rab proteins that are located on the cytoplasmic surface of distinct intracellular compartments. Cargo destined to recycling endosomes may be recycled back to the luminal membrane or to opposing abluminal membrane (transcytosis). Cargo within late endosomes may fuse with acidic lysosomes for degradation, or through a process of intra-vesicular budding, develop into a multivesicular body (MVB) and fuse with the plasma membrane releasing vesicular content as microvesicles and exosomes.

Nearly all endocytosed vesicles fuse with mildly acidic early endosomes, that serve as sorting stations for all internalised cargo and are predominantly localised in the cell periphery (Kalaidzidis et al., 2015). Early endosomes are pleomorphic organelles that consist of vacuolar and tubular components, which separate cargo to

be degraded from cargo to be recycled back to the cell surface, respectively (Zeigerer et al., 2012). These early endosomes may be identified for their positive expression of the small GTPase Ras-related protein (Rab) 5, and early endosomal antigen 1 (EEA1). Rab proteins are the largest GTPase sub-family, that function by cycling between GDP-bound (inactive) and GTP-bound (active) states (Mishra et al., 2010). They regulate intracellular trafficking mechanisms by interacting with effectors such as EEA1 and adaptor protein containing PH domain and leucine zipper motif 1 (APPL1), which facilitate endosome fusion, tethering and vesicular transport (Christoforidis et al., 1999; Mishra et al., 2010; Zhu et al., 2004). Studies have shown that early endosomes expressing EEA1 and APPL1 are distinct populations, however a proportion of the population express both effectors due to their ability to exchange content (Kalaidzidis et al., 2015).

Early endosomal sorting occurs via one of three pathways; recycling pathway, late endosomal and subsequently lysosomal pathway, and transcytotic pathway (De Bock et al., 2016). The slightly acidic microenvironment of early endosomes (pH ~5.7) causes internalised receptors to change conformation, releasing their bound ligand (Haqqani et al., 2017). Receptor cargos localised within the tubular regions of the early endosome are recycled primarily to the luminal membrane or transcytosed across polarised BCEC to the abluminal membrane. Furthermore, in polarised cells such as BCEC, endocytosis can occur at both the apical and basolateral sides of the plasma membrane, with each face possessing distinct early endosomal sorting compartments, but not lysosomal compartments (Brown et al., 2000; Sheff et al., 1999; Wilson et al., 2000).

Rab5 and Rab7 are the most highly characterised small GTPases, and are expressed on early endosomes and late endosomes, respectively (Rink et al., 2005). Rab5 is essential for endosomal organisation and in conjunction with soluble N-ethylmaleimide sensitive factor attachment protein receptor (SNARE) proteins, is responsible for mediating early endosomal biogenesis and fusion (McBride et al., 1999). When cargo is destined for degradation, early endosomes are transferred to late endosomes via a process of Rab conversion from Rab5 to Rab7. The mechanism is regulated by class C VPS/HOPS complex which interacts with the

Rab5 and recruits Rab7 during the conversion (Rink et al., 2005). Late endosomes are 0.25 – 1 μm in diameter and are localised within the perinuclear region of the cell. Late endosomes may form multivesicular bodies through the budding of late endosomal membranes which leads to the formation of a multivesicular body. These multivesicular bodies may subsequently fuse with the cell membrane releasing their vesicular cargo in the form of microvesicles (100 – 1000 nm diameter) and exosomes (50 – 120 nm diameter), (Hung and Leonard, 2015). Additional Rab proteins also mediate various intracellular trafficking and exocytosis processes. For instance, Rab4 mediates the release of recycled cargo from early endosomes whist recycling vesicles are targeted to plasma membrane mediated via Rab11 (S. W. Park et al., 2014; Zhao et al., 2015). Lysosomal-associated membrane protein 1 (LAMP1) is also localised on the vesicular membrane of lysosomes and plays a role in protecting the lysosomal membrane from proteolysis (Qingqing Wang et al., 2017).

1.6. Receptor mediated transcytosis at the BBB

Transcytosis is defined as the transport of endocytosed cargo across the cell cytoplasm to the opposing plasma membrane where it exits the cell via exocytosis. The rate of cellular trafficking occurring at the BBB is substantially lower than that from other endothelial cells. BCEC have been shown to possess only 15% the number vesicles observed within muscular capillary endothelial cells (Coomber and Stewart, 1986; Preston et al., 2014). Despite this finding, the BBB retains selective permeability to key nutrients such as iron-bound transferrin and lipoproteins, which are transported and acquired in the CNS via RMT.

RMT at the BBB has been suggested to primarily occur via a clathrin-mediated mechanism. Clathrin-coated pits are highly abundant at the luminal membrane suggesting that clathrin-dependant transcytosis occurs predominantly in the blood to brain direction, as is the case with Tf/TfR transport (Bien-Ly et al., 2014). In contrast, caveolae have been identified on both luminal and abluminal membranes and has been associated with bi-directional transport of cargo (Candela et al., 2010).

Several receptors have been identified on BCEC which mediate the transport of their constitutive ligands via RMT these include transferrin receptor, insulin receptor, leptin receptor, diphtheria toxin receptor and members of the low-density lipoprotein receptor (LDLR) family, LDLR and LDLR-related protein 1 (LRP1) (Uchida et al., 2011; Ohtsuki et al., 2013; Ueno et al., 2010; Ping Wang et al., 2010). These receptors have all been exploited for the transcytotic delivery of cargo across the BBB.

Researchers are continuously pursuing the ideal RMT strategies for drug transport across the BBB. One recently proposed approach describes the possibility of increasing the transcellular transport capacity of BCEC for drug delivery (Wang et al., 2016). It has been suggested that an exploitable pharmacological mechanism for increasing RMT delivery exists via the sodium-dependent lysophosphatidyl-choline (LPC) symporter 1 (NLS1) or Mfsd2a. NLS1 is a BCEC specific transporter that is expressed by pericytes and has been shown to play two critical roles at the BBB. Firstly, the transporter itself has been shown to facilitate the transport of LPC-DHA, an essential omega-3 fatty acid required for proper neural function (Nguyen et al., 2014). Secondly, NLS1 regulates transcellular delivery at the BBB through inhibition of transcytosis (Ben-Zvi et al., 2014). The group outlined the potential for targeting this transporter for delivery of small molecule drugs coupled with DHA or via the inhibition of NLS1 to temporarily attenuate suppression of transcytosis and therefore increase the uptake of RMT drug shuttles.

1.6.1. Insulin receptor

Insulin receptor (IR) is expressed at the BBB and throughout the various regions of the brain, and mediates the transport of insulin via RMT. This has made it an attractive target for exploitation of CNS drug delivery. Utilising the endogenous ligand insulin resulted in short serum half-life and demonstrated hypoglycaemic adverse effects (Lajoie and Shusta, 2015), thus subsequent targeting approaches have focused on the use of antibodies to IR. One promising antibody approach utilises a humanised antibody HIRMAb derived from a mouse anti-IR antibody (83-14). This antibody has shown promising pre-clinical results for the delivery IDUA for the treatment of mucopolysaccharidosis type I (Boado et al., 2016; Boado and

Pardridge, 2017; J. Z. Lu et al., 2011). HIRMAb has also been engineered as a quadrivalent fusion molecule proposed for the treatment of Alzheimer's disease, in which the HIRMAb antibody was fused to an anti-Aβ single-chain variable fragment (scFv) at the CH3 region of the Fc domain (Boado et al., 2007). The anti-Aβ acts as the therapeutic arms of the molecule whilst HIRMAb mediates the transcytosis across the BBB. The fusion molecule was shown to traverse the BBB in rhesus monkeys, with 1% of the injected dose reaching the CNS (Boado, Lu, et al., 2010).

1.6.2. Lipoprotein receptor family

Several members of the LDLR family have been identified on the surface of BCEC including LDLR, LRP1 and LRP2 (Gosselet et al., 2009; Molino et al., 2017). Functionally, LDLR is responsible for the transport of cholesterol via the cholesterol binding low-density lipoprotein (LDL). LDLR is also capable of binding to secondary form of LDL lipoprotein, beta very low-density lipoprotein (β-vLDL), which unlike LDL, contain multiple copies of Apolipoprotein-E (Apo-E), (Lane-Donovan and Herz, 2017).

The targeting of LDLR and LRP1 has predominantly consisted of the use of apolipoprotein ligand such as ApoB and ApoE (or their peptides components) coupled to nanoparticles (Dal Magro et al., 2017; Portioli et al., 2017; Wagner et al., 2012; Zensi, Begley, Pontikis, Legros, Mihoreanu, Wagner, Büchel, Briesen, and Kreuter, 2009a; Kreuter et al., 2002). The success of these nanocarrier ApoE conjugates has also led some groups to develop apolipoprotein-α-L-iduronidase (IDUA) fusion molecules for the enzyme replacement treatment of mucopolysaccharidosis type I (El-Amouri et al., 2014; Böckenhoff et al., 2014; Daren Wang et al., 2013).

Another promising lipoprotein receptor targeting approach utilises Angiopep-2 peptide, which targets LRP1 through the Kunitz domain found on ligands which bind the LDLR family (Demeule, Régina, et al., 2008; Demeule, Currie, et al., 2008). Since its identification, Angiopep-2 peptide has been conjugated to paclitaxel (ANG1005) and is currently in phase II clinical trials for the treatment of glioma (Drappatz et al., 2013). Angiopep-2 has since been conjugated to various

nanocarriers and shown to translocate the BBB *in vitro* and *in vivo* (F. Lu et al., 2017; Figueiredo et al., 2016; Kafa et al., 2016; Velasco-Aguirre et al., 2017).

Whilst LDLR has been shown to be expressed at the luminal membrane of BCEC and clearly mediates the transport of its ligands via RMT, its expression within the cerebral cortex is low, thus severely hindering it capacity for further target the subset of cells within the CNS (Molino et al., 2017). LRP1 has been shown be associated with BCEC transcytosis through a mechanism that does not involve acidification of cargo and is capable of mediating uptake in CNS cells, thus is a more viable RMT receptor for drug delivery at the BBB than LDLR (Tian et al., 2015). However, the use of LRP1 as an RMT drug delivery receptor has some potential disadvantages. Firstly, its expression has been shown to decrease in BCEC and total brain with aging (Silverberg et al., 2010). Furthermore, its expression is further reduced with Alzheimer's disease (Storck et al., 2016). These finding suggest that LRP1 may not be the most suitable RMT target for developing a drug delivery system, since neurodegenerative disorders are increasingly prevalent within the aging population (Gallagher et al., 2017).

Instead this thesis will explore the targeting of transferrin receptor, a widely targeted and highly expressed receptor on the surface of BCEC that has been shown to mediate the transport of its ligands via RMT at the BBB (discussed in section 1.7)

1.7. Transferrin receptor (TfR)

Transferrin receptor (TfR) is responsible for mediating the transport of iron into cells via endosomal internalisation of the iron-binding, carrier glycoprotein and natural ligand, transferrin (Tf) (Aasa et al., 1963). Serum Tf consists of two 40 kDa subunits (N and C lobes), and is primarily synthesised in hepatocytes. Each lobe contains an iron binding site and is capable of binding Fe^{3+} at a high affinity (Holmberg and Laurell, 1946). The oxidisation of Fe^{2+} in the portal circulation produces free circulating Fe^{3+} ions which are capable of inducing cell toxicity through the generation of free radicals and the formation of insoluble polymers (Eckenroth et al., 2011). Functioning as a carrier molecule, Tf therefore also indirectly prevents cell toxicity by 'mopping up' circulating Fe^{3+}.

Structurally TfR (CD71) is a homodimeric type II transmembranous glycoprotein consisting of two 760 amino acid monomers linked together via two disulphide linkages. The structure of TfR is shown in Figure 1.7.1. Each subunit is 90-95 kDa in size and is capable of binding a single Tf molecule. X-ray crystallography studies carried out by Lawrence *et al*. (1999) at 3.2 Å resolution set the novel foundations for structural work on TfR and also proposed a model of Tf binding to the TfR. The TfR monomer is composed of three distinct regions, a globular extracellular region (AA residues 90 – 760), a hydrophobic intramembranous region (AA residues 62 – 89) and an N-terminal intracellular cytoplasmic region (AA residues 1 – 61). The extracellular region is further subdivided into three distinct regions, the protease-like (AA residues 121 -188 and 384 – 606), apical (AA residues 189 – 383) and helical (AA residues 607 – 760) domains (Eckenroth et al., 2011).

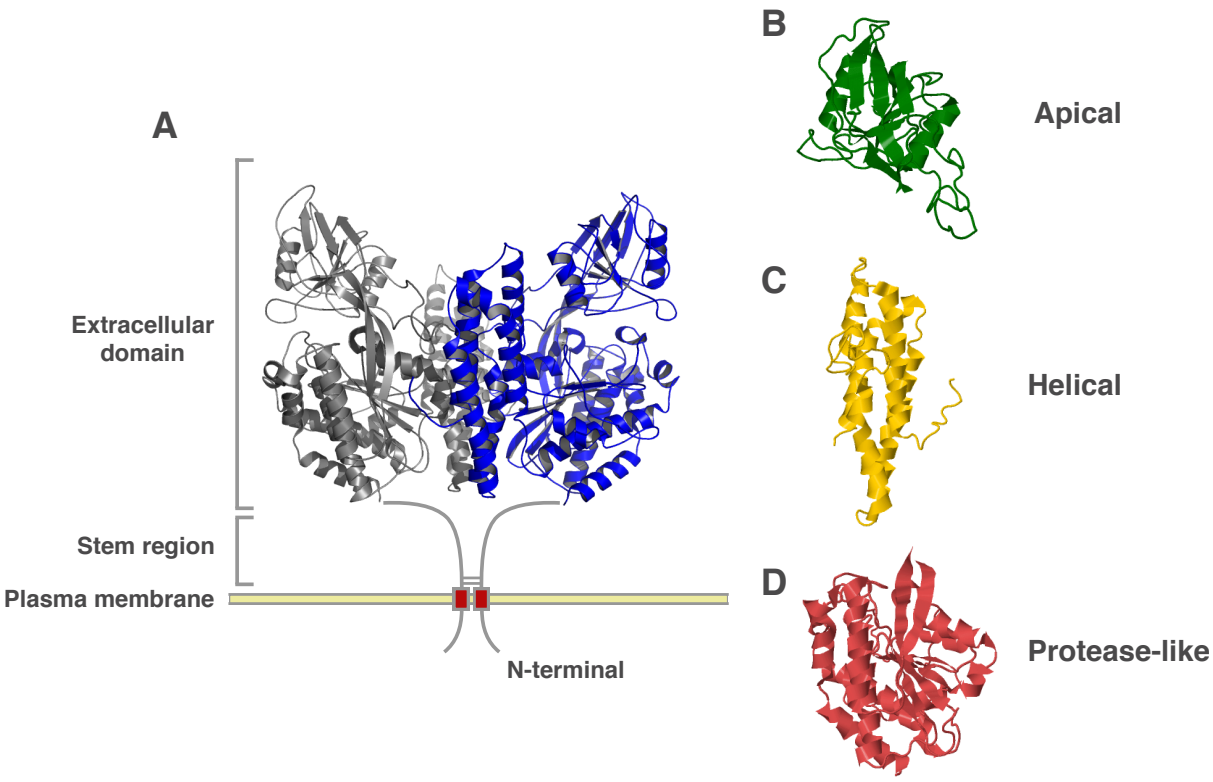

Figure 1.7.1: Extracellular structure of hTfR as determined by X-ray crystallography at 3.2 Å resolution.

Figure depicting the extracellular structure of the homodimeric TfR protein, anchored in the plasma membrane at the N-terminal region **(A).** The apical **(B)**, helical **(C)**, and protease-like **(D)** domains that make up each monomer of hTfR are also shown. Figure produced using PDB structure 1CX8 and JSmol software.

At the N-terminal intracellular region, an endocytosis motif consisting of amino acids tyrosine, threonine, arginine, and phenylalanine (YTRF) allows the correct orientation of the large ectodomain with respect to the plasma membrane. A phosphorylation site for protein kinase C is also present at serine24 (Davis et al., 1986). However, mutagenic studies have suggested that phosphorylation of serine24 does not induce an endocytosis signal (McGraw et al., 1988).

Two palmitoylation sites are located within the intramembranous region at cysteine residues 62 and 67, with cysteine 62 being the primary site for palmitoylation (Jing and Trowbridge, 1987). These sites enhance hydrophobicity through covalent attachment to fatty acids, thus anchoring the protein into the plasma membrane.

The stalk region (AA residues 89 – 120) contains a site for *O-linked* glycosylation (Threonine104), which is likely important for TfR transport to the plasma membrane (Do and Cummings, 1992; Hayes et al., 1992). At the plasma membrane side of the extracellular stalk, two intermolecular disulphide bonds are located at cysteine residues 89 and 98 (Jing and Trowbridge, 1987).

Multiple proteolytic sites have been identified within the extracellular stem region of TfR (Kaup et al., 2002; Rutledge et al., 1998; Turkewitz, Amatruda, et al., 1988). Although the most highly susceptible proteolytic cleavage site is present between arginine 100 and Leucine 101(Shih et al., 1990). Cleavage at this site results in the release of a solubilised form of the TfR extracellular domain into the circulation. This solubilised form consists of 660 AA per monomer and has been shown to stably maintain 95% homology to the extracellular protein structure of TfR (Turkewitz, Schwartz, et al., 1988). More importantly, its capability to bind Tf was also retained. Furthermore, Alvarez *et al*. (1989) revealed that dimerisation of the cleaved fragment occurred independent of the disulphide linkages, suggesting that homodimerisation occurs spontaneously through the helical domain of the globular extracellular region. Soluble TfR (sTfR) has also been observed as a component of serum under normal physiological conditions. This fragment was found to inversely correlate with iron storage levels within the body (Rutledge and Enns, 1996).

The extracellular domain contains the Tf binding site. Three *N-linked* glycosylation sites, (asparagine 251, 317 and 727) are also present and play a significant role in proper molecular folding. Mutation of these *N-linked* glycosylation sites leads to impaired Tf binding activity of TfR (A. M. Williams and Enns, 1991; Lawrence et al., 1999).

TfR is ubiquitously expressed in most cells of the body at low levels. Under physiological conditions, its expression is highest in cells that require high iron concentrations for cellular processes such as proliferation and the generation of mitochondrial ATP. However, although BCEC are non-proliferating cells, their expression of TfR remains high. This is due to the high demand for iron within the CNS for processes such as dopaminergic neurotransmitter synthesis and

myelination (Mills et al., 2010). In contrast, endothelial cells of the vasculature do not express detectable levels of TfR (Jefferies et al., 1984).

TfR is also highly expressed in various cancer cells. Iron requirement is increased within rapidly dividing cancer cells as it functions as a co-factor for ribonucleotide reductase enzyme in the DNA replication process. Moreover, the expression of TfR on various cancer cells has been correlated with advanced stage disease, as well as poor prognoses (Yang et al., 2001).

1.7.1. Iron transport at the BBB

The TfR mediated endocytotic internalisation of iron-bound Tf was first described by Cienchanover, Dautry-varsat, and Lodish (1983); prior to this discovery it was incorrectly assumed that iron was released from bound transferrin upon formation of the Tf/TfR complex at the cell surface (Jandl et al., 1959). The process of TfR mediated RMT at the BBB is outlined in Figure 1.7.2.

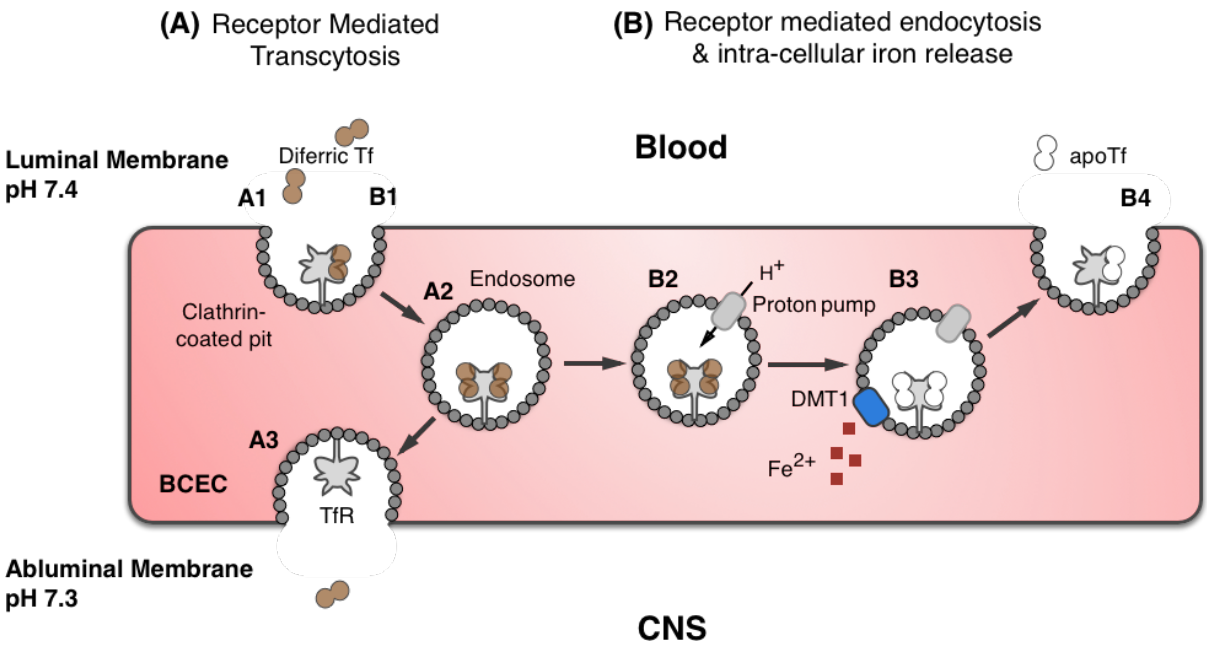

Figure 1.7.2: TfR mediated transcytosis and endocytosis of Tf/TfR complexes at the BBB.

Figure outlining the two proposed mechanisms for TfR mediated iron transport at the BBB, RMT **(A)** and receptor mediated endocytosis, followed by DMT1 mediated release of iron and subsequent receptor recycling **(B).** Both mechanisms initiate by binding of diferric transferrin to the TfR at the cell surface pH of 7.4. Binding of the ligand induces the invagination of the cell membrane into a clathrin-coated pit, which internalises via clathrin-dependent endocytoses and subsequently fuses with the early endosomal compartment **(A1, B1)**. RMT involves the complete traversal of the BCEC to the abluminal side exclusive of intra-endosomal release of iron bound Tf **(A2)**. Exocytosis of the

endosome at the abluminal side leads to the release of iron from Tf at the reduced pH of the interstitial fluid **(A3)**. The alternative and generally accepted mechanism for TfR mediated iron transport within the majority of cells involve proton pumps in endosomal membrane. These pumps facilitate the influx of H^+ ions into the endosome reducing the pH to 5.6 **(B2)**. Iron is then released from transferrin into the cytosol **(B3)**. The Tf/TfR complex is recycled via the fusion with a recycling endosome **(B4)**. Most recycling occurs to the luminal membrane via this mechanism. However, some recycling may also occur to the abluminal membrane.

Cienchanover *et al* (1983) showed that at the neutral cell surface pH of 7.4 only iron-bound Tf (monoferric and diferric) is capable of binding to the TfR. The unbound form, apotransferrin (apoTf) is ignored, thus preventing the competitive binding between the ubiquitously abundant apoTf species in contrast to the less abundant bound species. Furthermore, diferric Tf was shown to demonstrate a 30-fold increase in TfR association constant in contrast to monoferric Tf (Young et al., 1984). Following receptor association, the Tf/TfR complex is internalised via clathrin-coated pit formation, clathrin-dependant internalisation, and subsequently fusing with an early endosomal vesicle (described in section 1.5.3). The internal pH microenvironment of the endosome is then reduced via proton pumps to a pH of approximately 5.6, at which point iron is unbound from transferrin, reduced to Fe^{2+} and is transported across the endosomal membrane into the cytosol, via the aid of the divalent metal transporter 1 (DMT1). The residual apoTf/TfR complex is then sorted and re-localised to the luminal membrane where apoTf is released extracellularly into the plasma and can consequently bind iron at a neutral pH.

Although the aforementioned mechanism appears to be the primary mechanism for iron internalisation in the majority of cells within the body, it does not seem to be the case in BCEC. There has been conflicting evidence with regards to the exact mechanism by which TfR mediates the transport of iron into the CNS (Burdo et al., 2001; Moos and E. H. Morgan, 2000; Moos et al., 2006; Siddappa et al., 2002). Studies have previously demonstrated TfR transcytotic transport across BCEC to the abluminal side in endosomes (Bickel et al., 1994). More specifically, using OX26 (anti-rat TfR IgG2a antibody) coupled to gold nanoparticles and TEM, Bickel *et al*. (1994) demonstrated TfR to be mostly sub-localised to the luminal membrane and intracellularly in vesicles. Some expression was also observed on the abluminal membrane. However, it was not clear whether iron remained bound to

Tf and released at the abluminal membrane or transported into the cytosol following endocytosis via DMT1.

Utilising a bovine BCEC and astrocyte co-culture model Descamps *et al*. (1996) were able to study the uptake of labelled TfR. Endosomal internalisation was found to be temperature dependant, as endosomal uptake showed complete inhibition at lower temperatures. The group also observed no signs of intra-endothelial degradation of Tf, and therefore they concluded that the TfR internalisation pathway avoids the lysosomal degradation compartment. Moreover, by labelling both Tf and iron the group also demonstrated iron can be transported across the BCEC abluminal membrane bound to Tf. Interestingly they quantified 10% of Tf was recycled to the luminal membrane while the remaining 90% was found to recycle to the abluminal membrane. In support of these findings more recent studies by Moos *et al*. (2006) have also proposed a DMT1 independent mechanism for the transport of iron-bound Tf.

In contrast to the aforementioned mechanisms, iron uptake at BCEC may be more complex than initially thought and is likely to occur via various non-TfR dependant mechanisms. Mice that are severely deficient of circulating Tf have been reported to maintain normal brain iron content, thus suggesting alternative brain uptake mechanisms exist at the BBB (Beard et al., 2005). Tf homologous proteins such lactoferrin and melanotransferrin can also act as iron transporters across the BBB (Fillebeen et al., 1999; Rolland et al., 2009; Rothenberger et al., 1996; Ji et al., 2006). A study by Kumar *et al*. (2012) has identified that under situations of iron depletion, glyceraldehyde-3-phosphate dehydrogenase (GAPDH) can also function as a Tf binding protein, mediating iron uptake into non-TfR expressing CHO cells. Fe^{3+} bound ferritin has also been shown to act as a ligand for proteins such as Scara5 and Tim-2 (J. Y. Li et al., 2009; Todorich et al., 2008).

Regardless of the conflicting views over iron delivery to the CNS, TfR mediated transcytosis demonstrates great potential for clinically significant accumulation of a TfR targeted therapeutic within the CNS and this has been demonstrated in various pre-clinical studies, *in vitro* and *in vivo* (Webster et al., 2017;

Macdonald, Houghton, et al., 2016; Zuchero et al., 2016; Yu et al., 2014; Niewoehner et al., 2014; Manich et al., 2013; Macdonald, Henri, et al., 2016).

1.8. Targeting the BBB for drug delivery

Targeted drug delivery is the process of increasing the concentration of a drug in a specific site of action, mediated via delivery vectors and targeting moieties (e.g. antibodies). The targeted delivery of drugs improves their therapeutic index, a measure of the ratio of the therapeutically effective dose to the toxic dose of a therapeutic agent, thus reducing undesirable side effects due to non-target site interactions (Guo et al., 2012).

Several strategies have been used to overcome the transport limitations of the BBB. These can largely be divided into invasive and non-invasive approaches. Invasive approaches include transcranial surgical methods as well as methods that disrupt the BBB in order to increase drug permeability (Vykhodtseva et al., 2008). Non-invasive methods usually involve drug delivery approaches that utilise endogenous mechanisms such as pharmacological approaches (small lipophilic drug analogues and their endogenous transporters) (Pardridge, 2007) and biological drug delivery strategies (Lichota et al., 2010; L. B. Thomsen et al., 2012), the latter of which will be the focus of this study.

1.8.1. TfR targeted drug delivery

The most extensively targeted receptor for RMT drug delivery at the BBB is TfR (Yu et al., 2014; Pardridge, 2015; Webster et al., 2017). Many animal studies have demonstrated the use of TfR as an effective RMT delivery strategy for the transport of drug payloads across the BBB. The targeting of TfR for drug delivery has primarily consisted of two approaches. The first approach utilises the natural ligand Tf or a competitively binding domain that targets the same epitope (Pang et al., 2011; Staquicini et al., 2011; Huang et al., 2007). The second more popular approach has so far predominantly utilised antibodies for targeting an epitope independent of the ligand binding region (Bickel et al., 1994; Lee et al., 2000; Yu et al., 2014; Bien-Ly et al., 2014; Niewoehner et al., 2014; Webster et al., 2017)

Drug delivery using the natural transferrin ligand has so far predominantly consisted of nanocarrier conjugates and some of these have shown success in pre-clinical studies(Huang et al., 2007; Wiley et al., 2013). Huang *et al*. (2007) have previously shown that transferrin-polyamidoamine (PAMAM) conjugates can be successfully used for TfR-mediated uptake of gene vectors into the brain. Within this study the group demonstrated a 2.5-fold increase with PAMAM-PEG-Tf conjugates in comparison to the controls. Another study by Wiley *et al*. (2013) demonstrated the brain uptake of Tf-coated gold nanoparticles (45nm and 80nm in size). These gold nanoparticles were systemically administered in mice and assessed for accumulation in the brain parenchyma. The group concluded that the uptake of Tf-coated nanoparticles was avidity dependant on the density of Tf on gold nanoparticles. One recent notable example of Tf mediated RMT involved the use of an iron mimicking cyclic heptapeptide, CRTIGPSVC. This peptide competes with iron for binding to apoTf and was demonstrated to significantly reduce the brain tumour size in a mouse model of glioma (T. Kang et al., 2015; Staquicini et al., 2011). Although some studies have shown promising *in vivo* brain uptake using Tf as a RMT delivery vector, it is not an ideal targeting approach. This drug delivery strategy faces significant competition from circulating Tf which is present in the blood at 25 μM concentration (Qian et al., 2002).

The alternative approach of using a targeting molecule which binds to TfR at a ligand independent site is a more therapeutically viable option. Pioneering work by Pardridge *et al.* (1991) initially highlighted the concept of exploiting TfR mediated RMT for the delivery of macromolecular drugs across BCEC via a process later designated ‘molecular Trojan horse delivery’ (Pardridge, 2002). Although initially described for TfR, the same approach has also been applied to multiple target receptors that function via RMT (Dehouck et al., 1997; Demeule, Currie, et al., 2008). The process involves the use of a receptor specific molecular targeting domain, which is coupled to a therapeutic payload. The targeting domain binds TfR and is subsequently transported alongside the Tf/TfR complex via RMT to the

abluminal membrane of BCEC, where it can theoretically be released and made available within the CNS.

The concept was demonstrated using OX26, an IgG2a mouse monoclonal rat TfR-specific antibody generated against an extracellular region that does not interfere with Tf ligand binding and thus avoids any issues with competitive binding (Pardridge et al., 1991). Through an *in vivo* study in rats, OX26 was shown to only result in a 0.44% concentration of injected dose within the parenchyma. Studies have since described the conjugation OX26 to various payloads and demonstrated their capacity to be transported across the BBB via rat *in vivo* studies. Some of these payloads include, brain-derived neurotropic factor (BDNF), recombinant human CD4, vasoactive intestinal peptide analogue, nerve growth factor (Yun Zhang and Pardridge, 2006; Walus et al., 1996; D. Wu and Pardridge, 1996; Kordower et al., 1994). More recently, OX26 has increasingly been used in conjunction with nano-carriers to deliver various drug cargos across the BBB, these approaches are summarised in table 1.8.1.

Table 1.8.1: Recent OX26 Nano-carrier drug delivery approaches at the BBB.

Nano-carrier	Drug cargo	Proposed disease treatment	Study format (*in vitro/ in vivo*)	Reference
γ -PGA and l-PAE co-polymer (PHRO)	Ginsenoside Rg1	diabetic cerebral infarction	*In vivo*	(Shen et al., 2017)
liposomes	oxaliplatin	No proposed disease (generalised BBB drug delivery)	*In vitro* and *in vivo*	(Johnsen et al., 2017)
Pegylated liposomes	Dopamine	Parkinson's disease	*In vivo*	(Y.-S. Kang et al., 2016)
poly(lactic-co-glycolic acid) (PLGA) nanoparticles	iAβ_5 peptide (LPFFD)	Alzheimer's disease	*In vitro*	(Loureiro et al., 2016)
Pegylated liposomes	α -synuclein	Parkinson's disease	*In vitro*	(Loureiro et al., 2015)
Pegylated cationic solid lipid nanoparticles	Baicalin	Cerebral ischemic injury	*In vivo*	(Z. Liu et al., 2015)
Pegylated liposomes	chlorotoxin	Glioma	*In vitro* and *in vivo*	(Yue et al., 2014)
Pegylated liposomes	ApoE3	No proposed disease (generalised BBB drug delivery)	*In vitro* and *in vivo*	(Markoutsa et al., 2014)

Two rat anti-mouse TfR specific monoclonal antibodies, 8D3 and R17-217 have also been described within the literature (Kissel et al., 1998; Lesley et al., 1984). When comparing the brain uptake of both these antibodies, 8D3 exhibited a higher percentage uptake than R17-217 (3.1% and 1.7% injected dose/g, respectively) (Lee et al., 2000). However, upon further assessment R17-217 was observed to exhibit greater specificity towards the brain than to 8D3.

Although many *in vitro* and *in vivo* studies utilising monoclonal antibody delivery vectors have been successful in demonstrating some extent of drug delivery across BCEC, the observed rate of delivery *in vivo* is often poor (<1% of injected dose), resulting in a weak therapeutic concentration within the CNS. More recently, TfR bi-specific antibody targeting approaches have been described by (Yu et al., 2011). These studies propose a mechanism for TfR mediated transcytosis at the BBB, where antibody affinity and avidity of the targeting moiety plays an important

role in modulating intracellular fate of the internalised RMT vector. Through re-engineering approaches, the group demonstrated that lower to moderate affinity antibodies towards TfR in conjunction with therapeutic dosing, resulted in significantly increased accumulation within the CNS. In support of these findings, it has been reaffirmed that both OX26 and 8D3 are capable of binding to BCEC, however these do not undergo significant transcytosis and remain sequestered within BCEC (Moos and E. H. Morgan, 2001; Paris-Robidas et al., 2011). Once again, re-engineering approaches carried out on 8D3 to generate lower affinity variants resulted in significantly increased accumulation within the CNS (Webster et al., 2017).

1.9. Biopharmaceuticals

Biopharmaceuticals or biologics are a growing class of therapeutics. Multiple definitions have been used to describe biopharmaceuticals, and these definitions vary according to the source (e.g. scientific or business), manufacturing process and the inherent nature of the product. One of the most popular classic definitions refers to pharmaceuticals and biopharmaceuticals as being the major subsets for drugs, with biopharmaceuticals being inherently biological products that can be manufactured through biological processes, from biological sources. In contrast, a pharmaceutical is a product manufactured via chemical sources and processes (Rader, 2008). This definition encompasses all biological products including engineered proteins, blood/ plasma products and vaccines. However, under this definition, the categorisation of certain products becomes challenging since they can be interpreted as both pharmaceuticals and biopharmaceuticals. For instance, peptides and oligonucleotide agents (e.g. aptamers, small interfering RNA and miRNA) are inherently biological, however they may also be synthesised and modified via chemical approaches (Remuzgo et al., 2014; Tang et al., 2017).

Another definition of biopharmaceuticals, has a narrower view of the field, focusing only on the clinical successes of monoclonal antibodies (Mabs) and recombinant proteins, and this definition excludes proteins from non-recombinant sources, vaccines, blood/ plasma products. Instead of these aforementioned

definitions, it has been suggested that biotherapeutics should be defined as “pharmaceuticals inherently biological in nature and manufactured using biotechnology”, in order to avoid fragmentation of the literature (Rader, 2008). Examples of biopharmaceuticals described within this context include, peptides, recombinant proteins, enzymes, MAbs, small interfering RNA (siRNA), microRNA, gene therapies and aptamers (Andrews et al., 2015).

The push towards the development of recombinant human insulin in the early 1980’s bought about a revolutionary shift in the pharmaceutical industry that has changed the outlook for many patients suffering from diseases with previously very poor prognosis. As of 2014, a total of 212 biopharmaceuticals were marketed within the US and EU (Walsh, 2014). Biologics now make up approximately 45% of the world’s top 100 grossing drugs, and account for 25% of all pharmaceutical sales (Evaluate Pharma, 2015).

For many years, monoclonal antibodies (MAbs) have dominated the biologics arena, generating successful treatments towards various forms of cancer (Tan et al., 2013) and immuno-inflammatory diseases (reviewed in Willrich et al., 2015), in addition to contributing to the fields of disease diagnosis and bioscience research. Their success has primarily been attributed to their inherent target specificity.

Although proving highly successful for research, diagnostic and therapeutic applications, traditional MAbs based on the IgG structure have their limitations when used as biotherapeutics. The large size of IgG antibodies (150 kDa) leads to poor tissue penetration and in what is considered both an advantage and disadvantage, their long plasma half-life makes patient dosing convenient, but causes difficulty in regulating drug clearance (M. Schmidt and Wittrup, 2009; Bai et al., 2012). Moreover, their development and manufacturing complexity, batch-to-batch variation and requirement for cold storage, adds to the overall cost of bringing these drugs to market (Halim et al., 2016; Patel et al., 2015; Chames et al., 2009).

Given the shortcomings of antibodies and their clinical success, several engineering strategies have been employed to improve the properties of traditional antibodies. Many initial protein engineering attempts have focused on modifying the

IgG molecule e.g. bi-specific antibodies (Spiess et al., 2015), or using its modular fragments as independent binding domains, e.g. Fab and scFv (Holliger and Hudson, 2005). In addition to these approaches, several immunoglobulin-like molecules have been isolated from various animal sources and adapted into targeting domains such as camelids derived from camels and immunoglobulin new antigen receptor (IgNAR) derived from cartilaginous fish e.g. sharks (Rutgers et al., 2011; Dooley et al., 2003; Goodchild et al., 2011; T. Li et al., 2016). These antibody-like molecules differ from human immunoglobulin by being devoid of light chain regions (Feige et al., 2014; Hamers-Casterman et al., 1993).

More recently, developments on several forms of non-antibody engineered scaffolds have been described (Stefan et al., 2011; Oganesyan et al., 2013; Tiede et al., 2017; Škrlec et al., 2015). These scaffolds are based on backbones of a naturally occurring proteins (usually human origin), which normally carry out multiple functions within the body and therefore have complex binding regions (Lorey et al., 2014). Through mutagenesis engineering approaches, a library of these proteins is generated with randomised amino acids within the binding region (Tiede et al., 2014).

The work described herein focuses on the use of peptides and aptamers as antibody alternative targeting domains, these are described below.

1.10. Peptide therapeutics

Peptides are short chains consisting of two or more amino acids. Greater than 7000 naturally occurring peptides have been identified and many of these have crucial biological functions, acting as hormones, growth factors, ligands, antimicrobials and venoms (Murase et al., 2017; Modi et al., 2016; Orlandi et al., 2015; Seo et al., 2016; Wenzel et al., 2016; Soares et al., 2016; Oller-Salvia et al., 2013). Historically, peptides had been regarded as inferior to traditional chemical therapeutics, largely due to the fact that they are rapidly degraded by proteases upon intravenous administration (Julien et al., 2012; F. Xu et al., 2017). Systemically circulating unprotected peptides are rapidly degraded within minutes via exo-peptidases such as amino- and carboxy-peptidases (Alsters et al., 2015; John-White

et al., 2017). Moreover, peptides have limited oral bioavailability due to physiological (poor gastrointestinal solubility and permeability), and chemical and biochemical (acid hydrolysis and enzymatic degradation within gastrointestinal fluids) barriers, resulting in <2 % of orally administered dose reaching the circulation (Uhl et al., 2017; Diao and Meibohm, 2013). An exception to this is the approved immunosuppressant drug cyclosporine. This 11mer cyclic peptide (constrained via a disulphide bond between two cysteine residues) has greater resistance to peptidase degradation and demonstrates a 30 and 40% bioavailability following oral administration (Holt et al., 1995).

The advent of techniques such as DNA recombination, phage display, high throughput screening and combinatorial chemistry approaches, allowed the efficient selection, identification and modification of peptides from large combinatorial phage display libraries ('t Hoen et al., 2012; Staquicini et al., 2011; Ru et al., 2014; Wada, 2013). These libraries could be engineered to have structural features through the inclusion of fixed residues along the peptide chain (e.g. the peptide libraries used in this study) or via amino acids with particular properties to encourage overall structural and functional characteristics (O'Neil et al., 1992; Bonetto et al., 2009). Furthermore, the engineering of pre-identified peptides through rational design methods, such as alanine substitutions, structure-activity relationship studies and peptidomimetic modifications (Feng and B. Xu, 2016), allows the production of optimised protease resistant variants of peptides that maintain or improve upon biological and pharmacokinetic activity (Vlieghe et al., 2010). These modified peptides have the potential to bridge the gap between the stability and bioavailability of traditional small molecule drugs and the functionality and specificity of larger amino acid-based biologics. In total, approximately 60 peptide drugs have been approved, in addition to over 140 currently undergoing clinical trials (summarised in Fosgerau and Hoffmann, 2015; Hamzeh-Mivehroud et al., 2013).

Initial attempts at peptide delivery across the BBB involved the use cell-penetrating peptides originating from protein transduction domains such as TAT and penetratin (Cao et al., 2002; Joliot et al., 1991). Since these approaches relied on AMT transport, they were non-selective for the BBB and often resulted in the

accumulation of peptide within BCEC when not conjugated to secondary cationic moiety (Sharma et al., 2016). Selective peptides that target endogenous receptors expressed on the luminal membrane of BCEC and function through RMT, have been identified using *in vitro* phage display selections (Lee et al., 2001; Dai et al., 2014; Malcor et al., 2012). Studies have also employed *in vivo* phage display selections to identify brain penetrating peptides. However, this technique results in the identification of peptides without known target(s) and this poses many serious implications for safety and drug candidate development (Pasqualini and Ruoslahti, 1996).

Perhaps the greatest example for the viability of peptides as BBB shuttles, is the fact that many peptide-based venoms have evolved to circumvent the BBB and induce their biological effects within the CNS (Oller-Salvia et al., 2016). The ability of these venoms to function across a wide range of species signifies the potential for species cross-reactive targeting peptides. The identification of species cross-reactive binding domains is a highly sought after characteristic for biologic drug development, as it typically improves the safety, efficacy and the success rate of a drug candidate going forward from animal pre-clinical to human clinical studies (Irani et al., 2016; Farady et al., 2009; Eastwood et al., 2010).

1.10.1. Peptides targeting TfR

Four notable examples of peptides have been identified through phage display panning selections towards TfR, these are peptides B6 (GHKAKGPRK), THR (THRPPMWSPVWP), T7 (HAIYPRH) and BP9 (AHLHNRS) (Xia et al., 2000; Lee et al., 2001; Dai et al., 2014).

The B6 peptide was identified through screening of a nonamer phage display library towards hTfR (Xia et al., 2000). Following sequencing of selected pools, the majority of sequences were identified to contain the motifs AKxxK/R, KxKxPK/R, or KxK. The group utilised a model of mucopolysaccharidoses type VII to study the capability of several variants of peptide B6 to deliver gene therapies into BCEC. sequences for peptide B6 were cloned into the HI loop of adenovirus type 5 fibre and

and were shown to be bind hTfR expressing cells and BCEC. The group also observed a 2- to 34- fold increase in gene transfer with cells.

Studies by Prades *et al*. (2012) have re-introduced the TfR binding THR peptide for the purpose of drug delivery at the BBB. The 12mer linear peptide was initially identified via phage display panning selections and shown to bind to human TfR at a transferrin-independent receptor epitope, and traverse the plasma membrane of chicken embryo fibroblast cell lines via an endosomal pathway (Lee et al., 2001). The group combined this THR peptide alongside a β-sheet cleaving peptide, LPFFD, through conjugation to gold nanoparticles via a cysteine residue. The resultant THR/Aβ cleaving peptide conjugated nanoparticles demonstrated increased permeability *in vitro,* using a bovine BBB co-culture model and greater penetration of rat brain, *in vivo*. More recently, the same group were able to modify the THR peptide using a *retro-enantio* rational design approach to construct a mirrored version of the molecule that was more resistant to protease degradation. This modified molecule was shown to exhibit enhanced transport capability across the BBB when compared to the parent molecule (Prades and Salvia, 2015).

The BP9 peptide was identified through phage display selections of a 7-mer linear peptide library towards hTfR (Dai et al., 2014). Following three rounds of selection, 20 clones were picked and screened through phage ELISA. The group identified 6 clones that bind hTfR significantly higher than the negative control phage. Assessment of the sequences revealed the peptides share a two-amino acid motif ‘RS’ with transferrin. The group concluded that the negatively charged BP9 peptide binds through electrostatic interactions with TfR. The group also generated a BP9-EGFP fusion and assessed the binding of BP9 towards three human hepatocarcinoma cell lines expressing TfR, HepG2 and SMMC-7221 cells, and deficient for TfR, LO-2 cells. BP9 was shown to bind to the TfR positive cells, but not the deficient cells. Through inhibition of cell proliferation assays, BP9 was shown to interfere with Tf binding. The species cross-reactivity of this peptide has yet to be established, since the group have only assessed the binding of BP9 towards hTfR expressing cells. Furthermore, the capability of BP9 to mediate transport into cells was not established through internalisation assays.

1.11. Aptamers as novel targeting biologics

Aptamers are oligonucleotide-based targeting molecules that can bind molecular targets at high affinity and specificity via the three-dimensional hairpin structures they form through folding. The term aptamer stems from the Latin word *aptus* (to fit) and the Greek word *meros* (region) (Ellington and Szostak, 1990). Oligonucleotide aptamers consist of ribonucleic acid (RNA) or single stranded deoxyribonucleic acid (ssDNA) and are 20-100 nucleotides in length (5 to 25 kDa in weight) {Ni:2011vl}. Early studies into the human immunodeficiency virus (HIV) brought about the basic concept of oligonucleotide-protein molecular interaction. Studies carried out by Sullenger *et al.* (1990) to assess HIV viral replication established that a short RNA ligand, 5' transactivation response (TAR) element was responsible for binding Tat proteins and trans-activating viral replication.

Subsequently two groups working on aptamers in the 1990's brought about the development of an *in vitro* system for selecting and isolating aptamers (Tuerk and Gold, 1990; Ellington and Szostak, 1990). This system was termed Systematic Evolution of Ligands by Exponential Enrichment (SELEX) (described in section 1.12.2). The technique enabled the selective *in vitro* generation of specific aptamers to a variety of target molecules ranging from metal ions (C. H. Chung et al., 2013; Ling Zhang et al., 2013) and small bio-molecules, to large complex peptides, whole cells (Meng et al., 2010) and microorganisms (Y. S. Kim et al., 2013). The large range of potential target molecules provides aptamers with wide scope of applicational uses; some of these include diagnostic, analytical and therapeutic applications (Song et al., 2012).

Since their development in the 1990's, aptamers have only seen a significant surge in research over the past decade, primarily due to the expiry of key patents on their selection technology and use as ligands (McKeague and DeRosa, 2014). A recent success story for aptamers and their clinical significance came about with the FDA approval of the first aptamer based therapeutic, Macugen™ (pagaptanib sodium). This RNA aptamer-based drug offered a treatment for age related macular degeneration, by targeting an isoform of vascular endothelial growth factor (VEGF-

165), that is predominantly responsible for vascular permeability and ocular neovascularisation (Ng et al., 2006; Vinores, 2006).

Other aptamer-based drugs are currently undergoing clinical trials such as the anti-cancer drug, AS1411. This anti-proliferative guanosine rich DNA aptamer binds cell surface nucleolin, is internalised and inhibits growth by halting DNA replication (Ireson and Kelland, 2006). The G-rich sequence of AS1411 encourages the formation of intermolecular and intramolecular quadruplex structures, which are further stabilised through G-quartet loops (Dapić et al., 2003). Soundararajan *et al*. (2008) proposed an anti-tumour cell mechanism of action for AS1411. Overexpression of cytoplasmic nucleolin in some tumour cells in contrast to their healthy counterparts is likely to play a significant role in this mechanism. Functionally, nuceolin acts as a post-transcriptional regulator by binding the 3' untranslated region within the *bcl-2* mRNA sequence, and in doing so preventing its degradation. This protective mechanism prevents some tumour cells from undergoing apoptosis. By competitively binding to nucleolin, AS1411 effectively inhibits *bcl-2* protection and induces apoptosis in some tumour cells (Soundararajan et al., 2009).

AS1411 has shown promising results with phase 1 clinical trials exhibiting no toxicity in human participants and is currently in undergoing phase 2 for the treatment of acute myeloid leukaemia (Aravind et al., 2012). Other aptamers currently in phase 2 of clinical trials include; REG1/RB006 (coagulation factor IXa inhibitor) (Ahrens et al., 2011), ARC1779 (targets A1 domain of von Willebrand factor) (Gilbert et al., 2007; Bae, 2012), and NU172 (thrombin inhibitor) (Zavyalova et al., 2013).

The commonalities observed between aptamer and antibody- target binding has earned aptamers the title of 'chemical antibodies'. For this reason, aptamers are increasingly being investigated for their applicability in research, diagnostic, therapeutic applications, in all areas where antibodies have traditionally dominated (Z. Luo et al., 2017; Santos do Carmo et al., 2017; Sabet et al., 2017). The most compelling advantage for the use of aptamers is their highly stable nature. Antibodies being proteins are susceptible to irreversible denaturation with elevated

temperatures, leading to loss of tertiary structure. In contrast, oligonucleotide aptamers can be heat denatured, stored under harsh buffer conditions, and are capable of recovering their conformation by re-annealing (Song et al., 2012).

Aptamers have been found to bind to their targets with similar binding affinities to antibodies, with dissociation constants (K_d) in the nanomolar to picomolar range (Meng et al., 2010). Moreover, due to their small size (5 - 25kDa), aptamers have the added advantage of increased tissue penetration and the ability to access epitopes on targets otherwise inaccessible by larger antibodies (150kDa) (Simmons et al., 2012). The small molecular size of aptamers enhances their clearance rate from the blood. The plasma clearance rates can be further fine-tuned by conjugation of chemical moieties such as polyethylene glycol that bulk up the size of the aptamer, thus increasing plasma half-life (Tucker et al., 1999).

Nucleic acid aptamers also possess low immunogenic potential, as the immune system generally does not raise an immune response against nucleic acids. This allows aptamer drugs to be delivered at higher doses with little immunogenic resistance. Pre-clinical studies using pegaptanib sodium in rhesus monkeys presented no immunogenicity or toxicity (Drolet et al., 2000). Similar findings were also observed with early phase I clinical trials, where administered doses were 100-fold higher than those clinically relevant (Eyetech Study Group, 2002). In support of this, a recent study characterising the pharmacological properties of two angiotensin II binding aptamers has shown that immunisation using both aptamers did not induce a humoral immune response within BALB/c mice (Heiat et al., 2016). The selection and production of aptamers is carried out using chemical synthesis approaches *in vitro*, thus demonstrating a relatively cost effective and standardised means of production (Burmeister et al., 2006).

There is however one major limitation for the use of nucleotide-based aptamers as therapeutic targeting molecules *in vivo*. Nucleotides once injected into the circulation are rapidly degraded by serum and intracellular nucleases via catalysis of hydrolysis reactions (Kanwar et al., 2011). DNA-based aptamers are generally regarded as being more nuclease stable than their RNA counterparts. The presence of a 2' hydroxyl group within the ribose sugar backbone of RNA aptamers

makes them more susceptible to nuclease degradation (X. Yang et al., 2002). However, the existence of this 2' hydroxyl group offers RNA based aptamer libraries the added advantage of greater structural sequence diversity when compared to ssDNA libraries. This is due to non-Watson-Crick base pairing and to the generation of more complex tertiary structures (Dua et al., 2011). Generally pyrimidine nucleotide bases are modified to confer endonuclease stability through 2' incorporations of fluorine, amino groups (NH_2) or of iodide, bromide, chloride to the 5' end (Kanwar et al., 2011).

Several other approaches have been utilised in order to achieve nuclease stability. One of these approaches utilises synthetic nucleic acid analogues (e.g. locked nucleic acids) that are designed with nuclease-resistant sugar backbones (Lin Wang et al., 2005). However, the use of such analogues is not without limitations. Synthesis of pre-selected aptamers using nucleotide analogues can alter the binding capability of the aptamer, leading to self-aggregation and non-specific binding. Moreover, synthetic analogues often exhibit some toxicity when administered *in vivo* (Braasch and Corey, 2001). More recently studies have also highlighted that the conjugation of aptamers to gold nanoparticles provides some stability against nuclease degradation (Chung et al., 2013).

1.11.1. Aptamers targeting TfR

Several studies have highlighted the selection and rationale design of RNA and DNA aptamers towards TfR (C.-H. B. Chen et al., 2008; Macdonald, Houghton, et al., 2016; Macdonald, Henri, et al., 2016). Chen *et al.* (2008) were first to demonstrate the concept of TfR targeted delivery using selected aptamers conjugated to proteins. The group set out to identify both RNA and DNA aptamers towards mouse TfR for the purpose of enzyme replacement therapy, through the delivery of a lysosomal enzyme conjugated to a mTfR specific aptamer, which in turn allows for cellular uptake via receptor mediated endocytosis. The study highlighted the selection of two mouse TfR specific aptamers, an RNA aptamer (FB4) and a DNA aptamer (GS24). Both aptamers demonstrated TfR mediated endocytic transport within Ltk^- mouse fibroblast cells as determined by confocal microscopy. The GS24 DNA aptamer was also coupled to a lysosomal enzyme (α-L-iduronidase)

and was shown to correct glycosaminoglycan metabolism within IDua $^{-/-}$ cells. The group concluded that there was no evidence of these aptamers being involved in receptor mediated transcytosis and a cell selection approach may be required to identify aptamers that are capable of undergoing transcytosis.

Porciani *et al.* (2014) later investigated how the loop structures within GS24 relate to target TfR binding. Through the use of chromatographic based folding conformational analysis, the group identified two distinct structural folds (termed A-1F and A2-F). Incubating each isolated fold with mTfR and quantifying binding through a fluorescence anisotropy assay, the group showed that only one of the two folds, A-2F, was responsible for mTfR specific binding. Moreover, the binding observed using the individual A-2F fold demonstrated a greater affinity towards mTfR than the parental GS24 molecule, thus indicating that the presence of a secondary inactive fold limits the efficient binding of the aptamer towards target mTfR.

More recently, another rationale design study by Macdonald *et al.* (2016) outlined the generation a 14-mer truncated variant of the 64 nucleotide GS24 parent aptamer sequence. Through mutational studies of the binding region, the group generated 4 variants of this aptamer that demonstrated bEnd.3 cell binding at affinities ranging from 2.25 μM to 487.3 nM. The group characterised the functional ability of these aptamers to internalise within bEnd.3, and a human control cell line, (MOLT4), to assess any changes in target specificity. Varying levels of uptake were observed with the four mutant variants. Interestingly, the group found that highest degree of internalisation was observed with TfRA4 with a quantitated affinity towards the cells of 487.3 nM. However, no binding could be seen with the MOLT4 cell line, indicating that the epitope which these aptamer variants target is only present on mTfR.

Having demonstrated successful uptake of the mutant aptamers, Macdonald *et al*. (2016) generated several bi-functional aptamer conjugates, by coupling the truncated 14 nucleotide mTFR specific aptamer to 17 nucleotide truncated variants of SYL3C, an epithelial cell adhesion molecule (EpCAM) specific aptamer. EpCAM is a membrane glycoprotein overexpressed on brain metastasising cancer cells. Through the conjugation of the mTfR binding aptamer and variants of the EpCAM

aptamers, the group aimed to develop a dual targeting aptamer molecule, that undergoes transcytosis across the BBB and further targets the subset of cancer cells within the CNS. It was proposed that this would reduce widespread neurotoxicity caused through non-specific cellular uptake within the CNS, thus increasing the overall safety of the therapeutic conjugate. The bi-functional aptamers were found to maintain target bEnd.3 internalisation and were shown to transcytose across the BBB in mouse *in vivo* studies. One limitation to both the studies performed by Macdonald *et al.* (2016; 2016) was that the binding affinity of the identified aptamers was only determined towards cells and not recombinant protein. With cells typically expressing variable levels of receptor targets under different conditions, these binding affinities may or may not be entirely representative of the true affinity towards the target protein.

Wilner *et al.* (2012) have also previously highlighted the selection of a hTfR binding RNA aptamer which was found to bind competitively and with a similar affinity to transferrin. The group utilised a combinational recombinant protein and cell SELEX procedure in order to generate functionalised aptamers that bound under physiological conditions. Following just five rounds of SELEX, the group screened 13 clones and found three clones to bind robustly to Jurkat cells, known to overexpress TfR. One of these three clones, the c2 clone, was minimised to optimise binding affinity. Whilst the group had highlighted the potential for targeting the BBB, assessment of binding of the selected hTfR specific aptamer was not carried out on BCEC. Furthermore, the c2 clone aptamer was selected towards recombinant hTfR generated within the Sf9 insect cell line. This would suggest that post-translational glycosylation of the TfR protein used for selections would vary significantly from the glycosylation patterns found within mammalian cells. Although the described methods resulted in aptamers that functionally bound mammalian cell lines expressing hTfR, it is not an optimal selection approach. Some aptamers pre-identified through screening against TfR expressed in insect cells may not bind to mammalian TfR during cell screening.

Recently, Rhode *et al*. (2016) utilised the transferrin receptor RNA aptamer developed by Wilner *et al*. (2016) to deliver conjugated microRNA-126 and

demonstrated biological activity within human umbilical cord-derived venous endothelial cells (HUVEC) and murine endothelial cells (MEC).

1.12. *In vitro* enrichment selection techniques for the identification of target binding biologics

Combinatorial *in vitro* selection techniques provide a powerful and an efficient means of identifying specific molecular recognition domains towards a wide range of targets, from small molecules, proteins and cells to tissues and whole organisms (K. A. Noren and C. J. Noren, 2001; Stoltenburg et al., 2005) Target interacting molecules are isolated from large combinatorial libraries of random molecules with a theoretical diversity of up to 10^{16} unique species (Jijakli et al., 2016). Through iterative cycles of selection, amplification and purification, the selected pools become enriched with species that preferentially bind towards the target. These selections are usually performed with the target protein immobilised to an affinity matrix in order to allow effective separation of the unbound affinity domains from those that have bound to the target (Murphy et al., 2003).

Functional selections can also be performed towards live adherent cell cultures or in cell suspension. Furthermore, cell selections using iterative target positive and non-target expressing cells can be carried out in order to select domains that preferentially recognise certain cell types (Ohuchi, 2012). An advantage to this kind of *in vitro* selection procedure is that no prior knowledge of the target is required for target-site specific recognition.

1.12.1. Phage display

The most established *in vitro* affinity screening technique is phage display. This method was developed by Smith *et al*. (1985) and relies on bioengineering approaches to exploit the link between genotype and phenotype (Carmen and Jermutus, 2002). Principally, a foreign gene encoding a protein or peptide of interest is inserted into the genome of a bacteriophage, a virus capable of infecting bacteria. The inserted gene is fused with a coat protein encoding gene of the phage virion, and the resultant chimeric protein or peptide is then expressed and displayed by the

phage on its surface. The most commonly used bacteriophage for phage display is the M13 filamentous phage (G. P. Smith, 1985). Unlike lytic phages, filamentous phages do not result in cell lysis of the infected host cell and therefore can continue to replicate and be released from the cell as it grows and divides (G. P. Smith, 1988). The genome of M13 bacteriophage incorporates a total of 11 genes, five of which encode phage coat proteins. All of these five coat proteins have been exploited for phage display, but the gene-3 minor coat protein (g3p) remains the most popular fusion partner, due to the possibly of fusing larger proteins (Carmen and Jermutus, 2002).

The use of larger proteins or peptides in fusion with g3p has one major limitation, it hinders efficient infection of *E.coli* host cells (Holliger and Riechmann, 1997). G3p is responsible for the interaction of the phage with *E.coli* containing the F-pilus and thus the functioning of g3p is required for host cell infection (Omidfar and Daneshpour, 2015). In order to resolve this issue phagemid vectors were developed (Qi et al., 2012). These vectors are derived from filamentous phage vectors and typically contain the encoding material for replication origin of a plasmid, the phage coat protein and an antibiotic resistance marker. Whilst the phagmid DNA can be infected into a host cell via phage, it is not sufficient to allow the replication of phage particles following infection. Superinfection with a helper phage such as M13KO7 provides all the remaining genomic information required for replication to occur within the host cell (Carmen and Jermutus, 2002).

Library construction is an important aspect of phage display, since the diversity and quality of a library can alter the outcome of phage display selections. Phage display libraries typically range in diversity, demonstrating 10^9 - 10^{12} theoretically variable sequences (Omidfar and Daneshpour, 2015). Many functional proteins and peptides may be displayed as fusions to g3p. The simplest form of library construction involves the use of random oligonucleotides inserted into the phage genome as a fusion to g3p. These random oligonucleotides are phenotypically represented as randomised linear peptides. Alternatively, through the inclusion of two cysteine residues surrounding a random region, it is possible to generate cyclic peptides via the formation of a disulphide link. Additionally, antibody

libraries can be generated through the use of randomised cDNA sourced from immunoglobulin genes (Variable heavy and Variable light chains from immunised or native donors) (Pope et al., 1996; Goodchild et al., 2011).

The selection of phage particle towards a target is often referred to as biopanning and is outlined in Figure 1.12.1.

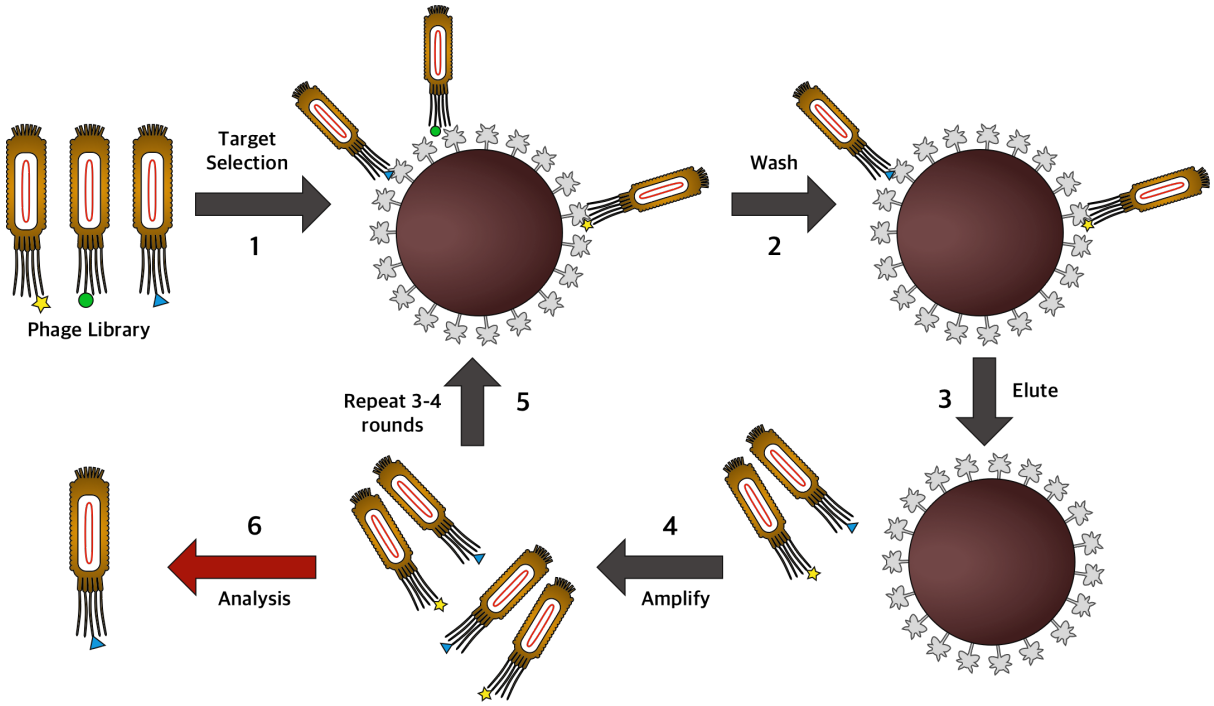

Figure 1.12.1: Schematic representation of soluble phage display selection.

A phage library is incubated with recombinant protein immobilised on an affinity matrix, (1). The unbound phage is removed through washing steps, (2) and the bound phage is eluted and amplified by infection of *E.coli,* (3). Amplified phage is purified and utilised in subsequent rounds of selection, (4). Following 3 – 4 rounds of selection, phage particles that preferentially bind towards the target are enriched, (5). DNA from enriched phage is amplified and sequenced to determine the nucleotide and amino acid sequences of binding domains.

Firstly, target antigen is immobilised onto a solid surface, via adsorption or affinity capture (e.g. streptavidin-biotin interaction) (Bakhshinejad and Sadeghizadeh, 2016). Subsequently, the phage library is incubated with the target, after which stringent washing steps are employed to remove non-binding and weakly binding phage. Phage is subsequently eluted from the target and used to infect *E.coli* for amplification. The amplified phage is purified and used in subsequent rounds of

selection towards the target. Phage particles are typically enriched to the target following 3 - 4 iterative selection rounds (Dai et al., 2014; J. Li et al., 2011).

1.12.2.Systematic evolution of ligands by exponential enrichment (SELEX)

SELEX is utilised to isolate aptamers enriched to specifically bind a given target from vast combinatorial oligonucleotide libraries (Ellington and Szostak, 1990). The general procedure consists of three steps, which are repeated cyclically to narrow down onto specifically binding oligonucleotides with the highest affinity towards the target. The number of rounds required for enrichment is dependent on the selection stringency and type of SELEX used, but typically ranges between 5 – 20 rounds. The generalised procedure of SELEX is outlined in Figure 1.12.2.

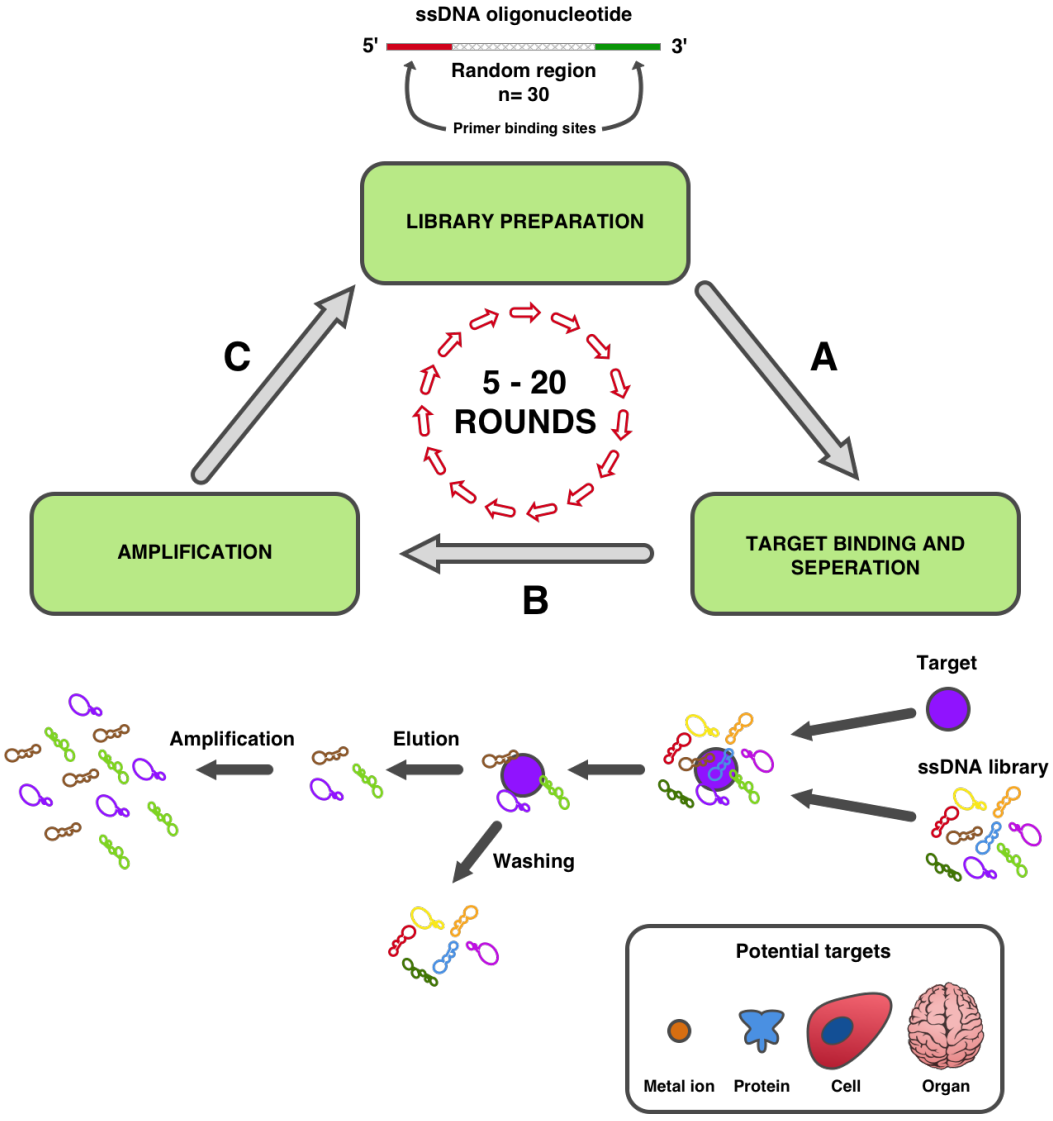

Figure 1.12.2: Schematic representation of typical aptamer SELEX procedure.

Figure outlining the typical aptamer selection cycle. **A.** A chemically synthesised library consisting of approximately 10^{15} theoretical sequences is incubated with target. **B.** The unbound sequences are removed through washing and the bound sequences are eluted. **C.** The eluted pool is amplified via PCR to generate an enriched pool for the subsequent round of aptamer selection.

Starting material for aptamer SELEX is a chemically synthesised ssDNA or RNA library, theoretically consisting of approximately 10^{13} - 10^{15} varying sequences (Song et al., 2012). Each sequence consists of a central degenerate nucleotide region of a selected length (generally 30-50 nucleotides). This random region is flanked by adjacent primer binding sites, which facilitate amplification of bound sequences. The library is incubated with the target and subsequently partitioned from unbound sequences. Bound sequences are then eluted and amplified by PCR in order to enrich the pool with target binding sequences. Amplified double-stranded DNA is purified by eluting the template strand from the complementary strand and this is utilised in the subsequent round of selection in order to further enrich those sequences that bind with highest affinities to the target.

Various methods and techniques have been developed and outlined in the literature for the selection of aptamers (Darmostuk et al., 2015). Stoltenburg *et al*. (2005) outlined a variation of the typical SELEX procedure termed fluorescence-monitored *in vitro* selection (FluMag). It involved the use of target immobilised to streptavidin-coated magnetic beads and the use of biotin and fluorescein isothiocyanate (FITC)-labelled primers for affinity immobilisation and detection, respectively. Another form of SELEX, Cell SELEX, allows selections to be performed on targets in their native conformations (Sefah et al., 2010). Furthermore, performing selections against recombinant protein targets accelerates the selection process by increasing the selection scrutiny to the specific target. It is therefore advantageous to carry out selections using a combination of both recombinant protein and cell SELEX techniques, as this generates high affinity aptamers that bind specifically to a functionalised target (Wilner et al., 2012).

More recently, a study by Cheng *et al*. (2013) highlighted the selection of brain penetrating aptamers via *in vivo* methods. The group injected a 2'-fluoro modified RNA aptamer library into the tail vein of C57BL/6 mice. The brain of these mice was harvested following 1 h circulation time and Dulbecco's phosphate

buffered saline (DPBS) infusion. RNA was extracted from the mouse brain, amplified, transcribed and purified before being utilised for another round of *in vivo* SELEX. A total of 22 rounds of selections were performed to isolate brain internalising aptamers. In contrast to *in vitro* methods this protocol required many more rounds in order to produce an enriched pool of aptamers. This was hypothesised to be due to two factors, the large random sequence of the RNA library (n= 40), and the vast complexity of targets available as baits using *in vivo* SELEX. Sub-localised binding of the selected aptamer (A15). The aptamer was observed to bind various regions of the brain including the cortex, cerebellum, hippocampus and striatum. However, this method results with aptamers without initial knowledge of the target.

1.13. Aims and Objectives

The overall aim of this project was to select and identify brain endothelial targeting non-antibody binding domains (cyclic peptides and ssDNA aptamers) via *in vitro* selection rounds of phage display and nucleic acid enrichment (SELEX) towards a suitable RMT functioning receptor candidate at the BBB, in this case TfR. Subsequently, selected and identified domains were screened and characterised for binding towards recombinant TfR and immortalised *in vitro* BCEC lines (hCMEC/D3 and bEnd.3 cells).

More specifically the study set out to:

1. Characterise cell surface receptor candidates that function via RMT at the BBB for use as exploitable delivery strategies across BCEC.
    a. Characterise endogenous surface receptor candidate expression in the hCMEC/D3 and CHO variant cell lines (CHO-TRVb).
    b. Evaluate endogenous expression of receptor candidates with long-term culture (cell passage), in order to determine optimal conditions for cell characterisation of identified domains.
2. Characterise the CHO-TRVb and -TRVb1 cell lines for hTfR expression and assess their suitability for use as hTfR positive and negative targets with *in vitro* cell selections.

3. Select and identify TfR species cross-reactive cyclic peptides.
    a. Conduct phage display selections to identify TfR binding and BCEC internalising cyclic peptides.
    b. Screen cyclic peptide domains for binding towards recombinant mouse, human and rat TfR by means of phage ELISA and elucidate the sequence homology of positively binding peptide clones.
4. Clone and express cyclic peptide lead candidates for characterisation.
    a. Clone out and express positive peptide clones as monovalent CPep-g3p-D1 fusion domains for lead identification and characterise these towards recombinant mTfR, hTfR and immortalised BCEC cells (bEnd.3 and hCMEC/D3).
    b. Express lead peptides as bivalent Fc-fusion domains coupled to a therapeutic payload, for characterising the cell delivery capability of the lead peptides.
5. Select and identify hTfR binding ssDNA aptamers
    a. Establish a protocol for aptamer SELEX utilising polyhistidine tagged recombinant protein immobilised on Ni-NTA magnetic agarose beads.
    b. Select ssDNA aptamers via rounds nucleic acid enrichment (SELEX) towards hTfR and CHO-TRVb1 cells (over-expressing hTfR).
    c. Carry out next generation sequencing of selected aptamer pools, analyse NGS data for overall enrichment with selection progression and identify potential lead aptamer candidates that have been highly enriched throughout the selection.

Chapter 2: Characterisation of candidate receptor targets that function via RMT at the BBB.

2.1. Introduction

Endogenous transport receptors expressed on the luminal surface of BCEC allow the movement of nutrients, proteins and other molecules across the BBB into the CNS for vital metabolic activities within the brain (Serlin et al., 2015; Abbott et al., 2010). These transport receptors have been proposed as exploitable targets for the delivery of therapeutic cargo across the BBB into the CNS (Georgieva et al., 2014). The expression of many of these transporters has been extensively explored both within *in vitro* models of the BBB (Carl et al., 2010; Ohtsuki et al., 2013) and *in vivo* (Cornford and Hyman, 2005). The most notable target mechanism for the purpose of exploitation is receptor mediated transcytosis (RMT) (Raub and Newton, 1991). Normally, RMT involves the binding of a ligand to its specific receptor, resulting in an endocytic event which leads to cellular internalisation of the receptor and its bound ligand. Consequently, the complex is trafficked through the cell to the abluminal membrane, where it is released and made available within the CNS (Bickel et al., 1994). By targeting an epitope on the transporter that does not interfere with ligand binding or internalisation, it is possible to 'hitch-hike' therapeutic molecules alongside the target transporter into the CNS. This mechanism is referred to as molecular 'Trojan horse' delivery and has been utilised in the past to deliver biologics such as monoclonal antibodies across the BBB (reviewed in Lajoie and Shusta, 2015).

The ideal candidate target receptor for exploitation would have the following characteristics. Firstly, the receptor should be specifically expressed by BCEC on both the luminal and abluminal membranes. It must also have a high blood to brain translocation capacity, to allow efficient delivery of neuro-therapeutic agents from the circulation. The cellular internalisation mechanism must also favour transcytosis by avoiding the lysosomal degradation compartment. Presently, there are no known receptors that meet all these criteria. Most BBB drug delivery efforts have focused on the exploitation of ubiquitously expressed receptors such as transferrin receptor and insulin receptor

(Yu et al., 2014; Niewoehner et al., 2014; Boado, Zhou, et al., 2010; Ulbrich et al., 2009; Huang et al., 2007; Lee et al., 2000; Pardridge et al., 1995; Coloma et al., 2000; Pardridge et al., 1991; Kuo and Shih-Huang, 2013).

Although some of these receptors are ubiquitously expressed, their expression is higher within BCEC than other cells, making them good candidates for delivery. Unfortunately, the ubiquitous nature of these receptors has also raised safety concerns regarding the off target side effects of their use (Ohshima-Hosoyama et al., 2012; Couch et al., 2013).

Although many *in vitro* and *in vivo* studies utilising monoclonal antibody delivery vectors have been successful in demonstrating transcytosis across BCEC, the rate of delivery is often poor. This amounts to a steady-state concentration of approximately 0.1% of circulating antibody being bio-available within the brain, thus resulting in a weak therapeutic concentration which does not usually elicit a pharmacologically relevant response (Niewoehner et al., 2014).

In recent years, alternative non-antibody biologics such as aptamers (Mattice and DeRosa, 2015), engineered antibody fragments (reviewed in Roque et al., 2004), peptides (Uhlig et al., 2014), fusion proteins (Czajkowsky et al., 2012), and non-antibody scaffolds (Skerra, 2007; Vazquez-Lombardi et al., 2015) have grown in popularity as novel targeting and therapeutic reagents. We hypothesise that the use of small non-antibody domains may prove advantageous alternatives to monoclonal antibodies in the context of delivering therapeutic cargo across the BBB.

Prior to commencing *in vitro* selections of non-antibody delivery domains, it was necessary to establish a target cell surface receptor protein that is highly expressed in brain endothelial cells and functions in the translocation of its natural ligand into the CNS via RMT. Three receptor candidates were selected for characterisation, these were; transferrin receptor (TfR), low-density lipoprotein receptor (LDLR) and low-density lipoprotein receptor-related protein 1 (LRP1). The primary aim of this chapter is to characterise the expression of these receptors on the human immortalised microvascular endothelial cell line, hCMEC/D3. The

characterisations were carried out to address three preliminary questions, these were as follows:

1. Are all three candidate receptors expressed on the surface of hCMEC/D3 cells?
2. Does the expression of the candidate receptors differ with long-term cell culture?
3. Which cell surface receptor would be the most suitable candidate to exploit for the purpose of molecular 'Trojan horse' delivery of therapeutic cargo across the BBB into the CNS?

Further to this main objective, it was also necessary to characterise two Chinese hamster ovary (CHO) transcript variant cell lines, CHO-TRVb (a hamster TfR deficient cell line) and CHO-TRVb-1 (the hTfR transfected form of the deficient cell line). These TfR variant cells were initially developed to allow the study of hTfR transfected CHO cells, without the interfering effects of endogenous Chinese hamster TfR (McGraw et al., 1987). We hypothesise that the CHO-TRVb cell lines could be valuable tools for accomplishing functional positive and negative cell selections towards TfR.

2.2. Materials and Methods

2.2.1. Pre-coating culture flasks and plates with collagen type I

Type I collagen 20x stock solution (1 mg/ml) (Sigma-Aldrich, Dorset, UK) was aliquoted into 1.5 ml Eppendorf tubes to reduce risk of contamination, and stored at 4 °C. Before use, the collagen was diluted to a working concentration 50 μg/ml in Hank's balanced salt solution (HBSS) with Ca^{2+} and Mg^{2+} (Sigma-Aldrich, Dorset, UK) and culture vessels were coated for 1 h at room temperature. Prior to cell seeding, the collagen was aspirated and the flasks were washed with HBSS (with Ca^{2+} and Mg^{2+}).

2.2.2. Cell culture of the hCMEC/D3 cell line

Growth media for the hCMEC/D3 cell line was made up using the following components and volumes outlined in Table 2.2.1. Prior to media preparation, culture media supplements were thawed at room temperature and foetal bovine serum (FBS) was thawed at 37 °C. Endothelial cell growth medium-2 (Lonza™, Basel, Switzerland) consists of Endothelial Basal Medium-2 (EBM-2) supplemented with 2.5% (v/v) FBS and growth factors to optimise growth.

Table 2.2.1: Preparing complete EGM-2 Growth medium.

Growth media component		**Volume (v/v)**
Media and Serum	Endothelial Basal Medium-2 (EBM-2) - (Lonza™)	97.11%
	Foetal bovine serum (FBS)	2.5%
Supplements	Human endothelial growth factor (hEGF)	0.025%
	Vascular endothelial growth factor (VEGF)	0.025%
	Human fibroblast growth factor (hFGF)	0.1%
	Gentamycin	0.1%
	Ascorbic acid	0.1%
	Hydrocortisone	0.4%

The supplemented media was inverted to mix and aliquoted into 50 ml falcon tubes when required to reduce risk of contamination and stored at 4 °C.

2.2.2.1. Thawing cells from cryostorage and initial culture

hCMEC/D3 cells were removed from cryostorage and thawed in a 37 °C water bath with gentle agitation. Cells were seeded into collagen pre-coated culture flasks containing pre-warmed EBM-2 culture media at a density of 40,000 cells/cm^2 and subsequently transferred to a humidified incubator set at 37 °C, 5% CO_2. Cell culture media was changed every two days until the cells were confluent. Cells were considered confluent when a contact inhibited monolayer was observed exhibiting phenotypic maturity; this took approximately 3-4 days. hCMEC/D3 cells were used between cell passages 23 – 35.

2.2.2.2. Sub-culture of adherent hCMEC/D3 cells

EBM-2 media, trypsin-ethylenediaminetetraacetic acid (EDTA) (Invitrogen, Paisley, UK), HBSS (without Ca^{2+} and Mg^{2+}) and FBS were pre-warmed in a water bath at 37 °C. Sub-culture of cells was performed by aspirating culture media from the culture flask, and washing cells with HBSS (without Ca^{2+} and Mg^{2+}). This wash step removes any traces of calcium and magnesium that would otherwise inhibit the action of trypsin.

Subsequently, enough trypsin-EDTA was added to cover the cell monolayer and the culture flask was placed in an incubator at 37°C for 2 min. Once cells had detached, the action of trypsin was inhibited by addition of 10% FBS in EBM-2 culture media to the culture flasks. The complete contents of the culture flask were then transferred to a 50 ml falcon tube and 10 µl of cell suspension was extracted for cell counting using a haemocytometer at 100x magnification.

Cells were centrifuged at 300 g for 5 min, the supernatant was discarded and the cell pellet was re-suspended in the appropriate volume of culture media. A volume equivalent to the seeding density of cells was then added to a collagen pre-coated culture flask containing pre-warmed EBM-2 culture medium and the flask was placed in a humidified incubator at 37°C, 5% CO_2.

Following sub-culture, remaining cells were prepared for cryostorage by addition of 10% (v/v) dimethyl sulfoxide (DMSO) (Sigma-Aldrich, Dorset, UK). Volumes equivalent to 1 million cells were then aliquoted into pre-labelled cryotubes. The cryotubes were frozen at a rate of -1°C per minute to -80°C before being transferred to liquid nitrogen for long-term storage.

2.2.3. Cell culture of CHO cell lines (TRVb and TRVb-1)

CHO-Transferrin Receptor Variant clone b cell lines, TRVb (endogenous TfR deficient) and CHO-TRVb-1 (human TfR stable transfection in TRVb cells) were kindly provided by Prof. Tim McGraw (Cornell University, New York).

The CHO-TRVb cell line was maintained in Ham's F12 nutrient mix + GlutaMAX media (Invitrogen, Paisley, UK) supplemented with 5% FBS and 100 U/ml penicillin and 100 µg/ml streptomycin. The human TFR expressing form of the deficient cell line, CHO-TRVb-1 was maintained in similar media to TRVb cells with the addition of 500 µg/ml Geneticin to prevent growth of non-transfected cells. Both cell lines were grown in a humidified incubator at 37°C, 5% CO_2. Growth media for each of the CHO cell lines was prepared as outlined in Table 2.2.2.

Table 2.2.2: CHO-TRVb and TRVb-1 cell culture media.

		TRVb (TfR deficient)	TRVb-1 (hTfR transfected)
Growth media component		**Percentage volume (v/v)**	
Media and Serum	Ham's F12 Nutrient mix + GlutaMAX (Invitrogen, Paisley, UK)	93%	92%
	Foetal bovine serum (Sigma-Aldrich, Dorset, UK)	5%	5%
Supplements	Penicillin/ streptomycin (Invitrogen, Paisley, UK)	2%	2%
	Geneticin solution (50 mg/ml) (Sigma-Aldrich, Dorset, UK)	-	1%

2.2.4. Assessment of cell-surface protein expression using Flow cytometry

Cell-surface receptor expression of the hCMEC/D3 and CHO-TRVb (CHO-TRVb and CHO-TRVb1) cell lines was assayed using flow cytometry. Mouse primary antibodies were chosen according to the criteria that they bind an epitope within the extracellular domain of each of the protein receptor candidates and are validated for the application of flow cytometry. These primary antibodies were subsequently indirectly labelled with a FITC conjugated sheep anti-mouse polyclonal IgG secondary antibody (Sigma-Aldrich, Dorset, UK). The antibodies selected are outlined in Table 2.2.3.

Table 2.2.3: Receptor protein specific antibodies utilised in FACS analysis.

Antigen	Description	Supplier	Catalogue No.	Working dilution
Human TfR	Mouse monoclonal IgG_1, Clone #29806	R&D Systems, Oxon, UK	MAB2474	1 mg/ml
Human LDLR	Mouse monoclonal IgG_1, Clone #472413	R&D Systems, Oxon, UK	MAB2148	1 mg/ml
Human LRP1α chain	Mouse monoclonal IgG_1	Invitrogen, Paisley, UK	37-3800	1 mg/ml
Isotype control antibody	Mouse IgG_1	Invitrogen, Paisley, UK	MG100	1mg/ml
Mouse IgG	Polyclonal sheep IgG_1 FITC conjugated	Sigma-Aldrich, Dorset, UK	F6257	1:50 (v/v)

Cells were cultured to confluence then harvested using the relevant cell detachment media, trypsin/ EDTA or accutase solution, for 2 min and 4 min, respectively. Cells were washed in HBSS and re-suspended at a concentration of 1 x 10^6 cells/ml in the relevant cell culture media.

All subsequent protocol stages were carried out on ice. 1.5 x 10^6 cells were isolated and washed in 9 ml of HBSS. This was carried out by centrifugation at 300 g for 5 min then discarding the supernatant. The wash step was then repeated using 9

ml of 1x phosphate buffered saline (PBS) to ensure removal of free protein that may bind primary antibody.

Cells were subsequently fixed for 30 min at room temperature in 1 ml of 2% paraformaldehyde solution made up in PBS. Fixed cells were then diluted in 9 ml of PBS and washed twice, before being re-suspended in antibody diluent solution consisting of 1 mg/ml bovine serum albumin (BSA) in PBS.

Following a cell count, 3 x 10^5 cells were aliquoted into relevantly labelled Eppendorf tubes. 2 μg of primary antibody was added to each sample tube. A negative control was prepared by inclusion of a primary isotype-matched irrelevant control antibody (Invitrogen, Paisley, UK).

Cells were incubated with primary antibody overnight on a shaker at 4 °C. The following day cells were washed in 1 ml of PBS twice via centrifugation at 500 g for 5 min. Subsequently, cells were re-suspended in a secondary antibody diluent consisting of 1:100 polyclonal sheep anti-mouse IgG1 conjugated to FITC (Sigma-Aldrich, Dorset, UK) in PBS and 1 mg/ml BSA. Cells were incubated with secondary antibody for 2 h, at 4 ˚C on a shaker, followed by another two washing steps in PBS. After washing, cells were re-suspended in 300 μl of HBSS and transferred to labelled FACS tubes before being analysed for fluorescence using a FACSCalibur machine and CellQuest software (Becton Dickinson, UK). The median fluorescence intensity of 10,000 sampled cells within a defined cell gate was acquired at a FL1 voltage of 360 V.

Characterisation of candidate receptor targets that function via RMT at the BBB.

2.2.5. Western Blotting

Denaturing polyacrylamide gels and buffers were prepared as outlined in Table 2.2.4.

Table 2.2.4: Table showing recipes for polyacrylamide gels and western blotting buffers.

		Composition
Polyacrylamide gels	**Resolving gel**	33% Protogel (30% acrylamide, 0.8% methylene bisacrylamide) (National diagnostics, Hull, UK), 0.1% w/v SDS, 0.37M tris HCl pH 8.8, 0.03% v/v tetramethyl-ethlenediamine (TEMED) (Sigma-Aldrich, Dorset, UK) and 0.1% w/v ammonium persulphate (APS) (Sigma-Aldrich, Dorset, UK).
	Stacking gel	16.7% Protogel (30% acrylamide, 0.8% methylene bisacrylamide), 0.03% w/v SDS, 0.12M tris HCl, pH 6.8, 0.03% v/v TEMED and 0.03% w/v APS.
Buffers	**RIPA lysis Buffer**	25mM Tris-HCl (pH 7.6), 150mM NaCl, 1% NP40, 1% sodium deoxycholate, 0.1% SDS
	4x SDS-PAGE (Laemmli's) reducing buffer	250mM tris HCl, 8% sodium dodecyl sulphate (SDS), 0.01% bromophenol blue, 40% glycerol, 10% 2-mercaptoethanol.
	Gel running buffer	25mM Tris, 192mM glycine, 1% SDS
	Gel transfer buffer	25mM Tris, 192mM glycine, 20% ethanol.
	Membrane blocking buffer	0.2% tween 20 (Sigma-Aldrich, Dorset, UK) and 5% fat free dried milk suspended in 1x PBS.
	Membrane washing buffer (PBST)	0.2% tween 20 suspended in 1xPBS.

CHO-TRVb and TRVb-1 cells were cultured to confluence in 12 well plates, supplemented with their relevant culture media. Cell lysates were prepared by addition of 0.5 ml of cold HBSS ($+Ca^{2+}$) and detached from the culture plates using a cell scraper. Detached cells were washed by centrifugation at 300 g for 5 min and re-suspended in 100 μl of RIPA lysis buffer per 1 x 10^6 cells. The cells were then cooled on ice and subsequently stored at -80°C for 30 min whilst frequently agitating cells by gentle shaking. Cells were thawed on ice, centrifuged at 300 g for 5 min and the supernatant, containing the protein extract, was recovered. Following protein extraction, sample total protein concentration was determined using detergent-

compatible (DC) colorimetric assay kit (Biorad, Hertfordshire, UK). This was performed by preparation of a standard curve using varying concentrations of the 1.5 mg/ml BSA standard stock solution. Successively, 45 μl aliquots of each protein extract was then added to 15 μl of 4x Laemmli's buffer in clean eppendorf tubes.

This mixture was then heated to 95°C for 10 min in order to denature the proteins. Poly-acrylamide 8% (v/v) resolving gels were cast and allowed to set, prior to the addition of the 5% (v/v) stacking gel and comb. The gel was placed in an electrophoresis tank containing running buffer and each lane was loaded with 15 μl of sample alongside a multicolour high range protein ladder (26625, ThermoFisher Scientific, Paisley, UK). Samples were run at 100V through the stacking gel and 150V through the resolving gel, until the bromophenol blue dye was observed to run off the gel. Proteins within the resolving gel were subsequently transferred onto a HyBond nitrocellulose membrane (Amersham, Buckinghamshire, UK) using 0.15 Amp, overnight at 4°C.

Following transfer, the membrane was briefly stained for 1 min in Ponceau red solution (Sigma-Aldrich, Dorset, UK). Staining was carried out in order to determine if protein and molecular marker migration was uniform. After staining the membrane was rinsed in water, before a 1 h incubation step with blocking buffer at room temperature. Post blocking, the membrane was washed and incubated overnight at 4°C with primary mouse monoclonal anti-human TfR (MAB2474, R&D Systems, Oxon, UK) antibody diluted in blocking buffer (10 μg/ml).

The following day, membranes were rinsed for 10 min in PBST washing buffer on a shaker. This process was repeated 4 more times using PBST washing buffer. The membrane was incubated with 1:80,000 dilution of polyclonal rabbit anti-mouse IgG HRP conjugated secondary antibody (Cat No. A9044, Sigma-Aldrich, Dorset, UK) at room temperature for 1 h. Following secondary incubation, the membrane was washed again in PBST washing buffer for 10 min (5 times) and then in 1x PBS for 5 min.

The membrane was then carefully dried on filter paper, briefly developed for 1 min using ECL detection reagent (Amersham, Buckinghamshire, UK) and exposed to Hyperfilm (Amersham, Buckinghamshire, UK) for 1 min.

2.2.6. Immunocytochemistry CHO-TRVb cell line internalisation assays

Immunocytochemistry (ICC) was used to assess TfR mediated uptake of antibodies directed towards hTfR and mTfR. CHO-TRVb and CHO-TRVb-1 cells were maintained as outlined in section 2.2.3. Cells were sub-cultured into 96-well special optics flat clear bottom black polystyrene TC-treated microplates (Corning, High Wycombe, UK) at a seeding density of 1.5 x 10^4 per well. Cells were grown to confluence for 48 h, media was aspirated from the culture wells and cells were washed twice in PBS, prior to commencing internalisation assays.

Anti-hTfR (Confidential protein, contact George Thom, MedImmune, Cambridge, UK) and an engineered variant of anti-mTfR (8D3) antibody (MedImmune, Cambridge, UK) were diluted to a working concentration of 2 μg/ml in 1% BSA/ unsupplemented media. Confluent cells were incubated with primary antibody within a humidified incubator for 5 min in 1% BSA in PBS. Post-incubation, cells were washed three times for 5 min in 1% BSA in PBS, and permeablised using 0.25% Triton X-100 (Sigma-Aldrich, Dorset, UK). Secondary labelling of antibodies was carried out using 10 μg/ml polyclonal F(ab')2 goat anti-human IgG (Fc specific) Alexa 488 conjugate (Thermo-Fisher Scientific, Paisley, UK). Nuclei were labelled with hoechst at a dilution of 1:10,000, for 1 min at room temperature. Immunofluorescent imaging of labelled cells within 96-well plates was carried out using an ImageXpress Micro XLS system (Molecular probes, Wokingham, UK). Mean grey value readings were acquired using FIJI (ImageJ), normalised to the number of cells in each image (imageJ), and averaged from three independent images taken per experimental replicate (n= 3).

2.2.7. Statistical analysis

Statistical analysis was performed using Graphpad Prism 6 statistical software on FACS triplicate sample runs by initially subtracting the irrelevant IgG_1 isotype control median fluorescence reading. One-way analysis of variance (ANOVA) tests were carried out where applicable alongside Tukey's multiple comparison post hoc-test. A *P* value <0.05 was considered to be significant.

2.3. Results

2.3.1. Expression of candidate receptor targets by hCMEC/D3 cells.

The initial characterisation study of the hCMEC/D3 cell line was undertaken in order to establish a suitable endothelial cell surface receptor candidate, and determine its optimal binding conditions for subsequent use as a bait during non-antibody domain selections. This study consisted of three parts.

2.3.1.1. Cell surface expression of TfR, LDLR and LRP1 on hCMEC/D3 cells

Firstly, the study set out to assess the expression of candidate receptors on the cell surface of the hCMEC/D3 cell line, whilst simultaneously assessing the binding effectiveness of the selected primary antibodies, targeted towards the extracellular portion of these receptors.

Flow cytometric analysis of the three receptor targets; TfR, LDLR and LRP1, were carried out using three separate biological replicates on hCMEC/D3 cells paired alongside the primary antibody matched IgG_1 isotype control. Results were normalised to the relevant IgG1 isotype controls and expressed as average fluorescence intensities +/- SEM.

All three receptor candidates exhibited expression on the cell surface of hCMEC/D3 cells, Figure 2.3.1. TfR presented with higher average median fluorescence intensity readings than LDLR and LRP1. However, it is not possible to discern whether this is directly due to the expression of each receptor candidate on

the hCMEC/D3 cell surface or whether it is due to the varying affinities of the detection antibodies towards their target epitopes.

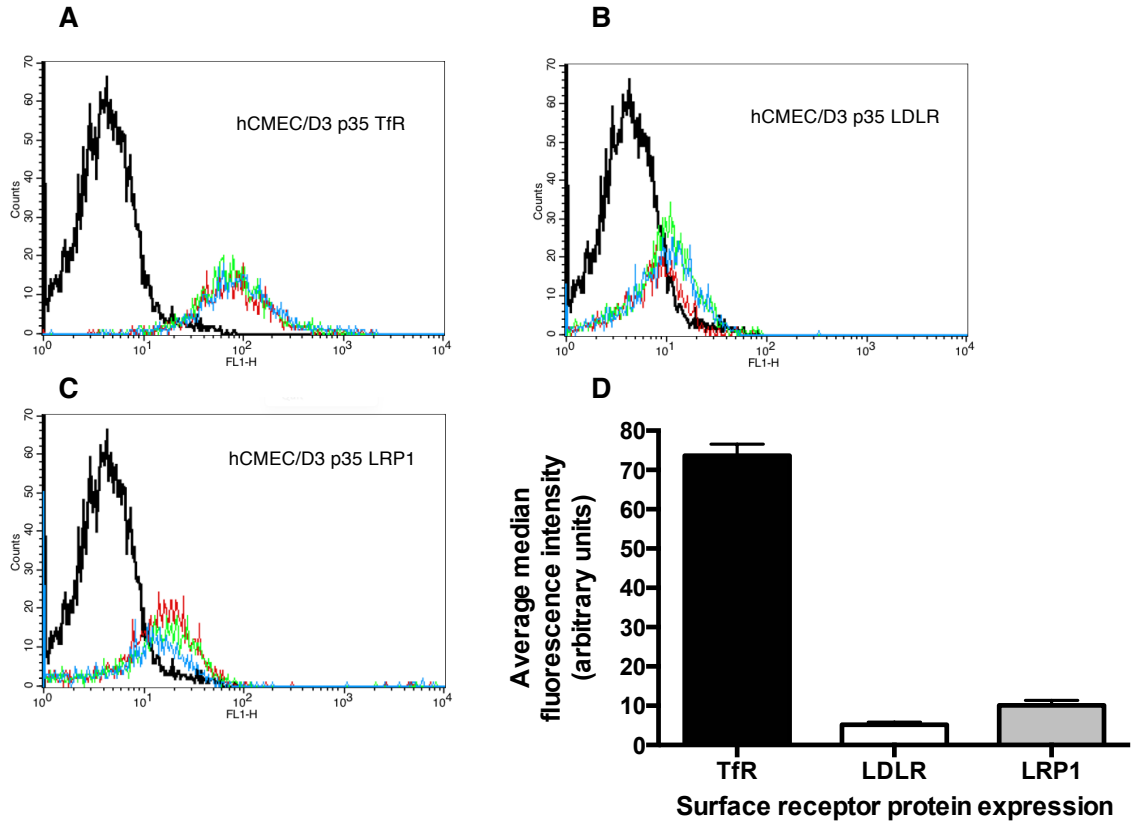

Figure 2.3.1: Facs detection of transport receptor proteins TfR, LDLR and LRP1 on hCMEC/D3 cells (p35)

FACS histogram overlay data showing expression of **(A)** TfR, **(B)** LDLR, and **(C)** LRP1 on the hCMEC/D3 cell line at (passage 35). Acquisition of FACS data was conducted on 10,000 gated events at an FL1 voltage of 360 V. Primary antibody matched (IgG_1) isotype control data is represented by a black line. Red, green and blue lines represent each of the three experimental replicates. **(D)** Summary of initial receptor candidate expression study on hCMEC/D3 cell line. Figure demonstrates expression of TfR, LDLR and LRP1 respectively. Median fluorescence intensity is presented as a mean ± SE of three experimental replicates (n= 3), with the average median fluorescence intensity of the relevant IgG_1 isotype control subtracted.

2.3.1.2. Expression of TfR, LDLR and LRP1 with long-term hCMEC/D3 culture

in vitro cultured cells de-differentiate with long-term culture, and inherently lose their desired phenotype through changes in gene and protein expression and cellular morphology (Schnabel et al., 2002). Therefore, it is essential to evaluate any variation in target receptor expression with increasing cell passage, in order to determine the optimal passage number when performing selections and binding assays.

Cultures of hCMEC/D3 cells at passages 25, 30 and 34 or 26, 29 and 36 were thawed from three independent batches of cells for each passage and grown to confluency under identical culture conditions, as described in section 2.2.2.2. Cells were detached using Trypsin/EDTA and assessed for cell surface receptor expression using FACS.

No significant changes in TfR expression were observed between passages 25, 30, and 34 ($P > 0.05$, n= 3). Fluorescence readings were relatively consistent throughout and remained high with increasing passage, as shown in 2.3.2, A and Figure 2.3.3, A.

LDLR expression was observed to significantly decrease by one third at passage 30 when compared to passage 25 ($P < 0.01$, n= 3) and this decrease was then maintained at passage 34, (2.3.2, B and Figure 2.3.3, B).

LRP1 exhibited a dramatic increase in expression with long-term culture (2.3.2, C and Figure 2.3.3, C). A statistically significant three-fold up-regulation in expression of LRP1 was observed with passage 36 in contrast to passage 26 ($P < 0.01$, n= 3). A significant two-fold increase was also observed with passage 36 over passage 29 ($P < 0.05$, n= 3). A greater degree of inter-variability between experimental replicates was observed for passage 29 (2.3.3, C).

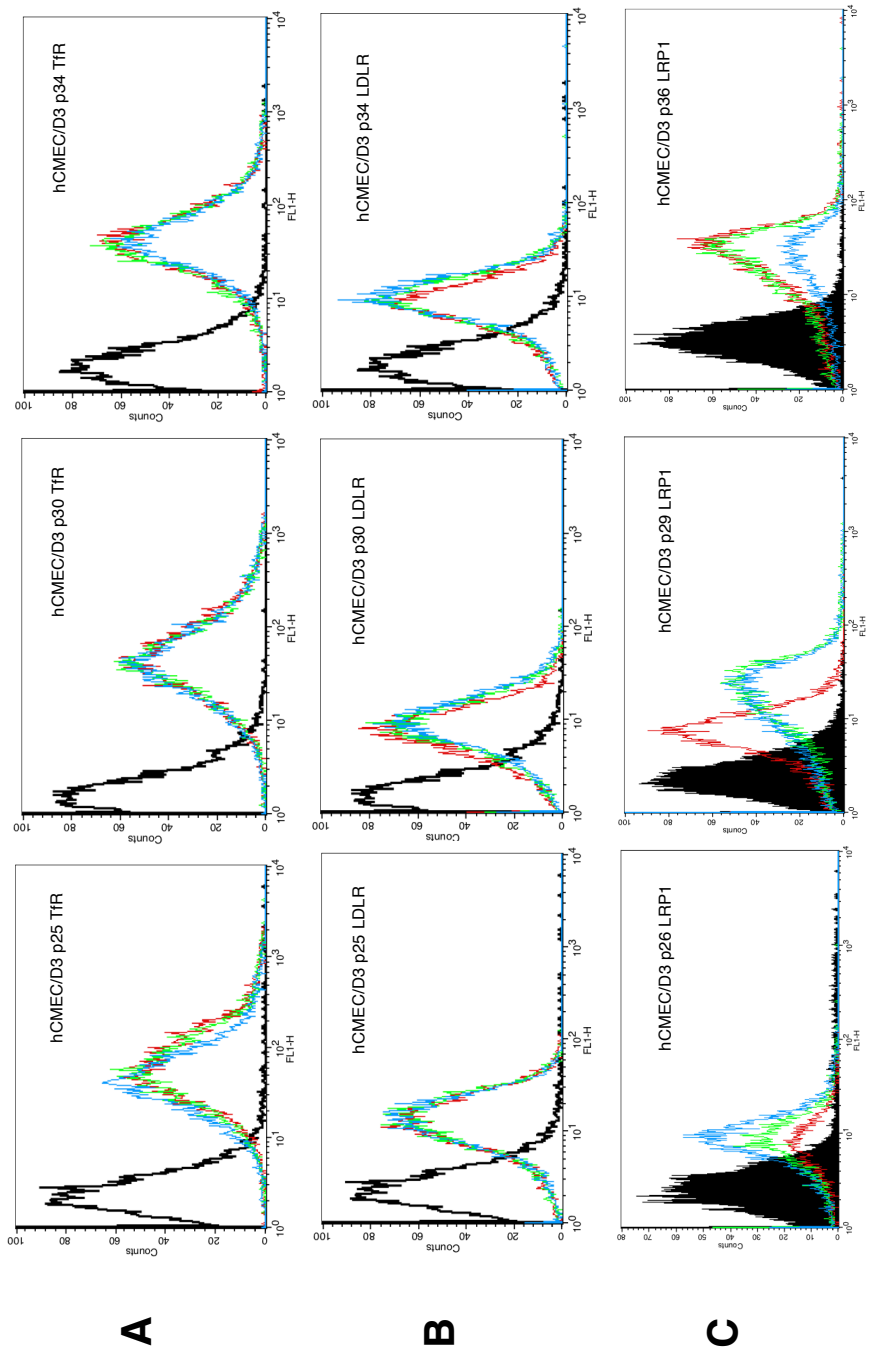

Figure 2.3.2: FACS detection of indirect antibody labelled, TfR, LDLR and LRP1 with long-term culture on the cell surface of hCMEC/D3 cells.

FACS histogram overlay data showing expression of **(A)** TfR (passages 25, 30, and 34), **(B)** LDLR (passages 25, 30, and 34), and **(C)** LRP1 (passages 26, 29, and 36) on the hCMEC/D3 cell line with increasing cell passage. FACS data was acquired on 10,000 gated events at an FL1 voltage of 360 V. Primary antibody matched (IgG_1) isotype control data is represented by a black line. Red, green and blue lines represent each of the experimental replicates.

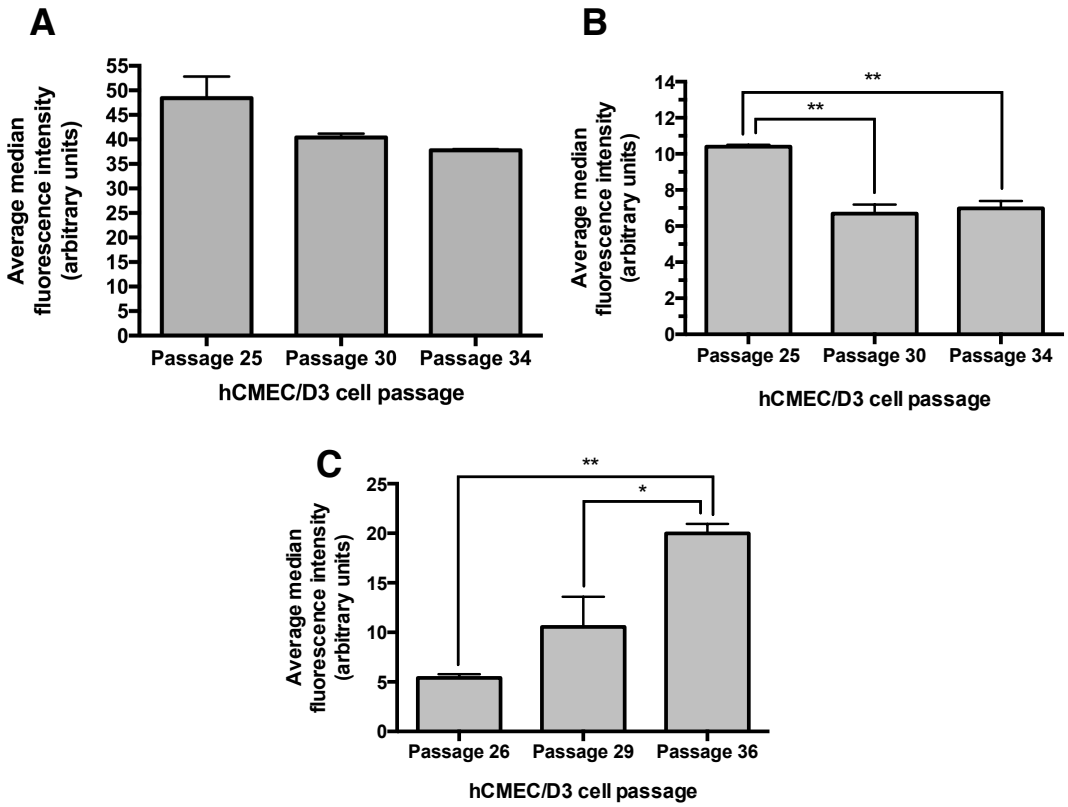

Figure 2.3.3: Summarised results of TfR, LDLR and LRP1 hCMEC/D3 cell surface expression with long-term culture.

Summarised receptor expression results from long-term culture study are shown in **(A)**, **(B)** and **(C)**, and demonstrate the expression of TfR, LDLR (passages 25, 30 and 34), and LRP1 (passages 26, 29, and 36), respectively. Median Fluorescence intensity is presented $\pm$ SE of three experimental replicates, with the average fluorescence intensity of the relevant IgG_1 isotype control subtracted. One-way ANOVA and Tukey's multiple comparison statistical tests were performed to assess statistically significant variations in receptor fluorescence intensity means. A *P* value of <0.05 was considered significant.

2.3.1.3. Effect of cell detachment protocol on surface TfR expression

When considering the protein structure of the TfR monomer, multiple sites for proteolytic cleavage had been described within the stem region of the extracellular domain, including a trypsin cleavage site at arginine 100 (Kaup et al., 2002; Rutledge et al., 1998; Turkewitz, Amatruda, et al., 1988). Biologically, cleavage at this site releases the solubilised extracellular domain of TfR into the circulation. It was consequently appropriate to assess whether trypsin detachment of cells had a potent cleaving effect on the expression of the membrane bound form. To evaluate this, a less potent secondary cell detachment solution (Accutase) was utilised for comparative purposes. The technique utilised for achieving the outlined goals of this study was flow cytometry.

hCMEC/D3 cells (passage 33) were cultured in six T25 flasks under the conditions described in section 2.2.2.2. Cells were detached using one of the two detachment solutions, trypsin EDTA or accutase, for the minimum incubation times required, 2 min or 4 min, respectively. Cells were fixed in 2% paraformaldehyde and evaluated for TfR cell surface expression via indirect antibody labelling and FACS analysis.

Cell membrane bound TfR expression was found to be consistent using both cell detachment solutions Figure 2.3.4. No observable advantage was identified with using Accutase detachment solution over short-term trypsin EDTA treatment.

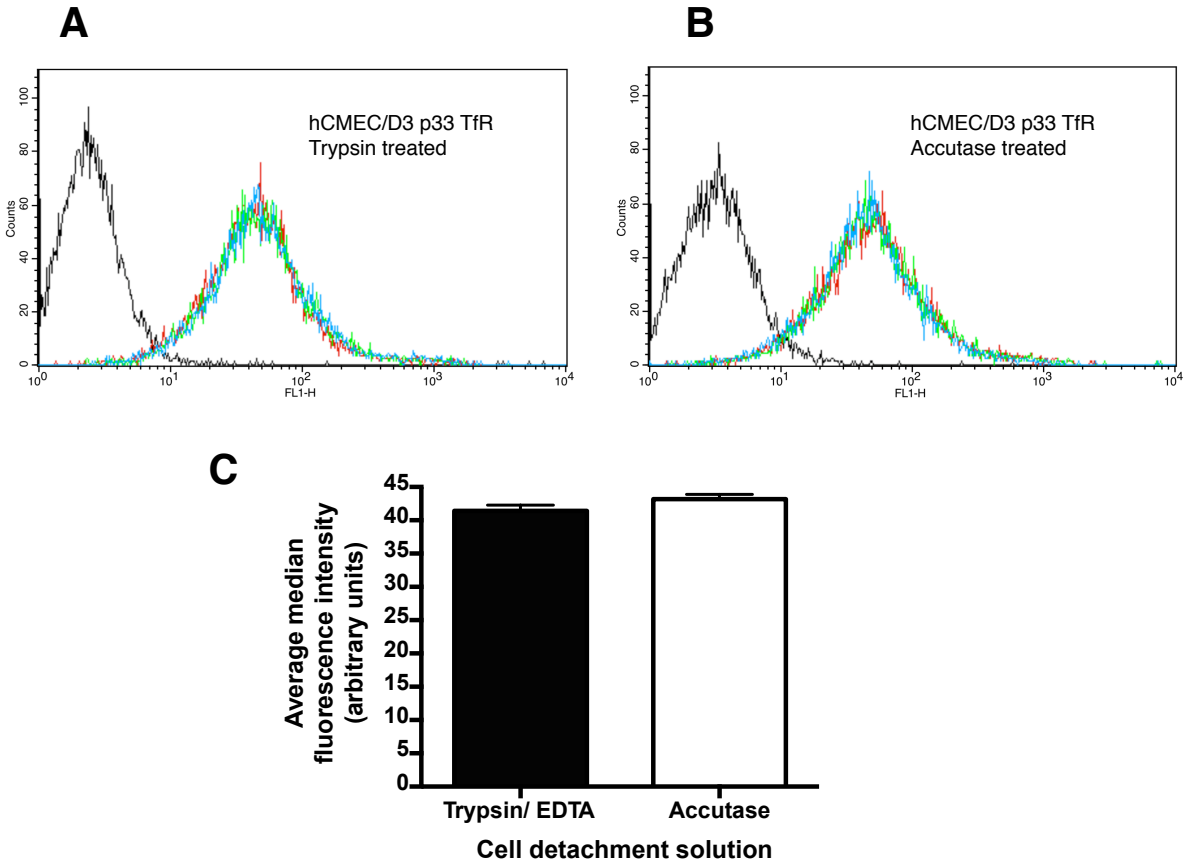

Figure 2.3.4: FACS detection of TfR on cell surface of hCMEC/D3 cells after Trypsin / EDTA or Accutase detachment.

FACS histogram overlay data showing expression of TfR following trypsin/EDTA detachment (A), and accutase detachment (B). Acquisition of FACS data was conducted on 10,000-gated events at an FL1 voltage of 360V. Primary antibody matched (IgG_1) isotype control data is represented by a black line. Red, green and blue lines represent each of the experimental replicates. Summarised results of trypsin EDTA and accutase hCMEC/D3 cell detachment study (C). Trypsin/EDTA potency on cell surface hTfR expression was compared to accutase detachment solution. No significant variations in TfR expression were observed. Median fluorescence intensity is presented as a mean ± SE of three experimental replicates, with the average median fluorescence intensity of the relevant IgG1 isotype control subtracted.

2.3.2. Characterising the expression of human TfR by CHO-TRVb cell lines.

TfR expression was also assessed on two other transferrin receptor variant cell lines, CHO-TRVb and TRVb-1 (McGraw et al., 1987). These were initially developed to allow the study of hTfR transfected CHO cells, without the interfering effects of endogenous Chinese hamster TfR. CHO-TRVb cell lines could potentially be valuable tools for accomplishing both positive and negative cell selections against the transfected and deficient forms of the cell line, respectively.

2.3.2.1. Expression of hTfR on CHO-TRVb cell lines

We characterised the expression of hTfR on both the endogenous hamster TfR deficient cell line (TRVb), and the hTfR stably transfected form of the cell line (TRVb-1) using FACS. The hTfR expression of both these cell lines was also simultaneously compared to expression on hCMEC/D3 cells.

Similar levels of hTfR expression were observed between the hCMEC/D3 cell line and the transfected CHO cell line (TRVb-1), however this similarity was not statistically significant, Figure 2.3.5.

Most notably, an antibody binding signal was also observed on the negative TRVb cell line. The signal on TRVb cells was found to be 5-fold less when compared to the hTfR TRVb-1 cell line and hCMEC/D3 cells ($P \leq 0.0001$, n= 3). These results suggest the TRVb cell line is not completely deficient and maybe a heterogeneous mix of hTfR expressing and hTfR deficient cells. Further assessment of the cell lines using the same primary antibody was performed by western blotting of the cell lysates.

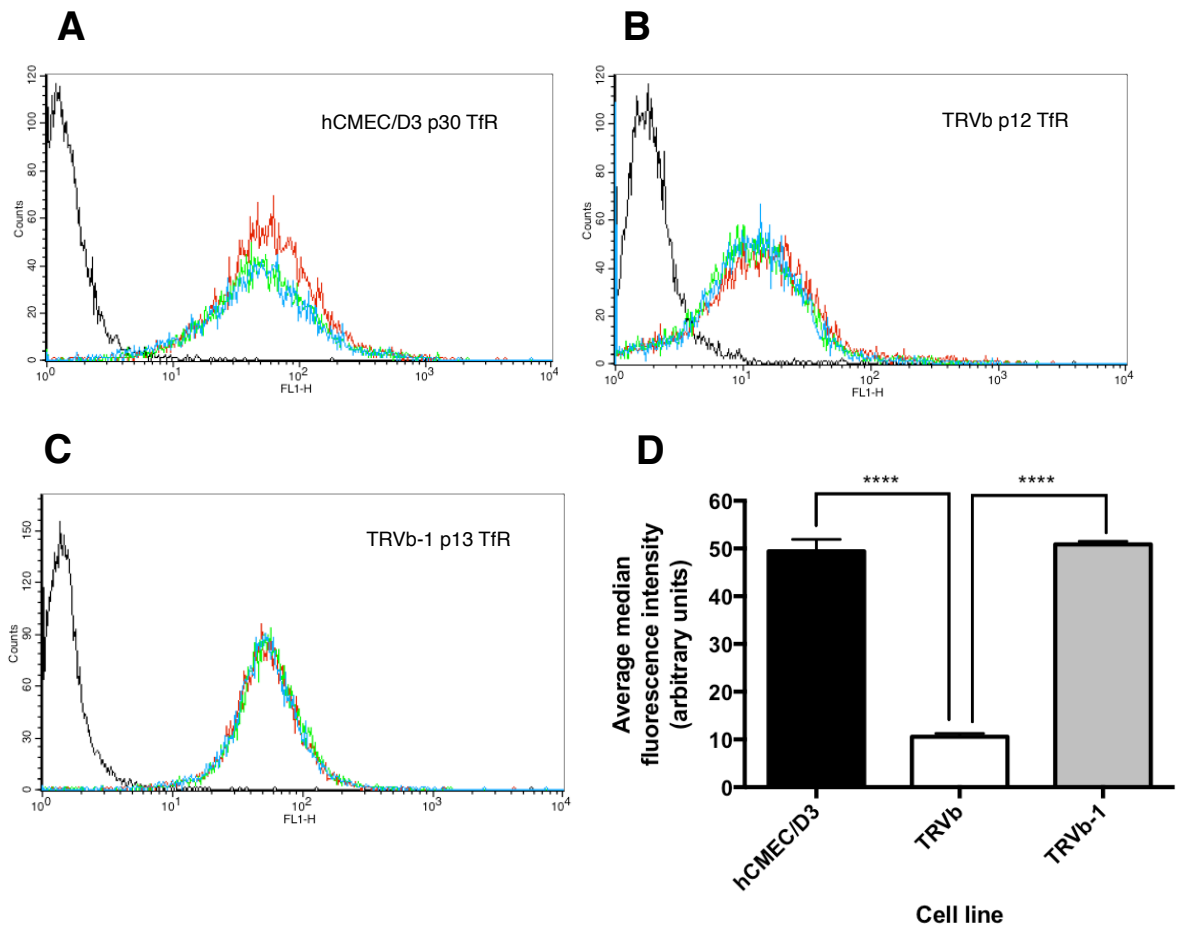

Figure 2.3.5: Characterisation of TfR expression on the cell surface of hCMEC/D3, TRVb and TRVb-1 cells.

FACS histogram overlay data showing expression of TfR on (A) hCMEC/D3 (p30), (B) TRVb (p12) and (C) TRVb-1 (p13) cell lines. Acquisition of FACS data was conducted on 10,000-gated events at an FL1 voltage of 360V. Primary antibody matched (IgG_1) isotype control data is represented by a black line. Red, green and blue lines represent each of the experimental replicates. Summarised results of surface TfR cell line comparison are shown in figure (D). Median fluorescence intensity is presented as a mean ± SE of three experimental replicates (n= 3), with the average median fluorescence intensity of the relevant IgG_1 isotype control subtracted. One-way ANOVA and Tukey's multiple comparison statistical tests were performed to assess statistically significant variations in receptor fluorescence intensity means. A *P* value of <0.05 was considered significant.

2.3.2.2. Immunoblotting of CHO-TRVb cell lysates

Immunoblotting was used for the phenotypic characterisation of hTfR on TRVb-1 (hTfR transfected) cells and also to validate the previously observed expression of hTfR on TRVb-1 (hTfR deficient) cell line. A visible band was observed with TRVb-1 cell lysate immunoblot (Lane 3, Figure 2.3.6). The observed band was at the correct expected size of the extracellular portion of hTfR (85kDa). However, no visible band was observed within TRVb cell lysate immunoblot (lane 2, Figure 2.3.6). Non-specific background binding was also observed in both lanes containing cell lysates. Expression of the β-actin housekeeping control was consistent between both cell line lysates.

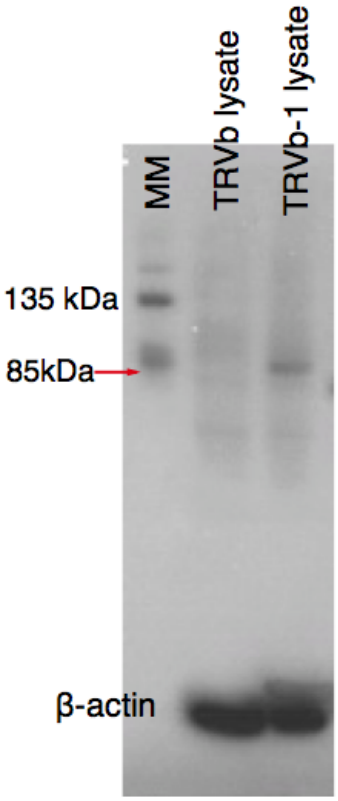

Figure 2.3.6: Immunoblot of hTfR in TRVb and TRVb-1 cell lysates.

Figure showing TfR expression (red arrow) on TRVb and TRVb-1 Chinese hamster ovary cells, as determined by immunoblotting, alongside β-actin (housekeeping control) expression.

2.3.2.3. Assessing the uptake of hTfR on CHO-TRVb and CHO-TRVb1 cell lines

Cell internalising antibodies, anti-hTfR (confidential protein, contact George Thom, MedImmune, Cambridge, UK) and an engineered variant of anti-mTfR (8D3) (Webster et al., 2017), were used to assess hTfR specific internalisation within CHO-TRVb and CHO-TRVb1 cell lines, via ICC. Results of the internalisation assay are shown in Figure 2.3.7 and Figure 2.3.8.

No fluorescence was observed with anti-hTfR within CHO-TRVb, the TfR deficient cell line, (Figure 2.3.7. A1 and A2). In contrast, a statistically significant 3.8-fold increase in fluorescence was observed with anti-hTfR within the hTfR over-expressing variant, CHO-TRVb-1, when compared to the secondary antibody control, (Figure 2.3.7, B1 and B2, Figure 2.3.8, B). The anti-mTfR antibody demonstrated no fluorescence with either the CHO-TRVb or the CHO-TRVb1 cell lines, (Figure 2.3.7, C1, C2, D1 and D2, Figure 2.3.8, A).

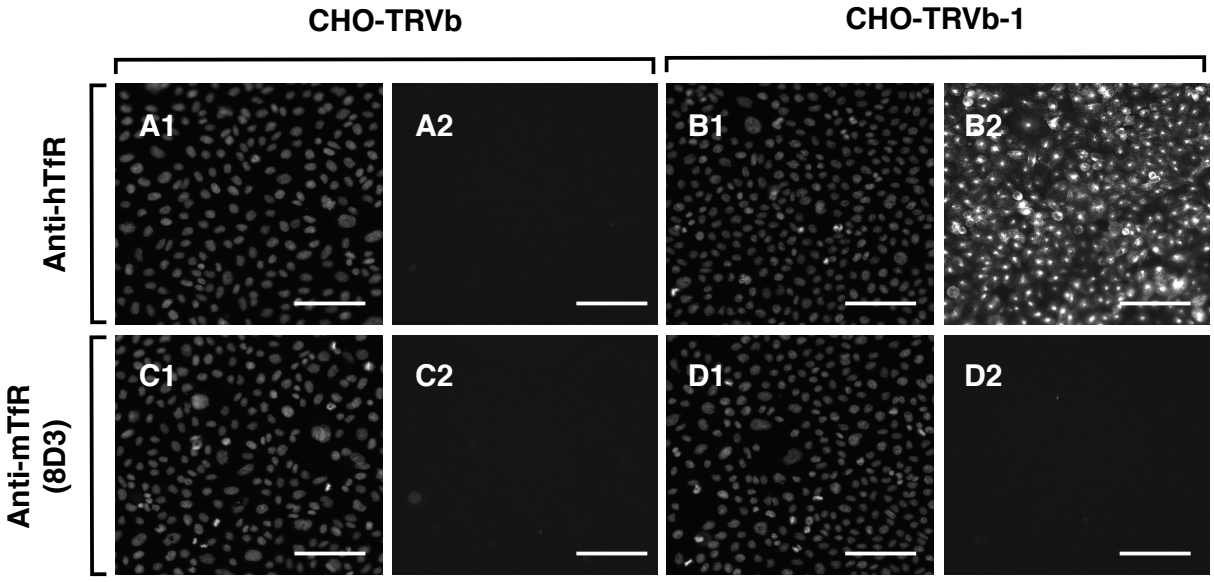

Figure 2.3.7: Uptake of anti-hTfR and anti-mTfR (8D3) antibodies in CHO-TRVb and -TRVb-1 cell lines.
Immunofluorescence images showing cellular uptake of anti-hTfR (A1, A2, B1, and B2), and anti-mTfR (8D3), (C1, C2, D1, and D2) in CHO-TRVb (Chinese hamster TfR deficient), (A1, A2, C1 and C2) and CHO-TRVb-1 (deficient cell line stably transfected with hTfR), (B1, B2, D1, and D2) cells. Hoechst nuclear staining is shown in A1, B1, C1 and D1, whilst secondary anti-human IgG-Fc specific Alexa 488 conjugate is shown in A2, B2, C2, and D2. Images were acquired at x20 magnification using a Molecular Probes ImageXpress XLS system and are representative of three experimental replicates (n= 3). Unlabeled scale bars = 100 μm.

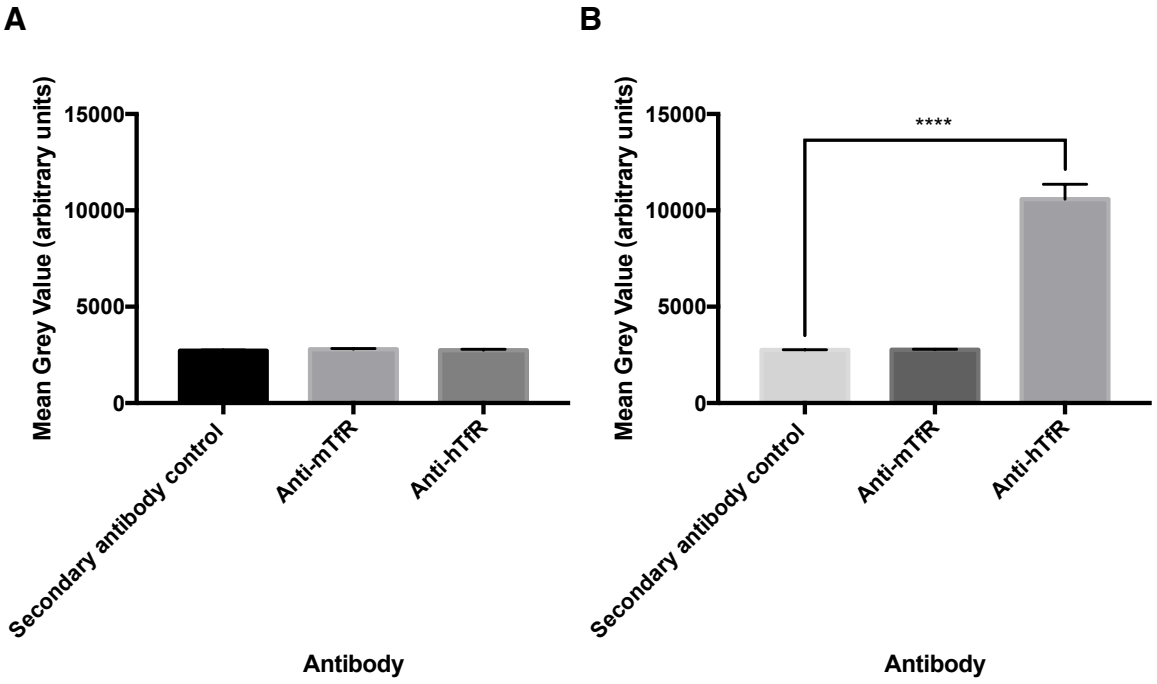

Figure 2.3.8: Summarised results of CHO-TRVb and -TRVb-1 cell line uptake study using anti-mTfR and anti-hTfR antibodies.

Quantitative summary of CHO-TRVb cell line anti-TfR uptake study. The cell uptake of anti-mTfR an anti-hTfR antibodies, within TRVb (A) and TRVb-1 (B) cells are shown. Mean grey value is presented as normalised average readings of three independent images acquired through ImageJ, per experimental replicate (n= 3), ± SEM. **** $P < 0.0001$.

2.4. Discussion

2.4.1. TfR, LDLR and LRP1 receptors are expressed on the cell surface of hCMEC/D3 cells

This chapter set out to assess the expression of the three receptor candidates on hCMEC/D3 cells, the differentiation in expression with long-term cell culture and consequently to determine which cell surface receptor would potentially be most suitable for targeted delivery of therapeutic cargo across the BBB. Furthermore, since TfR is proteolytically cleaved from the cell membrane releasing soluble TfR, it was necessary to evaluate the effect of short-term proteolytic detachment of hCMEC/D3 cells on the expression of TfR (Kaup et al., 2002).

In summary, within this chapter the expression of all three receptor candidates TfR, LDLR and LRP1 was confirmed on the cell surface of hCMEC/D3 cells, and

thus these findings support previous studies that have identified their expression at mRNA and protein level in hCMEC/D3 cells (Pinzón-Daza et al., 2012; Nazer et al., 2008; Ohtsuki et al., 2013). Additionally, the expression of the three receptor candidates was shown to differ with long-term *in vitro* culture, with TfR demonstrating relatively stable levels of expression in contrast to LDLR and LRP1. Furthermore, short-term trypsin/EDTA or accutase detachment was not found to have a detrimental effect on TfR expression within *in vitro* cultures of hCMEC/D3 cells.

The hCMEC/D3 cell line was chosen as a model of the BBB as it retains the majority of functional and morphological characteristics of primary BCEC in monoculture, and has been outlined as a good *in vitro* model for studying the BBB (Sade et al., 2014). Moreover, due to its stable expression of most transporters and receptors, it is a well suited model for studying therapeutic uptake and transporter influx (Weksler et al., 2013). However, like most *in vitro* BBB models, the hCMEC/D3 cells have been shown to exhibit some transporter expressional variances, and these are usually most prevalent with long-term culture of the cell line (Shawahna et al., 2013). *In vivo*, BCEC interact closely with pericytes and astrocytes forming the functionally adaptable neurovascular unit, which as a whole is responsible for producing the observable BBB phenotype. Therefore, it is no surprise that BCEC cells cultured *in vitro,* away from their natural microenvironment, exhibit de-differentiation with prolonged culture and variances in physiologically relevant receptor expression. Moreover, de-differentiation within *in vitro* cultured BCEC has been shown to be associated with a reduced TEER value (Patabendige et al., 2013). Data collected from *in vitro* BBB models can therefore be difficult to interpret on its own, and must be carefully interpreted alongside *in vivo* data.

The results of the flow cytometric assessment of membrane proteins demonstrated here highlight the expression of TfR, LDLR and LRP1 on the cell surface of hCMEC/D3 cells. However, since this detection was carried out using monoclonal antibodies directed towards the extracellular epitopes of these receptors, it was not possible to discern whether the fluorescence signals observed were due to the level of expression of each receptor candidate or whether this was due to the variances in binding affinity amongst the three selected receptor antibodies. The

expression of TfR and LRP1 receptors have previously been quantified on the surface of hCMEC/D3 cells (Ohtsuki et al., 2013).

Ohtsuki *et al.* (2013) previously quantified the expression of membrane proteins on hCMEC/D3 cells and primary BCEC. Using LC-MS/MS, the group quantified the membrane bound fractions for 91 target membrane proteins. They identified that 11 of these proteins were present at detectable levels in both cell types. GLUT1 and TfR were identified as exhibiting highest level of expression on hCMEC/D3. The group also compared the normalised expression levels between hCMEC/D3 cells and isolated primary human BCEC. They found TfR expression to be 18.5-fold higher within hCMEC/D3 cells in contrast to primary BCEC. Interestingly, within the same work LRP1 expression was noted to be below the limit of quantification in hCMEC/D3 cells, however its expression was detected in primary BCEC. The group concluded that differences between *in vitro* and *in vivo* conditions such as variances in cytokines, hormones and amino acids could be responsible for the variation between primary BCEC and the hCMEC/D3 cell line. The group did not identify the expression of LDLR on hCMEC/D3 cells or primary BCEC. A study by Holloway *et al.* (2007) has also shown that in contrast to brain endothelial cells, the expression of TfR is significantly lower in both dermal and lung microvascular endothelial cells, highlighting its great potential for BBB specific targeting over other endothelial cells of the body (Holloway et al., 2007).

The results presented in this chapter, also demonstrate that TfR had the least variable and most stable levels of expression of the three receptor candidates with long-term culture *in vitro*. This finding is important when considering the selection and characterisation of TfR targeting domains, since any variability in receptor expression between passages and batches of cells presents a significant problem for the reproducibility of characterisation results. TfR is vital for the uptake of iron into the brain, where iron is involved in various metabolic processes such as cellular division, neurotransmission and myelination (LeVine and Macklin, 1990). Expression of TfR in BCEC is observed from an early embryonic developmental stage, and highlights the importance of iron for proper CNS development and function. Furthermore, neonatal TfR knockout mouse models have been shown to exhibit

severe CNS developmental defects and are incapable of maintaining life (Levy et al., 1999). Importantly for therapeutic uptake and clearance, TfR is expressed on both luminal and abluminal membranes of BCEC and is also widely distributed within many cells of the of the CNS including; cortical neurons, oligodendrocytes and choroid plexus (J. Lu et al., 1995).

TfR expression is also known to be post-transcriptionally regulated at mRNA level via iron response elements (IRE) and iron regulatory proteins (Rouault and Cooperman, 1995). During a situation of iron deficiency, iron regulatory proteins bind IRE hairpin structures located within the un-translated region of TfR mRNA sequence. In doing so, iron regulatory proteins prevent the cleavage and degradation of TfR mRNA (Tong et al., 2002). Iron deficiency causes elevated levels of iron to concentrate within the brain parenchyma via increased iron transport (E. H. Morgan and Moos, 2002). Interestingly however, no simultaneous increase in expression of TfR is observed on the cell surface of BCEC (Moos and E. H. Morgan, 2001). It has been suggested that the observed increase of accumulated iron within the brain could be directly due to an increase in the cycling rate of TfR containing endosomes within BCEC (Moos et al., 2007). In support of this, intravenous injection of OX-26 anti-TfR antibody in normal and iron deficient rats did not result in increased binding within the iron deficient mice (Moos and E. H. Morgan, 2001). This theory could explain the reason why TfR expression was observed to remain relatively consistent with long-term culture (see Figure 2.3.3, A). Moreover, in support of this hypothesis, studies on primary porcine and bovine BCEC show that 80-90% of TfR is sub-localised in endosomes within the cytosol that are mobilised in situations of high iron requirement (Raub and Newton, 1991; van Gelder et al., 1995). Iron accumulation within the brain parenchyma has been shown to increase with age and also within the brains of individuals suffering from neurodegenerative conditions such as Parkinson's disease (Sofic et al., 1988; Zecca et al., 2004). The reason for this is poorly understood and there is no direct evidence to suggest that TfR activity increases with age or neurodegeneration.

In contrast to the relatively stable expression of TfR, the lipoprotein receptors; LDLR and LRP1, were both found to demonstrate varying cell surface protein

expression results with long-term culture. LDLR demonstrated a significant 0.3-fold reduction in expression between passages 25 and 30, and this significant reduction was maintained between passages 25 and 34. In contrast, LRP1 demonstrated a significant 3-fold increase in expression between passage 26 and 36.

Molino *et al*. (Molino et al., 2017) recently characterised the expression of LDLR at both protein and mRNA level. Within rat BCEC, the mRNA expression of LDLR was found to be 9-fold higher than that observed within the cerebral cortex, however in mice this expression difference was significantly lower. Molino *et al*. (Molino et al., 2017) also assessed the apical and basolateral distribution of LDLR on BCEC using a sucrose density gradient. Their results demonstrated that LDLR was localised to the apical fraction and was delivered to a Tf positive compartments avoiding lysosomal degradation.

Both LDLR and LRP1 are involved in the transport of lipoproteins and are known to be regulated through a feedback mechanism according to the level of LDL in their surrounding medium (Dehouck et al., 1994; Gosselet et al., 2009). Also, their expression has been shown to decrease with senescence *in vivo* (B. Wu et al., 2009). Pinzon-Daza *et al.* (2012) showed that lowering cholesterol synthesis in hCMEC/D3 cells using statins lead to elevated mRNA and protein expression of LDLR at 24 and 48 h, respectively. Interestingly, the group also outlined the potential for the prophylactic up-regulation of LDLR expression (using statins), prior to targeting with a liposome encapsulated therapeutic, conjugated to an LDLR ligand. Another study by Panzenboeck *et al*. (2006) demonstrated that Liver-X receptor (LXR) and peroxisome-proliferator activated receptor (PPAR) activation promoted the efflux of cholesterol from primary porcine BCEC. This efflux was mainly mediated by ATP binding cassette transporter A1 (ABCA1) and scavenger receptor class B type 1 (SR-BI). ABCA1 is primarily expressed on the basolateral side of BCEC and mediates the transport of cholesterol into the CNS, whereas SR-BI is abundantly expressed on the luminal side and mediates transport into the circulation.

The decrease in LDLR expression with long-term culture is potentially a result of a combination of factors. The 30% decrease is maintained at higher passages and could be related to LXR/ PPAR activated sterol transport pathways. The activation of

these nuclear receptors could be indirectly down-regulating the expression of LDLR via the efflux of cholesterol from endothelial cells into the culture media. In support of this hypothesis, Kamps and Berkel (1992) previously studied the regulatory response of LDLR expression within the hepatocarcinoma cell line, HepG2. They showed that 22h incubations with non-lipoprotein bound cholesterol in albumin containing media induced the complete down-regulation of LDLR expression at concentrations as low as 50μg/ml.

A study by Dehouck *et al*. (1994) has also shown LDLR expression to be highly regulated by astrocytes. Using a bovine BCEC and astrocyte co-culture model, the group identified a three-fold increase in LDL binding when compared to bovine BCEC alone. They proposed that this increase in LDLR expression at the luminal membrane of BCEC was due to the high lipid requirement of neighbouring astrocytes. The group concluded that receptor regulation was propagated through astrocyte secretory factors. The same group later confirmed that depletion of cholesterol from astrocytes, lead to an up-regulation of LDLR expression on the luminal surface of BCEC (Dehouck et al., 1997). Furthermore, unlike the traditional endocytotic recycling function of LDLR within most cells, LDLR on BCEC was observed to function through a caveolae dependant RMT mechanism. This specialised shift from recycling to a transcytotic mechanism is thought to be modulated by post-translational modifications of the cytoplasmic domain of the receptor. In support of their findings, previous studies have also demonstrated that phosphorylation of serine 664 on polymeric IgA receptor lead to an inactivation of the endocytosis signal allowing for transcytosis of the bound ligand (Aroeti and Mostov, 1994).

Similarly to LDLR, a variety of triggers within the cell also modulate cell surface expression of the large, multifunctional, scavenger protein, LRP1. For example, insulin has been shown to be involved in the regulation of LRP1 expression (Tamaki et al., 2007). Moreover, cellular cholesterol levels have also been shown to modulate the metalloproteinase dependant shedding of the extracellular ligand binding domain of LRP1 (Selvais et al., 2011). The relatively large size of the LRP1 extracellular domain in contrast to the other two studied receptors deprioritises its

feasibility as a targeted drug delivery transporter. Selections of non-antibody domains can only be carried out on small clusters of the LRP1 extracellular domain. Having identified that TfR expression was the most stable of the three receptor candidates, the focus of the rest of this thesis will be on targeting of TfR as a RMT drug delivery approach at the BBB.

Assessment of the effect of trypsin/EDTA detachment of hCMEC/D3 cells did not demonstrate any discernible difference in the expression of TfR. Trypsin is a membrane associated serine protease that breaks down peptide bonds through hydrolysis at accessible arginine and lysine residues. Alongside other membrane associated proteases, trypsin has been known to be involved in the shedding of membrane proteins (Ahram et al., 2005). Traditionally, trypsin is used alongside EDTA in cell culture applications to detach adherent cells from the culture vessel. However, trypsin detachment has been known to have detrimental effects on the structure of cell surface receptors and their epitopes (Deshui Zhang et al., 2012). Accutase was developed as a gentle alternative detachment solution to trypsin/EDTA. Accutase consists of a mixture of collagenolytic and proteolytic enzymes, which are isolated from shellfish sources (Bajpai et al., 2008).

Interestingly, short-term detachment using trypsin/EDTA solution showed no significant disadvantage in cell surface TfR expression over accutase solution. This observation was unexpected as studies had previously shown that the use of trypsin and other protease treatments lead to cleavage of TfR at one of multiple amino acid locations within the stem region of the amino acid sequence, and arginine 100 was found to be the most susceptible to proteolytic cleavage (Kaup et al., 2002; Rutledge et al., 1998; Turkewitz, Amatruda, et al., 1988). Biologically, cleavage within the stem region of the extracellular domain of TfR results in the release of sTfR into the circulation (Kaup et al., 2002). The result of the study herein could suggest that both detachment solutions exhibit equal potency on the surface expression of TfR when used for minimum detachment incubation times of 2 min and 4 min for trypsin and accutase, respectively. Longer treatment times using trypsin/EDTA may lead to an observable reduction in cell surface TfR expression, however this would need to be explored further.

Analysis of the FASTA sequence of TfR using the ExPASy peptide Cutter tool, reveals a total of 83 potential cleavage sites (Supplementary Figure S1), (Wilkins et al., 1999). Rutledge *et al*. (1994) have previously shown that the removal of the *O-linked* carbohydrate at threonine 104 results in the enhanced proteolytic cleavage of TfR at arginine 100. Through further studies, the group also demonstrated that the sialic acid of the *O-linked* carbohydrate conferred the greatest protection against TfR cleavage and concluded that the removal of this carbohydrate could allow the cell to regulate the proteolytic cleavage and subsequent release of sTfR (Rutledge and Enns, 1996).

Alternatively, the results herein could also imply that both treatments have equal potency towards the surface expression of TfR on hCMEC/D3 cells, but this finding may not be true of primary cells or other cell lines. Previous studies by Wachs *et al*. (2003) have demonstrated increased cell viability and survival rate of rat neural stem cells cultured as neurospheres when using accutase in contrast to trypsin. Accutase had no detrimental effects on the total cell viability of neural precursor cells immediately following detachment and following four days of culture. In contrast, trypsin significantly reduced the total cell viability of neural precursor cells by 66% following four days of culture. Several other studies have also showed the advantages of using accutase as a detachment solution for primary cell culture (Bajpai et al., 2008; Weikert et al., 2003). These studies suggest that primary cells are more susceptible to the damaging effects of trypsin treatment. It is not clear whether any observable reduction in the expression of TfR occurs in primary BCEC following enzymatic detachment using trypsin, and this would need to be explored further.

2.4.2. The CHO-TRVb-1 cell line expresses similar surface protein levels of TfR to hCMEC/D3 cells.

Functional selections using bio-combinatorial libraries against whole cells provides a means of selecting cell specific affinity reagents. Typically, iterative positive and negative selections are performed using target positive and negative cells in order to increase the specificity of the enriched pool to cells that highly express the target in its natural conformation (Ohuchi, 2012). CHO cells have long

been regarded as the cell line of choice for recombinant protein expression and the study of transfected forms of proteins due to their versatility, fast growth rate and long-term stable gene expression (Mariati et al., 2014).

However, the study of transfected forms of homologous proteins can sometimes be affected by the background endogenous expression of the host cell species. Iron is a vital nutritional requirement for cell growth within most cultured cell lines, and this is reflected by the expression of TfR on most cultured cells. In addition, TfR deficient mutant cell lines are usually incapable of sustaining cell growth *in vitro*. However, early TfR mutational studies characterising iron uptake in CHO cells identified a secondary non-TfR dependant mechanism for iron uptake in these cells.

Klausner *et al*. (1984) generated an endocytosis defective CHO cell line that was incapable of internalising and releasing iron from bound transferrin. Interestingly, they discovered the cells maintained sufficient iron uptake to support cellular growth. It was concluded that iron internalisation in these cells was also likely to occur via uptake of iron salts. McGraw *et al.* (1987) decided to exploit this feature by generating an endogenous hamster TfR deficient CHO cell line that could subsequently be stably transfected with the human form of TfR and studied without interfering effects of the homologous endogenous form. The group devised a strategy for isolating TfR-variant (TRV) CHO cells by selecting for resistance to one of two Tf-toxin conjugates. These chimeric Tf-toxin conjugates were generated by substituting the binding domain of ricin or diptheria toxin with Tf. In principle, The TfR deficient cells would not be able to bind the Tf-toxin conjugates and therefore would have a selective growth advantage over cells expressing TfR. The group subsequently stably transfected endogenous TfR deficient TRV cells with hTfR cDNA and demonstrated hTfR activity by assessing internalised ^{59}Fe presented as diferric Tf.

During our initial characterisation of hTfR expression on CHO-TRVb cell lines by FACS, similar levels of hTfR expression were observed on the CHO-TRVb-1 (hTfR expressing) cells when compared to hCMEC/D3 cells. Furthermore, the TRVb (TfR deficient) cell line by FACS also demonstrated some positive hTfR expression

on the surface of these cells. Suggesting the presence of a heterogeneous population of cells.

McGraw *et al.* (1987) had previously characterised the deficient cell line through functional uptake studies and shown that the cells did not internalise any fluorescein-Tf, suggesting that expression of endogenous TfR was absent within the cell line. More recently, Kumar *et al*. (2012) used these TfR deficient cell lines to elucidate alternative pathways for transferrin uptake. The same group had previously identified GAPDH as being a low affinity receptor for transferrin within macrophages and was involved in the uptake of iron bound transferrin (Raje et al., 2007). By knocking down GAPDH within the TfR deficient cells (CHO-TRVb), the group demonstrated a significant decrease in transferrin binding and also iron uptake. They concluded that the GAPDH mediated transferrin uptake occurred via a combination of clathrin-mediated and lipid raft endocytosis, in conjunction with macropinocytosis.

Further assessment of total protein expression by western blotting showed the deficient cell line was negative for hTfR protein expression. Upon closer examination of the immunoblotting results, a high level of background exposure was observed (Figure 2.3.6), suggesting some non-specific binding of the primary antibody. The described anti-hTfR antibody (R&D Systems, MAB2474) has not been validated for the application of western blotting. The background reading result seen on the gel could be due non-optimal binding of this antibody under immunoblotting conditions. Nevertheless, a clear band suggesting the expression of hTfR was observed on CHO-TRVb-1 (hTfR positive cell line).

To validate whether the negative cell line does express hTfR, a TfR functional cell uptake study was conducted using the CHO-TRVb cell lines and two antibodies, anti-hTfR (confidential protein, MedImmune, Cambridge, UK), and an engineered variant of anti-mTfR (8D3), (MedImmune, Cambridge, UK), (Webster et al., 2017). Cell uptake using the hTfR antibody was observed within the CHO-TRVb-1 cell line, but not the TRVb cell line, suggesting no expression of hTfR was present on that cell line. Furthermore, no cell uptake was observed with the anti-mTfR (8D3) antibody within both the CHO-TRVb and the -TRVb1 cell lines (Figure 2.3.7, and Figure 2.3.8). Due to the lack of an Chinese hamster specific antibody we, we were unable

to determine endogenous TfR uptake in relation to wild type CHO cells. However, recent studies have characterised these cell lines and detailed that they are deficient for the expression of endogenous hamster *TFRC* mRNA. Mehta *et al.* (2015) characterised the expression of both Chinese hamster and human *TFRC* mRNA within the hTfR transfected form of the deficient cell line. Their characterisation revealed that the CHO-TRVb-1 cells expressed human *TFRC* mRNA, but not the endogenous hamster form. This was compared with wild-type CHO cells which expressed endogenous hamster *TFRC* but not human *TFRC*.

Whilst we have identified hTfR expression within a small proportion of the CHO-TRVb cells via FACS analysis, functionally these cells do not appear to express TfR as identified via ICC cell uptake studies. These finding highlight that indeed; these cells may valuable tools for conducting positive and negative cell selections of non-antibody domains. Furthermore, the TfR deficient cell line would provide a valuable negative control for characterisation of identified domains.

To summarise, in support of previous findings, we have demonstrated that all three receptor candidates, TfR, LDLR and LRP1, are expressed on the cell surface of hCMEC/D3 cells. Furthermore, we have shown that TfR appears to be the most stably expressed of the three receptor candidates with long-term *in vitro* culture, and its expression on hCMEC/D3 cells was not altered following short-term trypsin treatment when compared to accutase, a more gentle proteolytic solution. The CHO-TRVb-1 cell line was observed to express similar levels of hTfR expression to hCMEC/D3 cells. Through uptake studies using antibodies directed to human and mouse TfR, the CHO-TRVb cell line was shown to be functionally deficient for the expression of hTfR and may be valuable tools for the selection and characterisation of non-antibody binding domains.

Chapter 3: Selection of TfR binding peptides for use as BBB drug delivery vectors.

3.1. Introduction

The BBB is the most significant obstacle for the delivery of neuro-therapeutic drugs into the CNS, thus hindering the development of successful treatments to the debilitating neurological disorders burdening our developed societies (Vigo et al., 2016). Biotherapeutics, are an increasingly popular choice for the therapeutic treatment of many disorders, primarily due to their highly specific targeting capability (Yanan Cui et al., 2017).

The leading class of biotherapeutics, MAbs, have restricted transport when used as RMT drug delivery shuttles at the BBB, this equates to 0.1 - 0.2% of circulatory antibody reaching the CNS (Yu and Watts, 2013). These limitations are primarily attributed to the large size and high affinity nature of antibodies, that have been shown to result in reduced CNS uptake via sequestration, and subsequent degradation within the late-endosomal and lysosomal compartments of BCEC (Bien-Ly et al., 2014). Additionally, the high specificity of antibodies results in the lack of species cross-reactivity which limits the translatability between animal and human models. In contrast to non-CNS drugs undergoing clinical trials, CNS therapies are more likely to fail during every phase, but most notably during phases II and III (McGonigle, 2014). Clinical trial failures particularly those that fail in later stages, have been partly attributed to the lack of suitable animal models and species cross-reactive molecules capable of producing translatable results (Yu et al., 2011; Irani et al., 2016). In addition to this, numerous factors such as poor drug efficacy, toxicity and the lack of understanding of complex CNS pathology, have further impeded progress in this research area (Ohshima-Hosoyama et al., 2012; Couch et al., 2013).

In recent years, there has been a resurgence in the popularity of peptides as an alternative amino acid based platform for use as highly selective and physiologically efficacious biochemical therapeutics (Craik et al., 2013; Kaspar and Reichert, 2013). Peptides are highly suited to affinity ligand screening approaches such as phage display, where expression of a diverse peptide library on the surface of bacteriophage coat proteins allows the selection towards a target of interest (van Rooy et al., 2010; Bonetto et al., 2009). In this respect, with peptides being

inherently smaller and lower affinity than antibodies, they have great potential for use as RMT drug delivery vectors at the BBB. The most notable examples of receptors exploited via peptides for molecular Trojan horse delivery across the BBB are the low-density lipoprotein receptor family (LDLR and LRP1) and transferrin receptor (TfR), (Demeule et al., 2008; Hultqvist et al., 2017; Malinovskaya et al., 2017; Manich et al., 2013; Bien-Ly et al., 2014; Niewoehner et al., 2014; Sorrentino et al., 2013; X. Tang et al., 2015; Wiley et al., 2013; Yu et al., 2014; Sakamoto et al., 2017).

Following the characterisation of candidate receptor targets expressed on human brain endothelial cells, the rationale of which is discussed in chapter two, the focus of this project is on TfR as a target for RMT drug delivery. We hypothesise that through the use of a combined target antigen and BBB cell phage display selection approach, we can identify novel peptide sequences that may have greater BBB specific transport capabilities. Additionally, the use of cyclic peptides in place of their linear counterparts may offer peptides with greater natural resistance to exopeptidases, whilst also demonstrating enhanced biological activity (Joo, 2012). In contrast to previously identified antibody-based BBB shuttles, peptide-based delivery shuttles would also likely confer greater transcytosis capacity through their inherently lower affinities (μM range), thus allowing the release of the delivery shuttle/ drug conjugate at the CNS side (Yu et al., 2011).

The overall aims of this study were to select and identify low to medium affinity TfR binding and BCEC cell internalising cyclic peptides via phage display selections. More specifically this study endeavoured to:

- Carry out soluble phage display selections towards mTfR and/ or hTFR recombinant protein antigens using three independent 16-mer cyclic peptide phage display libraries.
- Conduct a final functional selection round towards a mouse brain endothelial cell line (bEnd.3), in order to preferentially select cell internalising anti-TfR cyclic peptides.
- Screen for positive TfR species cross-reactive clones by means of a phage ELISA.

- Sequence and identify lead candidates for expression and further characterisation.
- Assess homology of identified peptides to each other and to the natural ligand of TfR, Tf.

3.2. Materials and methods

3.2.1. Preparation of TfR antigens for phage display selections

3.2.1.1. Biotinylation of recombinant transferrin receptor

Extracellular N-terminal 6x His tagged recombinant mouse TfR (Sino Biological Inc. Beijing, China, Figure 3.3.1, A) was biotinylated for soluble phage display selections. Biotin labelling was carried out using the optimised EZ Link Sulfo-NHS-biotin kit (ThermoFisher Scientific, Loughborough, UK) according to the provided protocol. Lyophilised mTfR-His6 was re-suspended in PBS at a concentration of 1 mg/ml. A protein:biotin molar ratio of 1:50 was used to label 200 µg of mTfR-His6 in volume of 200 µl. The reaction was incubated at room temperature for 30 min and the solution was buffer exchanged using a 2 ml Zeba Spin desalting column (ThermoFisher Scientific, Loughborough, UK). Biotinylated mTfR-His6 concentration was determined by spectrophotometry at 280 nm. Biotinylated recombinant human TfR-His10 was kindly provided by Miguel Carvalho (MedImmune, Cambridge, UK), (Figure 3.3.1, B). Biotinylated rat TfR-FLAG/HIS10 was kindly provided by Susan Fowler (MedImmune, Cambridge, UK), (Figure 3.3.1, C).

3.2.1.2. Antigen presentation ELISA

A streptavidin coated 96-well flat-bottomed microtiter plate (ThermoFisher Scientific, Loughborough, UK) was immobilised with triplicate serial dilution sets of biotinylated mTfR antigen ranging from 10 µg/ml to 0.01 µg/ml, in a dilution ratio of 1:2. Biotinylated insulin at a concentration of 10 µg/ml was also immobilised in separate wells as an irrelevant control antigen, alongside a PBS negative control. Plates were incubated with antigens overnight at 4°C and then washed three times with PBS to remove unbound antigen. Antigen immobilised plates were blocked in

3% (w/v) skimmed milk powder in PBS (MPBS) for 1 h at room temperature. Plates were washed three times with PBS and incubated with 2 µg/ml of human anti-mouse TfR (8D3) detection antibody made up in 3% (w/v) MPBS for 1 hour at room temperature. Plates were washed three times in PBS with 0.1% (w/v) tween 20 (PBST). Primary antibody was counter labelled with anti-human IgG (Fc Specific) horse radish peroxidase (HRP) conjugated secondary antibody (Cat No. A0170, Sigma-Aldrich, Dorset, UK) made up in 3% (w/v) MPBS at a dilution of 1:10,000 and incubated for 1 h at room temperature. Plates were washed three times in PBST and developed using 50 µl of 3,3',5,5'-SureBlue Tetramethylbenzidine (TMB) substrate (KPL, Maryland, USA) per well for 5 min at room temperature. The reaction was subsequently stopped by addition of 50 µl of 0.5 M H_2SO_4 to each well and plates were read using fluorescent plate reader at 450nm.

3.2.2. Cyclic peptide library growth.

Glycerol stocks of three pre-constructed cyclic peptide phage display libraries (Bonetto et al., 2009) were kindly provided by Siobhan O'brien (MedImmune, Cambridge, UK). Each of the three libraries encodes peptides 16 amino acid residues in length. However, these differ from one another through the size of the variable central region which is constrained via two flanking cysteine residues. Each library has a theoretical size of between 1.0 – 2.0 x 10^9 and incorporates a linker between the peptide and the gene-3-protein (g3p) domain in order to prevent steric hindrance of the peptide binding region. The amino acid formats of the cyclic peptide libraries are, CPEP1 ($X_5CX_4CX_5$), CPEP2 ($X_3CX_8CX_3$) and CPEP3 ($X_2CX_{10}CX_2$), where 'X' denotes a random amino acid.

Prior to soluble phage display selections (described in section 3.2.4), the libraries were grown and rescued as follows. For each library, 100 µl of glycerol stock was added to one 2 L Erlenmeyer flask containing 400 ml of 2x tryptone yeast media (16 g/L tryptone, 10 g/L yeast extract and 5 g NaCl) supplemented with 12.5 µg/ml tetracycline (2xTYTET). The culture was then grown overnight at 37°C within a shaking incubator at 280 rpm. The following day the phage particles were recovered by polyethylene glycol (PEG) precipitation (as described in section 3.2.3).

3.2.3. Phage purification via PEG precipitation

Cultures were transferred into two large, pre-cooled centrifuge pots and balanced by weight before spinning at 10,800 g for 20 min at 4°C. The supernatant was collected in pre-chilled 500 ml bottles before adding 120 ml of chilled 20% (w/v) PEG 8000/ 2.5 M NaCl to 400 ml of supernatant (3:10 ratio). The mixture was precipitated on ice for a minimum of 1 h. A phage pellet was concentrated by spinning at 10,800 g for 20 min at 4°C. The supernatant was then decanted and phage pellets were re-suspended in 10 ml of Tris-EDTA (TE) buffer (10 mM Tris-HCl and 1 mM EDTA), pH 8.0 and transferred to a 50 ml centrifuge tube. The centrifuge tubes were then spun in a pre-chilled rotor at 17,500 g for 15 min at 4°C and the supernatant containing re-suspended phage particles was collected into a fresh 50 ml centrifuge tube. Pre-chilled 20% PEG8000 solution was subsequently added to the collected phage supernatant at a ratio of 3:10 (v/v), mixed by inverting, and precipitated at 4°C for 1 h. After precipitation, the phage stock was centrifuged at 17,500 g for 20 min at 4°C. Supernatant was decanted, and each phage pellet was re-suspended in 5 ml of TE buffer, pH 8.0 and centrifuged at 17,500 g, 4°C for 10 min. Phage supernatant was transferred into a fresh 12 ml falcon tube without disturbing the bacterial pellet.

Prior to commencing phage display selections, phage input titres were calculated using an automated spiral petri dish plater and Acolyte colony counter (Synbiosis, Cambridge, UK).

3.2.4. Soluble phage display selection

Soluble phage display selections were carried out as outlined in Figure 3.2.1. The primary goal of these selections was to identify cyclic peptide domains that bound to both mouse and human TfR (species cross-reactive) and internalised within an *in vitro* model of the BBB, in this case, immortalised mouse brain endothelial cells, bEnd.3 (Montesano et al., 1990). Additionally, to encourage the selection of cross-species binding peptides, a cross-selection cascade was introduced at round 3, where a switch from human to mouse TfR antigen was included.

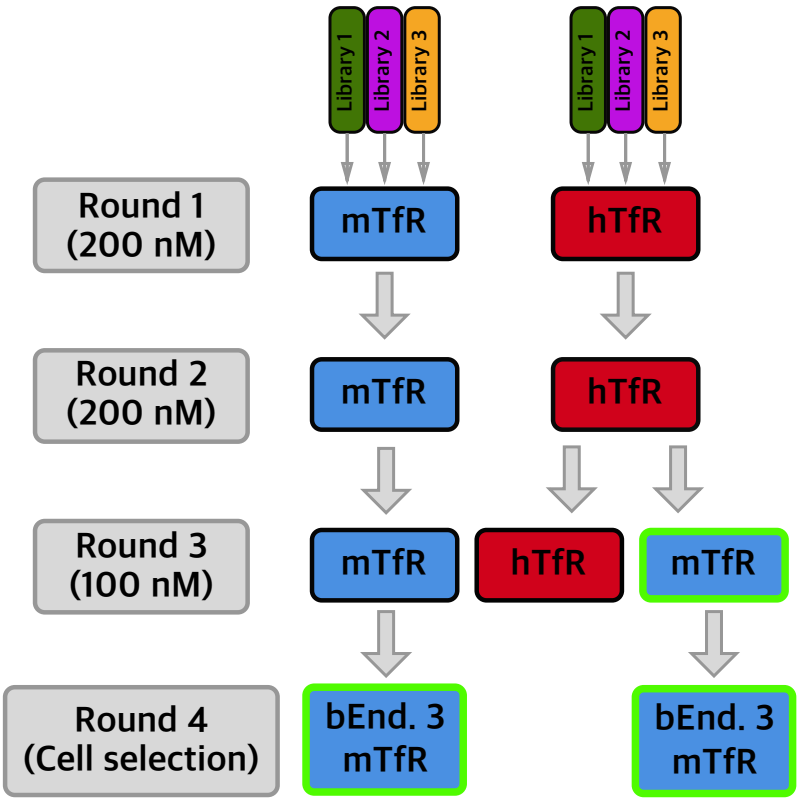

Figure 3.2.1: Schematic representation of soluble phage display selections conducted using cyclic peptide libraries.

Flow diagram showing cyclic peptide library selection cascades carried out against mouse and human TfR target antigen. A cross-selection cascade was introduced at round three to encourage the selection of TfR species cross-reactive peptides. The fourth round was conducted against mouse brain endothelial cells to encourage the selection of peptides that bind and are internalised via TfR expressed on the cell surface of mammalian cells. Selection output boxes highlighted in green were taken forward for phage ELISA screening against recombinant mouse and human TfR.

3.2.4.1. Inoculation of *E. coli* TG1 culture

E. coli TG1 cells were grown on a plate of M9 minimal media and a single colony was used to inoculate 50 ml of 2xTY media in a sterile 250 ml disposable flask under aseptic conditions. The flask was incubated at 37°C within a shaking incubator set to 300 rpm until the culture reached mid-logarithmic growth phase, as determined by an optical density (OD) 600 value of 0.5 – 1.0. Typically, TG1 cells reached an OD^{600} reading of 0.76 following 5 hours of culture.

3.2.4.2. Pre-blocking of phage library and streptavidin coated magnetic agarose beads

For the first round of selection a 50 µl aliquot of each library was added to 450 µl of 3% (w/v) MPBS in a 1.5 ml Eppendorf tube and allowed to incubate at room

temperature for 1 h on a rotary shaker. For later rounds of selection, a 10 µl aliquot of rescued phage output from the previous round of selection was transferred to an Eppendorf tube containing 490 µl of 3% (w/v) MPBS and incubated at room temperature for 1 h on a rotary shaker. A 10 µl aliquot taken from 1 ml total rescued phage volume equates to approximately 1.0 x 10^{10} colony forming units (cfu).

In addition to pre-blocking the phage library, streptavidin coated magnetic agarose beads (M-280 Dynabeads, ThermoFisher Scientific, Loughborough, UK) were also pre-blocked using 3% (w/v) MPBS. For each selection, a total of 100 µl of bead slurry was required, 50 µl for de-selection of library towards beads and 50 µl for capturing phage/ biotinylated antigen complexes at a later stage. Beads were pre-blocked in 1.5 ml Eppendorf tubes by removing the storage buffer using a magnetic separator, re-suspending in 1 ml of PBS, and subsequently discarding the PBS and re-suspending in 3% (w/v) MPBS. Beads were blocked in a rotary mixer at room temperature for 1 h.

3.2.4.3. De-selection of phage library against streptavidin coated magnetic agarose beads.

In order to limit the enrichment of peptide species that preferentially bind to the affinity matrix of the capture beads, a de-selection incubation step was performed using the pre-blocked phage library and an aliquot of pre-blocked beads.

Pre-blocked beads were separated using a magnetic separator, the supernatant was discarded and beads were then re-suspended in 100 µl of fresh 3% (w/v) MPBS. A 50 µl aliquot of the pre-blocked beads was transferred into the pre-blocked phage library and incubated at room temperature for 1 h. The remaining aliquots of beads were kept on ice for a later stage of the selection. Following de-selection beads were separated using a magnetic separator for 2 min and the supernatant containing the blocked and de-selected library was transferred into a fresh 1.5 ml Eppendorf tube.

3.2.4.4. Incubating de-selected phage library or rescued phage with biotinylated antigen

Biotinylated mouse or human TfR was added to 500 µl aliquots of blocked phage in 1.5 ml Eppendorf tubes at a final concentration of 200 nM for rounds 1 and 2 and 100 nM for round 3. The mixture was incubated at room temperature on a

rotary shaker for 2 hours in order to allow sufficient time for low affinity binding peptides to bind target TfR antigen.

3.2.4.5. Capturing binding phage particles

Following phage incubation, 50 µl of pre-blocked streptavidin magnetic agarose beads were added to each selection tube and allowed to equilibrate for 5 min on an orbital shaker. Beads were washed five times in PBST solution using a KingFisher mL purification system (Thermo-Fisher Scientific, Loughborough, UK) in order to remove unbound phage, and bound phage was subsequently eluted by re-suspending beads in 500 µl of 10 µg/ml trypsin solution and incubating on a rotary shaker at 37°C for 30 min. Streptavidin beads were captured using a magnetic separator and the eluted phage was isolated carefully in solution. Eluted phage was stored on ice until TG1 cells were ready at mid-logarithmic phase for infection.

3.2.4.6. Infecting TG1 cells with eluted phage

The total 500 µl volume of eluted phage was added to 0.8 ml of mid-log *E.coli* TG1 cells in a sterile 50 ml falcon tube and incubated at 37°C with shaking at 150 rpm. After phage infection of TG1 cells, an aliquot of the culture was used to create a dilution series, which was plated using a spiral plater and used to calculate output titres the following day. The remaining cultures were plated on 2xTYTET bioassay plates, and grown overnight in a 30°C incubator.

After calculating titres for rounds 3 and 4 outputs, the same dilution plates were used to carefully pick 176 individual colonies into 11 columns of two 96-well plates containing 100 µl of 2xTYTET. These master plates were sealed and grown overnight at 25°C, 250 rpm and the following morning 50 µl of 50% (v/v) glycerol solution was added to each well prior to storage at -80°C. The master plates were stored until ready to carry out phage ELISA screening.

3.2.5. Phage selection rescue

3.2.5.1. Harvesting cells from bioassay plates and freezing of glycerol selection outputs.

Bioassay plates (section 3.2.4.6) were harvested in a laminar flow hood and handled under aseptic conditions to avoid cross-contamination of selected outputs. Glycerol-medium mix was prepared by mixing 2xTY with 50% (v/v) glycerol in a 2:1

ratio. Harvesting of *E.coli* TG1 colonies grown on bioassay plates was carried out by addition of 10 ml of glycerol-medium per plate and scraping using a sterile disposable spreader. The cell suspension was subsequently transferred to a sterile 50 ml falcon tube and placed on a rotary shaker for 10 min at room temperature. For each selection output, two cryotubes were labelled, 1 ml of glycerol – cell suspension was added to the relevantly labelled cryotubes and the tubes were stored at -80°C.

Prior to commencing the subsequent round of selection glycerol stocks were thawed, 7 µl of glycerol stock was used to inoculate 25 ml of 2xTYTET and the culture was grown overnight at 30°C, 280 rpm. The following morning, phage was isolated from each 25 ml culture by PEG precipitation as outlined in section 3.2.2. The isolated and purified phage was used to inoculate *E.coli* TG1 cells at mid-log phase, and subsequently titred to determine the input titre alongside the commencement of a successive round of selection.

3.2.6. Live cell surface phage display selection

A fourth and final round of selection was carried out against cell surface antigens expressed by the immortalised mouse brain endothelial cell line, bEnd.3. This was done in order to select phage particles that specifically bind to TfR expressed in its natural conformation on the surface of mammalian cells, with all the relevant post-translational modifications.

3.2.6.1. Cell culture and harvesting of bEnd.3 cells

bEnd.3 cells were maintained in Dulbecco's Modified Eagle's Medium (DMEM) supplemented with 10% FBS and 100 U/ml penicillin and 100 µg/ml streptomycin (Invitrogen, Paisley, UK). Once cells had formed a confluent monolayer, they were harvested by washing in 10 ml of PBS and detached using 6 ml of accutase solution. Following detachment, the cells were collected in 10 ml of growth medium in a sterile 50 ml falcon tube. A viable cell count was carried out using trypan blue and a 10 µl aliquot of cell suspension, and the remaining cells were centrifuged at 1200 rpm, for 5 min. The supernatant was discarded and the cells were re-suspended at 1.3 x 10^7 cells per ml of media.

3.2.6.2. Pre-blocking phage and bEnd.3 cells

The cell suspension was blocked in 9 ml of 3% (w/v) skimmed milk powder in un-supplemented DMEM media for 1 h at room temperature on a rotary shaker. A 10 µl aliquot of round 3 selected and purified phage output was also blocked in 490 µl of MPBS, for 1 h at room temperature. Following the blocking steps, cells were centrifuged at 1200 rpm for 5 min and the supernatant was discarded. The cell pellet was then reconstituted in 500 µl of pre-blocked phage and transferred to an Eppendorf tube before incubating on a rotary shaker for 1 h at room temperature.

After incubation, the cells were centrifuged at 2000 rpm in a micro-centrifuge for 1 min. Unbound phage was carefully removed in solution and the pellet was re-suspended in 100 µl of PBS using a 1 ml pipette to avoid shearing stress on the cells. The re-suspended cell pellet was then transferred to a fresh Eppendorf tube, washed 8x in 1 ml PBS and inverted to mix.

3.2.6.3. Elution of internalised phage particles

In order to elute cell internalised phage particles, Triethylamine (TEA) was used to strip cell surface antigens and thus remove membrane bound phage. Post washing, the cell pellet was re-suspended in 500 µl of 100 mM TEA and incubated for 3 min at room temperature. Subsequently, the activity of TEA was neutralised using 1M Tris solution (pH 8.0). The phage was then used to infect mid-log *E.coli* TG1 cells and output titres were calculated as outlined in section 3.2.4.6.

3.2.7. Phage ELISA screening for cross-species TfR binding peptide hits

In total, three selection outputs from each of the three cyclic peptide libraries were screened for binding hits towards the extracellular domain of mouse and human TfR as highlighted in

Figure 3.2.1. 176 clones were picked into master plates for nine selections originating from rounds 3 and 4 (1584 clones in total) as shown in section 3.2.4.6.

Prior to commencing the phage ELISA screening, biotinylated antigens (mTfR, hTfR and Insulin) were diluted in DPBS to a concentration of 1 μg/ml and 50

µl per well was used to coat streptavidin coated 96-well plates, for a total of 18 plates per test antigen (54 plates in total).

Master plates were replicated into 96 deep-well plates. Selection, source plate and destination plate IDs are shown in supplementary Figure S3. Replication was then carried out using a microplate replicator, which was ethanol flame sterilised and cooled before being used to inoculate a labelled deep-well daughter plate containing 500 µl of 2xTYTET per well. The daughter plate was cultured overnight at 25°C, 280 rpm.

The following morning phage cultures were blocked for 1 h, at room temperature in equal volume of 6% (w/v) skimmed milk powder in 2xPBS solution. Concurrent to blocking phage cultures, antigen immobilised streptavidin plates were blocked with 300 µl per well of 3% (w/v) skimmed milk powder in 1xPBS, for 1 h at room temperature.

Following the blocking step, 96 deep-well plates containing blocked phage cultures were centrifuged for 5 min at 3200 rpm at room temperature. Antigen pre-coated and blocked 96-well plates were washed three times in PBS, and subsequently incubated with 50 µl per well phage supernatant for 1 h, at room temperature. Following phage incubation, plates were washed three times in PBST and detection was carried out by incubating with 50 µl per well anti-M13 HRP conjugated secondary antibody (27-9421-01, GE Healthcare Life Sciences, Little Chalfont, UK) at a dilution of 1/5000 for 1 h at room temperature.

Plates were washed three times in PBST and HRP was developed using 50 µl per well TMB substrate for 10 min at room temperature. To inhibit the reaction, 50 µl per well of 0.5 M H_2SO_4 was added and plates were read at 450 nm using an Envison fluorescent plate reader (Perkin Elmer, Beaconsfield, UK). Screening data was analysed using the software, Ignite (Continuity software package, MedImmune, Cambridge, UK).

Prior to analysis, the criteria for the identification of weak and strong antigen binding hits were assigned as reference absorbance values within the software. Weak hits were ≥ 0.2, but < 0.5 arbitrary units, and strong hits were ≥ 0.5 arbitrary

units. Additionally, a hTfR and mTfR specific hit was classified as binding weakly or strongly towards either hTfR or mTfR, respectively and not the irrelevant control antigen insulin. A species cross-reactive hit was classified as binding weakly or strongly to both hTfR and mTfR, but not the irrelevant control antigen insulin.

For phage ELISA repeat experiments, sequence validated clones containing the 16 unique peptide sequences were cultured from glycerol stocks and grown on 2xTYTET petri plates at 30°C overnight. Three independent colonies for each of the unique peptides were picked and inoculated into 96-deep well plates containing 500 *µ*l of 2xTYTET. Colonies were grown and subjected to phage ELISA binding assays, as outlined within this section.

3.2.8. Sequencing and identification of unique cross-species binding peptides.

Source plates identified to contain cross-species TfR binding clones were inoculated into fresh 96-well plates containing 100 µl per well of 2xTYTET using Freedom EVO automated liquid handling robot (Tecan, Männedorf, Switzerland), and grown overnight at 25°C. The following morning, aliquots of 30 µl per well were transferred into fresh 96-well plates for DNA amplification and sequencing. A total of 50 µl per well of 50% (v/v) glycerol solution was added to culture plates and these were stored at -80°C.

Sequencing of peptide hits within the fdDOG phage display vector was carried out using the relevant forward and reverse sequencing primers, as shown in Table 3.2.1.

Table 3.2.1: Sequencing primers used for amplifying insert region of fdDOG phage display vector.

Primer name	Sequence (5'-3')	LENGTH
fdDOGfor seq	GAAATTCACCTCGAAAGCAA	20
fdDOGrev seq	GACAGCCCTCATAGTTAGCGT	21

3.2.9. Sequence analysis of fdDOG positive hit sequencing data

Sequencing data from round 3 and 4 identified selection hits was analysed using the software Blaze 2.0 (Continuity software package, MedImmune, Cambridge

UK). All phage ELISA positive hits were assembled as fdDOG sequences and aligned according to the peptide insert region. After sequence alignment, identified unique sequences were summarised according to their sequence representation (i.e. number of times sequences had appeared), round of selection and library origin.

3.2.10. Multiple sequence alignment using ClustalW

ClustalW multiple sequence alignments were performed using Geneious R10 bio-informatics software package (Kearse et al., 2012). A global alignment of sequences with free end gaps was performed to determine the sequence homology amongst the 16 uniquely identified peptides. Additionally, this method was also used to determine the sequence homology between Pep1 and serotransferrin derived from human (accession №, P02787), mouse (accession №, Q921I1), and rat (accession №, P12346) species.

3.2.11. Predicting the molecular interaction of Pep1 with TfR

The molecular interaction of Tf with TfR was assessed using the previously described crystal structure (PDB ID 3S9M) and PDB Protein Workshop, (Moreland et al., 2005).

3.3. Results

3.3.1. Biotinylation of recombinant mouse TfR

Prior to initiating phage display selections using cyclic peptide libraries, it was necessary to introduce a secondary biotin affinity capture tag to the polyhistidine tagged recombinant mTfR material. This was done in order to utilise the strong biotin binding affinity towards streptavidin, for the purpose of antigenic immobilisation during soluble selections and protein binding assays.

The recombinant mTfR protein consists of the extracellular amino acids Cys89-Phe763, which are fused to an N-terminal polyhistidine tag. The complete sequences of the recombinant mTfR, hTfR and rat TfR (the latter only used for phage ELISA screening), are shown in Figure 3.3.1.

A **Mouse TFR extracellular domain (89-763), Length: 675AA**

CKRVEQKEECVKLAETEETDKSETMETEDVPTSS
RLYWADLKTLLSEKLNSIEFADTIKQLSQNTYTPRE
AGSQKDESLAYYIENQFHEFKFSKVWRDEHYVKI
QVKSSIGQNMVTIVQSNGNLDPVESPEGYVAFSK
PTEVSGKLVHANFGTKKDFEELSYSVNGSLVIVRA
GEITFAEKVANAQSFNAIGVLIYMDKNKFPVVEADL
ALFGHAHLGTGDPYTPGFPSFNHTQFPPSQSSGL
PNIPVQTISRAAAEKLFGKMEGSCPARWNIDSSCK
LELSQNQNVKLIVKNVLKERRILNIFGVIKGYEEPD
RYVVVGAQRDALGAGVAAKSSVGTGLLLKLAQVF
SDMISKDGFRPSRSIIFASWTAGDFGAVGATEWLE
GYLSSLHLKAFTYINLDKVVLGTSNFKVSASPLLYT
LMGKIMQDVKHPVDGKSLYRDSNWISKVEKLSFD
NAAYPFLAYSGIPAVSFCFCEDADYPYLGTRLDTY
EALTQKVPQLNQMVRTAAEVAGQLIIKLTHDVELN
LDYEMYNSKLLSFMKDLNQFKTDIRDMGLSLQWL
YSARGDYFRATSRLTTDFHNAEKTNRFVMREIND
RIMKVEYHFLSPYVSPRESPFRHIFWGSGSHTLSA
LVENLKLRQKNITAFNETLFRNQLALATWTIQGVA
NALSGDIWNIDNEFHHHHHH

B **Human TFR extracellular domain (119 – 761), Length: 671AA**

PAARRLYWDDLKRKLSEKLDSTDFTGTIKLLNENS
YVPREAGSQKDENLALYVENQFREFKLSKVWRDQ
HFVKIQVKDSAQNSVIIVDKNGRLVYLVENPGGYV
AYSKAATVTGKLVHANFGTKKDFEDLYTPVNGSIVI
VRAGKITFAEKVANAESLNAIGVLIYMDQTKFPIVN
AELSFFGHAHLGTGDPYTPGFPSFNHTQFPPSRS
SGLPNIPVQTISRAAAEKLFGNMEGDCPSDWKTD
STCRMVTSESKNVKLTVSNVLKEIKILNIFGVIKGFV
EPDHYVVVGAQRDAWGPGAAKSGVGTALLLKLA
QMFSDMVLKDGFQPSRSIIFASWSAGDFGSVGAT
EWLEGYLSSLHLKAFTYINLDKAVLGTSNFKVSAS
PLLYTLIEKTMQNVKHPVTGQFLYQDSNWASKVE
KLTLDNAAFPFLAYSGIPAVSFCFCEDTDYPYLGTT
MDTYKELIERIPELNKVARAAAEVAGQFVIKLTHDV
ELNLDYERYNSQLLSFVRDLNQYRADIKEMGLSLQ
WLYSARGDFFRATSRLTTDFGNAEKTDRFVMKKL
NDRVMRVEYHFLSPYVSPKESPFRHVFWGSGSH
TLPALLENLKLRKQNNGAFNETLFRNQLALATWTI
QGAANALSGDVWDIDNEFGLNDIFEAQKIEWHEG
GHHHHHHHHHH

C **Rat TFR extracellular domain (100-761), Length: 684AA**

LAEAEEADKSENDETEYVPKSSRLFWADLKTLLSEKLNSIEFTDIIKQLSQNTYTPREAGSQKDENLAYYIENL
FHDFKFSKVWRDEHYVKIQVKNSVSQNLVTINSGSNIDPVEAPEGYVAFSKAGEVTGKLVHANFGTKKDFEE
LNYSVNGSLVIVRAGKITFAEKVANAQSFNAIGVLIYMDRNTFPVVEADLQFFGHAHLGTGDPYTPGFPSFNH
TQFPPSQSSGLPSIPVQTISRAAAEKLFKNMEGNCPPSWNIDSSCKLELSQNQNVKLTVNNVLKETRILNIFGV
IKGYEEPDRYIVVGAQRDAWGPGVAKSSVGTGLLLKLAQVFSDMISKDGFRPSRSIIFASWTAGDYGAVGAT
EWLEGYLSSLHLKAFTYINLDKVVLGTSNFKVSASPLLYTLMGKIMQDVKHPIDGKYLYRDSNWISKIEELSLD
NAAFPFLAYSGIPAVSFCFCEDEDYPYLGTKLDTYEILIQKVPQLNQMVRTAAEVAGQFIIKLTHDIELTLDYEM
YNSKLLSFMKDLNQFKADIKDMGLSLQWLYSARGDYFRATSRLTTDFHNAEKTNRFVMREINDRIMKVEYHF
LSPYVSPRESPFRHIFWGSGSHTLSALVENLRLRQKNITAFNETLFRNQLALATWTIQGVANALSGDIWNIDN
EFAAADYKDDDDKAAHHHHHHHHHH

Figure 3.3.1: Amino acid sequence of the extracellular domain of mouse TfR.

Figure showing the amino acid sequence of the extracellular domains of recombinant mouse **(A)**, human **(B)**, and rat TfR **(C)**.

The biotinylation of mTfR was evaluated by means of a functional biotinylated antigen capture and presentation ELISA (Figure 3.3.2). A monoclonal anti-mTfR specific antibody (8D3) was used to detect the captured biotinylated mTfR on streptavidin coated 96-well plates. Biotinylated mTfR/8D3 binding demonstrated a sigmoid binding curve. Saturation of 8D3 anti-mTfR binding was observed at a bio-mTfR concentration of 1.1 µg/ml. As expected, no binding was observed with the irrelevant biotin-insulin and biotin-hTfR control antigens.

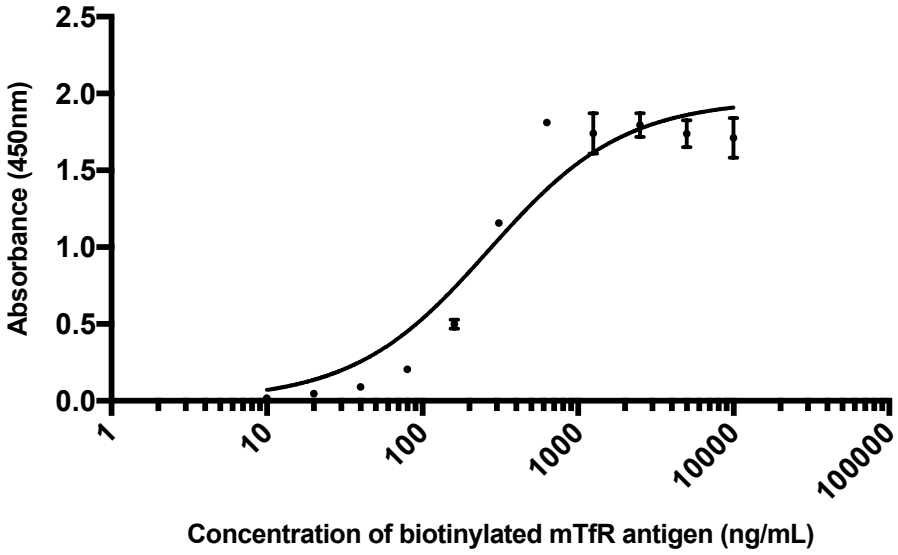

Figure 3.3.2: Validating the biotinylation of mTfR-His6 using anti-mouse TFR (8D3) antibody.

Summary of biotinylated mTfR-His6 antigen validation as determined via antigen presentation ELISA. Biotinylated mTfR-His6 was immobilised onto a streptavidin coated 96-well plate in a serial dilution starting at 10 µg/ml. Anti-mouse TfR antibody (8D3) was then used for detection at a concentration of 1 µg/ml. Results are expressed as averages of three experimental replicates (n= 3) ± SEM, with the average secondary antibody control reading subtracted.

3.3.2. Cyclic peptide phage display selection summary and input/ output titres.

A summary of the TfR CPEP library selection conditions are shown in Table 3.3.1. In order to assess the success of a selection round, it is necessary to evaluate the number phage particles that are to be introduced into a selection (input titre), and the number of phage particles that result from a selection (output titre). By comparing the input to output titres between rounds, it is possible to monitor the efficiency of the selection and hence the level of enrichment. The enrichment factor in relation to round 1 was calculated by dividing the input/output titres of round 1 to that of the relevant successive selection rounds.

Monitored phage input and output average titre results for the four rounds of selection are shown in Table 3.3.2. As expected, input titres were within the range of 5×10^{12} cfu and 5×10^{13} cfu throughout the four selection rounds. For the first round of selection, input/output titres were observed within the range of $10^{7} – 10^{8}$ cfu. Enrichment is observable from round 2 as indicated by a decrease in the input/output titres and an increase in the enrichment factor. The greatest degree of enrichment at round 2 was observed with hTfR selections (8, 10, 12) with the CPEP2 library demonstrating the highest enrichment factor.

The greatest degree of enrichment was observed at round 3 of the four selection rounds. Enrichment was substantially higher for the hTfR selections (14, 16 and 18) than the mTfR selections (13, 15 and 17), with the CPEP3 library selection (18) demonstrating the largest increase in enrichment factor. Interestingly, the switch from human to mouse TfR antigen at the round 3 cross-species antigen selected outputs (19, 20 and 21), resulted in a reduced enrichment factor for the CPEP1 and CPEP2 libraries when compared to the previous round. The CPEP3 library was the only cross selection to result in increased enrichment (21).

Following the fourth and final round of selection towards bEnd.3 cells, low enrichment factor values were observed for all sections (22 – 27) when compared to the relevant round 3 outputs. The lowest enrichment factor was noted with the three pools, 25, 26 and 27, originating from the cross antigen selected to mTfR selected phage pools.

Table 3.3.1: Cyclic peptide phage display selection round conditions.

Selection ID	Round	Peptide Library	Antigen	Antigen Conc. (nM)	Washes
1	1	CPEP1	mTfR	200	5
2	1		hTfR	200	5
3	1	CPEP2	mTfR	200	5
4	1		hTfR	200	5
5	1	CPEP3	mTfR	200	5
6	1		hTfR	200	5
7	2	CPEP1	mTfR	200	5
8	2		hTfR	200	5
9	2	CPEP2	mTfR	200	5
10	2		hTfR	200	5
11	2	CPEP3	mTfR	200	5
12	2		hTfR	200	5
13	3	CPEP1	mTfR	100	5
14	3		hTfR	100	5
15	3	CPEP2	mTfR	100	5
16	3		hTfR	100	5
17	3	CPEP3	mTfR	100	5
18	3		hTfR	100	5
19	3	CPEP1	hTfR → mTfR cross	100	5
20	3	CPEP2	hTfR → mTfR cross	100	5
21	3	CPEP3	hTfR → mTfR cross	100	5
22	4	CPEP1	R3 Library 1 mTfR	2 x 10^6 cells	5
23	4	CPEP2	R3 Library 2 mTfR	2 x 10^6 cells	5
24	4	CPEP3	R3 Library 3 mTfR	2 x 10^6 cells	5
25	4	CPEP1	R3 Library 1 cross → bEnd.3 cells	2 x 10^6 cells	5
26	4	CPEP2	R3 Library 2 cross → bEnd.3 cells	2 x 10^6 cells	5
27	4	CPEP3	R3 Library 3 cross → bEnd.3 cells	2 x 10^6 cells	5

Table 3.3.2: CPEP library phage input and output titres, and enrichment factor with TfR selection progression.

Table showing the average input and output titres for TfR selected CPEP libraries at each selection round. The input to output titre and calculated enrichment factor in relation to round 1 are also shown. cfu, colony forming units.

Selection ID	Round	Peptide Library	Input Titre (cfu/ml)	output Titre (cfu/ml)	Input/output (cfu/ml)	Enrichment factor (arbitrary units)
1	1	CPEP1	5.1×10^{13}	6.8×10^{5}	7.5×10^{7}	1
2	1		5.1×10^{13}	6.2×10^{5}	8.2×10^{7}	1
3	1	CPEP2	4.6×10^{13}	5.87×10^{5}	7.8×10^{7}	1
4	1		4.6×10^{13}	6.27×10^{5}	7.3×10^{7}	1
5	1	CPEP3	5.2×10^{13}	5.2×10^{5}	1.0×10^{8}	1
6	1		5.2×10^{13}	3.44×10^{5}	1.5×10^{8}	1
7	2	CPEP1	6.82×10^{13}	1.14×10^{5}	5.9×10^{8}	0.125
8	2		3.78×10^{13}	6.21×10^{6}	6.0×10^{6}	13.514
9	2	CPEP2	2.64×10^{13}	9.31×10^{5}	2.8×10^{7}	2.764
10	2		2.56×10^{13}	6.13×10^{7}	4.1×10^{5}	175.675
11	2	CPEP3	4.35×10^{13}	3.33×10^{5}	1.3×10^{8}	0.766
12	2		2.25×10^{13}	2.93×10^{6}	7.6×10^{6}	19.685
13	3	CPEP1	3.77×10^{13}	2.12×10^{7}	1.7×10^{6}	42.175
14	3		2.84×10^{13}	1.10×10^{9}	2.5×10^{4}	3186.052
15	3	CPEP2	9.08×10^{12}	7.2×10^{7}	1.2×10^{6}	62.139
16	3		1.02×10^{13}	3.92×10^{8}	2.6×10^{4}	2819.527
17	3	CPEP3	1.37×10^{13}	2.13×10^{7}	6.4×10^{5}	155.474
18	3		1.05×10^{13}	7.69×10^{8}	1.3×10^{4}	11070.875
19	3	CPEP1	2.84×10^{13}	1.01×10^{6}	2.8×10^{7}	2.925
20	3	CPEP2	1.02×10^{13}	1.8×10^{5}	5.6×10^{7}	1.295
21	3	CPEP3	1.05×10^{13}	8.23×10^{6}	1.2×10^{6}	118.483
22	4	CPEP1	1.23×10^{13}	8.9×10^{5}	1.3×10^{7}	5.427
23	4	CPEP2	2.03×10^{13}	5.8×10^{5}	3.5×10^{7}	2.239
24	4	CPEP3	1.02×10^{13}	8.0×10^{5}	1.2×10^{7}	7.843
25	4	CPEP1	1.15×10^{13}	2.8×10^{5}	4.1×10^{7}	2.003
26	4	CPEP2	2.33×10^{13}	1.02×10^{6}	2.2×10^{7}	3.212
27	4	CPEP3	7.17×10^{12}	1.4×10^{5}	5.1×10^{8}	0.295

3.3.3. Identification of species cross-reactive TfR binding cyclic peptides by phage ELISA.

Initial phage ELISA screening plate layout and screening reports are shown in supplementary Figure S4. A summary of the initial phage ELISA screen is shown in Figure 3.3.3. In total, of the 1584 clones that were screened for binding to mTfR, hTfR and the irrelevant control antigen (insulin), 875 (56%) specific TfR binding hits were identified across all selections. Identified hits were composed of, 197 (22.5%) TfR species cross-reactive, 367 (42%) human TfR specific and 311(35.5%) mouse TfR specific hits.

Interestingly, the majority of species cross-reactive hits were observed to originate from the round 4 non-cross antigen and bEnd.3 cell selected pool (135 hits). Moreover, this pool generated no human TfR specific binders. Most human TfR specific hits were observed within the round 3 antigen cross-selected pool. The switch from human TfR at rounds 1 and 2 towards mouse TfR antigen at round 3, did not result in the enrichment of many mTfR specific binders (four hits were identified). Also, the inclusion of a fourth bEnd.3 cell selection round to the round 3 antigen cross-selected pool resulted in an increase in the number of mTfR specific hits (12 up from 4) and a reduction of the number of hTfR specific (168 down from 199) and species cross-reactive hits (16 down from 46).

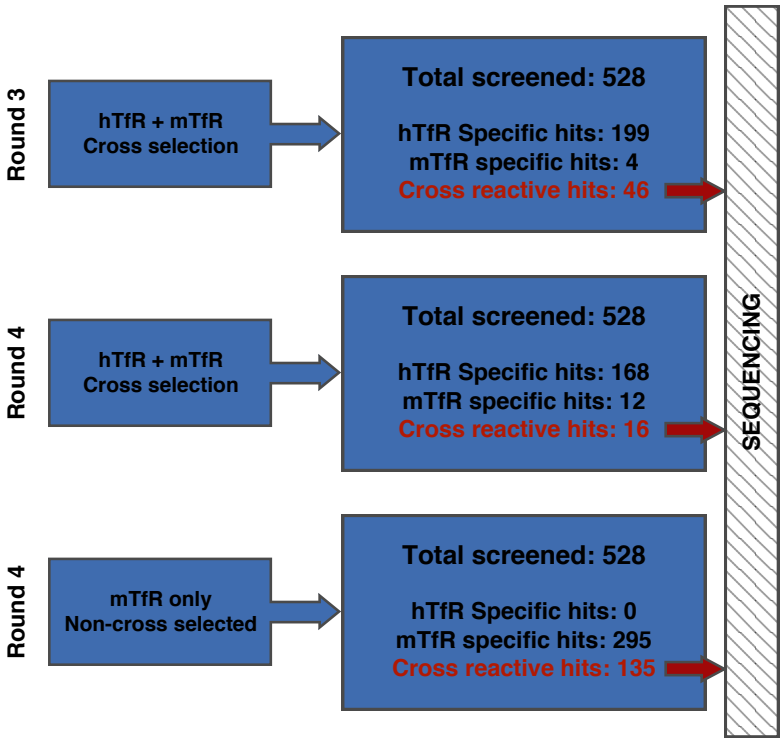

Figure 3.3.3: Phage ELISA initial screen hit output summary.

The numbers of mTfR specific, hTfR specific and species cross-reactive hits per selection cascade are shown. Only cross-species TfR binding hits were taken forward for sequence analysis.

3.3.4. Summary of fdDOG sequence analysis and lead peptide identification.

The phage ELISA pre-identified cross-species binding clones were sequenced and aligned according to the variable peptide coding region. Sequence alignment results are shown in supplementary figure S5. A summary of the peptide sequence analysis showing the amino acid sequence, nucleotide sequence and sequence representation is shown in Table 3.3.3. In total, 16 unique peptide sequences were identified. Six unique sequences were identified from CPEP1, four from CPEP2 and six from CPEP3. The most highly represented peptide sequence, Pep10, originated from the CPEP2 library which was selected against mTfR. Pep10 was represented 104 times, accounting for more than half of the total observed hits. The next top 4 candidates were Pep1 (represented 36 times), Pep9 (23 times), Pep6 (14 times) and Pep4 (5 times). Pep1 was identified from two independent selection cascades, Round 3 hTfR to mTfR cross-selection and the Round 4 mTfR only and cell selection cascade.

Table 3.3.3: Sequence analysis summary of identified cross-species TfR binding peptide hits.

Summary table showing the amino acid sequences, nucleotide sequences and sequence representation for each identified lead cross-species TfR binding cyclic peptide. Peptide sequences are sorted in descending order of highest sequence representation. Yellow highlights in the amino acid sequence show the position of the cysteine residues which form a constrained structure through disulphide linkages.

Peptide ID	Library	selection round	Description	AA sequence	Nucleotide sequence	Sequence representation
Pep10	CPEP2	Round 4	CPEP2 Non-cross mouse TfR selection	LHECTYYWWGLDCSFR	TTGCACGAGTGTACGTA CTACTGGTGGGGGTTG GACTGTTCCTTCCGG	104
Pep1	CPEP1	Round 3	CPEP1 human/ mouse TfR cross-selection	WSIIDCSMNYCLYIEG	TGGTCCATCATCGACTG TTCCATGAACTACTGTT TGTACATCGAGGGG	36
Pep9	CPEP2	Round 4	CPEP2 Non-cross mouse TfR selection	ARDCLETWYGFTCWNV	GCCCGGGACTGTTTGG AGACCTGGTACGGCTTC ACCTGTTGGAACGTC	23
Pep6	CPEP1	Round 4	CPEP1 Cross/ bEnd.3 cell selection	GWHPMCNLMACSQGRP	GGCTGGCACCCGATGT GTAACTTGATGGCGTGT TCCCAGGGGCGCCCG	14
Pep4	CPEP3	Round 4	CPEP3 Cross/ bEnd.3 cell selection	LYCYPTKLPWVEYCHE	CTCTACTGTTACCCGAC GAAGCTCCCCTGGGTC GAGTACTGTCATGAA	5
Pep3	CPEP1	Round 3	CPEP1 human/ mouse TfR cross-selection	TTFPSCHPQTCYDGVQ	ACGACCTTCCCCTCCTG TCACCCGCAGACGTGTT ACGACGGCGTGCAG	4
Pep11	CPEP1	Round 4	CPEP1 Non-cross mouse TfR selection	WTIAVCGKQGCEYVWE	TGGACCATCGCGGTCTG TGGCAAGCAGGGCTGT GAGTACGTGTGGGAG	2
Pep2	CPEP3	Round 3	CPEP3 human/ mouse TfR cross-selection	IHCHPQGDQSVSFCWR	ATCCACTGTCACCCCCA GGGCGACCAGAGCGTC TCCTTCTGTTGGCGG	1
Pep5	CPEP2	Round 4	CPEP2 Cross/ bEnd.3 cell selection	ADNCQTFYPLSWCESQ	GCCGACAACTGTCAGA CGTTCTACCCGTTGTCG TGGTGTGAGTCCCAG	1
Pep7	CPEP1	Round 4	CPEP1 Cross/ bEnd.3 cell selection	LPTKTCPCLWCCAEDW	CTCCCCACCAAGACCTG TCCGTGCTTGTGGTGTT GCGCCGAGGACTGG	1
Pep8	CPEP2	Round 4	CPEP2 Non-cross mouse TfR selection	SYNCVTRWWGITCEMY	AGCTACAACTGTGTGAC GCGCTGGTGGGGGATC ACCTGTGAGATGTAC	1
Pep12	CPEP1	Round 4	CPEP1 Non-cross mouse TfR selection	TWHYQCITMNCDVLVG	ACGTGGCACTACCAGT GTATCACCATGAACTGT GACGTGTTGGTGGGG	1
Pep13	CPEP3	Round 4	CPEP3 Non-cross mouse TfR selection	WVCTPLDSEIIEICQL	TGGGTCTGTACCCCGCT CGACTCCGAGATCATCG AGATCTGTCAGCTG	1
Pep14	CPEP3	Round 4	CPEP3 Non-cross mouse TfR selection	SICRTVILDTLYLCDE	TCCATCTGTCGCACCGT CATCTTGGACACGCTGT ACCTGTGTGACGAG	1
Pep15	CPEP3	Round 4	CPEP3 Non-cross mouse TfR selection	LHCTSIWSDVVQLCDL	TTGCACTGTACCTCCAT CTGGAGCGACGTGGTG CAGTTGTGTGACCTC	1
Pep16	CPEP3	Round 4	CPEP3 Non-cross mouse TfR selection	PLCTPIFPPFVLMCEE	CCCCTCTGTACGCCCAT CTTCCCGCCGTTCGTGT TGATGTGTGAGGAG	1

3.3.5. Sequence homology of the 16 unique peptides

A ClustalW sequence alignment was performed to determine whether the sequences of the 16 uniquely identified peptides shared any homologous amino acid residues or motifs (Figure 3.3.4). The two peptides Pep8 and Pep10, derived from the CPEP2 library, were identified to contain a highly hydrophobic, four amino acid motif consisting of 'WWGΘ' (where Θ refers to the hydrophobic amino acid residues I or L). Moreover, another peptide derived from CPEP2 library, Pep9 appears to be a variant containing 'WYGF' at identical locations to the 'WWGΘ' motif of Pep8 and Pep10 (peptide AA 8 – 11). Pep10 also shares homology with Pep1 and contains a three amino acid sequence of 'DCS' combined with 'WWGΘ' motif and a portion of a previously described Tf homologous '**FR**SETKD' (Dai et al., 2014).

Pep4 and Pep16 were also identified to contain a highly hydrophobic set of residues within their loop region. Pep13, Pep15 and Pep16 and Pep4 appear to also show preference for the motif 'CTPΘ' at AA positions 3 – 6. The streptavidin binding motifs 'HPQ' and 'HPM' were also identified within the sequences of Pep2, Pep3 and Pep6, and these are predicted to be streptavidin binding clones.

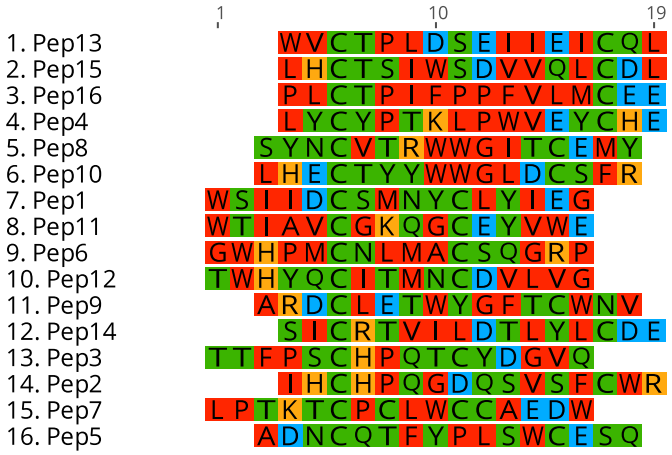

Figure 3.3.4: Sequence homology of 16 unique peptide sequences.

ClustalW multiple sequence alignment of the 16 uniquely identified peptides. Amino acid key, negatively charged (blue), positively charged (orange), polar (green) and non-polar (red). Figure generated using Geneious 11 software package.

3.3.6. Re-evaluation of the 16 sequence validated cross-species TfR binding cyclic peptides

Following the sequencing and identification of the 16 unique TfR species cross-reactive peptides, a repeat phage ELISA was conducted to validate the binding of these peptides towards mouse, human, and rat TfR antigens. Sequence validated clones containing the 16 unique peptide sequences were screened towards each of the three TfR antigens. A control antigen of similar size and charge to TfR was included to evaluate the specificity of the peptides towards TfR (confidential protein, contact George Thom, MedImmune, Cambridge, UK). A summary of the results is shown in Figure 2.3.5.

All sixteen peptides did not show any observable binding towards the control antigen. Fourteen of the sixteen uniquely pre-identified peptides were found to bind to mouse, human or rat TfR with varying binding profiles. Most notably, Pep1, Pep8, Pep9, and Pep10 exhibited the highest absorbance readings across all TfR antigens.

Interestingly, although initially identified as being positive for both mouse and human TfR, Pep2, Pep3 and Pep6 were discovered to be false positives following re-evaluation.

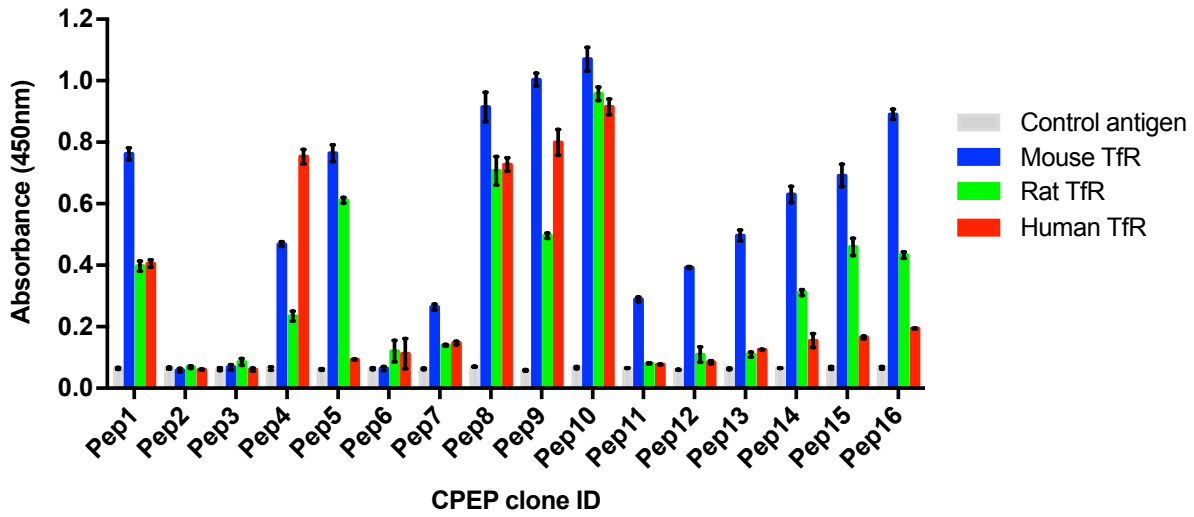

Figure 3.3.5: Phage ELISA screening summary of uniquely identified hits against mouse, human and rat TfR.

The sixteen unique anti-TfR species cross-reactive binding peptides were re-evaluated towards biotinylated mouse, human and rat TfR antigens by means of a phage ELISA. Two false positive hits, Pep2 and Pep3, were identified upon re-evaluation. The highest absorbance readings towards

mouse, human and rat TfR were observed with Pep1, Pep8, Pep9 and Pep10. Results are expressed as means of three experimental replicates (n= 3) ± SEM.

Some promising examples of peptides from the 16 unique clones were re-evaluated via a phage ELISA towards three additional control antigens (confidential proteins, contact George Thom, MedImmune, Cambridge, UK). This was carried out in order to confirm the target specificity of these peptides towards TfR. Results of the phage ELISA are shown in Figure 3.3.6.

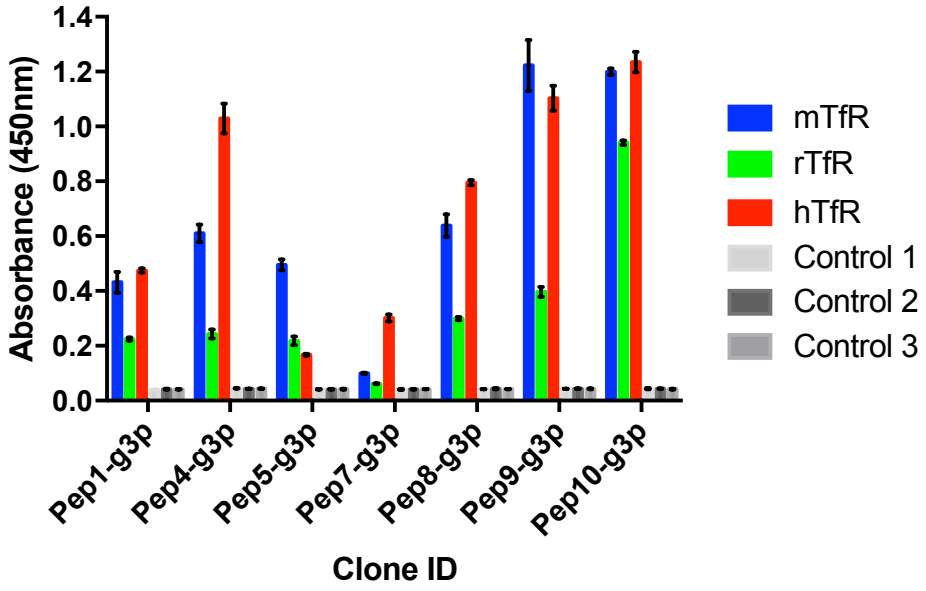

Figure 3.3.6: Binding re-evaluation of Pep-g3p clones towards biotinylated TfR by phage ELISA.

Peptides were re-evaluated for binding mouse, human and rat TfR in conjunction to an additional three control antigens, to validate specificity of the selected peptides towards TfR. Results are expressed as means of three experimental replicates (n=3) ± SEM.

All peptide candidates demonstrated various binding profiles towards mTfR, hTfR and rTfR. Once again Pep10 appears to demonstrate the highest absorbance readings towards the three TfR antigens. No binding was observed with any Pep-g3p clones towards the three control antigens, thus confirming the specificity of these peptide clones towards mouse, human and rat TfR.

3.3.7. Pep1 demonstrates homology with highly conserved residues on transferrin C-lobe.

To determine whether any of the identified unique peptide sequences shared sequence homology with the natural ligand of TfR, transferrin, a ClustalW multiple sequence alignment was performed using each of the 16 identified peptide sequences towards the sequence for human, mouse and rat serotransferrin (accession IDs: P02787, Q921I1, and P12346, respectively). Pep1 was identified to contain a homologous sequence to a highly conserved region of Tf (AA residues 633 – 648 within multiple alignment), consisting of the nine-amino acid sequence 'DCSGNFCLF', (Figure 3.3.7).

In order to predict a potential mechanism for Pep1 binding to TfR, the crystal structure previously described by Eckenroth *et al*. (2011) was analysed using PDB Protein Workshop, PDB ID: 3S9M. The homologous sequence of Pep1 (DCSGNFCLF) was identified at amino acid residues 614 - 622 and is located within the loop region within C1 subdomain of the C-lobe of Tf, (Figure 3.3.8). Furthermore, the amino acid asparagine 618 within this loop region appears to form an interaction with arginine 629, at αIII-2 helix of the helical domain of TfR, (Figure 3.3.8, B).

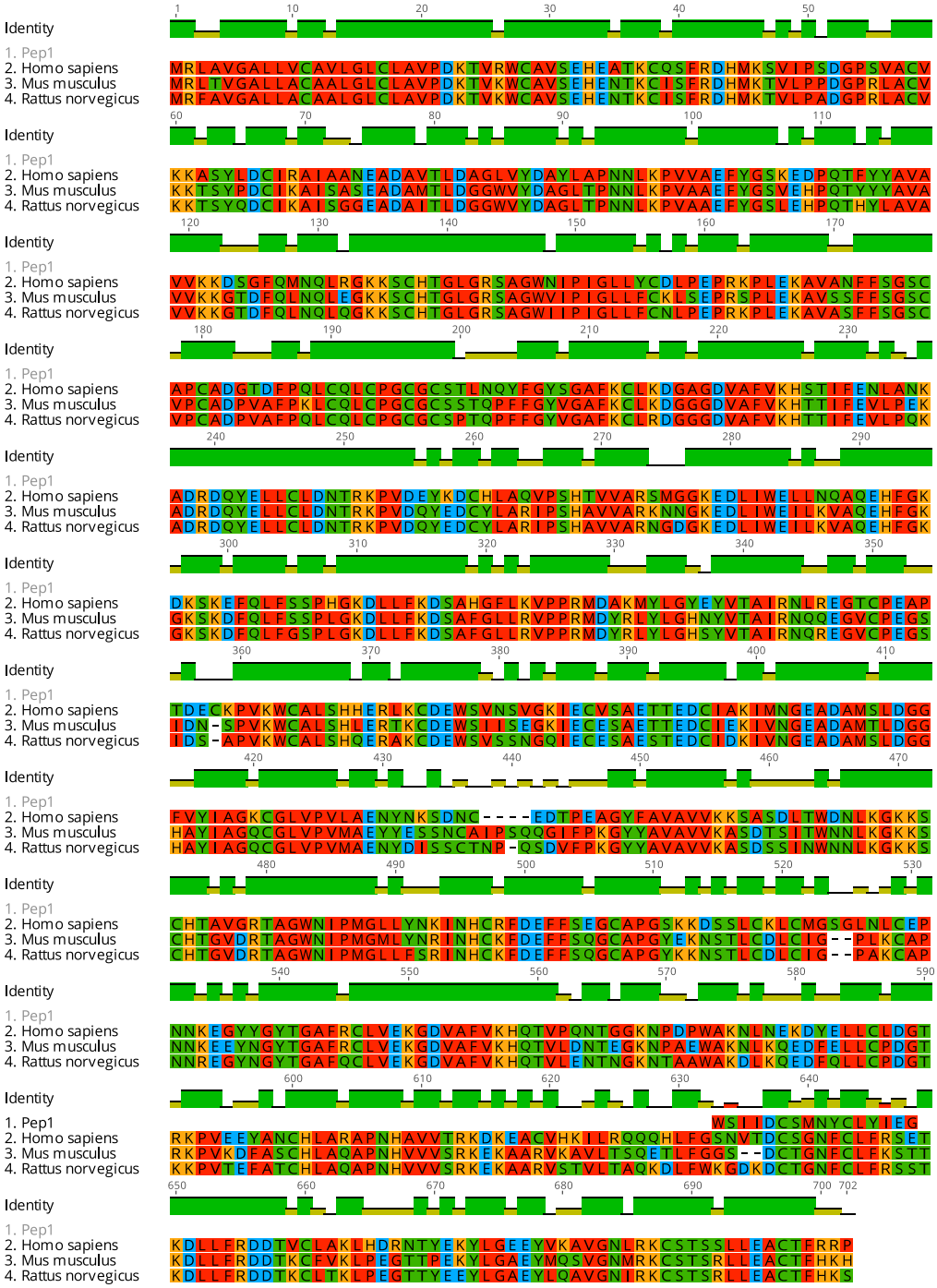

Figure 3.3.7: Sequence homology of Pep1 towards human, mouse and rat transferrin.

ClustalW multiple sequence alignment of transferrin derived from human (accession №, P02787), mouse (accession №, Q921I1), and rat (accession №, P12346). The sequence of Pep1 was also included in the alignment. Pep1 aligned with transferrin at amino acid residues 633 – 648 and demonstrated strong homology with a nine-residue motif that is highly conserved across the three evaluated species. Amino acid key, negatively charged (blue), positively charged (orange), polar (green) and non-polar (red). Figure generated using Geneious 10 software package.

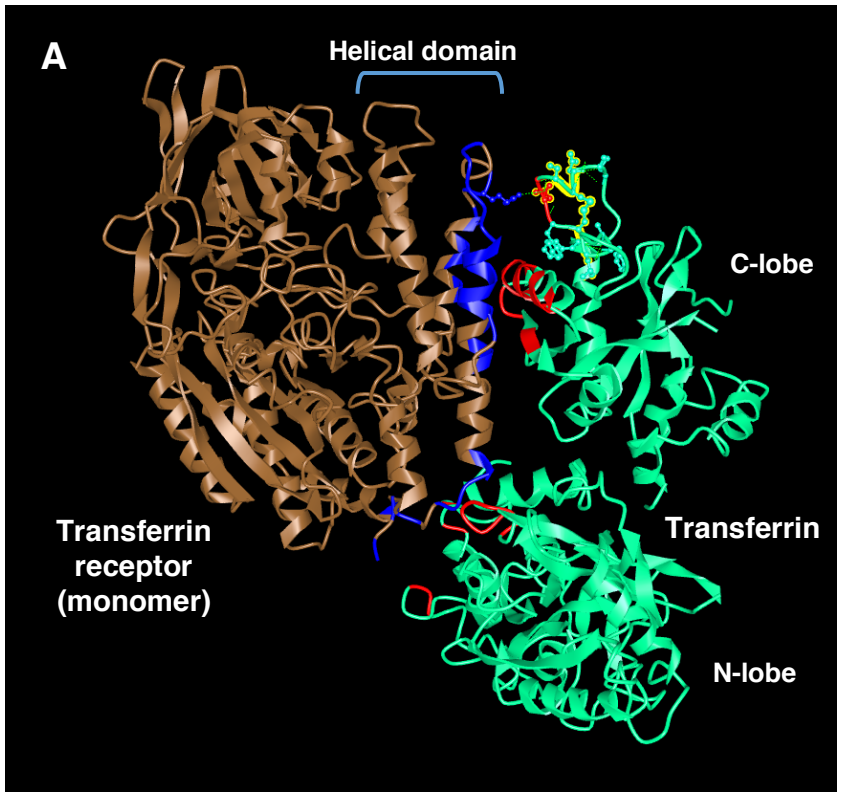

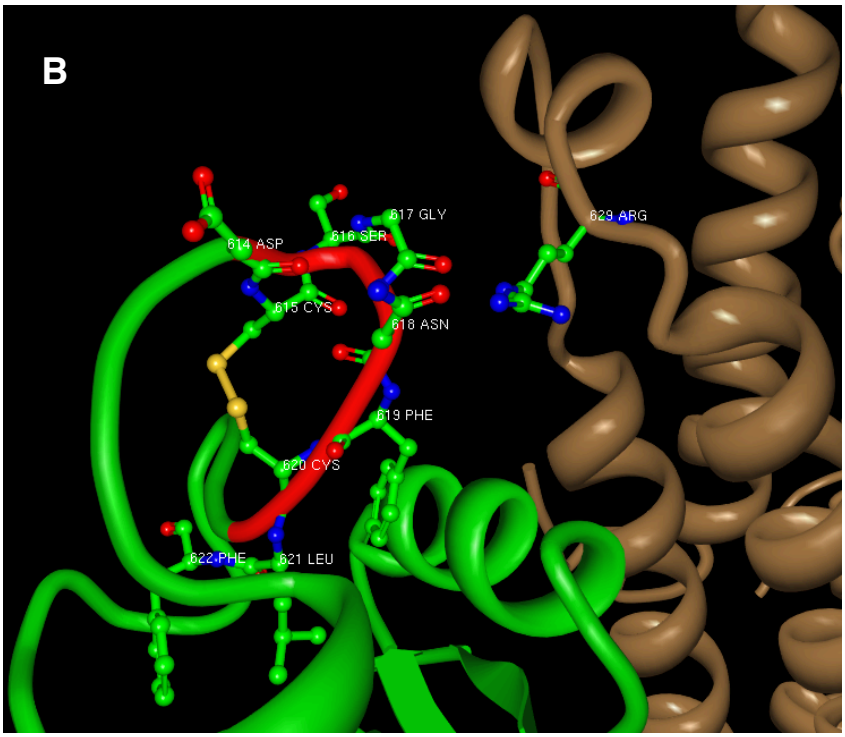

Figure 3.3.8: Predicted interaction of Pep1 with transferrin receptor monomer.

Figure showing the interaction sites between the TfR monomer (brown) and the C-lobe and N-lobe of transferrin (green), A. Interaction sites on the TfR monomer are labelled in blue, whilst interaction sites on transferrin are labelled in red. Conserved residues between Pep1 and the C-lobe of transferrin are highlighted in yellow. A close up of the interacting side chains of labeled Tf residues is shown in, B. The nine-residue sequence of Tf that demonstrates homology with Pep1 is highlighted

in red and the individual residues are labelled. The disulphide bond between the two cysteine residues is shown in yellow. The side chain of ASN618 on the Tf C-lobe interacts with the side chain of Arg629 located on the TfR helical domain (also shown). Figure produced using PDB Protein Workshop. PDB ID: 3S9M.

3.4. Discussion

3.4.1. Biotinylated mTfR maintains anti-mouse specific 8D3 antibody binding activity.

Phage display as an *in vitro* combinatorial library selection technique relies upon effective separation methods to partition the subset of target binding phage molecules from a large library of non-binding species (Carmen and Jermutus, 2002). In order to select molecules that bind to the target in its natural state, it is imperative that the solid phase immobilisation method does not interfere with the structure of the target molecule and that all epitopes of the molecule remain exposed for contact with phage particles (Koide et al., 2009). In early iterations of phage display, the use of non-specific adsorptive based target capture methods such as polystyrene coated plate surfaces, posed issues for the capture of targets and the separation of bound phage molecules from the unbound pool. These methods often lead to non-uniform immobilisation of targets (Adey et al., 1995), denaturation of target antigen (Friguet et al., 1984; Butler et al., 1992), blocking of target epitopes and through non-specific elution protocols, the recovery of phage molecules that non-specifically bound to the support surface (Koide et al., 2009). In order to overcome these problems, more specific affinity capture methods were introduced such as biotin capture using streptavidin.

Target proteins are labelled with biotin through enzymatic (Barat and A. M. Wu, 2007; Scholle et al., 2004) or most commonly via chemical approaches, the latter of which utilises reactive groups connected via a linker to a biotin moiety (Elia, 2008). Due to its small size (244 Da), biotin may be conjugated to proteins without disrupting biological activity (Alegria-Schaffer, 2014). In the context of phage display, immobilisation of biotinylated antigens to a streptavidin matrix was shown to not only provide greater density and bioactivity of molecules than non-specific adsorption, but also allowed the target antigen to be immobilised in solution phase on streptavidin-coated agarose beads (Hawkins et al., 1992). This protocol confers several

advantages over panning selections. Firstly, it allows for a greater number of epitopes to be available for phage interaction, whilst also avoiding the loss of low abundance high affinity clones through the preferential selection of high avidity molecules. N-Hydroxysuccinimide (NHS) esters of biotin react with primary amines available on the surface of proteins and these are mostly from the ε-amino and α-amino groups of lysine and N-terminal region, respectively (Tao et al., 2005).

Biotinylation was performed according to the optimised conditions described within the manufacturer protocol, which typically result in a maximum of 4 – 6 biotins per protein molecule (ThermoFisher Scientific, 2016). A functional assessment of the biotin labelled protein was carried out via streptavidin capture and antigen presentation ELISA titred against a protein specific antibody. Validation results for the biotinylation of mTfR material using an anti-mTfR (8D3) antibody resulted in dose dependant sigmoid binding curve, suggesting that biotinylated protein capture and detection was successful.

3.4.2. Sequence analysis resulted in the identification of thirteen cross-species binding sequences.

Since its conception in 1985, phage display has evolved over the years into a powerful tool for the efficient screening of ligands towards protein and non-protein targets from a diverse library consisting of peptides or proteins expressed as fusions to bacteriophage coat proteins. Through a process termed bio-panning, the phage libraries are screened against target molecules immobilised onto a solid phase matrix. Although this method is highly effective at selecting target specific ligands, target-unrelated phage (TUP) clones are often non-intentionally enriched through the interaction of the phage library with components of the screening technique (Bakhshinejad and Sadeghizadeh, 2016). Some of these non-target components include, the capture matrix (streptavidin, Ni-NTA, protein A), components of the blocking reagent (BSA or Milk), contaminating expression by-products within target antigen solution and solid phase immobilisation components (agarose and polystyrene plastic). By far, the most commonly identified TUPs tend to be polystyrene binding clones. Many polystyrene binding sequences have been identified even when using pre-blocking protocols (Adey et al., 1995).

In addition, TUP clones may be more readily propagated during replication, and their enrichment within a selected pool does not necessarily represent their affinity towards the target. This is usually due to the inherent structure of the peptide or protein displayed on the surface of the bacteriophage and its effect on virion infectivity. Phage displayed peptides or proteins expressed as multivalent g3p fusions can result in reduced overall infectivity due to steric hindrance between the N2 domain and F-pilus (Carmen and Jermutus, 2002). However, the expression of peptides shorter than 50 residues does not have a significant impact on infectivity. Also, since phage display functions on the principle linkage between genotype and phenotype, mutations arising within the phage genome can result in increased or decreased propagation of certain peptides dependant on how their structure effects the replication process. The use of fd-tet based libraries, such as the CPep libraries used for our TfR selections (Bonetto et al., 2009), minimises the possibility of propagation-related TUP mutations (Thomas et al., 2010).

A known example of a propagation related peptide is the HAIYPRH peptide. This peptide was initially discovered by Lee *et al*. (2001) when carrying out selections against human TfR using the commercially available Ph.D.-7 heptapeptide library, and later coined ‘T7’ peptide. Its specificity towards hTfR was later contested when several other labs were able to isolate the same sequence towards a host of different targets including, chromatin high mobility group protein 1 (Dintilhac and Bernués, 2002), Zn2+ ions (Brammer et al., 2008), and human umbilical vein endothelial cells (Maruta et al., 2003) intriguingly however, multiple studies have recently utilised this peptide as a glioma TfR targeting strategy and demonstrated its therapeutic targeting capability *in vitro* and *in vivo* (Yunke Bi et al., 2016; Yanna Cui et al., 2016; Yue Zhang et al., 2017).

To summarise the selection process, three cascades using three different cyclic peptide libraries were conducted in order to assess which protocol and library would generate the most target specific hits towards TfR. The rationale behind utilising a combined recombinant protein and cell selection approach was to identify species cross-reactive peptides that are capable of binding to TfR, and are internalised within functional brain endothelial cells.

Rodent models are extensively used within pre-clinical studies to evaluate the toxicity, efficacy, pharmacokinetics, and pharmacodynamics of drugs (Betts et al., 2016; Fan and Neubert, 2016; Myzithras et al., 2016) The specificity and precision targeting capability of biologics such as antibodies and peptides towards their target proteins, in most circumstances results in species specific domains that either only react with human protein variants, or their rodent counterparts with which they are evaluated. This results in difficulty with interpretation of pre-clinical data and its translatability to human studies (H. Park et al., 2017). The identification of species cross-reactive binding domains is a highly sought after characteristic for biologic drug development, as it typically improves the safety, efficacy and the success rate of a drug candidate going forward from animal pre-clinical to human clinical studies (Irani et al., 2016).

Assessment of the enrichment factor as calculated via input and output titres of each selection round revealed information about the selection rounds and the CPEP library that demonstrated the highest stringency. Beginning at round 2 greater enrichment was observed with the hTfR selections than the mTfR selections. The enrichment factor of hTfR selections at round 3 was substantially higher than that observed with round 2. One potential reason for this high degree of enrichment observed with hTfR selections is the propagation of sequences with an amplification bias or TUP clones towards the immobilisation matrix (Thomas et al., 2010). The mTfR selections did not demonstrate the highest degree of enrichment, however, they contributed the majority of TfR species cross-reactive unique peptides, (Table 3.3.3 and Figure 3.3.6).

The transition from hTfR to mTfR at round 3 resulted in low enrichment for CPEP1 and CPEP2 libraries (enrichment factor, 2.9 and 1.3, respectively). However, CPEP3 libraries showed a relatively high enrichment factor (118.5), suggesting further enrichment had occurred with that particular library. Interestingly, the introduction of a cross-selection cascade at round 3 lead to reduction in output titres when compared with the round 3 non-cross selected outputs. This was likely due to increased stringency of selection introduced by the inclusion of a secondary target antigen species, in this case mouse TfR. Very few of the phage particles that had

been pre-selected towards human TfR were also mouse specific, and therefore these are lost from the pool leading to a reduced output titre.

At round 4, this finding of reduced output titres is re-iterated with the introduction of cell selections against bEnd.3 mouse brain endothelial cells. The greater selection stringency requires enriched clones to not only bind to functional TfR expressed on cells in its natural conformation, but also to be internalised within cells, since a cell membrane stripping agent (TEA) was used in order to remove non-internalising phage particles.

Following initial phage ELISA screening we unexpectedly observed that the majority of cross-species binding hits originated from the round 4 non-cross antigen and bEnd.3 cell selected pool. This amounted to 68.5% of all cross-species binding hits. This finding was unexpected as this pool was preferentially partitioned towards mouse TfR throughout the entire selection cascade and one would expect that cross-species binding hits would mostly originate from cross-selected cascades. This was later identified to be due to the enrichment of one particular peptide sequence, LHECTYYWWGLDCSFR, which pre-dominated within the Round 4 non-cross selected output.

Sequence analysis of pre-identified species cross-reactive hits revealed a total of 16 unique peptide sequences. A unique peptide sequence is defined as a sequence that differs from another through at least one amino acid and is represented within a selected pool at least once. The most highly represented cross-species binding sequence was Pep10, LHECTYYWWGLDCSFR, which had originated from the aforementioned Round 4 mouse TfR selection cascade. Previous studies have established that peptide sequences that consist largely of aromatic amino acids (i.e. tyrosine, tryptophan, and phenylalanine) are most likely to be TUPs such as plastic specific binders (Adey et al., 1995; Gebhardt et al., 1996). However, it is important to note that not all highly hydrophobic sequences imply TUP specificity. The fact that this particular peptide sequence is highly enriched, was observed to bind both mouse and human TfR and not the irrelevant control antigen, could indicate that the mostly hydrophobic amino acids within the loop structure of this peptide play a role in binding to a hydrophobic TfR epitope. In the past this has

been true of tryptophan-rich peptide sequences which have been identified towards the highly hydrophobic extracellular regions of HIV-1 (Conley et al., 1994; Song et al., 2009; Zwick et al., 2001).

Homology between the 16 identified unique peptides was determined through a ClustalW multiple sequence alignment, (Figure 3.3.4). Pep8, Pep9, and Pep10 (derived from CPEP2 library) were identified to contain the four-hydrophobic amino acid motif 'WWGΘ' or a variant thereof (as with Pep9) at positions 8 – 11 within the peptide sequences. These three peptides were later identified to demonstrate the highest TfR species cross-reactive absorbance readings with phage ELISA screening (Figure 3.3.5).

During the selection of brain targeting peptides, Pasqualini *et al*. (1996) have previously highlighted the selection of a peptide sequence (CENWWGDVC) containing the motif 'WWG'. This peptide was derived from a CX_7C cyclic peptide library, and was identified alongside several other brain targeting peptides from various libraries, through *in vivo* organ selection in mice. The group intravenously injected the peptide library, subsequently recovered the brain and amplified phage, prior to subsequent rounds of selection to obtain brain enriched peptides. As isolated phage, the peptide was injected into mice and shown to demonstrate a 4-fold greater brain/ kidney tissue ratio. The disadvantage of *in vivo* selection methods is that the exact target could not be determined. The group concluded that since the peptides were only allowed to circulate for a few minutes the identified peptides are likely to be endothelial specific. Our identification of several peptides that potentially bind via this conserved 'WWGΘ' motif, could suggest that the CENWWGDVC peptide binds to TfR and further assessment would be needed to validate this theory.

Further assessment of the Pep10 sequence revealed that it contained the shared three-amino acid motif 'DCS' with pep1. In addition to this sequence, Pep10 also contained a portion of a previously described Tf region '**FR**SETKD', which was shown to bind TfR via the two amino acids 'RS' (Dai et al., 2014), (discussed further in section 3.4.3).

Another motif ‘CTPΘ’ or variants thereof, were also identified with Pep13, Pep16, Pep15 and Pep4. Peptides containing ‘CTPY’ and ‘CTPL’ have previously been described towards MHC class I and class II molecules (Allen et al., 2001; Schroers et al., 2003).

Re-evaluation of identified unique peptides was carried out through a secondary phage ELISA to validate the observed positive hits, (Figure 3.3.5 and Figure 3.3.6). Typically, phage ELISA screening provides a qualitative measure of binding towards a target antigen. It does not allow the affinity ranking of the screened clones as the expression of phage particles is not controlled, and thus some phage express more efficiently than others. Whilst phage ELISA screening is unrepresentative of affinity, a study by Watkins *et al*. (1997) showed that it is possible to perform phage ELISA screening that can provide a rough estimation of affinity ranking. By regulating the quantity of anti-fab capture reagent used to coat microtitre plates, the group were able normalise the variable *E.coli* expressions of fab fragments by saturating the immobilisation matrix. Following incubation with the target antigen, the group showed that absorbance readings were directly proportional to the relative affinity of assayed fab fragment.

Three peptide sequences, Pep2, Pep3 and Pep6 were identified to be false positives following re-evaluation via a phage ELISA (Figure 3.3.5). Upon closer examination of the peptide sequences of Pep2 and Pep3, a consensus tripeptide motif ‘HPQ’ was identified. The sequence of Pep6 did not contain the ‘HPQ’ motif, but it does appear to contain a similar variant, ‘HPM’, (Figure 3.3.4). The ‘HPQ’ motif was first described by Devlin *et al*. (1990) through screening of a 15mer linear peptide library with a diversity of 10^7 towards streptavidin. Since then, various studies have also identified the ‘HPQ’ motif from screening outputs of linear (Weber et al., 1992) and constrained (Giebel et al., 2002) peptide libraries. These peptides were either intentionally identified through selection towards streptavidin or avidin target antigens (Gissel, Jensen, Gregorius, Elsner, Svendsen, and Mouritsen, 1995a; Meyer et al., 2006) or non-intentionally as is the case when using streptavidin as a target antigen affinity capture reagent. The latter is usually unavoidable, and is often minimised through negative selection steps before each selection round towards

streptavidin, or via short incubations with 0.1 mM biotin in order to quickly displace any streptavidin binding phage particles without affecting the bound biotinylated target (I. Chen et al., 2007; Shan et al., 2016).

In all cases, the presence of the 'HPQ' sequence results in streptavidin binding. This is due to the fact the tripeptide very effectively mimics biotin, interacting with the four binding sites found on the tetrameric streptavidin molecule and therefore directly competing with biotin for binding one of the four binding sites of streptavidin (Katz, 1995; Weber et al., 1992). Giebel *et al*. (2002) screened for streptavidin binding clones using a cyclic peptide library (Ph.D.-C7C) and identified several 'HPQ' containing peptide sequences. Interestingly, their findings demonstrated that the constrained nature of these peptides added a 2- to 3-fold increase in binding affinity over the previously identified linear 'HPQ' containing heptapeptide equivalents (Weber et al., 1992). This finding exemplifies the greater binding complexity of cyclic peptides than their linear counterparts. In addition to the 'HPQ' motif, another previously reported variant 'HPM', has also been identified to bind streptavidin, though at a weaker affinity (Gissel, Jensen, Gregorius, Elsner, Svendsen, and Mouritsen, 1995b).

Given that both Pep2 and Pep3 had been incubated with antigen immobilised onto streptavidin coated plates, no observable streptavidin binding was detected. One possible explanation is that all the binding sites on streptavidin are saturated with biotinylated antigen and due to the significantly lower affinity of these peptides to streptavidin, no binding was observed. The 'HPQ' motif has previously been described as having an affinity towards streptavidin in the millimolar range (T. Schmidt et al., 1996). This is significantly lower than that of biotin/ streptavidin interaction which is within the picomolar range (Lakshmipriya et al., 2016). As a control, it may be beneficial to re-assess these peptides towards streptavidin coated plates alone, in order to determine whether binding occurs in the absence of biotinylated antigen.

Pep1, Pep8, Pep9 and Pep10 demonstrated the highest absorbance readings with phage ELISA screening. Moreover, these peptides were found to maintain specificity after re-assessment towards an additional three control antigens (Figure

3.3.5 and Figure 3.3.6). As previously described in this section, all four of these lead peptides share common motifs or variants of these motifs ('DCS', and 'WWGΘ'), and these could mediate binding to TfR.

3.4.3. Pep1 demonstrates sequence homology with a conserved motif on transferrin C1-lobe.

A ClustalW multiple sequence alignment was performed for each of the identified peptides towards the amino acid sequence of serotransferrin from mouse, human and rat species. This was conducted to determine whether any of the 16 unique peptides shared homology with the natural ligand to TfR, Tf. Pep1 was identified to share strong homology with a nine-amino acid peptide (DCSGNFCLF) that is conserved across all three analysed species. To the best of our knowledge this peptide sequence has not previously been described for targeting TfR. Interestingly, as previously mentioned in section 3.4.2, Pep10 appears to contain a motif that is homologous with Pep1 and the Tf (DCS), and this motif is followed by a portion of previously described Tf motif '**FR**SETKD', (Dai et al., 2014). Dai et al. (2014) previously highlighted the selection of a peptide designated BP9 (AHLHNRS). This peptide was identified through phage display selections towards recombinant hTfR, via biopanning of a linear 7-mer peptide library. From 20 clones that were screened 6 clones were identified that specifically target hTfR and share the two-amino acid motif 'RS' which was homologous with a Tf motif (F**RS**ETKD). Interestingly, the Tf homologous region identified by Dai *et al*. (2014), 'FRSETKD', follows directly after the 'DCSGNFCL' motif identified herein as homologous with Pep1. In our work, Pep10 in the form of isolated phage consistently demonstrated the highest absorbance values for TfR specific binding, (Figures 3.3.5 and 3.3.6), and this finding could be due to a combined effect of the 'DCS' motif in conjunction with the 'FR' motif. However, this would need to be evaluated through a comparison of Pep1 and BP9, to determine if a greater a degree of binding towards TfR is observed.

After establishing homology of Pep1 with Tf, we sought to assess a potential mechanism of binding with TfR. To do so, we studied the previously described crystal structures for the interaction of Tf with TfR at 3.2Å (Eckenroth et al., 2011), (PDB ID: 3S9M), Figure 3.3.8. Eckenroth *et al*. (Eckenroth et al., 2011) identified

extensive interactions between the α1 helix and β2 strand and loop regions within C1 lobe of Tf and the helical domain of TfR. Structurally, serum transferrin consists of 679 AA residues divided into two domains, N-lobe and C-lobe, which are connected via a short peptide linker. The N-lobe and the C-lobe can be further subdivided into N1 and N2, and C1 and C2 subdomains, respectively. Binding of a single iron ion occurs at each of the primary lobes, in between the two subdomains which open and close to accept and release an iron ion through a conformational change (Eckenroth et al., 2011). The interaction study showed that the binding of the Pep1 homologous sequence (DCSGNFCL) occurs via an interaction between a loop region located within the C1-lobe of Tf and the helical domain of TfR, Figure 3.3.8, A. Moreover, this binding appears to occur through the side chain of asparagine 618 on Tf, and Arginine 629 on the αIII-2 helix, of the TfR helical domain, Figure 3.3.8, B. The C-lobe and N-lobe of Tf, have numerous regions of interaction along the helical, and protease-like domains of TfR, Figure 3.3.8, A. an interaction between Glycine at position 617 of Tf was previously observed with Arginine 629 of TfR (Eckenroth et al., 2011). Pep1 binding with Arginine in this case could occur via the hydrophobic residue methionine at the same position as glycine within the sequence. It is not clear whether binding of Pep1 interferes with the binding of Tf to TfR. Further assessment through Tf competition assays is needed to elucidate whether Pep1 binds competitively with Tf.

In conclusion, combinational target antigen and cell selection strategies utilising the three cyclic peptide libraries were successful in identifying species cross-reactive peptides that bind to TfR. Following phage ELISA screening, 13 peptides were identified to bind specifically to TfR, with varying binding profiles towards mouse, human and rat TfR. Additionally, three peptide sequences were identified as false positive hits, and are predicted to be streptavidin binding peptides since they contain the consensus motifs ‘HPQ’ and ‘HPM’. The 13 peptides demonstrate regions of sequence homology amongst each other and with Tf. Through studying the crystal structure of Tf/TfR, we were able to predict a mechanism of binding for a novel peptide (Pep1) which showed the greatest degree of homology to Tf.

Chapter 4: Expression and characterisation of lead TfR binding peptides.

4.1. Introduction

The BBB limits the effective delivery of neuro-therapeutic agents into the CNS, preventing potentially life changing medicines from reaching their target site (Pardridge, 2015). Antibody alternative, molecular targeting domains such as peptides, can be selected through phage display towards specific targets, and have the potential to overcome the disadvantages posed by antibodies within the context of targeting the BBB (Molino et al., 2017).

Antibody-mediated RMT delivery shuttles are restricted in their ability to effectively deliver pharmacologically relevant concentrations of drugs into the CNS. This was later discovered to be due to the limits of the transcellular transport system and the binding affinity/ avidity of the BBB targeting domain (Bien-Ly et al., 2014; Niewoehner et al., 2014). The transport capabilities of anti-TfR antibody delivery molecules of varying affinities have shown that higher affinity antibody variants are more susceptible to lysosomal sorting and subsequent degradation than low affinity variants (Bien-Ly et al., 2014). Furthermore, the use of high affinity TfR binding antibody variants prevents dissociation at the abluminal membrane, and thus confine the delivery vector/ drug conjugate within BCEC (Yu and Watts, 2013; Yu et al., 2011). Bivalent Fab-anti-BACE1 fusion domains demonstrated a greater degree of colocalisation with lysosomes when compared to monovalent domains. No trans-BBB transport was observed with BCEC *in vitro* and *in vivo* transport studies and this was proposed to be due to receptor crosslinking of bivalent domains (Niewoehner et al., 2014).

Re-engineering of BBB targeting molecules as fusion domains has been carried out by several groups in order to improve uptake into the CNS (Webster et al., 2017; Yu et al., 2011; Boado, Lu, et al., 2010). Through the use of antibody engineering approaches, Yu *et al*. (2014; 2013) were able to optimise the binding properties of the anti-TfR antibodies and this resulted in favourable target binding, intracellular trafficking (i.e. avoiding lysosomal degradation) and transcytosis properties of delivery molecules.

Most recently, Webster *et al*. (2017) optimised the previously described 8D3 mouse TfR antibody through re-engineering approaches (Kissel et al., 1998). The group developed multiple 8D3 variants with lower affinity binding properties to mTfR. These antibody variants were then coupled to interleukin 1 receptor antagonist (IL1RA), an inhibitor of IL1 receptor, a key promoter of hyperalgesia with neuropathic pain. The group demonstrated CNS efficacy in a validated *in vivo* mouse model of neuropathic pain, induced through partial ligation of the sciatic nerve (Seltzer et al., 1990; Malmberg and Basbaum, 1998; Colleoni and Sacerdote, 2010).

Engineering approaches provide a means of enhancing the CNS uptake of biotherapeutic molecules. Peptides are amenable to such engineering approaches and can be expressed as fusions to small soluble domain or larger bivalent peptide-Fc fusion domains for enhanced expression and avidity (Foster et al., 2017; Costa et al., 2014). Despite the shortcomings, the mechanism of RMT continues to be exploited, since it provides a viable means of overcoming the macromolecular transport limitations of the BBB. in this respect, with peptides being inherently smaller and lower affinity antibodies, they have great potential for use as RMT drug delivery shuttles at the BBB.

This chapter focuses on the expression and characterisation of identified mouse and human TfR binding cyclic peptides for use as BBB targeting molecules (described in chapter 3).

The aims of this study were to:

- Generate a suitable periplasmic expression vector construct for expressing cyclic peptide g3p-domain 1 (CPep-D1) fusion proteins.
- Sub-clone the pre-identified cross-species TfR targeting CPep candidates into the expression vector and carry out periplasmic expression of soluble CPep-D1 domains.
- Affinity rank screening of lead peptide candidates according to their ability to selectively bind recombinant mouse and human TfR via soluble domain antigen binding ELISA assays.

- Assess the ability of selected lead CPep-D1 candidates to bind *in vitro* cultured BCEC, bEnd.3 and hCMEC/D3.
- Characterise the capacity of lead peptides expressed as Fc-fusion molecules to internalise and deliver a conjugated cargo within bEnd.3 and hCMEC/D3 cell lines.
- Assess the sub-cellular trafficking of CPep-Fc fusion domains within hCMEC/D3 cells.

4.2. Materials and Methods

4.2.1. Sub-cloning of cyclic peptides into pCANTAB6-D1/FLAGHIS expression vector

4.2.1.1. Modification of pC6-D1 expression vector to introduce a NotI and FLAG tag coding region

PCR primers were synthesised by the DNA chemistry team (MedImmune, Cambridge, UK), these are outlined in Table 4.2.1.

Table 4.2.1: Primers used for two-step pC6-D1 vector modification process.

Primer ID	Sequence	Length
pC6-D1/FLAGHISfor	CGGGCGGCCGCAGGTGGTTCTGG	23
pC6-D1/FLAGrev	CGCCGCTTTATCGTCATCGTCTTTGTAGTCAGAG CCACCACCCTCATTTTCAGG	54
pC6-D1/FLAHISrev2	CCAGTGAATTCTTAATGATGGTGGTGGTGATGA TGGTGGTGATGCGCCGCTTTATCGTCATCGTCTT TGTAGTC	74

A total of 10 ng of pC6-D1 vector stock was used in a 100 µl PCR reaction volume as outlined in Table 4.2.2. The PCR reaction was run with the following programme parameters: Hot start 94°C (3 min), denaturation 94°C (30 s), annealing 55°C (30 s), extension 72°C (90 s) and final extension 72°C (5 min). Denaturation, annealing and extension steps were repeated for 30 cycles. An aliquot of the PCR product was validated on a 1.5% agarose gel to confirm the insert size. Insert DNA was digested using NotI and EcoRI (New England Biolabs, Hitching, UK) and purified using a High-Pure PCR product purification kit (Roche Applied Science, Sussex, UK) according to the manufacturer's protocol.

Table 4.2.2. Amplification of pC6-D1 vector insert.

Reaction component	Volume (µl)
2x Thermo Ready mix PCR master mix	46
Nuclease free water	50
PD1-FHfor	1
PD1-FLrev2	1
pC6D1 vector stock (10 ng)	2

pCANTAB6 stock vector was digested using NotI and EcoRI (New England Biolabs, Hitching, UK). The digested vector was run on a 1% agarose gel, the double cut vector band was excised and gel purified using a QIAquick gel extraction kit (QIAGEN, Manchester, UK) according to the manufacturer's protocol, with the exception that the final elution step was carried out in 50 µl of nuclease free water. The digested and purified vector was 5' dephosphorylated using 1 unit of Antarctic phosphatase in a 55 µl reaction volume containing 5 µl of 10x Antarctic phosphatase buffer (New England Biolabs, Hitching, UK). Digested vector and modified insert were ligated using T4 DNA ligase (New England Biolabs, Hitching, UK) in a 20 µl reaction mix and transformed into chemically competent DH5α *E.coli* cells. Transformed cells were streaked onto 2xTYAG plates and grown overnight at 37°C. The following day, 8 colonies were picked and grown overnight in a shaking incubator at 37°C, 280rpm. Aliquots of grown up cultures were taken for sequence validation using the sequencing primers, CanFor (CCCAGGCTTTACACTTTATGCTTC) and CanRevGT (GTTGGGTAACGCCAGGG). Glycerol stocks of *E.coli* cells containing the pC6-D1/FLAGHIS construct were prepared following sequence validation.

4.2.1.2. Purification of pC6-D1/FLAGHIS plasmid DNA

A 400 ml culture of pC6-D1/FLAGHIS expressing *E.coli* DH5α cells was inoculated and grown overnight in a shaking incubator at 37°C, 280rpm. The following morning the culture was split into two 200 ml batches and plasmid DNA was purified using a HiSpeed Plasmid Maxiprep kit (QIAGEN, Manchester, UK) according to the manufacturer's protocol. Purified plasmid DNA was quantified using a Nanodrop spectrophotometer (ThermoFisher Scientific, Paisley, UK) and run on a 1.5% agarose gel to confirm plasmid size.

4.2.1.3. Restriction digestion of pC6-D1/FLAGHIS and CPep DNA vector

Purified pC6-D1/FLAGHIS DNA was restriction digested using the restriction enzymes NcoI and NotI (New England Biolabs, Hitching, UK). A total of 6 µg of plasmid DNA was digested in a volume of 100 µl with 10x NEB 3.1 buffer (New England Biolabs, Hitching, UK) and 2 units of NcoI. The sample was incubated with NcoI for 45 min at 37°C, then heat inactivated at 65°C for for 30 min. Subsequently, 2 units of NotI was added to the reaction and incubated for a further 1 hour at 37°C. Restriction digested products were run on a 1.5% agarose gel and gel purified using a QIAquick gel extraction kit (QIAGEN, Manchester, UK) according to the manufacturer's protocol. In order to prevent re-ligation of the vector, the digested vector DNA was 5' dephosphorylated using Antarctic phosphatase (New England Biolabs, Hitchin, UK) and incubation at 37°C for 1 hour.

Insert DNA of the 16 identified cross-species binding CPep sequences and an irrelevant control CPep of similar size was amplified from fdDOG vector using the PCR amplification primers fdpcrfor (CCAGCCGGCCATGGCGTCTCACAGTGCACAG) and fdpcrrev (TTCAACAGTTGCGGCCGCAGCGGTAGAACCAGAACCACCTTCTGCGGCCGC). A 40 µl PCR reaction was prepared for each of the identified clones as outlined Table 4.2.3.

Table 4.2.3: PCR reaction for amplification of CPep insert DNA from fdDOG phage vector.

Reaction component	Volume (µl)
2x Thermo Ready mix PCR master mix	20
Nuclease free water	17
Fdpcrfor (10 µM)	0.5
Fdpcrrev (10 µM)	0.5
Glycerol stock of CPep in fdDOG vector	2

The PCR reaction was run with the following programme parameters: Hot start 94°C (3 min), denaturation 94°C (30 s), annealing 55°C (30 s), extension 72°C (90 s) and final extension 72°C (5 min). Denaturation, annealing and extension steps were repeated for 30 cycles. CPep DNA inserts were purified using QIAquick Nucleotide removal kit (QIAGEN, Manchester, UK) according to the manufacturer's protocol. At the final stage of purification, insert DNA was eluted in 50 µl of nuclease

free water. Purified inserts were then restriction digested using NcoI and NotI as described earlier with the exception of the Antarctic phosphatase step. Inserts were subsequently re-purified using the QIAquick nucleotide removal kit (QIAGEN, Manchester, UK) according to the manufacturer's protocol.

4.2.1.4. Ligation reaction and transformation into E.coli Z' TG1 competent cells

NcoI and NotI digested CPep inserts and pC6-D1/FLAGHIS vector DNA were ligated using 400 units of T4 DNA ligase (New England Biolabs, Hitchin, UK). For each of the CPep sequences, a 20 µl reaction was set up as shown in Table 4.2.4.

Table 4.2.4: Ligation of insert into pC6-D1/FLAGHIS expression vector

Component	Volume (µl)
10x DNA ligase buffer	2
Nuclease free water	15
Digested vector (55 ng/µl)	1
Digested insert DNA	1
T4 DNA ligase	1
Total volume	20

The ligation reactions were incubated at room temperature for 1 h and subsequently transformed into Z-competent *E.coli* TG1 cells (MedImmune, Cambridge, UK). Cells were immediately plated out onto pre-warmed 2x Tryptone Yeast supplemented with 100 µg/ml ampicillin and 2% glucose (TYAG) agar plates and incubated overnight at 37°C. The following morning, 8 colonies per CPep were innoculated into columns within 96-well plates containing 2x TYAG media and cultured overnight at 30°C. Aliquots were then taken for sequencing and glycerol was added to remaining cultures in wells and plates were stored at -80°C.

4.2.2. *E.coli* periplasmic expression and affinity purification of CPep-D1 fusion domains.

4.2.2.1. Buffer preparation

In preparation for automated sample purification, buffers were prepared, sterile filtered and stored at 4°C. Buffers were made according to the recipes shown in Table 4.2.5.

Table 4.2.5: ASPEC purification buffer compositions.

Buffer	Composition
ASPEC buffer A (equilibration)	50 mM Tris-HCl, 300 mM Sodium chloride, pH 8.0
ASPEC buffer B (Binding)	50 mM Tris-HCl, 300 mM Sodium chloride, 40 mM Imidazole, pH 8.0
ASPEC buffer C (Elution)	50 mM Tris-HCl, 300 mM Sodium chloride, 400 mM Imidazole, pH 8.0
TES buffer	200 mM Tris-HCl, 0.5 mM EDTA, 0.5 M sucrose, pH 8.0
Test-tube buffer	1 M $MgCl_2$, 2 M Imidazole, pH 8.0

4.2.2.2. Expression, culture harvest, periplasm extraction and His capture affinity purification.

An agar plate was freshly streaked for each of the 16 identified CPep clones (including the two predicted streptavidin binding clones), in addition to an irrelevant control CPep of similar size and charge and grown overnight at 30°C. Starter cultures were then prepared by inoculating 10 ml aliquots of 2x TYAG with a single colony from each of the streaked plates, and these were grown overnight in a shaking incubator at 30°C, 300rpm. The following day, 0.3 ml was taken from each starter culture to prepare glycerol stocks, and the remaining cultures were used to inoculate 2L Erlenmeyer flasks containing 400 ml of 2x TYAG (100 µg/ml Ampicillin, 0.1% glucose). The flasks were then incubated for 2.5 h at 30°C, 300rpm. Subsequently, cultures were induced by addition of IPTG to a final concentration of 1 mM, and incubation was recommenced for a further 3 h.

The GX-274 ASPEC automated sample purification system (Gilson, Luton, UK) was setup by loading Ni-Sepharose FF columns, NAP10 desalting columns and 6 ml collection tubes. Lines were primed with the relevant buffers before use. Storage buffer was allowed to completely drain from the Ni-Sepharose FF and NAP10 column resins and the columns were allowed to equilibrate for 3 h in ASPEC buffers A and D, respectively.

Cultures were harvested via centrifugation at 6084 g for 10 min at 4°C using a pre-chilled SLA3000 rotor and a Sorvall RC5B centrifuge (ThermoFisher Scientific, Paisley, UK). Following centrifugation, the supernatant was discarded and the cell

pellet was re-suspended in Tris EDTA sucrose (TES) buffer, transferred to a 50 ml falcon tube and stored on ice. To each re-suspended cell pellet, 15 ml of a 1:5 diluted TES solution was added, mixed and stored on ice for 30 min. Subsequently, the samples were centrifuged at 3576 g for 30 min at 4°C and lysate was isolated.

Sample lysates were transferred to 25 ml glass test-tubes containing 125 µl of test-tube buffer and samples were loaded onto the ASPEC sample purification system and purified overnight. Purified material was quantified via a bicinchoninic acid (BCA) assay (ThermoFisher Scientific, Paisley, UK) according to the manufacturer's protocol. Expressed and purified peptides that resulted in concentrations below 25 µg/ml were considered failed expressions.

4.2.3. SDS-PAGE purity analysis of expressed CPep-D1 fusion domains.

Validation of expressed peptide purity and molecular weight was carried out via sodium dodecyl sulphate polyacrylamide gel electrophoresis (SDS-PAGE). Non-reducing sample buffer stock was prepared at a 1:2 (v/v) of MiliQ water to 4x LDS sample buffer. Sample buffer was added to a 25 µl aliquot of the expressed peptide, mixed, transferred to a heat block at 100°C for 3 min, and allowed to cool to room temperature.

Pre-cast NuPAGE 12% Bis-Tris gels (ThermoFisher Scientific, Paisley, UK) were placed in a buffer tank containing NuPAGE 1x MOPS SDS running buffer (ThermoFisher Scientific, Paisley, UK) and 10 µl of each peptide sample was loaded into individual wells alongside a well containing 5 µl of SeeBlue Plus pre-stained MW standard (ThermoFisher Scientific, Paisley, UK). The gel was run at 200 V, 400 mA for 45 min. Gels were subsequently stained for approximately 60 min in InstantBlue stain (Expedeon, Swavesey, UK) then de-stained by thoroughly rinsing in MiliQ water and allowing the gel to de-stain in water on a shaker for 30 min. Gels were imaged using a scanner.

4.2.4. Soluble CPep-D1 fusion TfR binding ELISA

Biotinylated mouse TfR, human TfR and an irrelevant control antigen (confidential proteins, contact George Thom, MedImmune, Cambridge, UK) of a

similar charge and molecular weight, were immobilised onto wells within streptavidin coated 96-well plates (Thermo-Fisher Scientific, Paisley, UK) at a concentration of 1 µg/ml overnight at 4°C. As a negative control, non-TfR immobilised streptavidin coated plates were also assayed alongside surface antigens. The following morning, plates were rinsed three times in PBS and wells were blocked in 3% (w/v) skimmed milk powder in PBS for 1 h at room temperature. Blocked plates were subsequently washed three times in PBS and expressed soluble CPep-D1 lead molecules were added to the relevant wells, at 10 µM concentration or 1:3 serial dilutions starting at 10 µM. Labelling of bound CPep-D1 domains was carried out by initially washing plates three times in PBS with 0.1% (v/v) Tween 20 (PBST) and incubating with a mouse monoclonal anti-FLAG M2 HRP conjugated secondary antibody (Sigma-Aldrich, Dorset, UK) at a dilution of 1:20,000 for 1 h at room temperature. Wells were re-washed in PBST, the reduction of HRP was catalysed by addition of TMB substrate for 10 min, sulphuric acid was added to stop the reaction and plates were read using an EnVision™ fluorescent plate reader (PerkinElmer, Beaconsfield, UK) at 450 nm.

4.2.5. Immunocytochemistry based cell binding, internalisation and intracellular co-localisation assays

ICC was used to assess the binding of lead peptides expressed as monomeric -D1 fusion domains towards bEnd.3 and hCMEC/D3 cell lines. ICC was also used to assess cellular uptake (within bEnd.3 and hCMEC/D3 cells) and intracellular localisation (within hCMEC/D3 cells) of CPep-Fc/ interleukin 1 receptor antagonist (IL1Ra) fusion domains.

4.2.5.1. Cell culture

Immortalised human brain endothelial cells (hCMEC/D3) were seeded into collagen coated flasks and maintained in endothelial cell basal medium-2 (Lonza, Basel, Switzerland) supplemented with 2.5% FBS and growth factors as outlined in Chapter 2, section 2.2.2. Immortalised mouse brain endothelial cells (bEnd.3) were maintained in Dulbecco's modified Eagle's medium (DMEM) supplemented with 10% FBS (Thermo-Fisher Scientific, Paisley, UK). Cells were cultured within a humidified

incubator at 37°C, 5% CO_2. All experiments were carried out with cell lines at passages 25 – 30.

For binding and internalisation assays, cells were sub-cultured into fibronectin- and collagen-coated Nunc Lab-Tek II 8-well glass chamber slides (ThermoFisher Scientific, Paisley, UK) or 96-well special optics flat clear bottom black polystyrene TC-treated microplates (Corning, High Wycombe, UK) at a seeding density of 5 x 10^4 per chamber or 1.5 x 10^4 per well, respectively. Cells were grown to confluence for 48 h, media was aspirated from the culture wells and cells were washed twice in PBS, prior to commencing cell binding and internalisation assays.

4.2.5.2. Cell binding assays

Cells were fixed in 4% *p*-formaldehyde in PBS, pH 7.4 for 15 min at room temperature. Post fixation, buffers were kept on ice and all subsequent steps were carried out at 4°C. Cells were washed three times in pre-chilled PBS and blocked in 5% BSA in PBS solution, 30 min at 4°C. Post blocking, cells were washed three times in PBS and incubated with expressed lead CPep-D1 fusion domains diluted to a concentration of 2 µM in 1% BSA in PBS, for 4 h at 4°C. Post Incubation, cells were washed three times in 1% BSA in PBS for 5 min at 4°C. Cell bound CPep-D1 domains were counter stained using a two-step secondary antibody labelling protocol. Cells were incubated for 1 h with 1 µg/ml secondary mouse anti-His monoclonal antibody (Millipore, Watford, UK) and subsequently 1:50 sheep anti-mouse IgG FITC conjugated polyclonal antibody (Sigma-Aldrich, Dorset, UK) diluted in 1% BSA in PBS. Post labelling, cells were washed and chamber slides were mounted to glass coverslips in DAPI Fluoromount-G mounting media (SouthernBiotech, Birmingham, USA).

Cells were imaged using a TCS SP5 confocal microscope (Leica, Milton Keynes, UK) and z-stack images were acquired using LAS AF software package. Max fluorescence intensity overlays were prepared from z-stack images using FIJI (imageJ). Mean grey value readings were acquired using FIJI (imageJ), normalised to the number of cells within each image and averaged from three independent images taken per experimental replicate (n= 3).

4.2.5.3. Cell internalisation and intracellular co-localisation assays

CPep-Fc/ interleukin 1 receptor antagonist (IL1Ra) fusion domains and human anti-mTfR specific 8D3 antibody were expressed, purified, and validated by the protein purification team (MedImmune, Cambridge, UK).

CPep-Fc/IL1Ra and anti-mTfR 8D3 antibody were diluted to a working concentration of 2 µM and 2 µg/ml in 1% BSA/ unsupplemented media, respectively. Confluent bEnd.3 or hCMEC/D3 cells were incubated with primary CPep-Fc/IL1Ra or anti-mTfR antibody within a humidified incubator at 37°C for 5, 15, 30, 60 and 120 min time intervals. Post-incubation, cells were washed three times for 5 min in 1% BSA in PBS, and permeabilised using 0.25% Triton X-100 (Sigma-Aldrich, Dorset, UK). Secondary labelling of CPep-Fc/IL1Ra domains and anti-mTfR antibody was carried out using 10 µg/ml polyclonal F(ab')2 goat anti-human IgG (Fc specific) Alexa 488 conjugate (Thermo-Fisher Scientific, Paisley, UK).

Intracellular co-localisation assays were carried out with hCMEC/D3 cells. In addition to CPep-Fc/IL1Ra labelling, cells were also labelled for EEA1 or LAMP1 using rabbit anti-EEA1(#3288, Cell Signalling Technology, Leiden, Netherlands) or anti-LAMP1 (#9091, Cell Signalling Technology, Leiden, Netherlands). Counter-staining of rabbit antibodies was carried out using goat anti-rabbit IgG (H+L) Alexa 647 conjugated secondary antibody (Thermo-Fisher Scientific, Paisley, UK). Nuclei were labelled with hoechst at a dilution of 1:10,000, for 1 min at room temperature. Immunofluorescent imaging of labelled cells within 96-well plates was carried out using an ImageXpress Micro XLS system (Molecular probes, Wokingham, UK). Normalised mean grey value reading were acquired as outlined in section 4.2.5.2.

4.2.6. Statistical analysis

Statistical analysis was conducted using Graphpad Prism 6 statistical software. Unpaired t-tests and one-way analysis of variance (ANOVA) tests were carried out where applicable, alongside Bonferroni's multiple comparison post-test. A p-value <0.05 was considered to be significant.

4.3. Results

4.3.1. Flag and His_{10} coding region successfully inserted into pC6-D1 expression vector.

The expression and purification of the small sized cyclic peptide (CPep) domains (approximately 1.8 kDa) poses a significant challenge for stability and effective purification. The solubility of peptides is typically poor due to the lack of a defined structure. This makes peptides susceptible to degradation by peptidases, and complicates their expression and purification steps through the formation of inclusion bodies and aggregates, respectively (Yuan Bi et al., 2006). To alleviate these issues, peptides may be expressed as fusion domains (Anderluh et al., 2003). A modified expression vector based on the pCANTAB6 phagemid vector (Figure 4.3.1), pCANTAB6-D1 (pC6-D1), was used to express monovalent cyclic peptides fused to the small and soluble N-terminal region of g3p-domain 1.

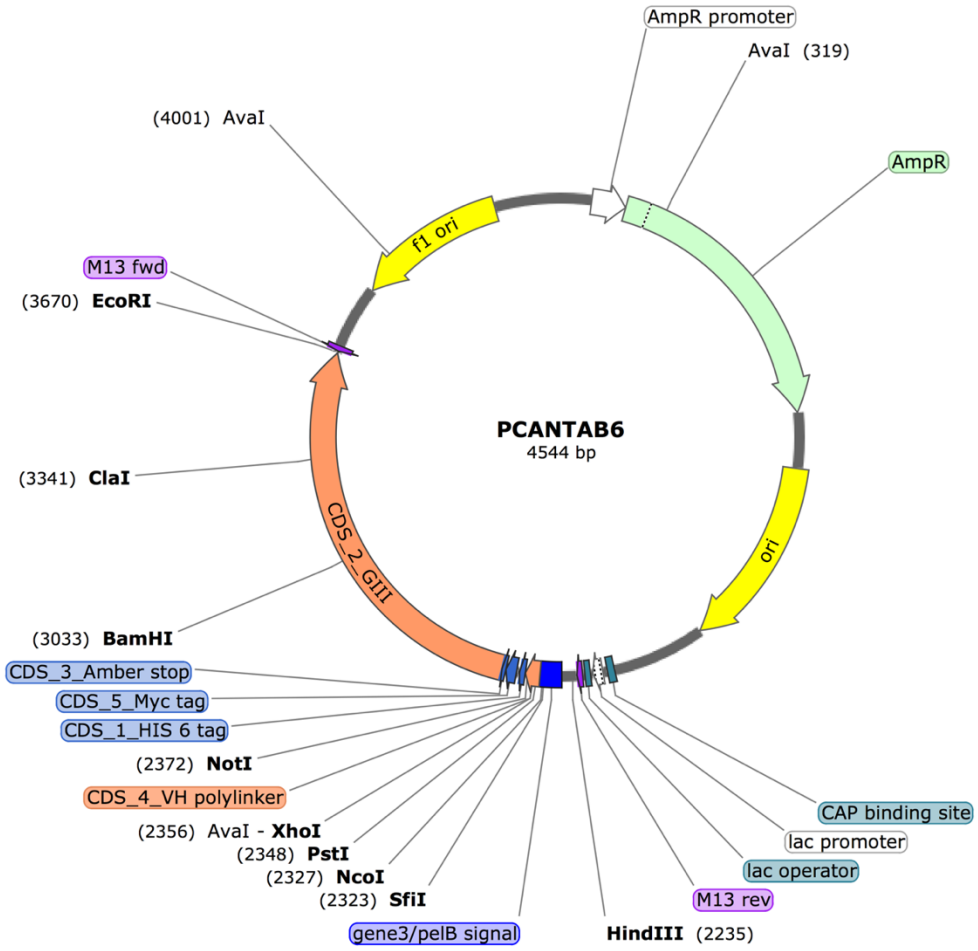

Figure 4.3.1: Circular vector map of stock pCANTAB6 expression vector.

Schematic representation of pCANTAB6 stock vector, showing the GIIIp encoding region, alongside the Myc tag, His6 tag and Pelb signaling regions. The insert region lies between NcoI and NotI restriction sites. Sourced from MedImmune (Cambridge, UK).

The pC6-D1 vector incorporates a LacZ promoter which drives the expression of CPep-D1 fusion domains to the periplasmic space through a *pelB* signalling peptide sequence (AQPAMA). To prevent steric hindrance of the peptide, this vector construct features a linker encoding region between the N-terminal domain of g3p-domain 1 and the peptide. The expression of peptides alongside a fusion partner also allows for the incorporation of affinity tags (Crowe et al., 1994; D. B. Smith and Johnson, 1988). The pC6-D1 expression vector encodes a His_{10} tag, which in turn generates CPep domains that incorporate a His tag for purification.

The presence of His tags on both the recombinant antigens and the expressed peptide domains poses an issue for the detection of peptide binding with ELISA based binding assays. Moreover, whilst the expression cassette within this vector incorporates a NcoI restriction site upstream of the peptide cloning region, it does not contain a unique downstream secondary restriction site. An alternative construct, pC6-D1/FLAGHIS, was therefore generated through a two-step PCR protocol in order to introduce a flag tag for detection of bound peptides and a NotI site for cloning.

Amplification of pC6-D1 expression cassette insert DNA via the two-step PCR modification primers resulted in an observable band at the expected size of 258bp, Figure 4.3.2, A, lane 3. Restriction digestion of the stock pCANTAB6 expression vector using EcoRI and NotI resulted in three observable bands relating to three independent DNA fragments, Figure 4.3.2, B. The largest fragment observed at 4544 bp represents the complete length of the pCANTAB6 stock expression vector and signifies the single digested vector product. The second largest band represents the double-digested vector product of interest and is observed at the expected size of 3250 bp. The smallest observable band relates to the size of the digest site and is at the expected size of 1300 bp.

Sequence validation of the modified pC6-D1/FLAGHIS vector revealed that the FLAG and NotI encoding sequences were successfully incorporated into the modified pC6-D1/FLAGHIS expression vector (Figure 4.3.3). The approximate molecular mass of a CPep-D1 fusion domain expressed using this construct is 13 kDa, with the peptide itself accounting for ≃ 1.8 kDa.

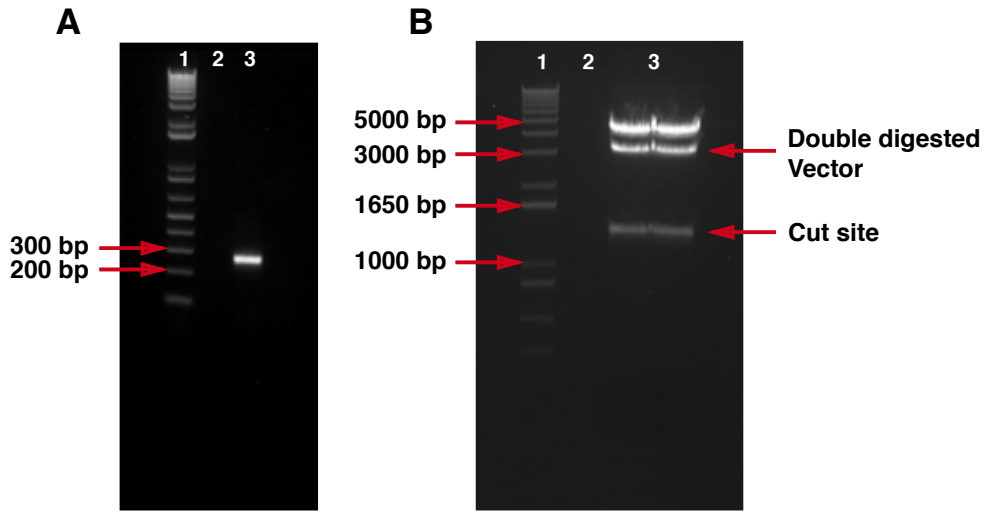

Figure 4.3.2: Validation of pC6-D1 FLAG modified insert DNA product and digested pCANTAB6 stock expression vector fragments via agarose gel electrophoresis.

Figure showing gel electrophoresis images of amplified insert DNA (A, lane 3) and restriction digested pCANTAB6 stock expression vector (B, lane 3). All gels were run alongside a 1 kbp DNA ladder.

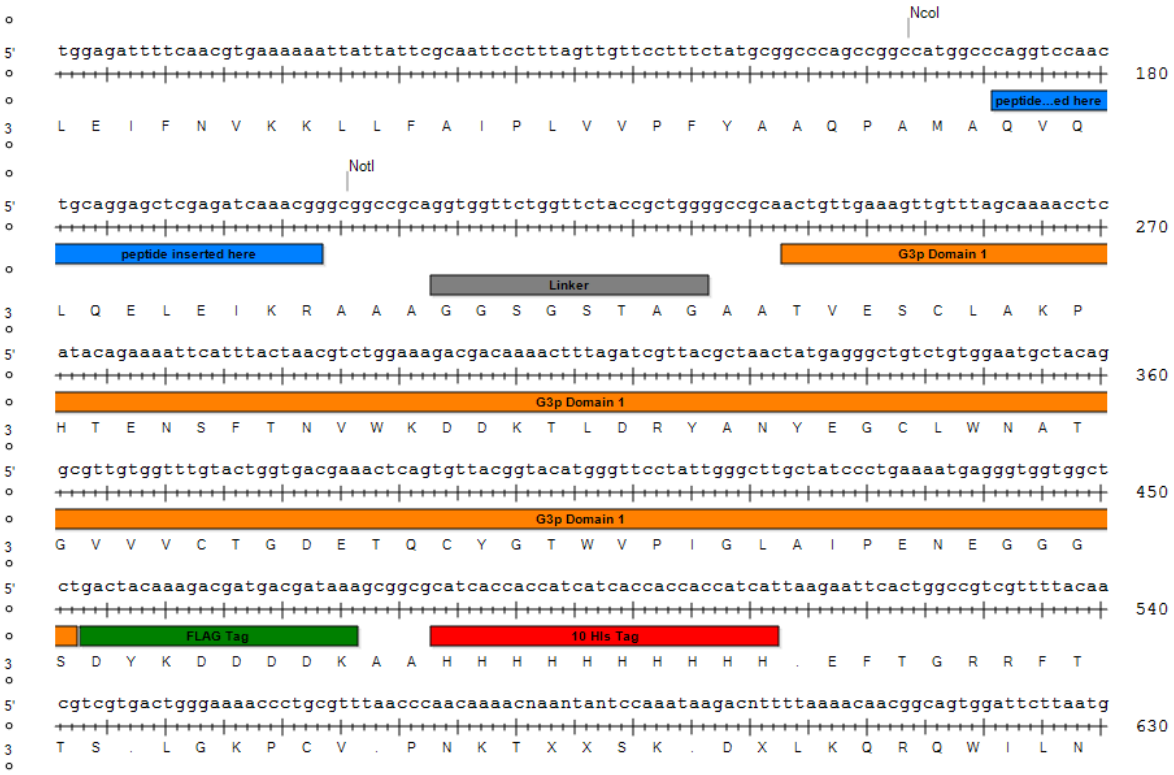

Figure 4.3.3: Sequence validation of the modified insert region of pC6-D1/FLAGHIS expression vector.

Schematic representation of the insert region within pC6-D1/FLAGHIS expression vector as determined by sequencing. The Flag and His_{10} coding regions were both validated in addition to the NotI restriction site introduced downstream of the peptide insert region.

4.3.2. Periplasmic expression of the CPep-D1 fusion domains resulted in variable yields of the uniquely identified peptides.

After establishing mouse and human TfR binding of uniquely identified CPep domains via phage ELISA, CPep-D1 domains were expressed via periplasmic expression for the subsequent characterisation of monovalent peptides expressed as fusions to g3p-domain 1. SDS-PAGE gel validation results are shown in 4.3.4.

Results revealed that not all of the CPep candidates expressed well as g3p-domain 1 fusions (4.3.4, A and B). Of the 16 identified peptide sequences that were expressed within this format, 14 peptides expressed to some extent as demonstrated by observable bands on SDS-PAGE gels 1 and 2 at 13kDa. Both Pep10 and Pep16 failed to express, showing no visible bands on the SDS-PAGE gel (4.3.4, A, lanes 12 and 19). Additionally, Pep2, Pep4, Pep12, Pep13 and Pep15 exhibited low expression which prevented their use in further studies, as they did not meet the minimum starting concentration of 10 µM required for soluble recombinant TfR binding assays (4.3.4, A, lanes 4, 6, 14, 16 and 18).

All Cpep-D1 fusion domains that expressed within this format demonstrated visible bands on SDS-PAGE gels within the expected region of 13 kDa (lanes 3-11, 13, 14, 16, 17 and 18, respectively). In addition to the 13 kDa band, the majority of these peptides showed secondary banding as noted with Pep1 – Pep3, Pep5 – Pep9 and Pep14 (lanes 3 – 5, 7 – 11 and 17, respectively). The secondary bands observed with Pep3, Pep5, Pep6, Pep7 and Pep14 (lanes 5, 7, 8, 9 and 17, respectively) are approximately 26 kDa in size. As well as demonstrating a secondary band at 26 kDa, Pep7 (lane 9) also demonstrated two additional bands which appear to be approximately 13 kDa apart and are visible at approximately 38 kDa and 52 kDa. Pep1, Pep8 and Pep9 demonstrate a secondary band that is within the range of 15 – 16 kDa (lanes 3, 10 and 11, respectively).

A

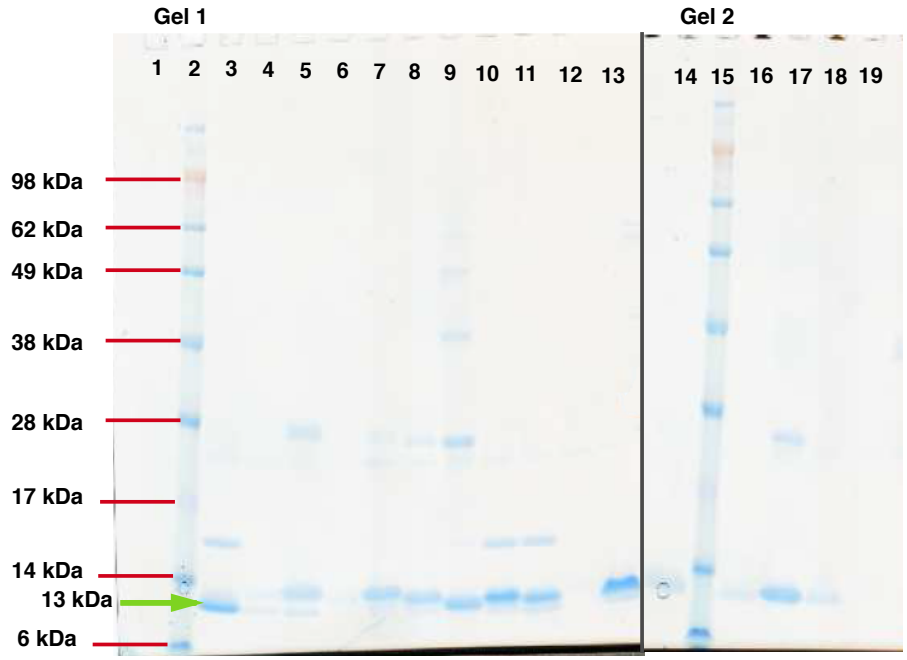

B

Gel	Lane	Lane content	Concentration (µg/ml)
Gel 1	1	Empty	N/A
	2	SeeBlue Plus2 protein standard	N/A
	3	Pep1	246
	4	Pep2	46 (Low)
	5	Pep3	212
	6	Pep4	27 (Low)
	7	Pep5	205
	8	Pep6	151
	9	Pep7	241
	10	Pep8	277
	11	Pep9	209
	12	Pep10	Fail
	13	Pep11	314
Gel 2	14	Pep12	48 (Low)
	15	SeeBlue Plus2 protein standard	N/A
	16	Pep13	29 (Low)
	17	Pep14	224
	18	Pep15	39 (Low)
	19	Pep16	Fail

Figure 4.3.4: Validation of expressed His_{10} tagged monovalent CPep-D1 fusion molecules by SDS-PAGE.

SDS-PAGE analysis of expressed monovalent CPep-D1 fusion molecules (**A**). CPep-D1 fusion domains were expressed in *E.coli* TG1 cells, purified on Ni-NTA affinity columns and run on a 12% Bis-Tris SDS-PAGE gels, which were later stained using Coomasie blue. The expected molecular weight of the CPep-D1 domain is 13 kDa. A summary table of peptide lane order and concentration as determined by BCA assay is shown in (**B**). The concentration column within the table also highlights peptides which failed to express and those that expressed below the usable requirement for further analysis via ELISA based screening assays i.e. 10 µM.

4.3.3. Four lead peptides identified to exhibit recombinant mouse and human TfR specific binding over the control antigen.

Characterisation of cyclic peptides expressed as monovalent fusions to g3p-domain 1 was carried out in order to establish lead candidates to be taken forward for cell binding studies and affinity ranking peptides towards mouse and human TfR. Lead peptides were selected according to criteria that they demonstrate higher absorbance readings towards both mouse and human TfR than those observed with the streptavidin and peptide controls.

Initial assessment of CPep-D1 domains was carried out at 10 μM concentration to establish lead peptide candidates. Results are summarised in Figure 4.3.5. Due to the poor periplasmic expression yields of some CPep-D1 domains and the large quantity required for further ICC cell binding studies, initial affinity screening of monovalent domains was carried out using two experimental replicates. Contrary to previous phage ELISA results (Chapter 3, Figure 3.3.3.), Pep7 did not bind mouse and human TfR when expressed within the CPep-D1 fusion format, as demonstrated by the lack of increased absorbance over the irrelevant control peptide. The predicted streptavidin binding clones containing the consensus 'HPQ' and 'HPM' motifs, Pep3 and Pep6, showed greater absorbance readings towards streptavidin than to the irrelevant control and TfR antigens.

Pep1, Pep8, Pep9 and Pep14 were all shown to exhibit greater absorbance readings with mouse and human TfR when compared with the irrelevant control antigen and were therefore taken forward for further study. In the case of Pep14, the absorbance readings observed appear to be only marginally greater than background absorbance of the irrelevant control peptide. Pep1 and Pep8 demonstrated similar absorbance readings towards both human and mouse TfR. Additionally, Pep1 and Pep8 also show a two-fold increase in non-specific binding towards the irrelevant control antigen when compared with the control CPep at 10 μM concentration.

To determine the binding profiles of lead peptides, Pep1, Pep8, Pep9 and Pep14 were all titred against biotinylated recombinant mTfR and hTfR antigens and an irrelevant control antigen (confidential protein, contact George Thom,

MedImmune, Cambridge, UK) at a 1:2 serial dilution starting from 10 μM concentration. Summarised results of the antigen presentation ELISAs are shown in Figure 4.3.6. All four lead peptides were observed to bind to mTfR and hTfR at greater absorbance readings than the control CPep. Pep1 demonstrated TfR specific binding at concentrations higher than 1.25 μM (Figure 4.3.6, A). Additionally, Pep1 also demonstrated greater absorbance readings towards hTfR at concentrations above 5 μM and this is consistent with previously observed results at 10 μM concentration, Figure 4.3.4.

Pep8 exhibits TfR specific binding at concentrations greater than 0.63 μM, (Figure 4.3.6, B). Overall, Pep1 and Pep8 demonstrate the highest absorbance values when compared to the irrelevant control antigen for both mouse and human TfR. However, with increasing concentration, Pep1 and Pep8 also show high levels of non-specific background binding as indicated by the gradual increase in absorbance readings observed with the irrelevant antigen and streptavidin controls (Figure 4.3.6, A and B). Moreover, a greater degree of non-specific binding towards the irrelevant control antigen and streptavidin coated plates was observed with Pep8 when compared to Pep1. Non-specific binding was also observed to gradually increase between 0.63 μM and 5 μM, with a more significant increase observed at 10 μM concentration.

Pep9 exhibits a greater affinity towards mTfR than hTfR (Figure 4.3.6, C). A gradual increase in mTfR specific binding was observed ranging from 0.63 μM to 10 μM concentration. Pep14 demonstrated a very weak affinity to mTfR and presented greater affinity towards hTfR at 5 μM and 10 μM concentrations (Figure 4.3.6, D). Contrary to Pep1 and Pep8 results, both Pep9 and Pep14 exhibited less non-specific binding towards the control antigen and streptavidin coated plates. However, overall absorbance values were lower for Pep9 and Pep14, suggesting significantly lower binding affinities than Pep1 and Pep8.

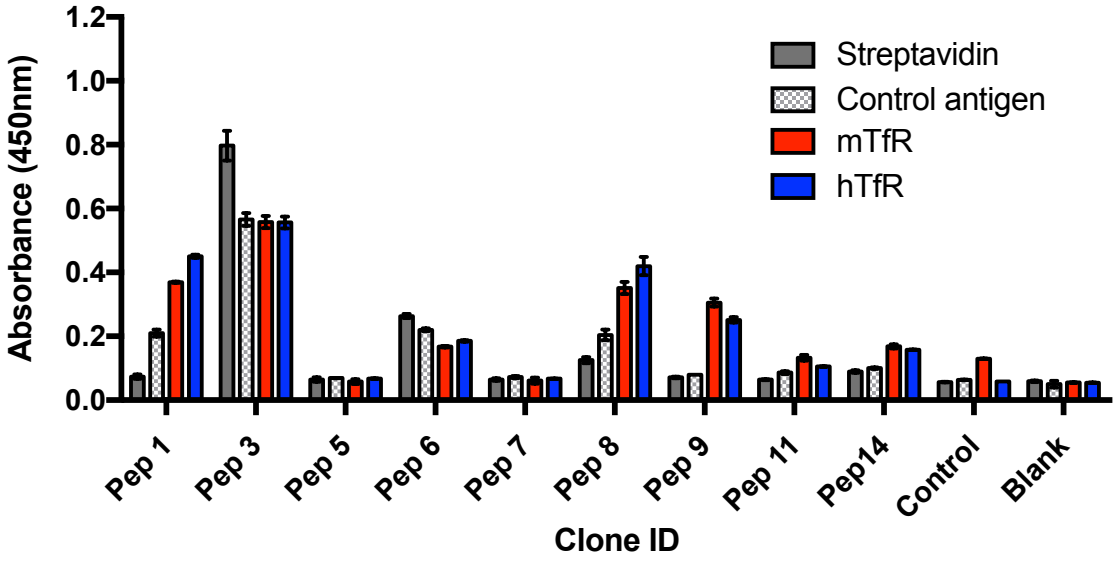

Figure 4.3.5: Summary of soluble CPep-D1 antigen binding ELISA and lead identification.

TfR binding ELISA performed with 10 µM of purified soluble CPep-D1 fusion domains titred against 1 µg/ml biotinylated human and mouse TfR immobilised onto streptavidin coated plates. Pep1, Pep8, Pep9 and Pep14 were identified as lead candidates and carried forward for further study. Summarised results are presented as averages of two experimental replicates, (n= 2).

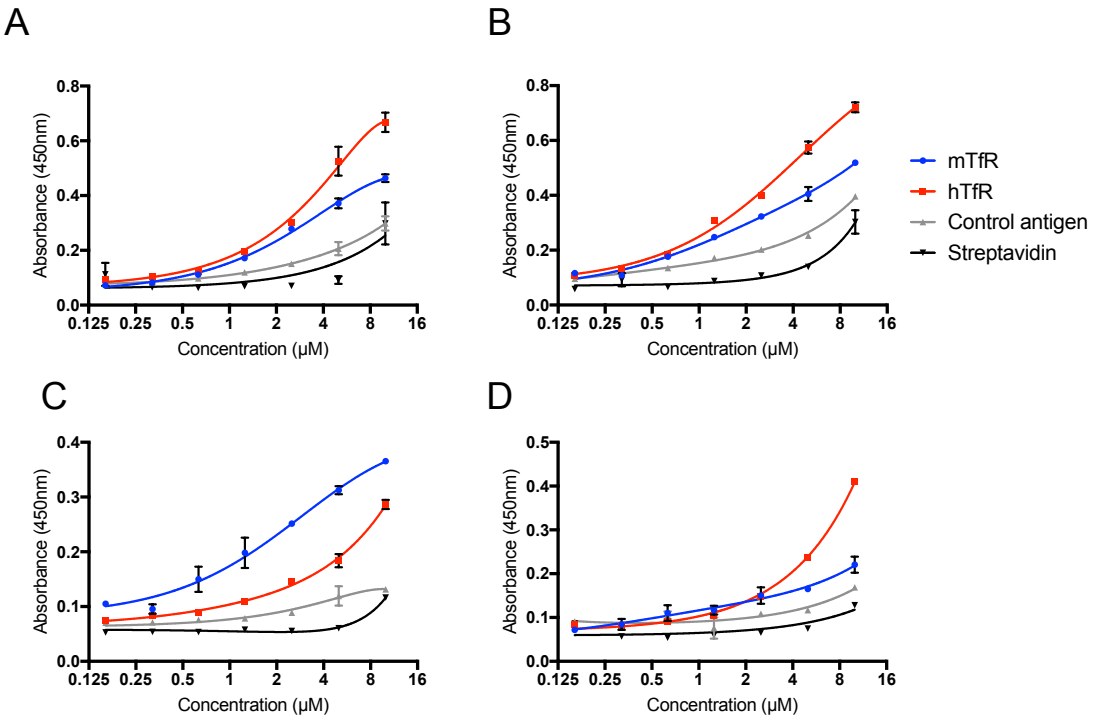

Figure 4.3.6: Titration summary of lead CPep-D1 soluble peptide binding to mouse and human TfR.

Titration of expressed CPep-D1 lead peptides, Pep1 (A), Pep8 (B), Pep9 (C) and Pep14 (D), towards 1 μg/ml biotinylated recombinant mTfR, hTfR, control antigen and non-TfR immobilised streptavidin coated plates, as determined by soluble peptide ELISA. Experiments were performed at a 1:2 serial dilution of CPep-D1 domains starting at 10 μM concentration. Summarised results are presented as averages of two experimental replicates, (n= 2).

4.3.4. Lead peptide candidates bind to immortalised mouse and human brain endothelial cell lines, bEnd.3 and hCMEC/D3.

ICC based cell binding assays were carried out using the four lead peptides Pep1, Pep8, Pep9 and Pep14 to establish whether CPep-D1 domains were capable of binding to TfR antigen expressed on the surface of brain endothelial cells, with all the relevant post-translational modifications (Davis et al., 1986; Jing and Trowbridge, 1990; Do and Cummings, 1992; Hayes et al., 1992; A. M. Williams and Enns, 1993).

Summarised results of the CPep-D1 cell binding assays are shown in Figure 4.3.7. All four lead CPep-D1 fusion domains were found to bind both mouse and human immortalised brain endothelial cell lines, bEnd.3 and hCMEC/D3, respectively (Figure 4.3.7, A). In order to quantitatively assess the extent of CPep-D1 domain binding towards bEnd.3 and hCMEC/D3 cells, mean grey value readings were

analysed using FIJI (ImageJ) from three images taken at random locations for each experimental replicate. The acquired mean grey value readings were multiplied with the number of cell nuclei within each image to normalise for cell density. A summary of the quantified results is shown in Figure 4.3.7, B and C.

The extent of cell binding was consistent with previous recombinant TfR affinity ranking ELISA based assays (Figure 4.3.6), thus confirming the binding profiles of lead candidates towards TfR. Pep1 and Pep8 exhibit the highest levels of cell binding with bEnd.3 and hCMEC/D3 (Figure 4.3.7, A and B). Pep9 and Pep14 also demonstrate cell binding towards mouse and human cell lines, (Figure 4.3.7, A and B).

Both Pep1 and Pep8 demonstrated a statistically significant 4.4- and 4.3-fold increase in binding towards bEnd.3 cells, when compared to the control CPep, respectively, (P= <0.0001), (Figure 4.3.7, A). In contrast, Pep9 and Pep14 demonstrated 2- and 1.7-fold increase in binding when compared to the control CPep, however these were not statistically significant, (Figure 4.3.7, A).

Pep1 and Pep8 exhibited a statistically significant 10.7- and -13.5-fold increase in binding towards hCMEC/D3 cells when compared with the control CPep, respectively, (P= <0.0001). Pep14 also demonstrated a statistically significant 3.8-fold increase in binding over the control CPep (P= 0.001 to 0.01). Pep9 demonstrated a 2.8-fold increase in binding in relation to the control, however this finding was not statistically significant.

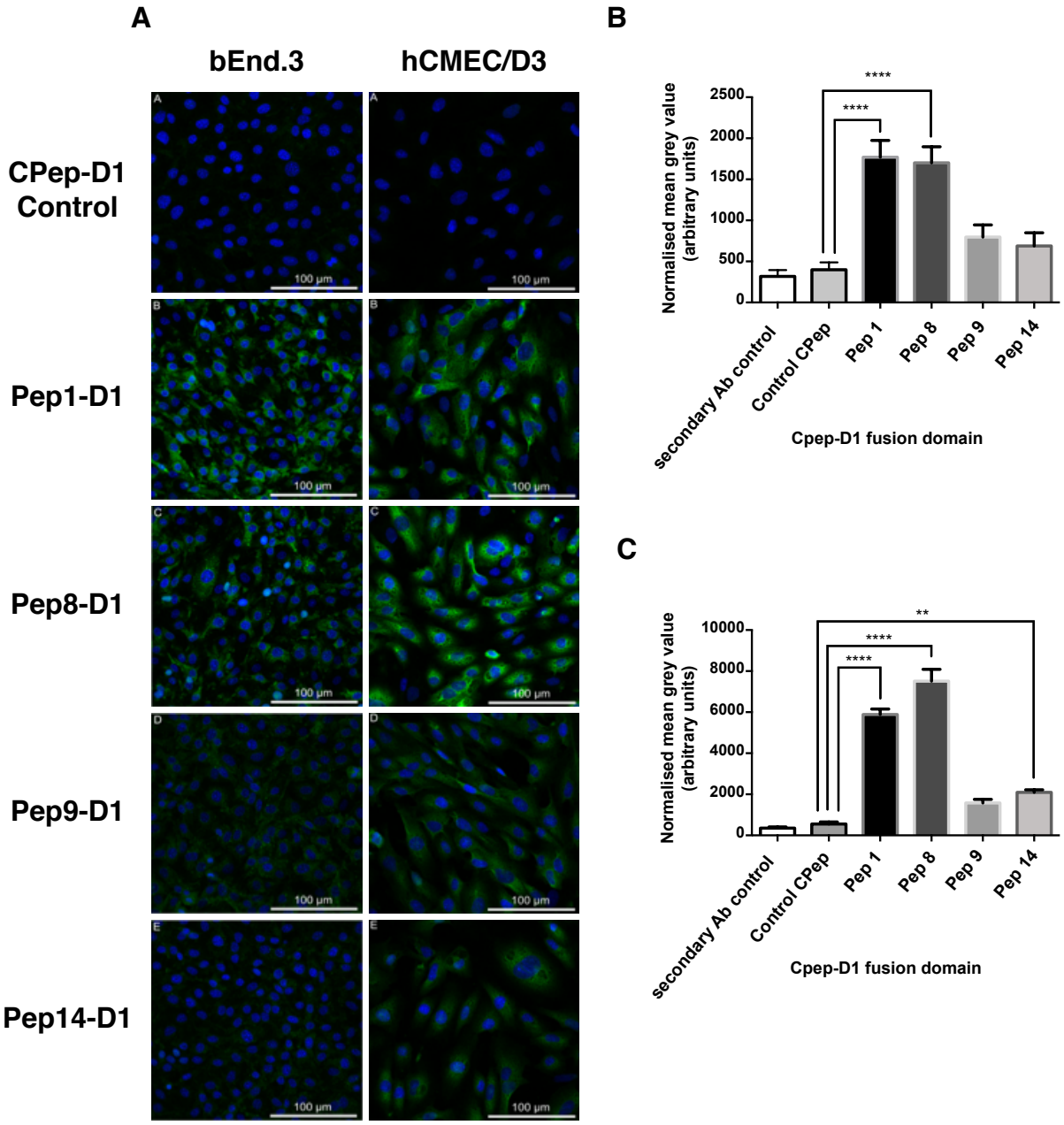

Figure 4.3.7: CPep-D1 bEnd.3 and hCMEC/D3 cell binding assay as determined by immunocytochemistry.

Figure summarising the results of the CPep-D1 brain endothelial cell binding study. bEnd.3 and hCMEC/D3 cells were grown in chamber slides for 48 hours, fixed in 4% PFA and incubated with 2 µM of monovalent Pep1, Pep8, Pep9 and Pep14 -D1 domains at 4°C for 4 hours. Secondary labelling was carried out with a mouse anti-his antibody and a goat anti-mouse FITC conjugated antibody. Z-stack images were acquired using a Leica SP5 confocal microscope, and max intensity images are shown (A). DAPI nuclear staining is represented by the blue channel, whilst CPep-D1 binding is represented by the green channel. A quantitative summary of ICC based CPep-D1 binding assays carried out against bEnd.3 (B) and hCMEC/D3 (C) is also shown. Mean grey value is presented as normalised average readings of three independent images acquired through ImageJ, per experimental replicate, ± SEM. ** P 0.001 to 0.01, **** $P < 0.0001$.

4.2.7. Pep1-Fc/IL1RA fusion molecule demonstrates mouse and human brain endothelial cell internalisation.

Pep1 and Pep8 were expressed as bivalent Fc-fusion proteins coupled to interleukin-1 receptor antagonist (IL1RA), (expressed by protein expression team, MedImmune, Cambridge, UK), in order to investigate the capacity these peptides to deliver a coupled cargo into mouse and human brain endothelial cells. To assess the optimal incubation time for peptide-Fc fusion domain internalisation within brain endothelial cells, an ICC time-course internalisation assay was carried out on bEnd.3 cells ranging from 5 min to 120 min time points. To quantitatively determine uptake at each internalisation time-point, the mean grey value readings were acquired via FIJI (ImageJ), and normalised to the number cells as outlined in section 4.2.5.2.

Summarised results of the internalisation time course and the quantitative mean grey value summary are shown in Figure 4.3.8 and Figure 4.3.9, respectively. As expected no staining was observed with the negative control CPep-Fc/IL1RA, Figure 4.3.8, A. Pep1-Fc/IL1RA demonstrated observable internalisation from the 15 min time point, saturating within cells by the 60 min time-point, Figure 4.3.8, B, and Figure 4.3.9. Unlike Pep1-Fc/IL1RA, Pep8-Fc/IL1RA demonstrates low levels of internalisation within bEnd.3 cells when compared to control CPep-Fc/ILRA, Figure 4.3.8, C, and Figure 4.3.9. In contrast, positive control anti-mTfR 8D3 antibody was internalised and saturated within cells after the 5 min time point Figure 4.3.8, D, and Figure 4.3.9. Since Pep8 demonstrated low bEnd.3 cell internalisation when expressed within the -Fc/IL1RA format, it was not carried forward for further studies.

Internalisation and sub-cellular co-localisation of Pep1-Fc/IL1RA was assessed towards hCMEC/D3 cells by means of ICC using labelled antibodies directed to the Fc domain of the fusion protein, a cellular early endosomal marker (EEA1) and a cellular lysosomal marker (LAMP1). Results are summarised in, Figure 4.3.10.

As expected control CPep-Fc/IL1RA did not present any internalisation within hCMEC/D3 cells as indicated by the lack of observable green staining (Figure 4.3.10, A, B, E and F). Pep1-Fc/IL1RA was observed to internalise within hCMEC/D3

cells (Figure 4.3.9, C, D, G and H). No distinct co-localisation was observed with EEA1 or LAMP1 at 60 and 120 min time points (Figure 4.3.10, G and H).

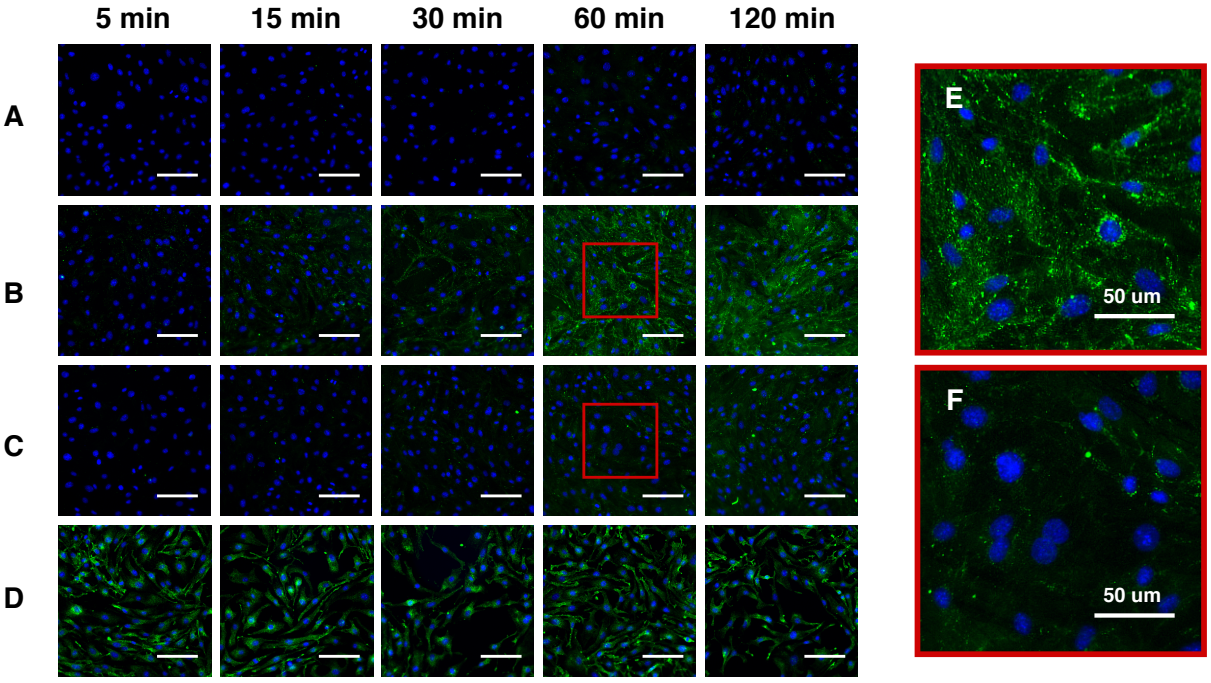

Figure 4.3.8: CPep-Fc/IL1RA bEnd.3 cell internalisation time course at 5, 15, 30, 60 and 120 min time points.

bEnd.3 cell internalisation of control CPep-Fc/IL1RA (A), Pep1-Fc/IL1RA (B), Pep8-Fc/IL1RA (C) and anti-mTfR 8D3 antibody (D). CPep-Fc fusions were incubated with cells at 5 µM concentration, whilst anti-mTfR 8D3 antibody was incubated at a concentration of 2 µg/ml. Blue channel represents nuclear staining. Green channel represents internalised CPep-Fc/IL1RA (A, B, C) or anti-mTfR 8D3 MAb (D). Enlarged representations of Pep1-Fc/IL1RA and Pep8-Fc/IL1RA internalisation at the 60 min interval are shown in (E) and (F), respectively. Images were acquired at x20 magnification using a Molecular Probes ImageXpress XLS system. Results are representative of three experimental replicates (n= 3).

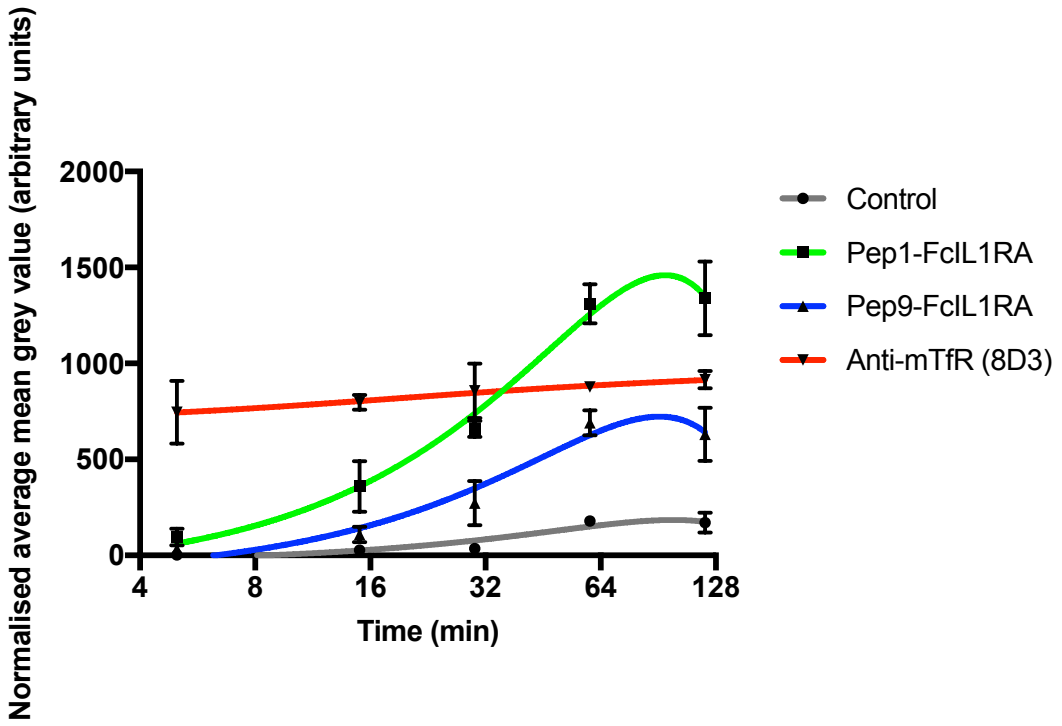

Figure 4.3.9: Quantified average mean grey values of CPep-Fc/IL1RA bEnd.3 internalisation assay.

A quantitative summary of the ICC based CPepFc/IL1RA internalisation time course carried out towards bEnd.3 cells. Mean grey value is presented as normalised average readings of three independent images acquired through ImageJ, per experimental replicate (n= 3), ± SEM.

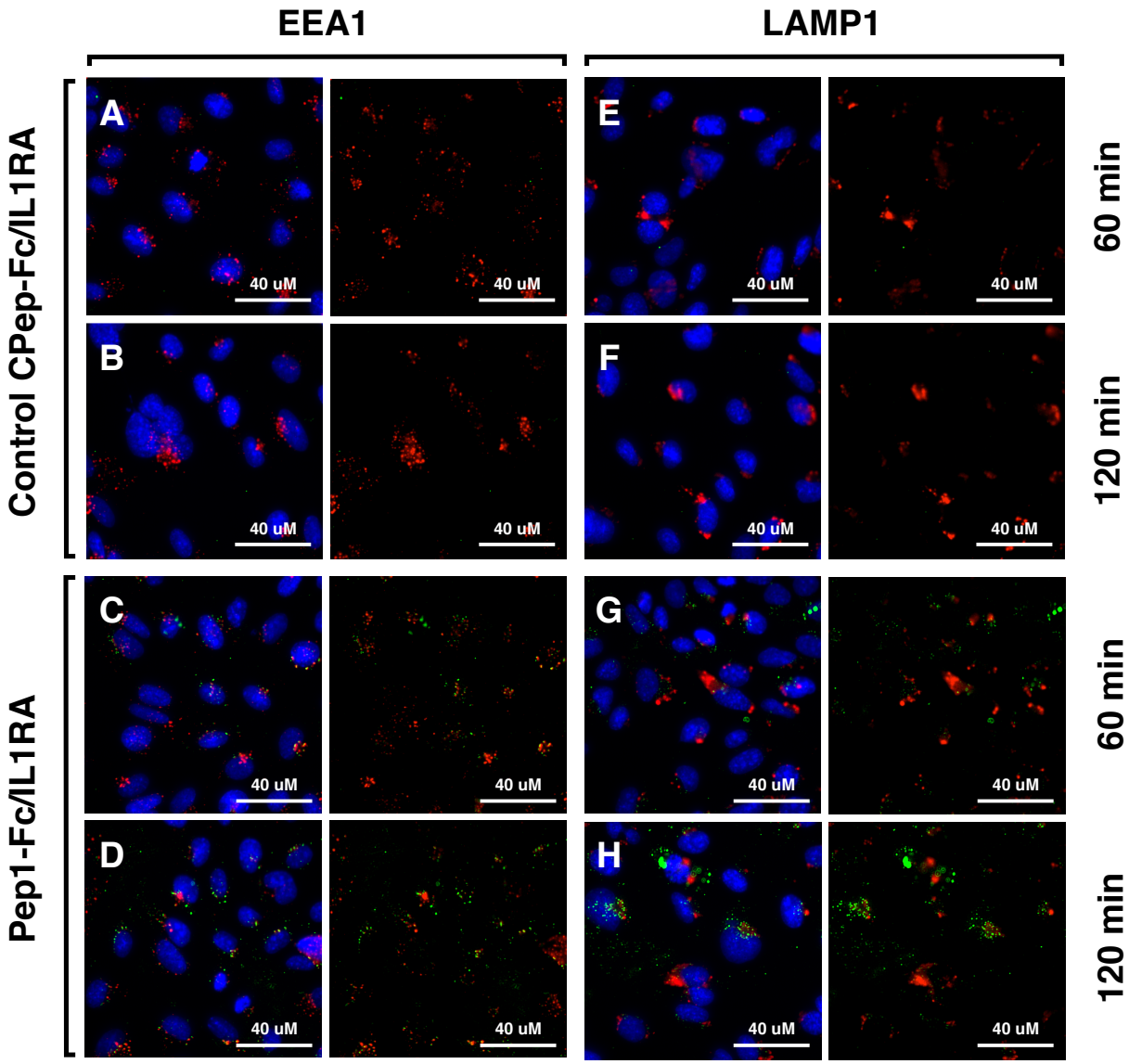

Figure 4.3.10: Pep1-Fc/IL1RA hCMEC/D3 cell internalisation and intracellular co-localisation assays.

Immunofluorescence images of hCMEC/D3 cells showing staining for control CPep-Fc/IL1RA (A, B, E and F) and Pep1-Fc/IL1RA (C, D, G and H) internalisation (green), with or without visible nuclear staining (blue). Intra-cellular trafficking of Pep1-Fc/IL1RA fusion domains was assessed using early endosomal antigen-1 (EEA1), (A, B, C, and D) or lysosomal-associated membrane protein 1 (LAMP1), (E, F, G and H) and are both represented by red staining. Control CPep-Fc/IL1RA and Pep1-Fc/IL1RA fusion molecules were both assessed at 60 and 120 min intervals. Images were acquired at x63 magnification using a Molecular Probes ImageXpress XLS system. Results are representative of three experimental replicates, (n= 3).

4.4. Discussion

4.4.1. Construction of pC6-D1/FLAGHIS expression vector and sub-cloning of CPep sequences.

Identified peptide candidates were initially screened as pentavalent g3p fusion domains which resulted in the observed multivalent binding towards target mouse and human TfR antigens (described in chapter 3). In order to evaluate the relative affinity of each peptide in the absence of avidity effects, peptides must be produced and characterised for binding as monovalent domains. Typically, the production of peptides can be achieved using solid phase chemical synthesis techniques. However, these techniques can be costly, which poses a problem for the efficient affinity ranking of large numbers of peptide candidates (Yuan Bi et al., 2006). Cellular expression systems provide a more viable approach to the production of relatively large quantities of recombinant peptide, whilst also allowing the simple incorporation of polypeptide affinity tags (Lindhout et al., 2003).

The most commonly utilised expression system, *E.coli*, has been exploited using a variety of expression vectors and is typically well suited for the expression of soluble domains under 60 kDa in size, although successful expression of larger proteins has also been reported (Rosano and Ceccarelli, 2014). The reducing environment of the cytoplasm, prevents the formation of di-sulphide linkages and often requires further steps to refold proteins *in vitro* (Rouet et al., 2012). However, researchers have overcome these issues by expressing proteins and peptides within the periplasmic space found in gram negative bacteria, an oxidising environment that is suitable for the formation of disulphide linkages (Lindhout et al., 2003). The direct expression of peptides remains challenging due to poor solubility and protease stability. The expression of peptides with a stable and highly soluble fusion partner domain can ameliorate these concerns (Amarasinghe and Jin, 2015). Typically, the yield of peptide obtained from *E.coli* periplasmic expression is dependent of the molecular weight of the coupled fusion partner. Smaller fusion partners tend to result in higher expression yields (Yuan Bi et al., 2006).

The pC6-D1 phagemid expression vector was chosen for the expression of peptide fusions to g3p-domain 1 as a means of enhancing solubility, reducing proteolytic degradation and facilitating cell expression and purification of the single domain peptides (Malik, 2016). This vector is based on the pCANTAB6 vector used to express single chain fragment variable (scFv) antibody domains (McCafferty and Johnson, 1996; Qi et al., 2012). The vector incorporates the complete coding region for g3p-domain 1 (g3p-D1), followed by a short flexible linker, a His_{10} tag and an ochre stop codon.

Structurally the 66 amino acid globular g3p-D1 is comprised of six stranded β-sheets that form a barrel unit which is capped at the N-terminal region with a short α-helix (Holliger and Riechmann, 1997; Holliger et al., 1999). Importantly for its use as fusion partner, g3p-D1 is a highly stable domain with a melting temperature of 66.8°C due to the presence of two disulphide linkages, and a N-terminal α-helical cap. The use of a short flexible GGSG linker between the peptide and the g3p-D1 fusion protein prevents steric hindrance of the cyclic peptide, allowing for greater freedom of interaction. The use of a suitable linker has also been shown to prevent protein mis-folding, whilst improving expression yields and bioactivity of the fusion domains (X. Chen et al., 2013).

For the purpose of this study, an alternative variant construct of the pC6-D1 vector, was generated in order to introduce a unique NotI restriction site to facilitate efficient sub-cloning of peptide sequences, and a FLAG tag for detection of peptide binding within ELISA based recombinant TfR binding assays. Although many affinity tags have been developed with varying sizes and functional properties (reviewed in Terpe, 2003), the FLAG tag was chosen in this case since it consists of a short, hydrophilic sequence and like the polyhistidine tag, does not usually interfere with the native folding and function of the fused protein (Einhauer and Jungbauer, 2001).

Results of the pCANTAB6 stock vector digestion with NotI and EcoRI showed a large proportion of the digested vector remained at its full length, as demonstrated by the band seen at 4544 bp (Figure 4.3.2, B). This observed band likely represents the single NotI digested product and is a result of the inefficiency of the EcoRI enzyme in NEBuffer 3.1 buffer, which only exhibits 50% activity in contrast to NotI which demonstrates 100% activity. Following ligation of the modified insert, the pC6-D1/FLAGHIS vector was transformed into competent *E.coli* DH5α cells and sequence validated, results are shown in. As expected the modified vector contained the inserted NotI restriction digest site downstream of the peptide insert region, in addition to the correct FLAG sequence, DYKDDDDK.

The precise FLAG sequence is vital for antibody recognition. Several monoclonal anti-FLAG antibodies have been identified towards the FLAG peptide sequence, namely anti-FLAG M1, M2 and M5, with each antibody having specific binding epitopes and properties (Einhauer and Jungbauer, 2001). The most commonly used and versatile of these antibodies is the mouse monoclonal anti-FLAG M2, which is capable of recognising the FLAG motif expressed at the N-, Met-N-, C- termini, and also within internal sites of the fusion protein, through a calcium independent manner. Utilising a peptide phage display library, Srila *et al*. (2013) carried out biopanning selections against anti-FLAG M2 to elucidate the consensus binding motif of this antibody. The group found that the consensus motif 'DYKxxD' was essential for proper binding of the FLAG peptide. Moreover, the group also discovered that C-terminal hydrophilic amino acid residues flanking this motif were preferentially selected towards the anti-FLAG M2 antibody, suggesting those residues also conferred some binding advantage towards anti-FLAG M2.

4.4.2. Periplasmic expression of monovalent CPep-D1 domains.

Although expression yields were within the expected range for nine of the expressed peptide candidates, the remaining candidates showed consistently low yields (Pep2, Pep4, Pep12, Pep13 and Pep15) or failed expressions (Pep10 and Pep16) with multiple expression attempts (Figure 4.3.3).

The poor or failed expressions observed with these peptides are likely to be due to the inherent sequence structure of the cyclic peptide and its effect on periplasmic expression within the *E.coli* host. Several factors have been shown to lead to poor or failed expressions (Rosano and Ceccarelli, 2014). The expressed peptide sequence may have a detrimental effect on a host cell function, which can lead to cell toxicity (Saïda, 2007). A lower yield may also be a result of low mRNA stability (Tegel et al., 2011) or mRNA secondary structure formation, which limits efficient translation. Furthermore, mRNA codons encoding the heterologous protein are not all equally translated within cellular hosts such as *E.coli* and this can lead to low or failed expression where minor codon usage is present within the peptide sequence (Kane, 1995). This results from an inherent frequency bias of codon use within *E.coli* and their cognate tRNA levels. Several factors lead to expression deficits with minor codon usage, these include the formation of truncated proteins via disrupted translation, reduced cell growth and frame shift mutations (Kleber-Janke and Becker, 2000). Kane *et al.* (1995) previously highlighted 18 minor codons with less than 1% frequency usage within *E.coli*. Of the 18 minor codons, 7 of the least prevalent codons are most commonly reported to interfere with heterologous expressions within *E.coli*, these are shown in Table 4.4.1.

Table 4.4.1: Most commonly reported minor codons and their frequency representation by *E.coli* (adapted from: Kane *et al*. 1995).

Minor codon	Encoded Amino acid	Frequency (per 1000 codons)
AGG	Arginine	1.4
AGA	Arginine	2.1
CGA	Arginine	3.1
CUA	Leucine	3.2
AUA	Isoleucine	4.1
CCC	Proline	4.3
CGG	Arginine	4.6
GGA	Glycine	7.0

Closer examination of the seven peptide sequences that exhibited low or failed expression revealed that four peptide sequences contained minor codons, with Pep2 and Pep16 containing two codons within their short 16 codon sequence (highlighted codons in Table 4.4.2). The minor codons that appear within the peptide sequences are CCC (Proline) and CGG (arginine). Previous studies have shown that minor codon presence close to the initiation codon of an mRNA sequence can significantly reduce its translational efficiency, through ribosomal stalling at minor codons and the limited availability of the less abundant tRNAs (G.-F. T. Chen and Inouye, 1994). These minor codons are commonly observed within the first 25 codons of *E.coli* genes, and are thought to be intrinsically involved in *E.coli* gene regulation via growth rate restriction.

Table 4.4.2: Minor codon usage within the variable peptide encoding region of poorly expressing CPep-D1 domains.

CPep ID	AA sequence	Nucleotide sequence (5' – 3')
Pep2	IHCHPQGDQSVSFCWR	ATC CAC TGT CAC CCC CAG GGC GAC CAG AGC GTC TCC TTC TGT TGG CGG
Pep4	LYCYPTKLPWVEYCHE	CTC TAC TGT TAC CCG ACG AAG CTC CCC TGG GTC GAG TAC TGT CAT GAA
Pep12	TWHYQCITMNCDVLVG	ACG TGG CAC TAC CAG TGT ATC ACC ATG AAC TGT GAC GTG TTG GTG GGG
Pep13	WVCTPLDSEIIEICQL	TGG GTC TGT ACC CCG CTC GAC TCC GAG ATC ATC GAG ATC TGT CAG CTG
Pep15	LHCTSIWSDVVQLCDL	TTG CAC TGT ACC TCC ATC TGG AGC GAC GTG GTG CAG TTG TGT GAC CTC
Pep10	LHECTYYWWGLDCSFR	TTG CAC GAG TGT ACG TAC TAC TGG TGG GGG TTG GAC TGT TCC TTC CGG
Pep16	PLCTPIFPPFVLMCEE	CCC CTC TGT ACG CCC ATC TTC CCG CCG TTC GTG TTG ATG TGT GAG GAG

The 16 codons that make up the peptide sequence all fall within the first 25 codons downstream of the initiator codon, any presence of minor codons within these peptide encoding sequences is therefore likely to interfere with efficient

translation. In the case of Pep16 which shows two CCC codons at the 5' region of the sequence, this resulted in a failed expression.

Several approaches have been used to overcome the translational issues posed by minor codon usage within recombinantly expressed proteins. The simplest method, codon optimisation, involves replacing minor codons with those more frequently represented in *E.coli* and code for the same amino acid residue (Marlatt et al., 2010; Tiwari et al., 2010).

Expressed CPep-D1 domains were primarily observed as soluble monomers at a size of 13 kDa on SDS-PAGE gels (Figure 4.3.4, A). However, nine of the expressed peptide candidates also demonstrated secondary bands on SDS-PAGE gels. The secondary band observed at approximately 15 kDa with Pep1, Pep8 and Pep9 could be due to translational read-through the ochre stop codon, resulting in the expression of a c-terminal extended fusion protein. The secondary bands observed at 26 kDa are likely due to dimerisation of the individual CPep-D1 domains. In addition to exhibiting a dimer band at 26kDa, Pep7 also demonstrated bands at 38 kDa and 52 kDa. These three bands appear to correspond to multimeric forms of the fusion protein, i.e. dimer, trimer and tetramer.

Protein aggregation is defined as the amalgamation of monomeric domains in their native or non-native states to form soluble or insoluble multimeric units (Moussa et al., 2016). The formation of aggregates during protein production is a multifactorial process, which initiates with the non-covalent interaction of proteins that form soluble reversible aggregates under the influence of a stressor or non-optimal storage conditions (e.g. temperature, pH, agitation, concentration). These reversible aggregates can subsequently act as foci for insoluble aggregate formation via a nucleation growth process. The formation of protein aggregates poses major challenges for the production of therapeutic proteins, since these aggregates often cause a loss in biological activity and have been shown to cause immunogenic responses, as demonstrated both *in vitro* and *in vivo* (Daha et al., 1982; Fradkin et al., 2009; Hermeling et al., 2006; Q. Luo et al., 2011; Joubert et al., 2012) .The intrinsic heterologous protein structure, expression vector, expression host cell and purification methods all play a significant role in the susceptibility of a protein to form

aggregates. These numerous factors make identifying the source of aggregation problematic and time-consuming. Although, the use of a fusion domain has been shown to minimise the formation of spontaneously occurring aggregates, studies have shown that hydrophobic regions within the fusion proteins are likely to also play role in aggregate formation (Lebendiker and Danieli, 2014). The intrinsic structure Pep7 appears to be the most susceptible to aggregation, since it resulted in the formation multimeric aggregates of varying sizes, as demonstrated by visible banding in increments of 13 kDa.

Although unnecessary at this stage of lead candidate discovery, it is possible to isolate and sequence the secondary band(s) via N-terminal sequencing (Edman sequencing) to identify the exact sequence of these contaminating bands (Joo et al., 2006).

4.4.3. Four CPep candidates bind specifically to recombinant mouse and human TfR expressed as CPep-D1 fusion domains.

Four cyclic peptide candidates (Pep1, Pep8, Pep9 and Pep14) were identified to bind specifically towards mouse and human TfR as soluble monovalent CPep-D1 domains (Figure 4.3.5). Detection of bound flag tagged CPep-D1 domains in this case was carried out via an anti-FLAG M2 antibody. In contrast to phage ELISA screening conducted using phage supernatant, the absorbance readings observed with these results are more insightful into the binding profiles of the monovalent peptide domains, and thus any variances in the overall binding curves of the peptides towards either mouse or human TfR, could reflect the relative binding affinity of the peptide towards the antigens. However, it is important to note that the binding affinity cannot be deduced using ELISA techniques, since the immobilisation of antigens via biotin tags onto streptavidin plates likely results in the steric hindrance of some epitopes (Underwood, 1993).

The precise binding affinity can be determined using more sensitive biomolecular interaction techniques such as surface plasmon resonance (SPR). These techniques rely on the use of optical-based biosensors to determine the one-to-one interaction of molecules in real-time without necessitating the need for labels

(Nguyen et al., 2015). The incorporation of a label to a biomolecule can in some cases detrimentally impact the overall structure and function of a given biomolecule, resulting in disrupted molecular interaction properties. The use of SPR therefore provides a means quantitatively assessing K_{on} and K_{off} kinetics for native biomolecular interactions, under label-free conditions (D. Yang et al., 2017).

Due to the aforementioned restrictions in CPep-D1 expression yields and cell binding assay requirements, ELISA screening of monovalent CPep-D1 domains was carried out using two experimental replicates. Contrary to phage ELISA screening results, Pep7 does not appear to bind mTfR, hTfR, or the control antigen when expressed within the CPep-D1 format, Figure 4.3.4 At first glance this appears to indicate that the peptide is a false positive clone identified via phage ELISA screening. However, since this peptide was observed to bind as a pentavalent fusions on phage particles throughout several experiments (Figure 3.3.5, and Figure 3.3.6), it is likely to be a weak affinity peptide that exhibits binding due to avidity effects of multivalent expression, a commonly observed phenomenon with phage display selections conducted in the g3p pentavalent fusion format (Gabryelczyk et al., 2015). Alternatively, with Pep7 being identified as the peptide most susceptible to aggregation, the lack of observed binding may be related to the presence of multimeric aggregate forms of the Pep7-D1 fusion protein observed on the SDS-PAGE gel (Figure 4.3.3), which may impede binding or interfere with effective detection of the FLAG tag. A study by Jannssen *et al*. (2015) have previously highlighted that the presence of oligomers within a protein sample can interfere with the accuracy of ELISA measurements. Using Aβ as an aggregate protein model, the group showed a decreased detection signal with highly oligomerised Aβ samples. Furthermore, disaggregating the oligomerised Aβ by treatment with trifluoroacetic acid and hexafluoroisopropanol, resulted in a recovery of the detection signal, which was not observed when monomeric protein was subjected to the same pre-treatment.

Pep3 (TTFPSCHPQTCYDGVQ) and Pep6 (GWHPMCNLMACSQGRP) both demonstrated higher absorbance readings towards streptavidin than mouse and human TfR, thus confirming they are TUP clones enriched throughout phage display

selections towards the streptavidin affinity capture matrix (Thomas et al., 2010). As previously predicted with phage ELISA positive clone sequence analysis, Pep3 binds to streptavidin via the consensus 'HPQ' motif within its sequence (Section 3.4.2). Interestingly, the 'HPM' motif binds streptavidin with a lower affinity than that seen with 'HPQ', as demonstrated by the lower absorbance reading seen with Pep6 in contrast to Pep3 (Figure 4.3.4), and these results are consistent with a previous study demonstrating the affinity of the two motifs (Gissel, Jensen, Gregorius, Elsner, Svendsen, and Mouritsen, 1995b). Binding could also be observed within the mTfR, hTfR and control antigen coated wells of Pep3 and Pep6 assays. This binding is likely to be towards non-occupied binding epitopes on streptavidin molecules, rather than non-specific binding. As discussed in chapter 3, avoiding the enrichment of TUP clones throughout phage display selections is difficult, even when de-selection steps are employed. The remaining peptide sequence surrounding the tripeptide 'HPQ' motif plays little to no role in mediating streptavidin binding, however preferential enrichment of phenylalanine, glycine, asparagine and valine residues have been reported following the glutamine residue of the 'HPQ 'motif (Menendez and Scott, 2005).

According to the CPep-D1 titration results, it appears that all four lead peptides, Pep1, Pep8, Pep9 and Pep14 demonstrate weak affinity profiles (Figure 4.3.5). When compared to the CPep-D1 control, all four lead peptides exhibit specific binding within the micro-molar range. This finding was anticipated, since peptides selected in this phage display format tend to be significantly weaker affinity than antibodies also selected via phage display. Additionally, selections were conducted in manner to encourage the identification of lower affinity peptides by maintaining higher concentrations of target TfR antigen throughout later selection rounds. Theoretically, the identification of low to medium affinity peptides in the context of targeting the BBB would be advantageous since it has been shown to positively influence the fate of transcellular trafficking across the BCEC by avoiding lysosomal degradation (Bien-Ly et al., 2014).

Once again, Pep1 and Pep8 exhibited the highest degree of binding towards mouse and human TfR of the four lead candidates. Interestingly, even though

blocking steps were carried out, both of these lead peptides also demonstrated non-specific binding, which was observed at higher concentrations towards the irrelevant control antigen and streptavidin coated plates. In contrast, non-specific binding was not observed when these peptides were expressed as pentavalent g3p fusions during phage ELISA screening, Figure 3.3.6.

The poor potency of these peptides, in combination with the crude purification method used to generate the monovalent g3p-domain 1 fusions, may be one reason for the observed non-specific binding. However, it appears that the inherent amino acid makeup of the peptides also plays a role in non-specific activity since Pep8 appears to be more pre-disposed to non-specific binding than Pep1, as demonstrated by the increased non-specific binding from 0.63 – 10 µM concentrations.

4.4.4. Lead cyclic peptide candidates bind bEnd.3 and hCMEC/D3 cells

CPep cell binding assays were conducted towards bEnd.3 and hCMEC/D3 cells in order to assess whether the four identified lead peptide candidates could recognise TfR expressed natively on the cell surface of *in vitro* cultured immortalised brain endothelial cells. TfR undergoes significant post-translational modifications within the mammalian cell (Davis et al., 1986; Jing and Trowbridge, 1990; Do and Cummings, 1992; Hayes et al., 1992; A. M. Williams and Enns, 1993). These modifications are not always reflected correctly with expressed recombinant protein. The validation of peptide binding towards cells is therefore important for the identification of functionally relevant peptides.

The four lead peptide candidates Pep1, Pep8, Pep9 and Pep14 all bound with various binding profiles towards the two cell lines when compared to the CPep-D1 control, (Figure 4.3.7). As anticipated, the highest fluorescence intensities were observed with Pep1 and Pep8 for both cell lines. These results are consistent with previous recombinant TfR binding assays, where Pep1 and Pep8 persistently demonstrate the highest degree of binding towards recombinant mTfR and hTfR, (Figure 3.3.5 and Figure 3.3.6).

Due to time and reagent limitations, it was not possible to determine whether cell binding occurs competitively with Tf. As previously discussed in section 3.3.5, the sequences of Pep1 and Pep10 share a homologous 'DCS' motif with Tf, and this motif amongst others ('WGG' and FR) may mediate the identified peptides to TfR.

Eckenroth *et al.* (2011), have previously shown that arginine 646 which located within a canonical 'RGD' sequence (arginine 646, glycine 647, and asparagine 648) of TfR is vital for binding to Tf. Furthermore, it was suggested that these residues are within binding range of Tf residues 356, 359 and 366 located within the C1-lobe of Tf and are vital for Tf binding to TfR. The group concluded that the remaining van der Walls interactions between the C1-lobe of Tf and TfR likely show limited conservation with the specificity for binding between Tf and TfR. This finding alongside the proposed site of binding discussed in section 3.4.3, could suggest that binding of Pep1 to TfR residue arginine629 may or may not interfere with Tf interaction, and this would need to be demonstrated experimentally. One means of assessing this, would be to incubate cells with Pep1 and recombinant TfR protein at equimolar concentration, and determine whether there is a reduction in binding when compared to Pep1 alone.

4.4.5. Pep1-Fc/IL1RA internalises within bEnd.3 and hCMEC/D3 cells

Targeting TfR has been extensively shown to be an effective strategy for the delivery of macromolecular drugs and large nano-carrier conjugates into cancer cells and across the BBB (Q. Ye et al., 2012; Yue Zhang et al., 2017; Yu et al., 2014; T. Kang et al., 2015; Webster et al., 2017). Ligands that are multivalent or contain multiple pharmacophores, can synergistically interact with targets and this leads to an apparent increase in their 'functional affinity' or more commonly referred to as avidity. Naturally occurring multivalent immunoglobulins, such as IgG typically have strong affinities towards their targets due to their bivalent structure. The increased avidity is a result of cross-linkages formed between two target antigens. When one pharmacophore binds towards a target site, the local co-presence of the secondary pharmacophore within close proximity leads to a higher local concentration and increased residency time, which results in an increased probability of secondary site binding and rebinding of the dissociated, tethered pharmacophore (Vauquelin and

Charlton, 2013). Researchers have exploited the multivalent nature of IgG antibodies by generating highly engineered Fc-Fusion molecules which mimic the bivalent structure of IgG. The first instance of fc-fusion use was described in 1989 (Czajkowsky et al., 2012). Since then, many Fc-fusion domain therapies have been researched, developed and approved, with one example etanercept reaching 'blockbuster drug' status (Willrich et al., 2015; Beck and Reichert, 2014).

An engineered Fc-fusion molecule is typically constructed by fusing a peptide or protein encoding sequence to the N-terminal encoding sequence of the Fc-domain, via the use of a linker. The appropriate choice of linker can vary with the required structural properties and pharmacokinetic characteristics (X. Chen et al., 2013). However, typically the most versatile are the flexible glycine-rich repeat linker, e.g. $(G_4S)_n$ of a suitable length to avoid steric hindrance or interaction of the effector molecule with the Fc-domain. The primary advantage for the fusion of an effector molecule to the Fc-domain is the ability to take advantage of extended half-life through the pH dependant binding to FcRn, and averting degradation in endo-lysosomal compartments (Beck and Reichert, 2014; Strohl, 2015). Furthermore, expression of the effector domain as an Fc-fusion also facilitates with protein or peptide stability, expression and label-free purification via protein A affinity chromatography (Stanislaus et al., 2017; Zwolak et al., 2017). Whilst FcRn mediated receptor recycling extends the half-life of Fc containing therapeutics, studies have demonstrated that FcRn expressed on BCEC primarily functions in the efflux of IgG from the CNS into the blood via a process of 'reverse transcytosis' (Cooper et al., 2013; Deane et al., 2005; Schlachetzki et al., 2002). Nevertheless, the inclusion of an Fc-domain does confer an advantage for the transcytosis of macromolecules across the BBB. Haqqani *et al*. (2017) recently reported that the inclusion of an Fc domain to single domain antibodies results in a redistribution from late endosomes and lysosomes to early endosomes and multi-vesicular bodies, which increases transcytosis to the abluminal side of the BBB.

In order to improve avidity and also determine the capability of the lead peptides (Pep1 and Pep8) to deliver a cargo into BCEC, the lead peptides were engineered as CPep/Fc-fusion domains. These domains were also expressed

coupled to IL1RA on the C-terminal CH3 region of the Fc domain (the rationale of which is discussed later on in this section). The overall structure of the CPep-Fc/IL1RA molecule is shown in Figure 4.4.1.

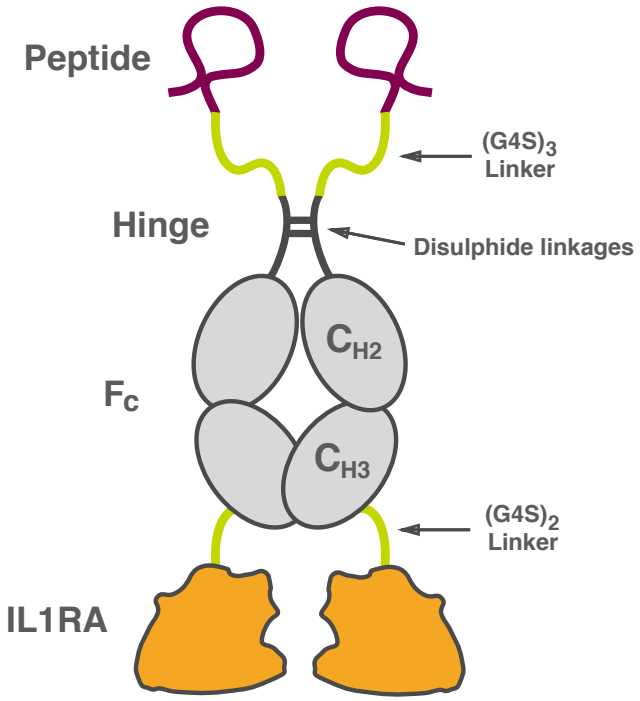

Figure 4.4.1: Schematic representation of CPep-Fc/Il1Ra structure.

Figure depicting the engineered structure of CPep-Fc/IL1RA. The molecule consists of the peptide fused to the N-terminal hinge region of the Fc domain via a flexible $(G4S)^3$ linker. IL1RA is fused to the C-terminal, CH_3 region of the Fc domain. Image not to scale. Approximate size of molecule is 70 kDa.

A bEnd.3 cell internalisation time course ICC assay was carried out in order to assess the optimal cellular uptake time for lead peptides, Pep1 and Pep8, expressed as CPep-Fc/IL1RA domains, (Figure 4.3.7 and Figure 4.3.8). A stark difference in fluorescence was observed between Pep1 and Pep8. When expressed as an Fc-IL1RA fusion domain, it appears Pep8 no longer maintains its potent activity as demonstrated by the disperse faint fluorescence observed throughout Pep8 time points and the lower normalised mean grey value readings as determined through quantification of images. Furthermore, none to very little specific internalisation can be seen within cells. The reason for this is unclear, since the specific binding of Pep8 as a monovalent CPep-D1 fusion had already been successfully demonstrated towards bEnd.3 and hCMEC/D3 cells, (Figure 3.3.5, Figure 3.3.6, Figure 4.3.4, and

Figure 4.3.5). Additionally, Webster *et al*. (2017) have previously reported that the expression of monoclonal antibodies fused to IL1RA demonstrated no observable effect on binding activity of Fab domains.

The variation in biological activity observed for Pep8 expressed as –g3p, –D1 and –Fc fusion formats could be due to the inherent structure of Pep8, the way it interacts with the –Fc/IL1RA domain and the feasibility of expression within mammalian cells. Whilst mammalian expression systems generate proteins that are properly folded with post-translational modifications, the overexpression of these proteins within the mammalian cell can overwhelm protein folding mechanisms, leading to the production of misfolded or partially processed proteins which are prone to aggregation (Schröder et al., 2002). Strand *et al*. (2013) have previously studied the aggregation mechanisms of glycosylated Fc-fusion domains produced in CHO cells. The group utilised the high molecular weight species of activin receptor-like kinase 1 Fc-fusion protein as a model for soluble aggregate formation, and highlighted the existence of two populations of aggregates. The majority of aggregates were found to be covalently linked via non-native intermolecular disulphide linkages, whilst the smaller population associated via non-covalent interactions. The group also demonstrated that secondary structure and glycan micro-heterogeneity of proteins differ according to the overall size of the aggregates. Another study has also suggested that Fc-fusion protein aggregates are formed through free thiol cross-linking at the peptide moiety of the fusion protein (Wei Wang and Roberts, 2010).

Conversely to Pep8, Pep1 shows a linear increase in specific internalisation from 5 min to 30 min, saturating at 60 – 120 min time points as indicated through quantification of normalised mean grey value readings (Figure 4.3.9). At the 5 and 15 min time points, internalisation appears to be primarily localised to outer regions of cells with few internalised vesicles visible. In contrast to the anti-mTfR 8D3 antibody control, Pep1 mediated uptake occurs at a slower rate. He *et al*. (2015) have previously studied the trafficking of TfR within an engineered CHO cell line expressing TfR-EGFP fusions. Through live cell ICC assessment, the group were able to study the time-dependant internalisation of a hTfR specific antibody. The

group highlighted the fast turnover of TfR through co-localisation of EGFP with EEA1, which was detected after 5 min and LAMP1 following 30 min. The results described herein show that the high binding affinity 8D3 antibody and the fast turnover of TfR lead to saturated internalisation in less than the minimum 5 min time point. In contrast to Pep1- and Pep8- Fc/IL1RA, no linear increase in internalisation was observed with the quantified 8D3 antibody mean grey values, (Figure 4.3.9). These results further highlight the low binding affinity of these peptides, which even when expressed as higher avidity bivalent fusion domains, retain a slow rate of cell uptake in contrast to antibodies. As previously described by Yu *et al*. (2011), the use of high affinity antibodies and therapeutic dosing strategies, detrimentally effects the fate of internalised vesicles by triggering the carriage transfer from late endosomes to acidic lysosomes, which results in protein degradation, and reduced transcellular transport. In this case, the observed reduced rate of internalisation of Pep1-Fc/IL1RA may be a favourable trait for transcellular delivery, however this would need to be explored further using BCEC cell transcytosis studies.

In order to assess the capacity of Pep1-Fc/IL1RA molecules to internalise within hCMEC/D3 cells and examine their intracellular fate, an ICC internalisation and preliminary co-localisation study was carried out at 30 and 60 min time points, Figure 4.3.10. As observed with bEnd.3 cells, internalisation of Pep1-Fc/IL1RA was observed with both time points in hCMEC/D3 cells. However, no distinctive co-localisation was observed with LAMP1 or EEA1. This initial finding is promising as it indicates that at these late time points in TfR trafficking cycle no distinct co-localisation is visible between Pep1-FcIL1RA and lysosomes. However, imaging for this study was conducted using epifluorescence microscopy rather than confocal microscopy and this does not provide the relevant information on whether the two fluorescently labelled molecules of interest are co-localised or whether they overlap within the Z-dimension (Dunn et al., 2011). Further intracellular trafficking studies conducted via confocal microscopy are needed to determine the exact mechanism of uptake for Pep1-Fc/IL1RA.

Our knowledge of intracellular trafficking is expanding at a rapid rate. Recent evidence has emerged to suggest that regardless of the entry and trafficking routes

taken by vesicles, exocytosis occurs via a dedicated cellular mechanisms which are mediated via several proteins including, Rab proteins (Rab27, Rab11 and Rab35), soluble NSF attachment protein (SNAP) and the transSNARE complex formed via interaction of vesicular SNAREs (e.g. synaptobrevin) and target SNAREs (e.g. syntaxin) (Biesemann et al., 2017; H H Wang et al., 2016; van Breevoort et al., 2014; Zhao et al., 2015; Q. M. Zhu et al., 2015; L. Yang et al., 2012; Naskar and Puri, 2017). These function to translocate vesicles to within close proximity of the plasma membrane. Further categorisation of endosomal co-localisation and subcellular trafficking can be elucidated via the use of antibodies directed towards more specific markers of early endosomes (Rab5), late-endosomes (Rab 7), recycling endosomes (Rab 4 and 11) and transcytotic endosomes (Rab 27) (De Bock et al., 2016). Furthermore, labelling of CD133 would also confirm whether these peptides are being taken up through an additional non-specific macropinocytosis mechanism (Müller-Greven et al., 2017).

The conjugation of IL1RA to Fc domain was carried out in anticipation of further work to demonstrate the capacity of the peptides to deliver a therapeutic cargo and elicit a detectable response *in vivo*. IL1 (α and β) are pro-inflammatory and regulatory cytokines that are involved regulating acute inflammatory responses, in a wide variety of cells by exerting their effects through binding to IL1 receptor (IL1R). Within the peripheral nervous system, these cytokines are involved in the induction and propagation of pain and as such have warranted drug targeting for the treatment of neuropathic pain, a condition that does not respond well to traditional analgesics (Webster et al., 2017). IL1RA (kineret) is a natural antagonist of IL1R and an anti-inflammatory regulator which has been shown to block the effects of the IL1 *in vitro* and *in vivo* (Arend and Guthridge, 2000).

A pilot study of *in vivo* CNS uptake was performed using a C57BL/6 mouse pre-clinical neuropathic pain model induced through partial sciatic nerve ligation, (Thom and Hatcher, 2016). The mouse model had been adapted from the original rat model reported by Seltzer *et al*. (1990), and its viability for use as a model for studying the uptake of biologics into the CNS has recently been validated by Webster *et al.* (2017). Partial nerve ligation (PNL) results in a neuropathic pain

phenotype, the extent of which is quantifiable through mechanical pressure at the ipsilateral paw (Malmberg and Basbaum, 1998).

Results of the study are shown in Supplementary Figure S5. PNL of the sciatic nerve resulted in mechanical hyperalgesia which demonstrated a significant reduction in ipsilateral/contralateral (ipsi/contra) ratio on day 7 and 10, in comparison to the sham + PBS control. Operated mice treated with PBS did not show any variation in the level of mechanical hyperalgesia from pre-dose levels, suggesting no effect of the PBS control. Administration of Pep1- and Pep8-FcIL1RA resulted in a brief but statistically significant reversal in mechanical hyperalgesia that was only observable at 4 hours post dose, and rapidly diminished thereafter. The control CPep-Fc/IL1RA showed no significant effect. Further optimisation of the peptides for increased affinity may be necessary to improve their uptake and therapeutic delivery capability across the BBB.

In conclusion, when expressed as soluble CPep-D1 fusion domains Pep1 and Pep8 were shown to bind specifically towards recombinant mouse and human TfR and also demonstrated statistically significant binding with both *in vitro* cell models of the BBB (bEnd3 and hCMEC/D3). Furthermore, Pep9 and Pep14 demonstrated weak affinity binding towards recombinant mouse and human TfR protein, in addition to bEnd.3 and hCMEC/D3 cells. When expressed as a peptide-Fc/IL1RA fusion domain, Pep1 and Pep8 were both shown to internalise within bEnd.3 and hCMEC/D3 cells. In contrast to an anti-mTfR antibody (8D3), uptake within bEnd.3 cells were observed to occur at slower rate, saturating at the 60 and 120 min time points in contrast to 5 min observed with the antibody. When administered in a validated CNS uptake model of neuropathic pain, Pep1- and Pep8-Fc/IL1RA demonstrated significant short-term reversal of mechanical hyperalgesia, suggesting CNS uptake, (Thom and Hatcher, 2016).

Chapter 5: Selection of hTfR binding DNA aptamers for use as alternative BBB shuttles.

5.1. Introduction

Biologic based delivery molecules such as antibodies, peptides and engineered proteins have been extensively researched for use as delivery shuttles, via exploiting RMT at the BBB and these have shown some success in pre-clinical studies (Yu et al., 2014; Demeule, Currie, et al., 2008; Haqqani et al., 2017). Novel molecular delivery approaches diversify our capacity to access previously inaccessible targets, and are highly sought after within the context of targeting the BBB.

Aptamers are an emerging class of targeting molecules, which consist of ssDNA or RNA and have several proposed advantages over traditional biologics (J. Zhou and Rossi, 2017). Much like antibodies, aptamers are capable of binding epitopes on targets with a high affinity and avidity, through the adoption of three-dimensional hairpin-loop structures (Porciani et al., 2014). Target binding aptamers are identified from large combinatorial libraries through an *in vitro* selection technique, termed SELEX, which much like phage display, relies on the enrichment of target binding aptamers through iterative rounds of selection towards the target. Multiple adaptations to the traditional SELEX technique have been developed and utilised to select target binding aptamers (Stoltenburg et al., 2005; Soldevilla et al., 2017; Duan et al., 2017; Renders et al., 2017).

By far the most significant advantage for the use of aptamers as drug delivery shuttles across the BBB, is their low immunogenic potential. The toxicity concerns related to the use of anti-TfR and anti-IR antibodies have been highlighted (Couch et al., 2013; Ohshima-Hosoyama et al., 2012). Unlike, amino acid based biologics, aptamers have been shown to mostly avoid immunogenic response at clinically relevant concentrations (Drolet et al., 2000; Heiat et al., 2016). Furthermore, in contrast to protein based biologics, aptamers are chemically synthesised through a consistent and cost effective chemical synthesis process, which eliminates the safety implications of batch-to-batch variability (Lakhin et al., 2013). Moreover, the small size of aptamers (average 10 - 25 kDa) in contrast to MAb results in increased tissue penetration and accessibility of smaller epitopes (Catuogno et al., 2016).

Selection of hTfR binding DNA aptamers for use as alternative BBB shuttles.

Transferrin receptor is the most commonly researched target receptor for biologic drug delivery across the BBB via RMT (discussed in chapters 1 and 2), and its over expression on highly proliferating cells has also made it a desirable target for cancer therapies (Dai et al., 2014; T. Kang et al., 2015; Yue Zhang et al., 2017).

The major body of current literature on TfR targeting using aptamers is derived from two parental aptamer sequences, GS24 ssDNA aptamer and the c2 RNA aptamer (C.-H. B. Chen et al., 2008; Wilner et al., 2012). Subsequent studies have predominantly focused on the truncation and optimisation of the GS24 ssDNA aptamer (Porciani et al., 2014; Macdonald, Houghton, et al., 2016). Thus, novel aptamers that target TfR and mediate uptake into cells are needed.

The overall aim of this study was to select DNA aptamers that specifically target human TfR, through a combinatorial approach towards recombinant protein and cell SELEX. DNA based aptamers were chosen for hTfR aptamer selections. DNA is significantly more stable than RNA, facilitating lab handling procedures and improving the potential therapeutic aptamer bioavailability when administered *in vivo*, without the requirement for chemical modifications.

More specifically the study endeavoured to:

- Characterise the optimal immobilisation capacity of Ni-NTA magnetic agarose beads for recombinant polyhistidine tagged human TfR.
- Establish an aptamer SELEX protocol that utilises recombinant TfR material immobilised onto Ni-NTA magnetic agarose beads.
- Conduct aptamer selections using a combined approach of recombinant hTfR and CHO-TRVb-1 cells overexpressing the hTfR (described in chapter 2).
- Screen selected pools for enrichment and identify potential lead aptamer sequences through next generation sequencing (NGS).

5.2. Materials and Methods

5.2.1. Western blotting

Denaturing polyacrylamide gels and buffers were prepared as outlined in chapter 2, table 2.2.4. Carrier free, N-terminal polyhistidine tagged recombinant hTfR (2474-TR, R&D Systems, Oxon, UK) aliquoted in 1 µg, 2.5 µg, 5 µg and 10 µg amounts was re-suspended in a final volume of 500 µl of protein binding/ wash buffer (Table 5.2.1). Storage media was removed from 100 µl aliquots of 5% Nickel-Nitrilotriacetic acid (Ni-NTA)-coated magnetic agarose bead suspensions (36111, Qiagen, Manchester, UK) by separating with a magnetic separator for 1 min and disposing the supernatant using a pipette. The beads were then washed twice in protein binding/ wash buffer, and re-suspended in the relevant 500 µl hTFR-His6 protein solution. Beads were incubated with recombinant hTfR-His6 on a rotary mixer for 1 h at room temperature.

Table 5.2.1 : Composition of buffers used for Ni-NTA Magnetic agarose bead aptamer selections.

Buffer	Composition
Protein binding/ Wash buffer	- 50 mM NaH_2PO_4 - 300 mM NaCl - 20 mM imidazole - Corrected to pH 8.0
Interaction buffer	- 50 mM NaH_2PO_4 - 50 mM NaCl - 20 mM imidazole - Corrected to pH 8.0
Elution buffer	- 50 mM NaH_2PO_4 - 300 mM NaCl - 20 mM imidazole - Corrected to pH 8.0

Following incubation, the beads were separated using a magnetic separator and the supernatant containing unbound material was isolated into a fresh Eppendorf tube and stored at 4°C. For each experimental tube, 500 µl of protein binding buffer was then added to immobilised beads and the volume was split into two aliquots of 250 µl. The first aliquot was used to assess protein loss and elution efficiency following one wash step, whilst the second aliquot was used to assess the

same criteria following three wash steps. This was accomplished by washing once or three times in wash buffer and eluting immobilised beads by re-suspension in 40 µl of SDS-PAGE sample buffer and heating to 95°C for 5 min. Similarly, 100 µl of SDS-PAGE sample buffer was added to the unbound supernatant, and these were also heated to 95°C for 5 min.

The remaining western blotting protocol was carried out as outlined in Chapter 2, section 2.2.5, from the poly-acrylamide casting step onwards.

5.2.2. ssDNA aptamer SELEX

Aptamer selections were carried out using a N30 ssDNA library (TriLink Biotechnologies, California, USA). The library was supplied as a random 30 nucleotide region, flanked by two primer binding sites, each 23 nucleotides in length (overall aptamer length 76bp). The ssDNA library, forward and reverse primer sequences used in the SELEX procedure are outlined below:

- **Trilink (n=30) ssDNA library:** 5' TAG GGA AGA GAA GGA CAT ATG AT(N30) TTG ACT AGT ACA TGA CCA CTT GA 3'
- **Trilink (n=30) forward primer:** 5’ TAG GGA AGA GAA GGA CAT ATG AT 3’
- **Trilink (n=30) reverse primer:** 5’ TCA AGT GGT CAT GTA CTA GTC AA 3'

Two aptamer selection protocols were carried out in a combinational approach for the selection of receptor specific aptamers. Selections were primarily conducted towards hTFR-His6 (2474-TR, R&D Systems, Oxon, UK) for a total of 12 rounds. However, at round 5 a functional cell selection round was introduced towards CHO-TRVb-1 cells overexpressing human TfR in the absence of endogenous hamster TfR (described in chapter 2).

Recombinant protein SELEX was performed using hTfR-His6 immobilised onto Ni-NTA-coated magnetic agarose beads (Qiagen, Manchester, UK). The procedure described for recombinant protein selections was a modification of the original “Flu-Mag SELEX” magnetic bead based aptamer selection protocol outlined

by Stolenburg *et al*. (2005). The cell selection round towards CHO-TRVb-1 cells was carried out according to the cell SELEX protocol outlined by Sefah *et al*. (2010).

5.2.2.1. Recombinant hTfR aptamer SELEX

The procedure used for recombinant protein SELEX is outlined in Figure 5.2.1. Ni-NTA washing/ binding, interaction and elution buffers were prepared as suggested within the QIAGEN Ni-NTA magnetic agarose beads handbook (QIAGEN, 2001), (outlined in Table 5.2.1). Prepared buffers were autoclaved and stored at 4˚C. Prior to incubation, 10 nmoles of the lyophilised ssDNA library was re-constituted in 370 µl of binding buffer. The re-suspended library was then heated to 95˚C and cooled on ice to encourage ssDNA folding and the formation of secondary structures (Sefah et al., 2010).

For each selection round, the relevant volume of Ni-NTA magnetic agarose bead slurry was transferred into a clean Eppendorf tube (outlined in Table 5.2.1), the storage buffer was removed and the beads were washed in washing buffer. Pre-washed beads were subsequently immobilised by incubating with 5 µg of hTfR-His6 on a rotary shaker for 1 h at room temperature.

A de-selection step was employed at the start of each round using the pre-folded library stock (round 1) or pre-folded, and reconstituted aptamer pool (subsequent rounds), incubated with non-immobilised Ni-NTA magnetic agarose beads. This was achieved by incubating the ssDNA pool with 100 µl of pre-washed beads in binding buffer for 1 h on a rotary shaker at room temperature. The beads were then pulled down using a magnetic separator and the non-bound supernatant was transferred onto pre-washed and target hTfR-His6 immobilised beads. The immobilised beads and de-selected library were incubated at room temperature for the relevant incubation times shown in Table 5.2.2.

Following incubation, the beads were pulled down with a magnetic separator, the unbound ssDNA pool was transferred into a clean Eppendorf tube and stored at -20°C. The beads were subsequently washed in washing buffer with increasing wash volumes and number of wash steps as the selection progressed (outlined in Table 5.2.1). Bound aptamers were sequentially eluted in five 100 µl volumes of elution

buffer (Table 5.2.1) for the first round, and three 100 µl volumes for subsequent rounds. At round 5 onwards multiple selections were simultaneously carried out in order to achieve appropriate yields of ssDNA for selection progression.

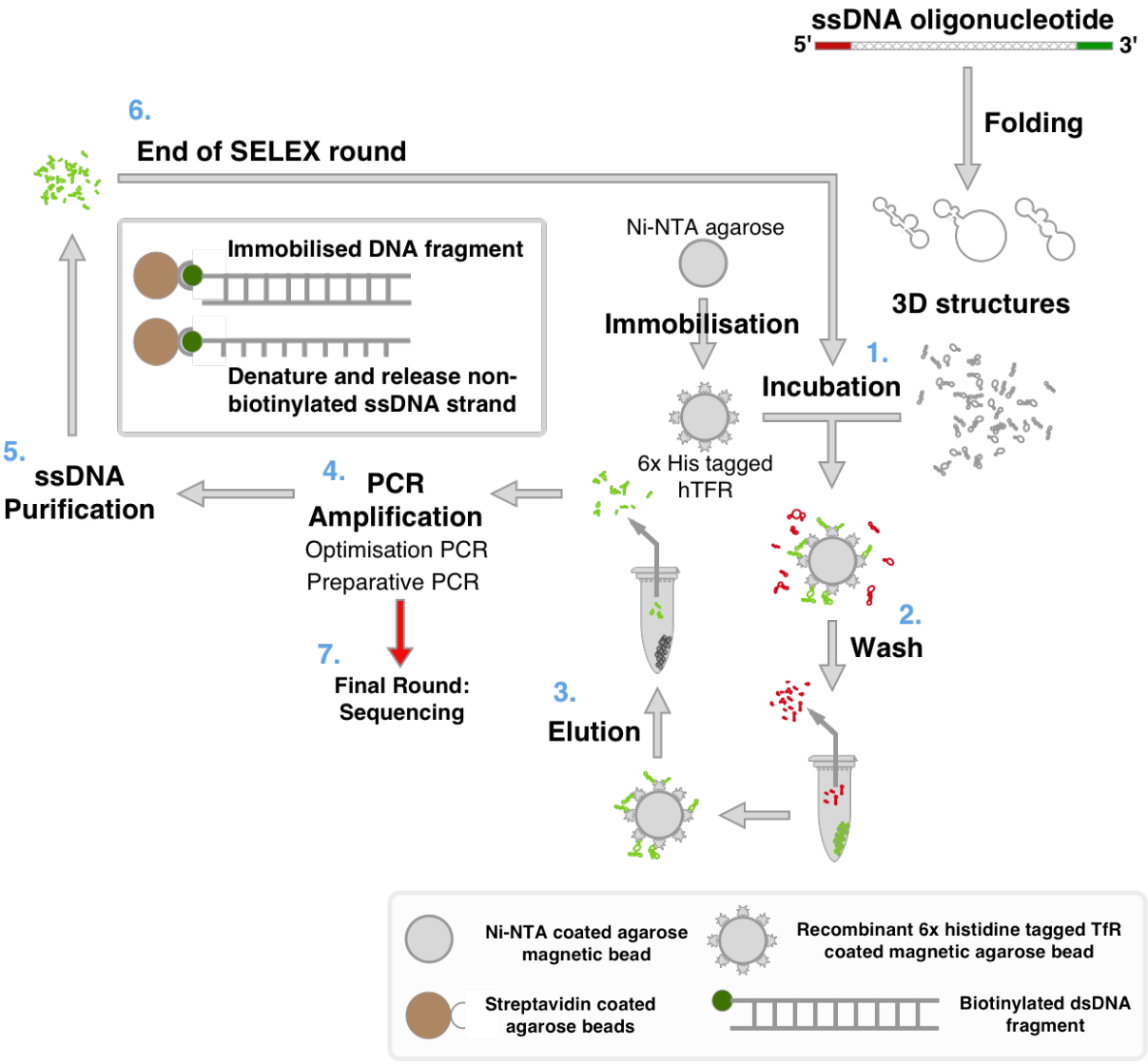

Figure 5.2.1: Schematic representation of DNA aptamer selection using recombinant protein immobilised on Ni-NTA coated magnetic agarose beads.

1. The chemically synthesised random oligonucleotide library is incubated with Ni-NTA magnetic agarose beads immobilized with polyhistidine tagged recombinant protein. **2.** Magnetic beads are separated and unbound sequences are removed with the supernatant. Wash steps are performed in washing buffer and remnant unbound and poorly bound sequences are removed. **3.** Binding sequences are detached and collected from protein-bound beads in elution buffer. **4.** Amplification steps are carried out to amplify the bound sequences within the selected pool. A biotin tag is incorporated to the 3' end of the non-template strand via a specific biotinylated primer **5.** The non-biotinylated strand is separated from the template strand via alkaline denaturation and affinity purification methods, utilising streptavidin-coated beads. **6.** The enriched and purified pool is

utilised in the following round of selection and the cycle is repeated. **7.** Following 6 – 15 rounds, the selected pool is sequenced to identify the exact nucleotide base sequences for selected aptamers.

Table 5.2.2: Table showing an overview of selection conditions for recombinant hTfR-His6 SELEX.

Selection Round	Target	Ni-NTA Bead slurry	Incubation time (minutes)	Wash volume (µl)	Wash steps
1	hTfR-His6	100	60	500	3
2	hTfR-His6	100	60	500	3
3	hTfR-His6	100	60	500	3
4	hTfR-His6	100	60	500	3
5	CHO-TRVb-1 cells	N/A	60	500	3
6	hTfR-His6	85	60	500	4
7	hTfR-His6	70	50	500	4
8	hTfR-His6	55	40	750	5
9	hTfR-His6	40	30	750	5
10	hTfR-His6	40	30	900	5
11	hTfR-His6	40	30	900	5
12	hTfR-His6	40	30	900	5

5.2.2.2. CHO-TRVB-1 cell SELEX

Cell SELEX washing and binding buffers were prepared as follows:

- **Washing buffer:** 4.5 g of glucose and 5 ml of 1M $MgCl_2$ were added to 1 L of DPBS (Sigma-Aldrich, Dorset, UK).
- **Binding buffer:** 4.5 g of glucose, 100 mg of baker's yeast tRNA (Sigma-Aldrich, Dorset, UK), 1 g BSA (Sigma-Aldrich, Dorset, UK), and 5 ml of 1 M $MgCl_2$ were all added to 1 L of DPBS.

Target TRVb-1 CHO cells were cultured to confluence according to the cell culture protocol outlined in chapter 2, section 2.2.3. Adherent cells were dissociated via a short-term trypsin treatment (2 min), the action of trypsin was inhibited using culture media. Following cell detachment and counting, cells were washed and 1 x 10^7 cells were isolated for cell selection. The isolated cells were washed twice in 3

ml of washing buffer and re-suspended in 330 µl of binding buffer. The purified and desiccated ssDNA pool from round 4 was re-suspended in binding buffer at a concentration of 1000 nM, added to the cell suspension, and incubated on a rotary shaker at 4 ˚C for 1 h.

Post incubation, cells were centrifuged at 150 g for 3 min at 4˚C; the supernatant containing unbound ssDNA sequences was then carefully collected and stored at -20˚C. The remaining cell pellet was carefully washed three times in 3 ml of washing buffer and elution of bound aptamers was accomplished by re-suspending the cell pellet in 500 µl of DNase free water, heating to 95˚C for 10 min, and centrifuging the suspension at 13,100 g for 5 min. Cell membrane bound and internalised aptamers were isolated by carefully collecting the supernatant.

5.2.3. PCR amplification of selected aptamer pool outputs

5.2.3.1. Initial PCR amplification of Round 1 selected pool

Following the first round of selection, the entire first round selected pool was used as a template for a 1000 µl PCR reaction mixture. A master mix was prepared as outlined in Table 5.2.3. The purpose of this initial amplification was to increase the frequency of bound ssDNA sequences for the preparative PCR amplification step to follow.

Table 5.2.3: Initial PCR amplification of entire first round selected pool.

PCR reaction component	Reaction Mixture Volume (µl)
DNase free water	290
MyTaq 5x PCR reaction buffer (Bioline, UK) – Containing dNTPs and $MgCl_2$	200
Forward/ Reverse Primer Mix (100 µM)	10
MyTaq Hot start DNA polymerase (5 units /µl)	3
Template ssDNA – Round 1 selected pool	500

The total reaction mixture was separated into 20 x 50 µl aliquots in PCR reaction tubes. Amplification was carried out using a Bio-Rad icycler PCR machine, (Bio-Rad, Hertfordshire, UK). PCR reaction conditions used are outlined in Table 5.2.4.

Table 5.2.4: PCR amplification programme reaction conditions.

Step	Temperature (°C)	Time (s)
Hot start	95	150
Amplification - 10 cycles for first round or optimised cycle number for later rounds		
Denaturation	95	30
Annealing	49	30
Extension	72	30
Final extension	72	180
Hold	4	∞

The melting temperature of the primer pair was calculated using OligoAnalyzer 3.1 software (Integrated DNA technologies, Leuven, Belgium). Initial amplification of the first round selected pool was performed for 10 cycles to minimise the formation of non-specific amplicons. Following amplification, all reaction mixtures were pooled.

5.2.3.2. Optimisation PCR

A 250 µl reaction master mix was prepared alongside a negative control as outlined in Table 5.2.5. The reaction mix was split into 5 x 50 µl aliquots in PCR reaction tubes. Reaction tubes were removed incrementally at cycle number ranges determined from the previously selected optimal cycle number for amplification. For amplification of round one selected pool, 4, 6, 8, 10, 12 cycles were used. In later rounds, cycle numbers in the range of 12 – 22 cycles were used. The negative control tube was amplified for the maximum number of cycles carried out for the optimisation PCR. For cell selection rounds, 5 µl supernatant of cell lysate was included within the amplification negative control.

Table 5.2.5: Optimisation PCR reaction setup.

Reagents	Reaction mixture volume (µl)	Control (µl)
MyTaq 5x reaction buffer (Bioline, UK) – containing dNTPs and $MgCL_2$	25	5
Forward/ Reverse Primer mix (10 µM)	25	5
DNase-free water	166.75	35
Template DNA – Amplified selected pool (10% of reaction volume)	25	-
MyTaq Hot start DNA polymerase (5 units/ µl)	0.75	0.15

PCR products were separated on a 3% agarose gel containing 2.5 µg ethidium bromide. 10 µl aliquots of each PCR amplification product was mixed with 2 µl of 6x loading dye (Promega, Southampton, UK) and loaded on the gel alongside a 25 bp DNA ladder (Promega, Southampton, UK). Agarose gel electrophoresis was performed in 1x TAE buffer at 100 V for 45 min. Visualisation of gels was carried out on a gel doc G:Box system (Syngene, Cambridge, UK). The optimal cycle number for the preparative PCR was determined as the brightest single observable band, lacking non-specific amplification bands.

5.2.3.3. Preparative PCR

Large scale amplification was carried out using an unmodified forward primer in conjunction with a biotinylated reverse primer to allow affinity capture, separation and purification of the single stranded complementary DNA identical to the original aptamer strand. A 1000 µl reaction mix was prepared as outlined in Table 5.2.6, with the selected aptamer pool serving as 10% of the reaction mix. The reaction was then distributed into 10 x 100 µl aliquots in PCR tubes and pooled following amplification. A 10 µl aliquot was run on a 3% agarose gel to verify efficient amplification.

Table 5.2.6: Preparative PCR amplification reaction setup.

Reagents	Reaction mixture volume (µl)
MyTaq™ 5x PCR reaction buffer (Bioline™, UK) – Containing dNTPs and $MgCl_2$	200
Forward primer (100µM)	5
Biotinylated Reverse primer (100µM)	5
Template DNA - Amplified Round 1 selected pool (10% of reaction mixture)	100
DNase-free water	690
MyTaq™ Hot start DNA polymerase	3

5.2.4. Purification of ssDNA from PCR product

Separation and isolation of the non-biotinylated strand from the dsDNA PCR product was performed using alkaline denaturation and affinity purification techniques. DNA synthesis columns (Glen-Research, Virginia, USA) were prepared by inserting a filter into the lower end of the column. A plunger from a 10 ml syringe was removed, and the empty syringe was inserted into the top of the column. 200 µl of streptavidin sepharose bead suspension (GE Healthcare Life Sciences, Little Chalfont, UK) was loaded into the syringe. The plunger was then gradually inserted to allow the storage buffer to drain out of the filter. Between each draining step, the DNA synthesis column was disconnected prior to removal of the syringe plunger. The beads were subsequently washed using 2.5 ml of Dulbecco's PBS (DPBS) and the round 1 preparative PCR product was run through the column three times. The beads were washed again in 2.5 ml of DPBS, prior to elution of the non-biotinylated strand using 500 µl of 200 mM NaOH solution. The eluate was gradually collected in a clean Eppendorf tube.

5.2.5. Desalting, quantification and lyophilisation of purified ssDNA

Desalting was performed using Illustra NAP5 columns containing G25 Sephadex (GE Healthcare Life Science, Little Chalfont, UK). The NAP5 column was completely drained of storage buffer and then the column was equilibrated using a minimum of 15 ml of nuclease free water, in 3 ml volumes. 500 µl of eluted ssDNA was then added to the column and allowed to drain into the gel completely. The

purified and desalted ssDNA pool was then eluted off the NAP5 column into a clean Eppendorf tube using 1 ml of DNase free water. The concentration of purified ssDNA was determined at a UV absorbance of 260 nm, on a nanodrop spectrophotometer (ThermoFisher Scientific, Paisley, UK). Following quantification, the aqueous sample was vacuum desiccated at 60°C in an Eppendorf concentrator plus (Eppendorf, Stevenage, UK) for 6 h. The lyophilised ssDNA pool was re-constituted at a concentration of 200 nM for subsequent selection rounds.

5.2.6. Next-generation sequencing of aptamer selected pools

5.2.6.1. DNA pool preparation for Illumina MiSeq sequencing

The round 5 cell selected, round 6, 7, 9, 10, and 12 hTfR-His6 selected, and the round 1 unbound pool (negative control), were all amplified by carrying out preparative PCR amplification steps (as outlined in section 5.2.3.3) using unmodified n30 Trilink library amplification forward and reverse primers, (outlined in section 5.2.2). Following preparative PCR amplification, the dsDNA products were lyophilised using an Eppendorf concentrator plus (Eppendorf, Stevenage, UK) and re-constituted in 65 µl of DNase free water. A 10 µl aliquot was taken for validation on a pre-cast 4% Hi-ReSolution agarose E-gel (G501804, ThermoFisher Scientific, Paisley, UK). Purification of dsDNA product was carried out using a nucleotide removal kit, according to the manufacturer protocol. Elution from the purification column was carried out in 60 µl of DNA free water. Quantification of purified samples was carried out using a Qubit 3.0 Fluorimeter (ThermoFisher Scientific, Paisley, UK) and a Qubit dsDNA High Sensitivity assay kit (Q32851, ThermoFisher Scientific, Paisley, UK).

5.2.6.2. Enrichment analysis of NGS sequencing Data

A sequence count analysis was performed by Colin Hardman (MedImmune, Cambridge, UK). Paired reads were assembled using PandaSeq (Masella et al., 2012). Viable assembled reads were then aligned according to the forward and reverse primer binding regions as outlined below:

AGGGAAGAGAAGGACATATGAT ({30}) TTGACTAGTACATGACCACTTGA

The random regions were then clustered according to uniqueness.

5.3. Results

5.3.1. Assaying recombinant hTfR immobilisation onto Ni-NTA agarose beads.

An immunoblot was carried out to validate the size of the recombinant polyhistidine tagged hTfR (R&D Systems, Oxon, UK), and also to assess the optimal binding capacity and immobilisation integrity of Ni-NTA magnetic agarose beads to be used as bait in subsequent SELEX protocols. This was performed by incubating 100 µl of bead slurry with varying amounts of recombinant hTfR (1 µg, 10 µg, 2.5 µg and 5 µg).

Results of the 1 µg and 10 µg immobilisation study are shown in A and B, respectively. No protein was observed in the supernatant of the 1 µg incubation following magnetic separation (Figure 5.3.1, A, lane 4). However, in contrast to the 1 µg incubation, the 10 µg incubation presented a significant quantity of unbound protein within the supernatant (Figure 5.3.1, A, lane 7).

The beads were washed once and three times in order to assess the loss of bead-bound recombinant hTfR. Remaining bound protein was eluted off the beads and quantified. For the 1 µg sample a faint band was observed bound to the Ni-NTA agarose beads following one wash step and elution (Figure 5.3.1, A, lane 2). A fainter band was observed with three washing steps, suggesting greater loss of recombinant protein had occurred with three wash steps in contrast to one wash step. (Figure 5.3.1, A, lane 3). Incubation, subsequent washing and elution of beads with 10 *µ*g of recombinant TfR produced two intense bands of similar thickness. This finding suggests a large proportion of protein remained bound to the beads after washing steps and were successfully isolated following elution. Observable bands appeared at the correct expected length of 85 kDa.

A follow up experiment was performed using 2.5 µg and 5 µg of recombinant TfR to determine a quantity of protein that exhibited optimal saturation of beads with minimal protein wastage (Figure 5.3.1, B). During this experiment Eppendorf protein Lo-bind (Eppendorf, Stevenage, UK) tubes were used in an attempt to reduce bead to tube adhesion. At 2.5 µg some protein remained unbound within the supernatant (Figure 5.3.1, B, lane 1), This observation was more notable with 5 µg of supernatant

(Figure 5.3.1, B, lane 2). Following one and three wash steps, the 2.5 µg eluted samples showed no visible variation in hTfR recovery. However, observable bands were faint indicating a small quantity of protein had been eluted from the beads (Figure 5.3.1, B, lanes 3 and 4). Likewise, at 5 µg little to no protein loss was observed with three wash steps in contrast to one wash step (Figure 5.3.1, B, lanes 5 and 6). However, significantly more protein was eluted from the beads, when compared with the 2.5 µg eluted samples. Overall, 5 µg gave the most efficient levels of recovery of eluted hTfR, without excessive protein loss.

hTfR-His6 was validated at the correct size of 76 kDa. Interestingly, the 10 µg sample wash and supernatant also contained a faint secondary band at a size of approximately 150 kDa, indicating the presence of TfR in the dimeric form.

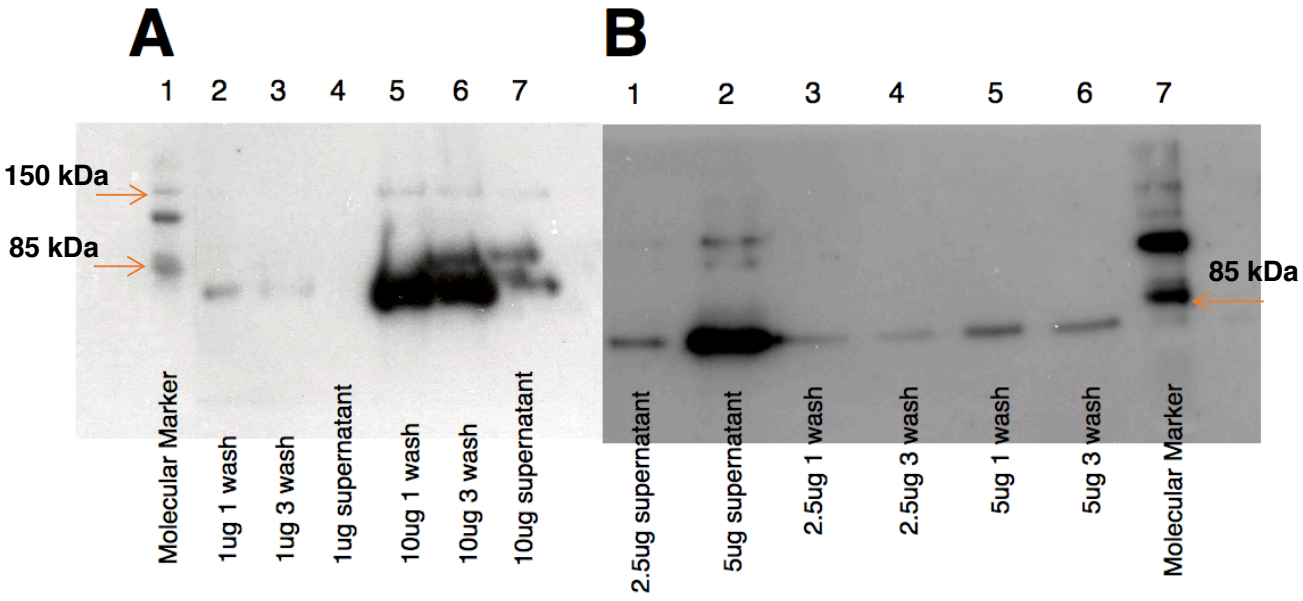

Figure 5.3.1: Assessing immobilisation of recombinant hTfR to Ni-NTA magnetic agarose beads.

Immunoblot assessment of hTfR was performed by incubating **(A)** 1 µg, 10 µg or **(B)** 2.5 µg and 5 µg of recombinant hTfR with 100 µl of bead slurry. Unbound protein was measured in supernatant. Loss of protein with one and three protocol wash steps was also assessed by eluting beads following relevant wash steps. Recombinant hTFR-His6 was observed at the expected size of the soluble hTFR monomer (76 kDa). Bands were also noted at a size equivalent to the dimeric form (152 kDa) with the 10 µg samples. Due to an error in technical handling of the membrane, secondary exposure bands are visible in lanes 6 and 7.

5.3.2. Adapted SELEX protocol for the selection of hTfR binding ssDNA aptamers immobilised on Ni-NTA beads.

Optimisation PCRs were performed in order to determine the optimal PCR amplification cycle numbers to carry out for large scale preparative amplifications of the selected ssDNA pool, without over-amplification or the formation of non-specific amplification products. The amplified preparative pool would then be purified and used for the successive SELEX round.

Optimisation PCR gel electrophoresis results are shown in Figure 5.3.2. The determined optimal cycle number used for preparative PCR amplifications is highlighted in blue. Throughout the selection a primary band representing the n30 library can be seen at the expected size of 76 base pairs (bp). Initial amplification of the round 1 selected pool only required 6 cycles to produce a clean single visible band on agarose gels. However, for rounds two and three the number of cycles required was increased to 14 cycles. From round four onwards, the number of cycles required to amplify a clean PCR product fluctuated between 18 and 22 cycles.

An observable non-specific secondary band can be seen at round 11 on the optimisation PCR gel at a size of 50 bp. Although the presence of this band could not be detected on agarose gel runs of the preparative PCR amplified product, the non-specific band prevented further progression of the selection past selection round 12, where its presence was as prevalent as the primary PCR product in all optimisation PCR cycles (results not shown).

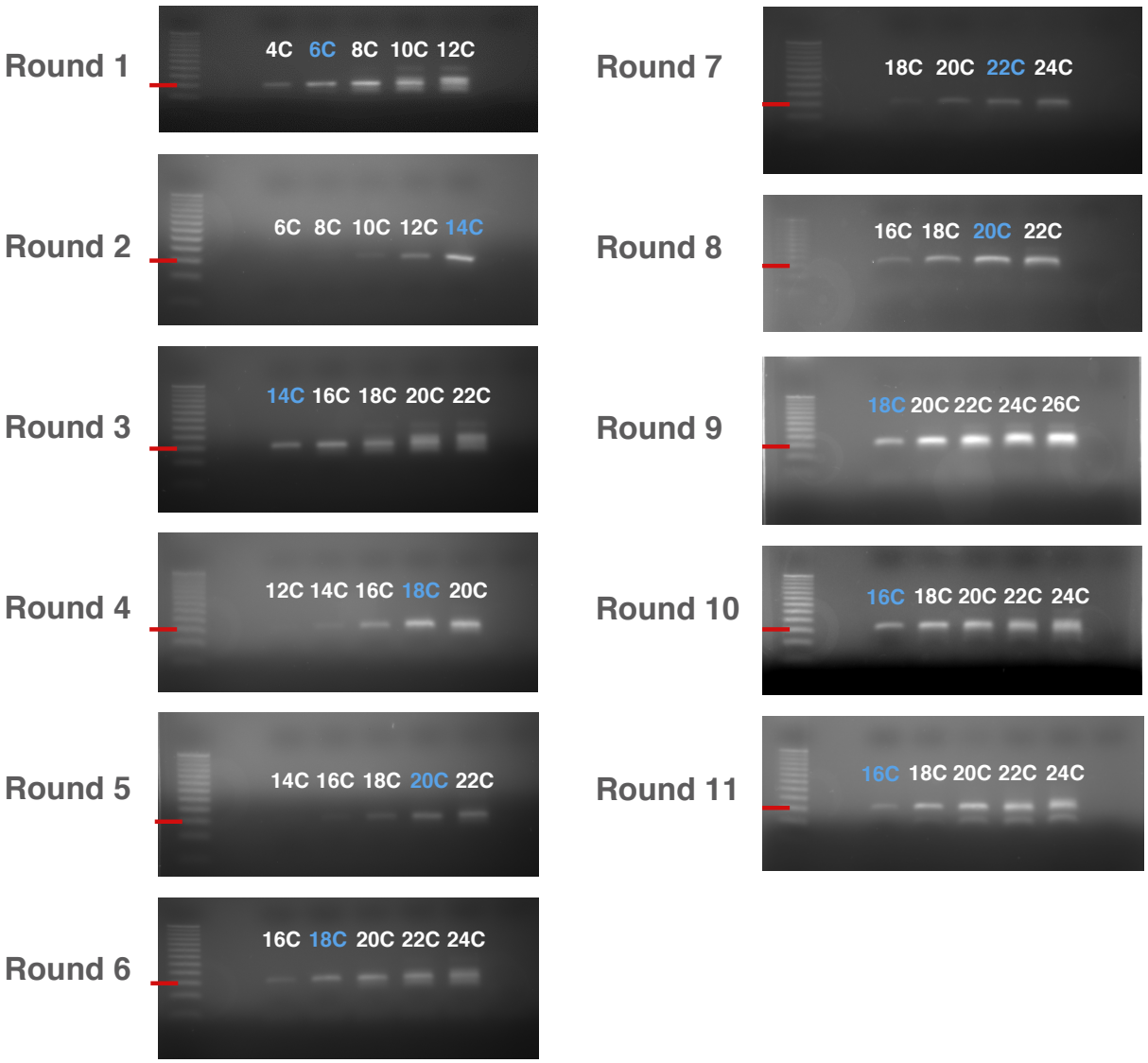

Figure 5.3.2: Optimisation PCR amplification results.

Figure showing optimisation PCR gel electrophoresis runs for each round of selection. The amplification cycle numbers used are shown in each lane. The red line indicates the position of the 75 bp marker on the 25 bp incremental marker DNA ladder. The optimal cycle number determined for each round is highlighted in blue.

5.3.3. Enrichment observed following 12 rounds of SELEX

Following 12 rounds of ssDNA aptamer SELEX, high throughput sequencing (HTS) in the form of Illumina Miseq sequencing, was carried out to assess the pools for overall enrichment. The sequencing output results would also be used for subsequent screening and identification of conserved aptamer sequences that have been enriched throughout the selection process. A summary of the count analysis conducted on NGS data is shown in Figure 5.3.3. In total, out of 13 million reads, approximately 9.6 million reads could be aligned and sorted according to the forward and reverse primer binding sites. This equates to 74% of total reads.

As expected, the R0 unbound library control showed complete diversity, with all sorted sequences being represented once as indicated by the total number of unique sequences within that pool (Figure 5.3.3, A and B). As the selection progresses from round 0 onwards, the number of unique sequences and therefore diversity of the selected pools is gradually reduced up until round 9. From round 9 to round 10 a 30% reduction in the diversity of the selected pool was observed. A reduction of approximately 15% was also noted from round 10 to round 12. Overall, a 62% reduction in pool diversity was observed between round 0 and round 12.

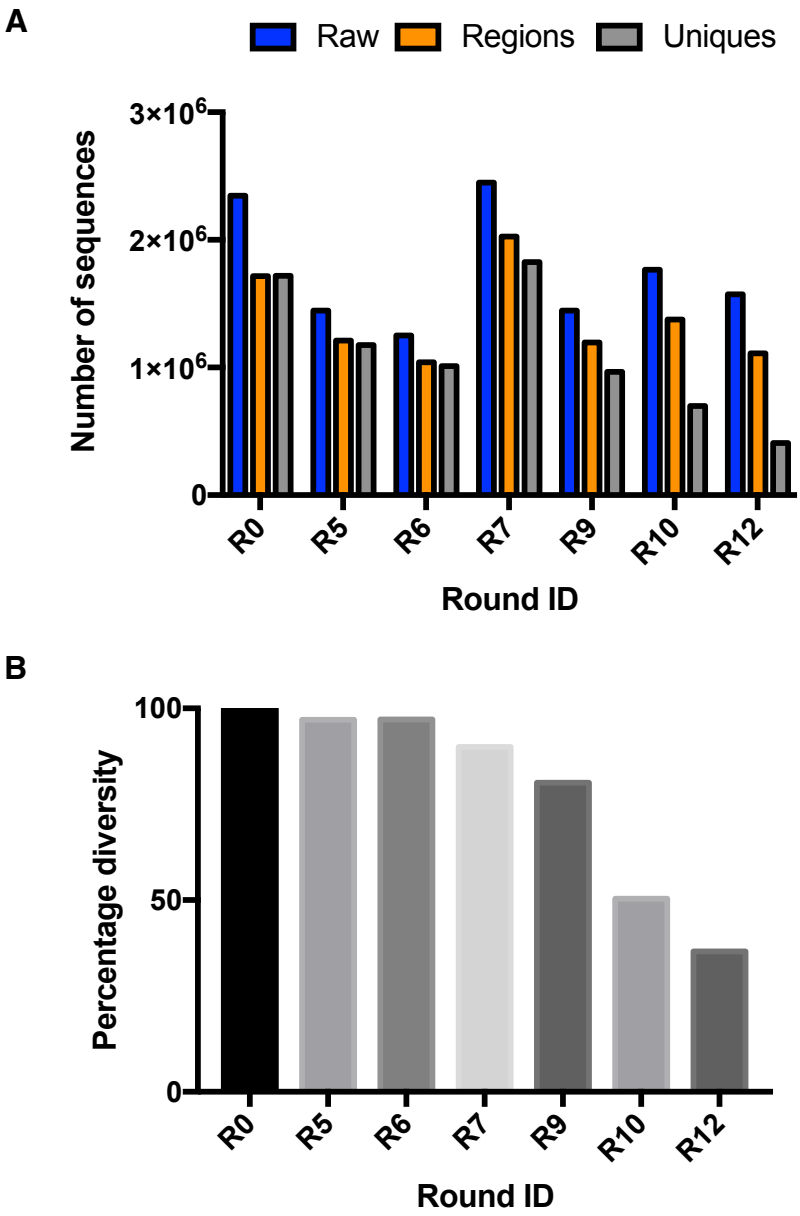

Figure 5.3.3: Summary of NGS count analysis as an overall assessment of aptamer enrichment.

Figure showing a summary of the count analysis conducted using NGS data. **(A)** For each of the sequenced selection rounds, the number of raw sequences (blue), the number of primer aligned sequences (orange) and the number of unique sequences within the n30 random region (grey) are shown. A unique sequence in this case is defined as a sequence that differs from another by at least one nucleotide. **(B)** Figure showing the percentage diversity presented as a ratio of primer aligned to unique sequences. Significant enrichment is observed at round 10, with further enrichment observed at round 12.

5.4. Discussion

5.4.1. hTfR-His6 efficiently immobilised to Ni-NTA magnetic agarose beads

Validation of hTfR-His6 on an SDS-PAGE gel revealed a band at the correct size of the hTfR extracellular domain (76 kDa). Moreover, at 10 µM concentration, some of this material was also observed in the dimeric form (152 kDa). The extracellular domain of TfR has previously been identified to be natively present in a soluble form that arises through trypsin proteolytic cleavage of the TfR stem region. This extracellular domain has been shown to maintain the dimeric globular structure and functionality of transferrin binding, via the spontaneous dimerisation of monomeric helical domains (Aisen, 2004; Mason et al., 2009).

Ni-NTA magnetic agarose beads were assessed for their ability to immobilise hTfR-His6. Additionally, the capacity of these beads to maintain hTfR-His6 with multiple wash steps was also assessed (Figure 5.3.1). Results show that the beads were capable of effectively capturing recombinant hTfR-His6. Optimal binding was determined at 5 µg of hTfR-His6, since immobilised beads showed equal amounts of protein following elution after one or three wash steps, with minimal recombinant protein usage in the process.

Binding of the polyhistidine tag occurs to a Ni-NTA chelated atom, with an affinity of $K_D = 10^{-6}$ M (Nieba et al., 1997). Although immobilisation via streptavidin and biotin interaction would allow the target protein to remain bound to the beads with a stronger affinity interaction ($K_D = 10^{-14}$ M), it also makes elution of target aptamers together with their bound interaction partners (in this case, hTFR-His6) impossible without the use of denaturing conditions (A. Holmberg et al., 2005). Furthermore, due to the size of biotin, and the biotin labelling process, there is potential to block epitopes on the target protein, thus limiting the availability of accessible epitopes for aptamer interaction (Murphy et al., 2003). His-tag immobilisation to beads also allows the homogenous native (n-terminal) orientation of TfR protein on the surface of magnetic agarose beads for selections.

A key component of aptamer selection relies on the efficient separation and purification of the relevant strand from the complementary strand. The use of Ni-NTA

for the immobilisation of target protein in this case also allows the subsequent utilisation of streptavidin as an affinity capture matrix during separation and purification stages of SELEX, as carried out for this study.

A similar approach to aptamer SELEX and ssDNA purification had previously been described for the successful selection of high affinity thyroid transcription factor (TTF) specific aptamers (Murphy et al., 2003). In support of the practicality of this SELEX approach, several other aptamer SELEX studies have also described the use of the polyhistidine tag in order to effectively immobilise and select target specific aptamers (Wilner et al., 2012; Tanaka et al., 2009; Barfod et al., 2009).

5.4.2. Analysis of PCR amplification steps

Aptamer selection by the various forms of SELEX is liable to failure due to several inherent issues including, the retention of non-target specific aptamers due to inefficient pool partitioning methods, interaction of the primer binding sites with the random region of the library leading to by-product amplification, and the enrichment of non-target specific aptamers towards affinity capture matrix (Tolle et al., 2014; Ouellet et al., 2015). The failure of aptamer SELEX via these factors results from an increased number of rounds required for enrichment of target specific aptamers or the complete takeover of the amplified pool with non-specific by-products.

In total, 12 rounds of aptamer SELEX were carried out. The summary of the PCR amplification steps and relevant cycle numbers used for preparative PCR are shown in Figure 5.3.2. At round 11 the presence of truncated secondary band 50 bp in size was observed. This band indicates the presence of a non-specific amplification product. The formation of aptamer amplification by-products is a well-established phenomenon that interferes with aptamer enrichment and reduces library specific amplification (Ouellet et al., 2015). Tolle *et al.* (2014) have previously examined the process of by-product formation during the amplification stages of aptamer SELEX. The group reported two distinct forms of amplification by-products, termed ladder and non-ladder, and proposed a mechanism by which these by-products were formed. The ladder class of by-products result from the annealing of the 3’ end fixed region of one strand to a complementary sequence within the

random region of another strand. This annealing and amplification process results in a double reverse primer PCR product that can subsequently be further amplified to form copies with multiple reverse primer binding sites. The non-ladder class of by-products occurs when there is incomplete annealing of the reverse primer to the random region, which results in a gap that prevents further re-annealing and the production of a slightly larger, single sized PCR product.

Both these types of by-products describe larger amplicons which were not observed within our optimisation and preparative PCR stages. The smaller amplification product observed within the round 11 pool may instead be due to primer-primer hybridisation, a major cause of by-product formation within conventional PCR methods (Tolle et al., 2014). Furthermore, calculated annealing temperature for the library amplification primers was low (49°C). Although a low primer melting temperature has been demonstrated to significantly reduce preferential PCR amplification biases (Sipos et al., 2007), it has also been well established to increase non-specific annealing of primers to non-target sequences and can lead to a reduction in the yields of the desired product. The low annealing temperature of the primers could have also contributed to the formation of non-specific amplification by-products observed with the round 11 PCR step.

The presence of this by-product prevented further progression past round 12, during which, there was a clear amplification of the two visible bands at equal band intensities (result not shown). Re-selection attempts were carried out starting from the round 9 selection output pool, with increased selection stringency (via increased wash steps and volumes). However, the same amplification by-products re-emerged by round 12.

5.4.3. Significant enrichment observed following 12 rounds of hTfR SELEX

Although NGS was initially developed for whole genome sequencing its use has been expanded to many other research areas, including the screening of ligands following library selections carried out via phage display and SELEX (Blind and Blank, 2015). Screening via HTS is highly advantageous in this respect, as it has previously been shown to allow the identification of low abundance, target binding aptamers (<1%) in fewer selection rounds, whilst also allowing a highly representative, in depth analysis of sequenced aptamer pools (Nguyen Quang et al., 2016). Furthermore, it also allows the tracking of aptamer species and conserved motifs with selection progression (Alam et al., 2015).

The results of the NGS of hTfR selected pools demonstrate an overall 62% reduction in sequence diversity between the unselected pool and round 12. Although a significant amount of enrichment was observed, further rounds could still be carried out in order to further enrich the pool for aptamers with the strongest binding affinity towards hTfR. The level of enrichment observed with the current hTfR selection protocol correlates with other studies that have required on average, between 6 – 15 rounds for enrichment. Studies have previously highlighted the selection of TfR specific aptamers using traditional SELEX approaches in as few as 5 to 9 rounds (C.-H. B. Chen et al., 2008; Wilner et al., 2012). The current study required more rounds to achieve enrichment, and this may have been due to several factors including selection stringency, which has been shown to play a significant role in the number of rounds required to achieve high levels of enrichment (K. M. Ahmad et al., 2011).

Using a similar SELEX approach to the one described here, Murphy *et al*. (2003) demonstrated the identification of high affinity aptamers towards TTP following 15 rounds of selection. The binding affinities of these aptamers was characterised and shown to be within the low nanomolar range (10^{-8} to 10^{-9}). However, the advantage of screening earlier rounds is that this allows the identification of lower to moderate affinity aptamer variants which are highly sought after for the purpose of identifying aptamer species capable of translocating the BBB via RMT. Macdonald *et al*. (2016) have demonstrated that TfR binding aptamers with

a moderate affinity of approximately 500 nM exhibited the greatest degree of internalisation within bEnd.3 cells. Similarly, optimised antibody based BBB delivery molecules which also appear to have moderate binding affinities have been described, and these were reported as 111 ± 16 nM (Yu et al., 2011) and 130 nM (Webster et al., 2017). From these findings, it appears the optimal affinity for TfR mediated biologic targeting of RMT occurs within the range of 100 – 500 nM. However, this is also likely dependant on the targeted epitope and its effect on overall fate of transcellular trafficking within BCEC.

Current aptamer TfR targeting approaches have focused on the rational design or use of pre-existing aptamers that have specificity towards either mTfR (GS24 ssDNA aptamer and its variants) or hTfR (c2 RNA aptamer) independently. As discussed in chapter 3, there is a significant requirement in the area of biologic therapeutics to produce species cross-reactive molecular recognition domains, that are capable of recognising molecules on multiple species homologues for translatability of pre-clinical to clinical studies and improved biologic safety and efficacy rate (Irani et al., 2016). Further work into identifying novel TfR species cross-reactive aptamers is needed.

In conclusion, this study has highlighted the enrichment of a heterogeneous pool of aptamers, that have been preferentially selected towards recombinant target hTfR protein and hTfR overexpressed on CHO-TRVb1 cells. Through the use of high throughput sequencing, it was possible to establish the extent of enrichment with selection progression from round 0 to round 12.

Aptamers are proving to be promising alternatives to antibodies for many applications including drug delivery. However, they have yet to become as established as antibodies, partly due to a lack of awareness and commercial backing. Further research into the pharmacokinetic, pharmacodynamic and safety profiles of aptamer-based therapies is required *in vivo* to meet the increased demand for delivery of DNA and RNA based therapies such as siRNAs and miRNAs.

Chapter 6: General Discussion

Through the course of this thesis, we have explored the use of phage display and SELEX for the selection of TfR binding cyclic peptides and aptamers, respectively. Specifically, we aimed to utilise the selected domains as the targeting moiety for a generalised drug delivery system, capable of transporting a conjugated macromolecular therapeutic cargo e.g. protein, miRNA, siRNA or drug carriers (gold nanoparticles and liposomes) across the BBB into the CNS. To achieve this goal, endogenous receptors that are localised on the cell surface of BCEC and function in transcellular transport were exploited.

6.1. Assessment of receptor targets that function via RMT at the BBB

It was necessary to identify a suitable receptor candidate for exploiting the mechanism of RMT prior to conducting selections of binding domains, therefore chapter two focused on the characterisation of three receptor candidates; TfR, LDLR and LRP1, which were selected based on the criteria that they transport their natural ligands across the BBB via RMT. Although, these receptor candidates are not exclusively expressed by BCEC and by definition are not target specific in nature, they have been successfully targeted for the delivery of therapeutic cargos across the BBB (Yu et al., 2014; Hultqvist et al., 2017; Demeule, Currie, et al., 2008; Zensi, Begley, Pontikis, Legros, Mihoreanu, Wagner, Büchel, Briesen, and Kreuter, 2009b).

Three principle research aims needed to be addressed within this chapter; are the receptor candidates expressed on the surface of the hCMEC/D3 cell line? If so, to what extent is their expression stable with long-term culture? Does the proteolytic detachment of cells impact the expression of TfR?

Cell surface protein expression of TfR, LDLR and LRP1 was demonstrated on hCMEC/D3 cells and the suitability of these receptors as potential targets for RMT mediated drug delivery across the BBB was assessed. Concurrent with the literature we found that all three receptors were expressed on hCMEC/D3 cells (Ohtsuki et al., 2013; Pinzón-Daza et al., 2012). TfR was found to exhibit the most stable levels of expression with long-term *in vitro* culture. In contrast to TfR expression, LDLR and LRP1 expressions appeared to vary significantly with long-term culture. Additionally,

although TfR has been shown to have a functional trypsin cleavage site at arginine 100 within the stem region of its extracellular domain and is bio-available in a soluble form within the circulation, use of trypsin/ EDTA as a short-term cell detachment solution did not appear to affect the cell surface expression of TfR on hCMEC/D3 cells. Considering our findings, in conjunction with previous studies that have shown the expression of TfR to be amongst the most highly expressed membrane receptors on BCEC both *in vitro* and *in vivo*, together with the observed fast endocytotic turnover of TfR (He et al., 2015), we decided to pursue TfR as our receptor candidate of interest (He et al., 2015; Ohtsuki et al., 2013; W. M. Yang et al., 2011).

Within chapter two, we had also set out to evaluate the hTfR protein expression of two CHO-transcript variant cell lines, CHO-TRVb (TfR deficient) and -TRVb-1 (deficient cells transfected with hTfR) and assess their applicability for use as target cells for accomplishing positive and negative *in vitro* selections. Through flow cytometric analysis, the human TfR transfected form of the deficient cell line (TRVb-1) was observed to express similar levels of hTfR to hCMEC/D3 cells.

Similarly to the work presented herein, Mehta *et al*. (2015) have also demonstrated the cell surface hTfR expression of CHO-TRVb1 cells by FACS analysis. The group highlighted that TfR expression remained consistent following 5 g/L holotransferrin treatment at 24h and 48h time points, and expression was observed in 70% of the cell population. In contrast, the group found that the HepG2 cell line demonstrated a 2-fold reduction of hTfR following the same holotransferrin treatment, and its expression of hTfR was seen in 30% of cells at 24h and 15% of cells at 48h. However, considering the higher levels of hTfR the group did not see an increase in uptake of iron within these cells, suggesting that iron may be regulated through increased expression of *slc40a1* which mediates the efflux of iron from these cells.

Within our work, we identified some expression of hTfR by FACS analysis on the deficient cell line suggesting presence of a heterogeneous population of cells. However, our assessment of TfR uptake within these cell lines showed no observable uptake of anti-hTfR or anti-mTfR within the deficient cells suggesting they

are functionally deficient of hTfR. This finding corresponds to existing evidence showing TfR mediated uptake with these cell lines (McGraw et al., 1987).

Further exploration of these cell lines was not within the remit of our work. Being functionally deficient for the expression of hTfR, these cells may prove to be useful tools for selecting and characterising conformationally relevant TfR cell binding domains, and this would need to be explored further. Such selections could be performed through positive and negative cell selections towards the hTfR expressing and the hTfR deficient cells, a commonly used approach for identifying target cell specific domains (Cerchia et al., 2009; M. Lu et al., 2015).

Further characterisation of TfR expression under various culture conditions such as serum starvation within hCMEC/D3 cells has yet to be established and would be beneficial in deducing the optimal conditions for cell selections, when expression of TfR is highest. Utilising live cell imaging of Hela cells, Tacheva-Grigorova *et al*. (2013) demonstrated a substantial increase in the expression of surface TfR following incubation with ligand at 4°C and subsequent re-initiation of endocytosis at 37°C. It has not yet been established whether a similar increase in TfR expression is observed with BCEC under the same culture conditions and this could be explored further.

Also, another under-explored area with BBB cell models is the circadian regulation of genes. The levels of iron found in the brain fluctuate in diurnal patterns, and these have been shown to be associated with Alzheimer's disease, Parkinson's disease and restless leg syndrome (Simpson et al., 2015). In iron-deficient mice, brain iron levels were found to be to be reduced by 25% (in relation to control fed mice), during the light phase when compared to the active dark phase (Unger et al., 2009). The circadian regulation of TfR could be one of the factors involved in the observed diurnal variations in brain iron content. A previous study utilising hexapeptide (dalagrin) conjugated nanoparticles has demonstrated a dose and time dependant antinociceptive effect and this was suggested to potentially be due to an increased rate of endocytosis and exocytosis occurring within BCEC during the rest phase (Ramge et al., 1999; Kreuter, 2015). Characterisation of the diurnal profiles of

BCEC receptors with *in vitro* and *in vivo* models of the BBB could be an important factor for future drug transport studies.

6.2. Selection and identification of TfR binding cyclic peptides

Following the identification of TfR as a suitable drug delivery candidate receptor that functions through RMT on BCEC, a study was set up to select and identify suitable peptides targeting TfR. Chapter three focused on the selection and identification of cyclic peptides capable of recognising TfR variants from multiple species.

The primary research goal of this chapter was to devise a phage display selection strategy that would facilitate the identification of low to medium affinity TfR species cross-reactive cyclic peptides. Secondly, this study endeavoured to utilise a suitable screening method for the identification of species cross-reactive peptides. Lastly, identified species cross-reactive peptides were compared for sequence homology.

Multiple phage display selection cascades were performed using three CPEP libraries towards biotinylated target human and mouse TfR immobilised on streptavidin-coated magnetic agarose beads. A cross-selection cascade was performed to encourage the identification of species cross-reactive domains. selections towards target receptors from multiple species, aid in the identification of species cross-targeting peptides, which are likely to fare more positively during the later stages of clinical trials, where the transition from animal models to human participants is the major cause of clinical trial failure (Eastwood et al., 2010). This is particularly important in the case of CNS biotherapeutics, where the lack of suitable BBB *in vitro* models and species cross-reactive domains has been amongst the reasons for the clinical trial failure of CNS candidates (Stanimirovic et al., 2015).

Similar phage display methods have previously been utilised to select and identify species cross-reactive domains to various targets including VEGF receptor, serum albumin, and notch receptors (Henry et al., 2015; Popkov et al., 2004; Y. Wu et al., 2010).

Furthermore, functional cell selections towards bEnd.3 cells were also carried out in a manner to encourage the identification of cell internalising domains. In a partially similar approach, a previous study has highlighted the selection of BBB crossing camelid single domain antibodies through phenotypic phage display selections towards cells (Muruganandam et al., 2002). This method relied on de-selection steps against lung endothelial cells to remove non-BBB specific domains. Subsequently, multiple rounds of cell selection were performed in order to identify human BCEC binding domains. The enriched pool of binding domains was phenotypically screened to identify cell internalising domains, in a similar approach to that described within our phage display selection strategy.

Interestingly, to identify a subset of cell transmigrating domains Muruganandam *et al*. (2002) further subjected the enriched pool to cell transcytosis assays using an *in vitro* model of the BBB consisting of human brain endothelial cells grown in transwell filters. The group identified two transmigrating domains Fc5 and Fc44, that demonstrated 4.5 ± 2.7% and 2.9 ± 1.7% brain uptake when intravenously administered as phage in mice, respectively. Whilst this approach resulted in BBB transmigrating domains, the exact binding receptor could not be determined without further studies (Abulrob et al., 2005). This is undesired, since identification of the unknown target(s) post-selection can be cumbersome and may hinder drug development due to a lack of understanding of the specific mechanism of action. This is further exemplified through the *in vivo* selection study carried out by Pasqualini *et al*. (1996), where intravenous injection of a peptide phage library and isolating the brain at each round led to the enrichment of cyclic peptides without a known target, and this target has not yet been elucidated. In contrast, our selection approach utilised a pre-selection to recombinant TfR protein prior to further enrichment through functional cell selections. This combined selection strategy avoids the selection of binding domains to unknown targets whilst also conferring functionally relevant domains.

From screening three phage output pools, we have identified 13 lead peptide sequences that were all shown to exhibit specific binding towards mouse, rat and human forms of TfR, as determined through phage ELISA studies using crude phage

supernatants. Moreover, the antigen cross-selection strategy was successful in identifying three species cross-reactive candidates (Pep1, Pep4 and Pep7). Furthermore, mTfR only selections were also successful in identifying species cross-reactive domains. In addition to the identification of TfR binding peptide candidates, three TUP clones that bind streptavidin through the consensus 'HPQ' and 'HPM' motifs were also observed.

Homology assessment of the 16 unique peptides revealed various conserved motifs that likely confer binding of peptides towards TfR including 'DCS', 'CTPΘ', and a hydrophobic motif 'WWGΘ'. Two of these motifs, 'CTPΘ' and 'WWG' have previously been described within peptides that bind MHC molecules and an unknown brain targeting protein, respectively (Allen et al., 2001; Pasqualini and Ruoslahti, 1996; Schroers et al., 2003). Since the brain targeting peptide described by Pasqualini *et al*. (1996), (CENWWGDVC), shares the 'WWG' motif with three of the strongest binding domains as identified by phage ELISA (Pep8, Pep9 and Pep10), we predict that it could be targeting the brain via TfR mediated uptake across BCEC. Further work would be required to elucidate the binding of 'CENWWGDVC' to recombinant TfR and BCEC targets.

Through homology studies with the natural ligand transferrin, Pep1 was identified to share strong homology with a nine-residue motif (DCSGNFCL) located within the sequence of Tf (AA 614 – 622). This sequence was conserved across human mouse and rat TfR and has not previously been described for targeting of TfR. Through studying the previously described crystal structures and interactions of Tf with TfR (Eckenroth et al., 2011), we have identified a potential mechanism of binding for Pep1. The corresponding peptide motif to Pep1 was identified on Tf C1 subdomain of the C-lobe and was shown to bind through electrostatic interactions between Tf and Arginine 629 of TfR. Dai *et al*. (2014) have previously described a phage display selected linear peptide (BP9) that contains two amino acid motif (FR) and bears homology with Tf Herein, we have shown that the 'FR' motif lies downstream of our identified homologous sequence (DCSGNFCL). It is not clear whether both of these peptide interact with TfR through a consensus epitope and this would need to be explored further through competition binding assays utilising both peptides.

During the course of our phage ELISA screening analysis, we also identified hTfR and mTfR specific positive clones that could not be investigated further due to time constraints (see supplementary Figure S3). Whilst this project has solely focused on the identification of TfR species cross-reactive peptides, it may also be interesting to sequence, express and characterise these unique TfR binding clones for their ability to internalise and traverse BCEC. Furthermore, whilst these peptides were identified to be species specific via phage ELISA screening, they may still be useful candidates for obtaining species cross-reactive peptides. Studies have previously shown that it is possible to confer species cross-reactivity through affinity maturation and computational design approaches of the binding region of peptides and antibodies (Garcia-Rodriguez et al., 2007; Farady et al., 2009).

Additionally, due to time constraints, only a small number of clones were screened per output pool (528 clones). It may therefore be valuable to re-screen the output pools using a greater number of clones. Typically, several thousands of clones are screened per output pool in order to obtain a representative overview of the entire pool and identify binding sequences with low representation (Lee et al., 2004; Kehoe et al., 2006). Although phage ELISA screening methods are the most extensively reported methods in the literature for phage clone screening, the difficulty in initially recognising whether affinity molecules exhibit TUP binding properties and the time-consuming protocols involved for screening a large number of clones has led some researchers to transition to alternative screening methods. In recent years, some groups have transitioned to high throughput sequencing as an alternative means of predicting sequences that may potentially be involved in target specific binding ('t Hoen et al., 2012). This is done through the alignment of millions of sequence reads from a heterogeneous selection output pool and the study of conserved sequence motifs across the most highly enriched sequences. Sequence enrichment can also be monitored with selection round progress, allowing for correlations to be made with preserved sequences seen in later rounds. Subsequently, lead sequences can be synthesised and assayed for binding towards the target antigen.

Ngubane *et al*. (W. M. Yang et al., 2011) compared the results of both random clone picking and HTS as screening approaches when carrying out phage display selections towards *Mycobacterium tuberculosis* using a cyclic heptapeptide library (CX_7C). The group discovered that target specific clones could be identified following just one round of selection when using HTS. Moreover, the most highly enriched sequence identified using the HTS approach demonstrated a greater binding affinity towards the target than the three identified leads discovered via the random colony screening approach. Interestingly, the most highly enriched sequence discovered via HTS (80% representation), was not identified using the random colony screening approach.

Further work on assessing the physiochemical properties of the identified peptide sequences is needed. The functional groups of amino acids confer distinct physical properties that determine the overall solubility and charge of a peptide. The isoelectric point (pI) of a peptide or a protein is the pH at which the molecule has a net charge of zero (Kozlowski, 2016). Peptides and proteins have poor solubility at the isoelectric point making them more likely to precipitate and bind non-specifically (McDonald et al., 2009). Additionally, short positively charged or hydrophobic peptides are more susceptible to passive adsorption to polystyrene surfaces (Kogot et al., 2012). Importantly, determining the pI of a peptide will allow the calculation of its charge at physiological pH of 7.4 which can give an indication of its specificity and solubility within circulation (Kohn et al., 2007). The lipophilicity of a peptide is also an important factor to consider. Highly hydrophobic peptides are more prone to bind plasma proteins such as albumin within the circulation significantly increasing serum half-life and reducing elimination (Plum et al., 2013).

6.3. Characterisation of binding and internalisation of lead peptides

Following the identification of 13 positive cross-species binding peptides from phage ELISA screening towards TfR, peptides needed to be expressed as soluble domains for characterisation. Chapter four focuses on the expression and characterisation of lead peptides towards recombinant protein and BCEC targets.

The primary research aim of this chapter was to characterise the binding and cell uptake of peptide candidates expressed as soluble fusion domains, towards recombinant TfR and BCEC cells derived from both mouse and human species.

For the initial characterisation towards recombinant TfR and BCEC cell lines, peptide candidates were cloned into a modified pCANTAB6-D1/FLAGHIS10 vector and expressed as soluble monovalent fusion domains to g3p-D1 via periplasmic expression. Subsequently, promising lead candidates that expressed within the g3p-D1 fusion format were taken forward for further characterisation as bivalent CPep-Fc fusion domains. Finally, the internalisation and subcellular trafficking of CPep-Fc lead domains was assessed on bEnd.3 and hCMEC/D3 cells.

Periplasmic expression of monovalent CPep-D1 fusion domains resulted in the efficient expression of 9 of the 16 peptides identified through phage ELISA screening. Five peptides demonstrated poor periplasmic expression yields, (Pep2, Pep4, Pep12, Pep13 and Pep15) and two peptides (Pep10 and Pep16) failed to express completely with the current periplasmic expression protocol. The most significant peptide that failed to express was Pep10, which consistently demonstrated the highest specific absorbance readings during phage ELISA screening towards all three species of TfR and was the most highly enriched sequence identified throughout the selection process. Some fusion molecules have been known to be problematic to expressed within *E.coli* and it has been suggested that this may be due to the inappropriate physiochemical properties of microbial hosts (H.-J. Kang et al., 2017).

Due to time constraints, it was not possible to optimise the re-expression conditions for the CPep-D1 domains that exhibited low yields or failed to express. Further optimisations of growth conditions using different growth temperatures, IPTG concentrations, and induction times may be necessary to optimise yields (Rouet et al., 2012). Additionally, optimisations of minor codon usage within peptide coding sequences and the use of *E.coli* strains that re-introduce less abundant tRNA may also ameliorate heterologous expression issues (Nouri et al., 2016). Another approach would be to utilise an alternative fusion domain to the g3p-D1 domain described here. Various fusion domains have been described for the stable and

efficient periplasmic expression of peptides and proteins, these include the small ubiquitin-like modifier 3 (SUMO 3), Cytochrome b5 and Fh8 tag (Besir, 2017; Dormeshkin et al., 2016; Costa et al., 2013).

If optimisation approaches fail to yield suitable quantities of peptide, then chemical synthesis approaches may be necessary for characterising the remaining peptide candidates. Typically, the peptides are synthesised coupled to polyethylene glycol (PEG) in place of the fusion domain to aid in peptide stability and solubility, whilst also reducing immunogenicity and decreasing clearance rate (Dozier and Distefano, 2015).

Following monovalent peptide screening, four lead peptides (Pep1, Pep8, Pep9, and Pep14) were identified to specifically bind to recombinant mouse and human TfR and immortalised mouse and human BCEC (bEnd.3 and hCMEC/D3). Pep1 and Pep8 demonstrated the greatest degree of binding towards recombinant TfR and BCEC, whilst Pep9 and Pep14 appear to be very weak affinity peptides.

Alanine scanning and other structure-based design studies may be carried out on the four lead peptide candidates to identify key amino acid residues involved in TfR binding. Rationale design approaches such as these can aid in the identification of peptide variants with improved binding affinity, stability and desired physiochemical properties (Savio et al., 2012). Furthermore, the precise binding affinities of these lead peptides has yet to be determined via SPR based approaches such Biacore (Kamat and Rafique, 2017; Yau and Shochat, 2014).

The two promising lead peptides (Pep1 and Pep8) were subsequently expressed as divalent CPep-Fc/IL1RA fusions and assessed for their capacity to transport a conjugated cargo within BCEC. Pep1 demonstrated a specific, time dependant uptake within bEnd.3 and its internalisation demonstrated with hCMEC/D3 cells at 60 and 120 min time points. At both time-points, no observable co-localisation was observed with EEA1 and LAMP1 suggesting that at those particular time-points it was avoiding the lysosomal degradation pathway. However, this preliminary finding needs to be validated using confocal microscopy since

epifluorescence microscopy is not capable of distinguishing overlapping vesicles within the Z-dimension from co-localised points (Dunn et al., 2011).

Pep8 demonstrated a low specific uptake when expressed as a -Fc/IL1RA fusion. A study by Daniel *et al*. (Danial et al., 2017) has recently reported a similar loss in peptide binding potency when a PEG polymer was conjugated to heptad repeat 2 peptide. Further work is needed to determine whether the low uptake observed with Pep8 was due to expression within this format.

Results of the early *in vivo* pilot study carried out using the mouse neuropathic pain model indicate that these peptides demonstrate some promise for use as BBB delivery shuttles (Thom and Hatcher, 2016). A significant increase in CNS uptake as demonstrated via an increase in analgesic effect on the mice was observed at the four-hour time-point in relation to sham controls. However, the observed effects were rapidly diminished thereafter. It is not clear whether renal filtration is the cause for this rapid clearance. The threshold for glomerular filtration is a molecule size of approximately 60 kDa, however it has also been suggested that the radius of a molecule is the limiting factor for renal filtration (Meibohm and H. Zhou, 2012). The size of these fusion domains could suggest that renal filtration may be the cause of the rapid clearance, however further assessment is needed. As they currently stand, these peptide-Fc conjugates do not provide a viable proposition for therapeutic dosing, primarily due to the fact that frequent dosing strategies using biologics is not economically viable and increases the risks of adverse drug events.

The use of strategies to increase the size of these molecules significantly beyond the renal threshold may be required for optimisation. Alternatively, the extent of binding of peptides towards plasma proteins such as albumin can also influence drug distribution *in vivo*, limiting the free compound available for binding and uptake at target cells. Dennis *et al*. (2002) have selected an albumin binding peptide through phage display that binds albumin derived from various species. The group demonstrated extended half-life of a short lived Fab domain after recombinant fusion with the peptide ‘DICLPRWGCLW’. Such an approach may be useful in reducing the rapid elimination of Pep1-Fc/IL1RA.

The transcytosis capacity of Pep1-Fc/IL1RA has yet to be explored using *in vitro* BBB transcytosis models. Transcytosis within *in vitro* cell models may be assessed two ways. Firstly, the most commonly utilised method involves the use of *in vitro* immortalised BCEC cultured in trans-well filters in order to assess apical to basolateral transport. However, these models are highly susceptible to significant para-cellular flux due to low TEER values, which mask the measurement of specific transcellular transport. One promising study describes an approach which overcomes this problem through the use of a 'pulse-chase' method (Sade et al., 2014). Alternatively, the use of TEM approaches is also a well-established method for assessing apical to basolateral transport within *in vitro* models of the BBB (D. Ye et al., 2014). Conducting transcytosis assays using the CPep-Fc/IL1RA domains in addition to determining brain uptake with *in vivo* animal models, will greatly aid in evaluating the viability of CPep1 as a potential BBB drug delivery shuttle.

6.4. Selection and enrichment analysis of aptamer selected pools

Aptamers have recently emerged as promising alternatives to antibodies as molecular recognition domains (Alshaer et al., 2017; Ruscito et al., 2017). Chapter five focuses on the establishment of a SELEX protocol and the selection of ssDNA aptamers that target and bind hTfR.

The overall aim of this chapter was to establish a protocol for the selection of hTfR binding aptamers and subsequently screen selected pools for the identification of enriched aptamer species. Several considerations were made when deciding upon the selection approach and SELEX library to use. Firstly, a ssDNA library was chosen in place of its RNA counterpart, since DNA is significantly more stable than RNA. This facilitates lab handling procedures and potentially produces aptamers that can be utilised natively *in vivo* (Heiat et al., 2016). Furthermore, the size of the library chosen for this study consisted of 30 nucleotides within the random region. Smaller aptamers are likely to have better tissue penetration and better accessibility of epitopes (Xiang et al., 2015). In order to improve the likelihood of selecting physiologically relevant aptamers, a combinatorial selection strategy consisting of selections towards recombinant hTfR and hTfR overexpressing CHO cells was

chosen. Such an approach has previously been described by Wilner *et al*. (Wilner et al., 2012) during the selection of hTfR binding RNA aptamers.

The preferential separation of target binding aptamer from the unbound pool was carried out through the immobilisation of polyhistidine tagged hTfR onto Ni-NTA magnetic agarose beads, a commonly utilised affinity capture matrix for utilised for SELEX (Murphy et al., 2003; Wilner et al., 2012; Bartnicki et al., 2015). Prior to commencing with selections, it was necessary validate Ni-NTA magnetic bead capture of hTfR-His6 and assess whether the beads could maintain captured protein through multiple wash steps. Captured and eluted hTfR protein from Ni-NTA magnetic agarose beads following wash steps, was characterised using immunoblot analysis. Our findings indicate that that 5 μg was optimal for minimising loss of protein with one and three wash steps.

Initially, the goal of these selections was to perform 5 rounds of aptamer SELEX towards recombinant hTfR-His6 and subsequently one or more rounds of cell selections towards CHO-TRVb-1 (hTfR overexpressing) cells. A similar number of rounds was previously carried out to identify target hTfR binding RNA aptamers (Wilner et al., 2012). A total of 6 rounds were initially carried out, five rounds of selection towards hTfR-His6 and one round towards CHO-TRVb-1 cells. Using a colony screening approach, it was not possible to identify any enriched sequences following the screening of approximately 88 colonies originating from each of the round 5 and 6 selected pools (results not shown). Selections were subsequently continued to round 12, where non-specific amplification products were observed to contaminate the amplified aptamer pool and limited further progression of the selection.

As discussed in chapter 5, the formation of non-specific by-products is a commonly observed artefact of selections and can originate from various sources (Tolle et al., 2014). In the case of our selections the source of contamination likely originated from primer dimerisation. Some of these by-products may be overcome through the use of emulsion PCR, a technique that ameliorates the need for optimisation PCR steps, allows the amplification of small amounts of DNA and prevents PCR amplification bias (Tolle et al., 2014; R. Williams et al., 2006).

Following 12 rounds of SELEX, HTS was carried out on several selected pools in order to determine enrichment and allow further identification of potential lead candidate aptamer sequences for screening. A count analysis revealed an overall 62% reduction in pool diversity between the unselected pool and round 12 selected pool. Having established enrichment following 12 rounds, further analysis of clustered NGS data is required to identify conserved whole sequences or regions within groups of aptamers. Once identified, lead candidates may then be chemically synthesised and screened using aptamer linked immunosorbent assays (ALISA) (Modh et al., 2016), Fluorescent dye-linked aptamer assays (FLAA) (Schütze et al., 2011) or FACS analysis (Macdonald, Houghton, et al., 2016; Sefah et al., 2010) to identify target hTfR binding aptamers.

The cell selection approach used at round 4 to successfully identify functional cell internalising peptides can be applied within the context of aptamer selections (described in chapter 3). This approach may be applied in order to increase selection stringency and preferentially identify BCEC cell internalising aptamers. A similar approach has previously been described with cell-internalising SELEX (Mallikaratchy, 2017). Following the incubation of the aptamer library with live cells, cells are washed in a high salt solution in order eliminate slow or non-internalising aptamers leaving only aptamers that have been internalised within cells.

6.5. Conclusion and personal reflections

This thesis has explored the use of antibody alternative biologic domains for use as drug delivery shuttles across the BCECs that form the primary physical barrier component of the neurovascular unit. TfR was confirmed as a suitable candidate RMT receptor at the BCEC and targeted through phage display and SELEX to identify cyclic peptides and aptamers, respectively.

Through the use of a multifaceted phage display selection approach, we have identified 13 species cross-reactive peptides that demonstrate specific binding towards human and mouse TfR. Through homology sequence alignment, we have identified that our lead peptide candidate (Pep1) shares significant homology with a highly conserved nine amino acid sequence on transferrin (DCSGNFCLF), which

has not previously been described for targeting TfR. Furthermore, when expressed as a bivalent Fc-fusion domain, Pep1 demonstrated a significant time-dependant uptake within bEnd.3 cells and was shown to internalise within hCMEC/D3 cells at 60 and 120 min time points.

ssDNA aptamers, were also selected through a cascade of *in vitro* rounds of enrichment towards recombinant hTfR and CHO cells overexpressing hTfR. Following 12 rounds of nucleic acid enrichment, a count analysis of NGS data revealed that the selection resulted in 62% enrichment of the round 12 selected pool in contrast to the unselected pool. This result warrants further detailed assessment of the selected pools for sequence enriched aptamers which may be characterised for binding recombinant hTfR and BCEC.

The versatile and specific nature of biotherapeutics has revolutionised the way we tackle the treatment of many conditions (Gasser and Waaga-Gasser, 2016). Non-antibody biologic domains (such as peptides and aptamers) provide an effective approach to circumventing the transport limitations of the BBB, and have the potential to overcome the longstanding limitations of traditional MAb within this context. There is a vastly unmet demand for the treatment of neurological disorders. Whilst evidently there are high financial risks involved in the pursuit of strategies that enhance therapeutic uptake of macromolecules at the CNS, the promise of opening a largely untapped pharmaceutical market has continued to push research and development within this area (Stanimirovic et al., 2015). With our ever-growing knowledge of the BBB and continued commitment to research into targeted therapeutic approaches, it is only a matter of time and effort before the capabilities of this fascinating class of drugs is realised within the area neurotherapeutic treatments.

Bibliography

't Hoen, P. A. C. et al. (2012) Phage display screening without repetitious selection rounds. *Analytical biochemistry*. [Online] 421 (2), 622–631.

Aasa, R. et al. (1963) The specific binding of iron(III) and copper(II) to transferrin and conalbumin. *Biochimica et biophysica acta*. [Online] 75203–222.

Abbott, N. J. (2013) *Blood–brain barrier structure and function and the challenges for CNS drug delivery*. [Online] 36 (3), 437–449.

Abbott, N. J. et al. (2010) Structure and function of the blood-brain barrier. *Neurobiology of Disease*. [Online] 37 (1), 13–25.

Abraham, J. et al. (2010) Structural basis for receptor recognition by New World hemorrhagic fever arenaviruses. *Nature structural & molecular biology*. [Online] 17 (4), 438–444.

Abulrob, A. et al. (2005) The blood-brain barrier transmigrating single domain antibody: mechanisms of transport and antigenic epitopes in human brain endothelial cells. *Journal of neurochemistry*. [Online] 95 (4), 1201–1214.

Adey, N. B. et al. (1995) Characterization of phage that bind plastic from phage-displayed random peptide libraries. *Gene*. 156 (1), 27–31. [online]. Available from: http://eutils.ncbi.nlm.nih.gov/entrez/eutils/elink.fcgi?dbfrom=pubmed&id=7737512&retmode=ref&cmd=prlinks.

Ahmad, K. M. et al. (2011) Probing the limits of aptamer affinity with a microfluidic SELEX platform. Maxim Antopolsky (ed.). *PloS one*. [Online] 6 (11), e27051.

Ahmad, W. et al. (2017) Rabies virus co-localizes with early (Rab5) and late (Rab7) endosomal proteins in neuronal and SH-SY5Y cells. *Virologica Sinica*. [Online] 32 (3), 207–215.

Ahram, M. et al. (2005) A proteomic approach to characterize protein shedding. *Proteomics*. [Online] 5 (1), 123–131.

Ahrens, I. et al. (2011) *Reg1, a Novel RNA-Aptamer Direct Factor IXa-inhibitor (pegnivacogin) Reduces Platelet Activation in Healthy Volunteers and Residual Platelet Aggregation in ….*

Airan, R. D. et al. (2017) MR-Guided Delivery of Hydrophilic Molecular Imaging Agents Across the Blood-Brain Barrier Through Focused Ultrasound. *Molecular imaging and biology : MIB : the official publication of the Academy of Molecular Imaging*. [Online] 19 (1), 24–30.

Aisen, P. (2004) Transferrin receptor 1. *The international journal of biochemistry & cell biology*. [Online] 36 (11), 2137–2143.

Alam, K. K. et al. (2015) FASTAptamer: A Bioinformatic Toolkit for High-throughput Sequence Analysis of Combinatorial Selections. *Molecular therapy. Nucleic acids*. [Online] 4 (3), e230.

Alegria-Schaffer, A. (2014) 'Protein Biotinylation', in *Laboratory Methods in Enzymology: Protein Part A*. Methods in Enzymology. [Online]. Elsevier. pp. 109–114.

Allen, T. M. et al. (2001) CD8(+) lymphocytes from simian immunodeficiency virus-infected rhesus macaques recognize 14 different epitopes bound by the major histocompatibility complex class I molecule mamu-A*01: implications for vaccine design and testing. *Journal of virology*. [Online] 75 (2), 738–749.

Alshaer, W. et al. (2017) Selection and targeting of EpCAM protein by ssDNA aptamer. Vittorio de Franciscis (ed.). *PloS one*. [Online] 12 (12), e0189558.

Alsters, S. I. M. et al. (2015) Truncating Homozygous Mutation of Carboxypeptidase E (CPE) in a Morbidly Obese Female with Type 2 Diabetes Mellitus, Intellectual Disability and Hypogonadotrophic Hypogonadism. Daniela Cota (ed.). *PloS one*. [Online] 10 (6), e0131417.

Alvarez, E. et al. (1989) Intermolecular disulfide bonds are not required for the expression of the dimeric state and functional activity of the transferrin receptor. *The EMBO journal*. 8 (8), 2231–2240.

Amarasinghe, C. & Jin, J.-P. (2015) *The Use of Affinity Tags to Overcome Obstacles in Recombinant Protein Expression and Purification.* 22 (10), 885–892.

Anderluh, G. et al. (2003) Expression of proteins using the third domain of the Escherichia coli periplasmic-protein TolA as a fusion partner. *Protein expression and purification*. 28 (1), 173–181.

Andreone, B. J. et al. (2017) Blood-Brain Barrier Permeability Is Regulated by Lipid Transport-Dependent Suppression of Caveolae-Mediated Transcytosis. *Neuron*. [Online] 94 (3), 581–594.e585.

Andrews, L. et al. (2015) A snapshot of biologic drug development: Challenges and opportunities. *Human & Experimental Toxicology*. [Online] 34 (12), 1279–1285.

Apodaca, G. et al. (2012) Role of membrane traffic in the generation of epithelial cell asymmetry. *Nature cell biology*. [Online] 14 (12), 1235–1243.

Aravind, A. et al. (2012) AS1411 aptamer tagged PLGA-lecithin-PEG nanoparticles for tumor cell targeting and drug delivery. *Biotechnology and bioengineering*. [Online] 109 (11), 2920–2931.

Arend, W. P. & Guthridge, C. J. (2000) Biological role of interleukin 1 receptor antagonist isoforms. *Annals of the rheumatic diseases*. [Online]

Aroeti, B. & Mostov, K. E. (1994) Polarized sorting of the polymeric immunoglobulin receptor in the exocytotic and endocytotic pathways is controlled by the same amino acids. *The EMBO journal*. 13 (10), 2297–2304.

Artus, C. et al. (2014) The Wnt/planar cell polarity signaling pathway contributes to the integrity of tight junctions in brain endothelial cells. *Journal of cerebral blood flow and metabolism : official journal of the International Society of Cerebral Blood Flow and Metabolism*. [Online] 34 (3), 433–440.

Asmat, T. M. et al. (2014) Endocytosis of Streptococcus pneumoniae via the polymeric immunoglobulin receptor of epithelial cells relies on clathrin and caveolin dependent mechanisms. *International journal of medical microbiology : IJMM*. [Online] 304 (8), 1233–1246.

Avinoam, O. et al. (2015) ENDOCYTOSIS. Endocytic sites mature by continuous bending and remodeling of the clathrin coat. *Science (New York, N.Y.)*. [Online] 348 (6241), 1369–1372.

Bae, O.-N. (2012) Targeting von Willebrand factor as a novel anti-platelet therapy; application of ARC1779, an Anti-vWF aptamer, against thrombotic risk. *Archives of pharmacal research*. [Online] 35 (10), 1693–1699.

Bai, S. et al. (2012) A guide to rational dosing of monoclonal antibodies. *Clinical pharmacokinetics*. [Online] 51 (2), 119–135.

Bajpai, R. et al. (2008) Efficient propagation of single cells Accutase-dissociated human embryonic stem cells. *Molecular reproduction and development*. [Online] 75 (5), 818–827.

Bakhshinejad, B. & Sadeghizadeh, M. (2016) A polystyrene binding target-unrelated peptide isolated in the screening of phage display library. *Analytical biochemistry*. [Online] 512120–128.

Barat, B. & Wu, A. M. (2007) Metabolic biotinylation of recombinant antibody by biotin ligase retained in the endoplasmic reticulum. *Biomolecular engineering*. [Online] 24 (3), 283–291.

Barfod, A. et al. (2009) In vitro selection of RNA aptamers against a conserved region of the Plasmodium falciparum erythrocyte membrane protein 1. *Parasitology research*. [Online] 105 (6), 1557–1566.

Bartnicki, F. et al. (2015) Imidazole-free purification of His3-tagged recombinant proteins using ssDNA aptamer-based affinity chromatography. *Journal of chromatography. A*. [Online] 1418130–139.

Bauer, H.-C. et al. (2014) 'You Shall Not Pass'-tight junctions of the blood brain barrier. *Frontiers in neuroscience*. [Online] 8392.

Beard, J. L. et al. (2005) Brain iron uptake in hypotransferrinemic mice: influence of systemic iron status. *Journal of neuroscience research*. [Online] 79 (1-2), 254–261.

Beck, A. & Reichert, J. M. (2014) Therapeutic Fc-fusion proteins and peptides as successful alternatives to antibodies. *mAbs*. [Online] 3 (5), 415–416.

Begley, D. J. (2004) ABC transporters and the blood-brain barrier. *Current pharmaceutical design*. 10 (12), 1295–1312.

Ben-Zvi, A. et al. (2014) Mfsd2a is critical for the formation and function of the blood-brain barrier. *Nature*. [Online] 509 (7501), 507–511.

Besir, H. (2017) A Generic Protocol for Purifying Disulfide-Bonded Domains and Random Protein Fragments Using Fusion Proteins with SUMO3 and Cleavage by SenP2 Protease. *Methods in molecular biology (Clifton, N.J.)*. [Online] 1586 (Chapter 9), 141–154.

Betts, A. M. et al. (2016) Preclinical to Clinical Translation of Antibody-Drug Conjugates Using PK/PD Modeling: a Retrospective Analysis of Inotuzumab Ozogamicin. *The AAPS journal*. [Online] 18 (5), 1101–1116.

Bi, Yuan et al. (2006) Efficient high level expression of peptides and proteins as fusion proteins with the N-terminal domain of L9: application to the villin headpiece helical subdomain. *Protein expression and purification*. [Online] 47 (1), 234–240.

Bi, Yunke et al. (2016) T7 Peptide-Functionalized PEG-PLGA Micelles Loaded with Carmustine for Targeting Therapy of Glioma. *ACS applied materials & interfaces*. [Online] 8 (41), 27465–27473. [online]. Available from: http://pubs.acs.org/doi/abs/10.1021/acsami.6b05572.

Bian, F. et al. (2017) Reactive oxygen species mediate angiotensin II-induced transcytosis of low-density lipoprotein across endothelial cells. *International journal of molecular medicine*. [Online] 39 (3), 629–635.

Bickel, U. et al. (1994) In vivo demonstration of subcellular localization of anti-transferrin receptor monoclonal antibody-colloidal gold conjugate in brain capillary endothelium. *The journal of histochemistry and cytochemistry : official journal of the Histochemistry Society*. [Online] 42 (11), 1493–1497.

Bien-Ly, N. et al. (2014) Transferrin receptor (TfR) trafficking determines brain uptake of TfR antibody affinity variants. *The Journal of experimental medicine*. [Online] 211 (2), 233–244.

Biesemann, A. et al. (2017) Rab35 protein regulates evoked exocytosis of endothelial Weibel-Palade bodies. *The Journal of biological chemistry*. [Online] 292 (28), 11631–11640.

Blind, M. & Blank, M. (2015) Aptamer Selection Technology and Recent Advances. *Molecular therapy. Nucleic acids*. [Online] 4 (1), e223.

Boado, R. J. & Pardridge, W. M. (2017) Brain and Organ Uptake in the Rhesus Monkey in Vivo of Recombinant Iduronidase Compared to an Insulin Receptor Antibody-Iduronidase Fusion Protein. *Molecular Pharmaceutics*. [Online] 14 (4), 1271–1277.

Boado, R. J. et al. (2007) Fusion antibody for Alzheimer's disease with bidirectional transport across the blood-brain barrier and abeta fibril disaggregation. *Bioconjugate chemistry*. [Online] 18 (2), 447–455.

Boado, R. J. et al. (2016) Insulin Receptor Antibody-α-N-Acetylglucosaminidase Fusion Protein Penetrates the Primate Blood-Brain Barrier and Reduces Glycosoaminoglycans in Sanfilippo Type B Fibroblasts. *Molecular Pharmaceutics*. [Online] 13 (4), 1385–1392.

Boado, R. J., Lu, J. Z., et al. (2010) IgG-single chain Fv fusion protein therapeutic for Alzheimer's disease: Expression in CHO cells and pharmacokinetics and brain delivery in the rhesus monkey. *Biotechnology and bioengineering*. [Online] 105 (3), 627–635.

Boado, R. J., Zhou, Q.-H., et al. (2010) Pharmacokinetics and Brain Uptake of a Genetically Engineered Bifunctional Fusion Antibody Targeting the Mouse Transferrin Receptor. *Molecular Pharmaceutics*. [Online] 7 (1), 237–244.

Bonazzi, M. et al. (2012) A common clathrin-mediated machinery co-ordinates cell-cell adhesion and bacterial internalization. *Traffic (Copenhagen, Denmark)*. [Online] 13 (12), 1653–1666.

Bonetto, S. et al. (2009) Identification of cyclic peptides able to mimic the functional epitope of IgG1-Fc for human Fc gammaRI. *FASEB journal : official publication of the Federation of American Societies for Experimental Biology*. [Online] 23 (2), 575–585.

Botero-Kleiven, S. et al. (2001) Receptor-Mediated Endocytosis in an Apicomplexan Parasite (Toxoplasma gondii). *Experimental Parasitology*. [Online] 98 (3), 134–144.

Boucrot, E. et al. (2010) Roles of AP-2 in clathrin-mediated endocytosis. Richard Steinhardt (ed.). *PloS one*. [Online] 5 (5), e10597.

Böckenhoff, A. et al. (2014) Comparison of five peptide vectors for improved brain delivery of the lysosomal enzyme arylsulfatase A. *The Journal of neuroscience : the official journal of the Society for Neuroscience*. [Online] 34 (9), 3122–3129.

Braasch, D. A. & Corey, D. R. (2001) Locked nucleic acid (LNA): fine-tuning the recognition of DNA and RNA. *Chemistry & biology*. 8 (1), 1–7.

Brammer, L. A. et al. (2008) A target-unrelated peptide in an M13 phage display library traced to an advantageous mutation in the gene II ribosome-binding site. *Analytical biochemistry*. [Online] 373 (1), 88–98.

Brown, P. S. et al. (2000) Definition of distinct compartments in polarized Madin-Darby canine kidney (MDCK) cells for membrane-volume sorting, polarized sorting and apical recycling. *Traffic (Copenhagen, Denmark)*. 1 (2), 124–140.

Burdo, J. R. et al. (2001) Distribution of divalent metal transporter 1 and metal transport protein 1 in the normal and Belgrade rat. *Journal of neuroscience research*. [Online] 66 (6), 1198–1207.

Burmeister, P. E. et al. (2006) 2‘-Deoxy purine, 2’-O-methyl pyrimidine (dRmY) aptamers as candidate therapeutics. *Oligonucleotides*. [Online] 16 (4), 337–351.

Butler, J. E. et al. (1992) The physical and functional behavior of capture antibodies adsorbed on polystyrene. *Journal of Immunological Methods*. [Online] 150 (1-2), 77–90.

Byland, R. et al. (2007) A conserved dileucine motif mediates clathrin and AP-2-dependent endocytosis of the HIV-1 envelope protein. *Molecular biology of the cell*. [Online] 18 (2), 414–425.

Candela, P. et al. (2010) Apical-to-basolateral transport of amyloid-β peptides through blood-brain barrier cells is mediated by the receptor for advanced glycation end-products and is restricted by P-glycoprotein. *Journal of Alzheimer's disease : JAD*. [Online] 22 (3), 849–859. [online]. Available from: http://www.medra.org/servlet/aliasResolver?alias=iospress&doi=10.3233/JAD-2010-100462.

Candela, P. et al. (2008) Physiological pathway for low-density lipoproteins across the blood-brain barrier: transcytosis through brain capillary endothelial cells in vitro. *Endothelium : journal of endothelial cell research*. [Online] 15 (5-6), 254–264.

Cao, G. et al. (2002) In Vivo Delivery of a Bcl-xL Fusion Protein Containing the TAT Protein Transduction Domain Protects against Ischemic Brain Injury and Neuronal Apoptosis. *The Journal of neuroscience : the official journal of the Society for Neuroscience*. 22 (13), 5423–5431.

Cardoso, F. L. et al. (2010) Looking at the blood-brain barrier: molecular anatomy and possible investigation approaches. *Brain research reviews*. [Online] 64 (2), 328–363.

Carl, S. M. et al. (2010) ABC and SLC Transporter Expression and Pot Substrate Characterization across the Human CMEC/D3 Blood–Brain Barrier Cell Line. *Molecular Pharmaceutics*. [Online] 7 (4), 1057–1068.

Carmen, S. & Jermutus, L. (2002) Concepts in antibody phage display. *Briefings in functional genomics & proteomics*. [Online] 1 (2), 189–203.

Carpentier, J. L. et al. (1982) Co-localization of 125I-epidermal growth factor and ferritin-low density lipoprotein in coated pits: a quantitative electron microscopic study in normal and mutant human fibroblasts. *The Journal of cell biology*. 95 (1), 73–77.

Catuogno, S. et al. (2016) Aptamer-Mediated Targeted Delivery of Therapeutics: An Update. *Pharmaceuticals (Basel, Switzerland)*. [Online] 9 (4), 69. [online]. Available from: http://www.mdpi.com/1424-8247/9/4/69/htm.

Cerchia, L. et al. (2009) Differential SELEX in Human Glioma Cell Lines Dong-Yan Jin (ed.). *PloS one*. [Online] 4 (11).

Chames, P. et al. (2009) Therapeutic antibodies: successes, limitations and hopes for the future. *British journal of pharmacology*. [Online] 157 (2), 220–233.

Chen, C.-H. B. et al. (2008) Aptamer-based endocytosis of a lysosomal enzyme. *Proceedings of the National Academy of Sciences of the United States of America*. [Online] 105 (41), 15908–15913.

Chen, G.-F. T. & Inouye, M. (1994) Role of the AGA/AGG codons, the rarest codons in global gene expression in Escherichia coli. *Genes & development*. 8 (21), 2641–2652.

Chen, I. et al. (2007) Phage display evolution of a peptide substrate for yeast biotin ligase and application to two-color quantum dot labeling of cell surface proteins. *Journal of the American Chemical Society*. [Online] 129 (20), 6619–6625.

Chen, X. et al. (2013) Fusion protein linkers: property, design and functionality. *Advanced drug delivery reviews*. [Online] 65 (10), 1357–1369.

Chen, Z.-L. et al. (2013) Ablation of astrocytic laminin impairs vascular smooth muscle cell function and leads to hemorrhagic stroke. *The Journal of cell biology*. [Online] 202 (2), 381–395.

Cheng, C. et al. (2013) In vivo SELEX for Identification of Brain-penetrating Aptamers. *Molecular therapy. Nucleic acids*. [Online] 2 (1), e67.

Christoforidis, S. et al. (1999) The Rab5 effector EEA1 is a core component of endosome docking. *Nature*. [Online] 397 (6720), 621–625.

Chung, C. H. et al. (2013) Nuclease-resistant DNA aptamer on gold nanoparticles for the simultaneous detection of Pb2+ and Hg2+ in human serum. *Biosensors & bioelectronics*. [Online] 41827–832.

Chung, Y. C. et al. (2013) MMP-3 contributes to nigrostriatal dopaminergic neuronal loss, BBB damage, and neuroinflammation in an MPTP mouse model of Parkinson's disease. *Mediators of inflammation*. [Online] 2013 (9157), 370526–11.

Ciechanover, A. et al. (1983) Kinetics of internalization and recycling of transferrin and the transferrin receptor in a human hepatoma cell line. Effect of lysosomotropic agents. *The Journal of biological chemistry*. 258 (16), 9681–9689.

Clark, D. E. (2003) In silico prediction of blood-brain barrier permeation. *Drug discovery today*. 8 (20), 927–933.

Collawn, J. F. et al. (1990) Transferrin receptor internalization sequence YXRF implicates a tight turn as the structural recognition motif for endocytosis. *Cell*. 63 (5), 1061–1072.

Colleoni, M. & Sacerdote, P. (2010) Murine models of human neuropathic pain. *Biochimica et biophysica acta*. [Online] 1802 (10), 924–933.

Coloma, M. J. et al. (2000) Transport across the primate blood-brain barrier of a genetically engineered chimeric monoclonal antibody to the human insulin receptor. *Pharmaceutical research*. 17 (3), 266–274.

Conley, A. J. et al. (1994) Neutralization of divergent human immunodeficiency virus type 1 variants and primary isolates by IAM-41-2F5, an anti-gp41 human monoclonal antibody. *Proceedings of the National Academy of Sciences*. 91 (8), 3348–3352.

Coomber, B. L. & Stewart, P. A. (1986) Three-dimensional reconstruction of vesicles in endothelium of blood-brain barrier versus highly permeable microvessels. *The Anatomical record*. [Online] 215 (3), 256–261.

Cooper, P. R. et al. (2013) Efflux of monoclonal antibodies from rat brain by neonatal Fc receptor, FcRn. *Brain research*. [Online] 153413–21.

Cornford, E. M. & Hyman, S. (2005) Localization of brain endothelial luminal and abluminal transporters with immunogold electron microscopy. *NeuroRx : the journal of the American Society for Experimental NeuroTherapeutics*. [Online] 2 (1), 27–43.

Costa, S. et al. (2014) Fusion tags for protein solubility, purification and immunogenicity in Escherichia coli: the novel Fh8 system. *Frontiers in microbiology*. [Online] 563.

Costa, S. J. et al. (2013) The Fh8 tag: a fusion partner for simple and cost-effective protein purification in Escherichia coli. *Protein expression and purification*. [Online] 92 (2), 163–170.

Couch, J. A. et al. (2013) Addressing Safety Liabilities of TfR Bispecific Antibodies That Cross the Blood-Brain Barrier. *Science translational medicine*. [Online] 5 (183), 183ra57–183ra57.

Craik, D. J. et al. (2013) The future of peptide-based drugs. *Chemical biology & drug design*. [Online] 81 (1), 136–147.

Cramm-Behrens, C. I. et al. (2008) Apical cargo traverses endosomal compartments on the passage to the cell surface. *Traffic (Copenhagen, Denmark)*. [Online] 9 (12), 2206–2220.

Crowe, J. et al. (1994) 6xHis-Ni-NTA chromatography as a superior technique in recombinant protein expression/purification. *Methods in molecular biology (Clifton, N.J.)*. [Online] 31371–387.

Cui, Yanan et al. (2017) Monoclonal antibodies: formulations of marketed products and recent advances in novel delivery system. *Drug development and industrial pharmacy*. [Online] 43 (4), 519–530.

Cui, Yanna et al. (2016) Dual-Targeting Magnetic PLGA Nanoparticles for Codelivery of Paclitaxel and Curcumin for Brain Tumor Therapy. *ACS applied materials & interfaces*. [Online] 8 (47), 32159–32169.

Czajkowsky, D. M. et al. (2012) Fc-fusion proteins: new developments and future perspectives. *EMBO Molecular Medicine*. [Online] 4 (10), 1015–1028.

Daha, M. R. et al. (1982) Degradation of soluble immunoglobulin aggregates in vitro by monocytes from normal subjects and from patients with systemic lupus erythematosus. *Scandinavian journal of immunology*. 16 (2), 117–122.

Dai, X. et al. (2014) TfR Binding Peptide Screened by Phage Display Technology - Characterization to Target Cancer Cells. *Tropical Journal of Pharmaceutical Research*. [Online] 13 (3), 331–338.

Dal Magro, R. et al. (2017) ApoE-modified solid lipid nanoparticles: A feasible strategy to cross the blood-brain barrier. *Journal of controlled release : official journal of the Controlled Release Society*. [Online] 249103–110.

Danial, M. et al. (2017) Site-Specific Polymer Attachment to HR2 Peptide Fusion Inhibitors against HIV-1 Decreases Binding Association Rates and Dissociation Rates Rather Than Binding Affinity. *Bioconjugate chemistry*. [Online] 28 (3), 701–712.

Dapić, V. et al. (2003) Biophysical and biological properties of quadruplex oligodeoxyribonucleotides. *Nucleic acids research*. 31 (8), 2097–2107.

Darmostuk, M. et al. (2015) Current approaches in SELEX: An update to aptamer selection technology. *Biotechnology advances*. [Online] 33 (6 Pt 2), 1141–1161.

Davis, R. J. et al. (1986) Identification of serine 24 as the unique site on the transferrin receptor phosphorylated by protein kinase C. *The Journal of biological chemistry*. 261 (19), 9034–9041.

De Bock, M. et al. (2016) Into rather unexplored terrain-transcellular transport across the blood-brain barrier. *Glia*. [Online] 64 (7), 1097–1123.

De Bock, M. et al. (2012) Low extracellular Ca2+ conditions induce an increase in brain endothelial permeability that involves intercellular Ca2+ waves. *Brain research*. [Online] 148778–87.

de Lange, E. C. (2013) The mastermind approach to CNS drug therapy: translational prediction of human brain distribution, target site kinetics, and therapeutic effects. *Fluids and barriers of the CNS*. [Online] 10 (1), 12.

Deane, R. et al. (2005) IgG-assisted age-dependent clearance of Alzheimer's amyloid beta peptide by the blood-brain barrier neonatal Fc receptor. *The Journal of neuroscience : the official journal of the Society for Neuroscience*. [Online] 25 (50), 11495–11503.

Dehouck, B. et al. (1997) A new function for the LDL receptor: transcytosis of LDL across the blood-brain barrier. *The Journal of cell biology*. 138 (4), 877–889.

Dehouck, B. et al. (1994) Upregulation of the low density lipoprotein receptor at the blood-brain barrier: intercommunications between brain capillary endothelial cells and astrocytes. *The Journal of cell biology*. 126 (2), 465–473.

Demeule, M., Currie, J.-C., et al. (2008) Involvement of the low-density lipoprotein receptor-related protein in the transcytosis of the brain delivery vector angiopep-2. *Journal of neurochemistry*. [Online] 106 (4), 1534–1544. [online]. Available from: http://doi.wiley.com/10.1111/j.1471-4159.2008.05492.x.

Demeule, M., Régina, A., et al. (2008) Identification and design of peptides as a new drug delivery system for the brain. *The Journal of pharmacology and experimental therapeutics*. [Online] 324 (3), 1064–1072.

Dennis, M. S. et al. (2002) Albumin binding as a general strategy for improving the pharmacokinetics of proteins. *The Journal of biological chemistry*. [Online] 277 (38), 35035–35043.

Descamps, L. et al. (1996) Receptor-mediated transcytosis of transferrin through blood-brain barrier endothelial cells. *The American journal of physiology*. [Online] 270 (4 Pt 2), H1149–H1158.

Devlin, J. J. et al. (1990) Random peptide libraries: a source of specific protein binding molecules. *Science (New York, N.Y.)*. 249 (4967), 404–406.

Diao, L. & Meibohm, B. (2013) Pharmacokinetics and pharmacokinetic-pharmacodynamic correlations of therapeutic peptides. *Clinical pharmacokinetics*. [Online] 52 (10), 855–868.

Dintilhac, A. & Bernués, J. (2002) HMGB1 interacts with many apparently unrelated proteins by recognizing short amino acid sequences. *The Journal of biological chemistry*. [Online] 277 (9), 7021–7028.

Do, S. I. & Cummings, R. D. (1992) Presence of O-linked oligosaccharide on a threonine residue in the human transferrin receptor. *Glycobiology*. 2 (4), 345–353.

Dooley, H. et al. (2003) Selection and characterization of naturally occurring single-domain (IgNAR) antibody fragments from immunized sharks by phage display. *Molecular immunology*. 40 (1), 25–33.

Dormeshkin, D. et al. (2016) Development of CYB5-fusion monitoring system for efficient periplasmic expression of multimeric proteins in Escherichia coli. *Protein expression and purification*. [Online] 12860–66.

Dozier, J. K. & Distefano, M. D. (2015) Site-Specific PEGylation of Therapeutic Proteins. *International journal of molecular sciences*. [Online] 16 (10), 25831–25864.

Drappatz, J. et al. (2013) Phase I study of GRN1005 in recurrent malignant glioma. *Clinical cancer research : an official journal of the American Association for Cancer Research*. [Online] 19 (6), 1567–1576.

Drolet, D. W. et al. (2000) Pharmacokinetics and safety of an anti-vascular endothelial growth factor aptamer (NX1838) following injection into the vitreous humor of rhesus monkeys. *Pharmaceutical research*. 17 (12), 1503–1510.

Dua, P. et al. (2011) Nucleic acid aptamers targeting cell-surface proteins. *Methods (San Diego, Calif.)*. [Online] 54 (2), 215–225.

Duan, N. et al. (2017) Selection and Application of ssDNA Aptamers against Clenbuterol Hydrochloride Based on ssDNA Library Immobilized SELEX. *Journal of agricultural and food chemistry*. [Online] 65 (8), 1771–1777.

Dunn, K. W. et al. (2011) A practical guide to evaluating colocalization in biological microscopy. *American journal of physiology. Cell physiology*. [Online] 300 (4), C723–C742.

Duvernoy, H. et al. (1983) The vascularization of the human cerebellar cortex. *Brain research bulletin*. 11 (4), 419–480.

Eastwood, D. et al. (2010) Monoclonal antibody TGN1412 trial failure explained by species differences in CD28 expression on CD4+ effector memory T-cells. *British journal of pharmacology*. [Online] 161 (3), 512–526.

Eckenroth, B. E. et al. (2011) How the binding of human transferrin primes the transferrin receptor potentiating iron release at endosomal pH. *Proceedings of the National Academy of Sciences of the United States of America*. [Online] 108 (32), 13089–13094.

Einhauer, A. & Jungbauer, A. (2001) The FLAG™ peptide, a versatile fusion tag for the purification of recombinant proteins. *Journal of biochemical and biophysical methods*. [Online] 49 (1-3), 455–465.

El-Amouri, S. S. et al. (2014) Normalization and improvement of CNS deficits in mice with Hurler syndrome after long-term peripheral delivery of BBB-targeted iduronidase. *Molecular therapy : the journal of the American Society of Gene Therapy*. [Online] 22 (12), 2028–2037.

Elia, G. (2008) Biotinylation reagents for the study of cell surface proteins. *Proteomics*. [Online]

Ellington, A. D. & Szostak, J. W. (1990) In vitro selection of RNA molecules that bind specific ligands. *Nature*. [Online] 346 (6287), 818–822.

Evaluate Pharma (2015) *World Preview 2015, Outlook to 2020*. 9 (1), 1–8.

Eyetech Study Group (2002) Preclinical and phase 1A clinical evaluation of an anti-VEGF pegylated aptamer (EYE001) for the treatment of exudative age-related macular degeneration. *Retina (Philadelphia, Pa.)*. 22 (2), 143–152.

Ezan, P. et al. (2012) Deletion of astroglial connexins weakens the blood-brain barrier. *Journal of cerebral blood flow and metabolism : official journal of the International Society of Cerebral Blood Flow and Metabolism*. [Online] 32 (8), 1457–1467. [online]. Available from: http://journals.sagepub.com/doi/10.1038/jcbfm.2012.45.

Fan, Y.-Y. & Neubert, H. (2016) Quantitative Analysis of Human Neonatal Fc Receptor (FcRn) Tissue Expression in Transgenic Mice by Online Peptide Immuno-Affinity LC-HRMS. *Analytical chemistry*. [Online] 88 (8), 4239–4247.

Farady, C. J. et al. (2009) Improving the species cross-reactivity of an antibody using computational design. *Bioorganic & medicinal chemistry letters*. [Online] 19 (14), 3744–3747.

Feige, M. J. et al. (2014) The structural analysis of shark IgNAR antibodies reveals evolutionary principles of immunoglobulins. *Proceedings of the National Academy of Sciences of the United States of America*. [Online] 111 (22), 8155–8160.

Feng, Z. & Xu, B. (2016) Inspiration from the mirror: D-amino acid containing peptides in biomedical approaches. *Biomolecular concepts*. [Online] 7 (3), 179–187.

Figueiredo, P. et al. (2016) Angiopep2-functionalized polymersomes for targeted doxorubicin delivery to glioblastoma cells. *International journal of pharmaceutics*. [Online] 511 (2), 794–803.

Fillebeen, C. et al. (1999) Receptor-mediated transcytosis of lactoferrin through the blood-brain barrier. *The Journal of biological chemistry*. 274 (11), 7011–7017.

Fletcher, S. J. et al. (2014) Analysis of occludin trafficking, demonstrating continuous endocytosis, degradation, recycling and biosynthetic secretory trafficking. Ludger Johannes (ed.). *PloS one*. [Online] 9 (11), e111176.

Fosgerau, K. & Hoffmann, T. (2015) Peptide therapeutics: current status and future directions. *Drug discovery today*. [Online] 20 (1), 122–128.

Foster, J. S. et al. (2017) Preliminary characterization of a novel peptide-Fc-fusion construct for targeting amyloid deposits. *Amyloid : the international journal of experimental and clinical investigation : the official journal of the International Society of Amyloidosis*. [Online] 24 (sup1), 26–27.

Fradkin, A. H. et al. (2009) Immunogenicity of aggregates of recombinant human growth hormone in mouse models. *Journal of pharmaceutical sciences*. [Online] 98 (9), 3247–3264.

Friguet, B. et al. (1984) Some monoclonal antibodies raised with a native protein bind preferentially to the denatured antigen. *Molecular immunology*. 21 (7), 673–677.

Fukuda, S. et al. (2004) Focal cerebral ischemia induces active proteases that degrade microvascular matrix. *Stroke; a journal of cerebral circulation*. [Online] 35 (4), 998–1004.

Gabryelczyk, B. et al. (2015) Engineering of the Function of Diamond-like Carbon Binding Peptides through Structural Design. *Biomacromolecules*. [Online] 16 (2), 476–482.

Gaillard, P. J. et al. (2012) Targeted blood-to-brain drug delivery --10 key development criteria. *Current pharmaceutical biotechnology*. 13 (12), 2328–2339.

Gallagher, M. D. et al. (2017) A Dementia-Associated Risk Variant near TMEM106B Alters Chromatin Architecture and Gene Expression. *American journal of human genetics*. [Online] 101 (5), 643–663.

Garcia-Rodriguez, C. et al. (2007) Molecular evolution of antibody cross-reactivity for two subtypes of type A botulinum neurotoxin. *Nature biotechnology*. [Online] 25 (1), 107–116.

Gasser, M. & Waaga-Gasser, A. M. (2016) Therapeutic Antibodies in Cancer Therapy. *Advances in experimental medicine and biology*. [Online] 917 (Suppl 1), 95–120.

Gebhardt, K. et al. (1996) Adhesive peptides selected by phage display: characterization, applications and similarities with fibrinogen. *Peptide research*. 9 (6), 269–278.

Georgieva, J. et al. (2014) Smuggling Drugs into the Brain: An Overview of Ligands Targeting Transcytosis for Drug Delivery across the Blood–Brain Barrier. *Pharmaceutics*. [Online] 6 (4), 557–583.

Giebel, L. B. et al. (2002) Screening of cyclic peptide phage libraries identifies ligands that bind streptavidin with high affinities. *Biochemistry*. [Online] 34 (47), 15430–15435.

Gilbert, J. C. et al. (2007) First-in-human evaluation of anti von Willebrand factor therapeutic aptamer ARC1779 in healthy volunteers. *Circulation*. [Online] 116 (23), 2678–2686.

Gissel, B., Jensen, M. R., Gregorius, K., Elsner, H. I., Svendsen, I. & Mouritsen, S. (1995a) Identification of avidin and streptavidin binding motifs among peptides selected from a synthetic peptide library consisting solely of D-amino acids. *Journal of peptide science : an official publication of the European Peptide Society*. [Online] 1 (4), 217–226.

Goodchild, S. A. et al. (2011) Isolation and characterisation of Ebolavirus-specific recombinant antibody fragments from murine and shark immune libraries. *Molecular immunology*. [Online] 48 (15-16), 2027–2037.

Gosselet, F. et al. (2009) Transcriptional profiles of receptors and transporters involved in brain cholesterol homeostasis at the blood-brain barrier: use of an in vitro model. *Brain research*. [Online] 124934–42.

Gray, S. M. et al. (2017) Unravelling the regulation of insulin transport across the brain endothelial cell. *Diabetologia*. [Online] 60 (8), 1512–1521.

Gribkoff, V. K. & Kaczmarek, L. K. (2017) The need for new approaches in CNS drug discovery: Why drugs have failed, and what can be done to improve outcomes. *Neuropharmacology*. [Online] 12011–19.

Groenendaal, D. et al. (2007) Population pharmacokinetic modelling of non-linear brain distribution of morphine: influence of active saturable influx and P-glycoprotein mediated efflux. *British journal of pharmacology*. [Online] 151 (5), 701–712.

Guo, L. et al. (2012) Perspectives on brain-targeting drug delivery systems. *Current pharmaceutical biotechnology*. 13 (12), 2310–2318.

Haarmann, A. et al. (2015) Soluble VCAM-1 impairs human brain endothelial barrier integrity via integrin α-4-transduced outside-in signalling. *Acta neuropathologica*. [Online] 129 (5), 639–652.

Halim, L. A. et al. (2016) Quality and Batch-to-Batch Consistency of Original and Biosimilar Epoetin Products. *Journal of pharmaceutical sciences*. [Online] 105 (2), 542–550.

Halliday, M. R. et al. (2016) Accelerated pericyte degeneration and blood-brain barrier breakdown in apolipoprotein E4 carriers with Alzheimer's disease. *Journal of cerebral blood flow and metabolism : official journal of the International Society of Cerebral Blood Flow and Metabolism*. [Online] 36 (1), 216–227.

Hamers-Casterman, C. et al. (1993) Naturally occurring antibodies devoid of light chains. *Nature*. [Online] 363 (6428), 446–448.

Hamzeh-Mivehroud, M. et al. (2013) Phage display as a technology delivering on the promise of peptide drug discovery. *Drug discovery today*. [Online] 18 (23-24), 1144–1157.

Haqqani, A. S. et al. (2017) Endosomal trafficking regulates receptor-mediated transcytosis of antibodies across the blood brain barrier. *Journal of cerebral blood flow and metabolism : official journal of the International Society of Cerebral Blood Flow and Metabolism*. [Online] 259271678X17740031.

Hawkes, C. A. et al. (2013) Regional differences in the morphological and functional effects of aging on cerebral basement membranes and perivascular drainage of amyloid-β from the mouse brain. *Aging cell*. [Online] 12 (2), 224–236.

Hawkins, R. E. et al. (1992) Selection of phage antibodies by binding affinity. Mimicking affinity maturation. *Journal of molecular biology*. 226 (3), 889–896.

Hayes, G. R. et al. (1992) Identification of the O-linked glycosylation site of the human transferrin receptor. *Glycobiology*. 2 (4), 355–359.

He, Q. et al. (2015) Endocytosis of a functionally enhanced GFP-tagged transferrin receptor in CHO cells. *PloS one*. [Online] 10 (3), e0122452.

Heiat, M. et al. (2016) Characterization of pharmacological properties of isolated single-stranded DNA aptamers against angiotensin II. *Molecular and cellular probes*. [Online] 30 (4), 238–245.

Held, F. et al. (2017) Vascular basement membrane alterations and β-amyloid accumulations in an animal model of cerebral small vessel disease. *Clinical science (London, England : 1979)*. [Online] 131 (10), 1001–1013.

Henne, W. M. et al. (2010) FCHo proteins are nucleators of clathrin-mediated endocytosis. *Science (New York, N.Y.)*. [Online] 328 (5983), 1281–1284.

Henry, K. A. et al. (2015) Identification of cross-reactive single-domain antibodies against serum albumin using next-generation DNA sequencing. *Protein engineering, design & selection : PEDS*. [Online] 28 (10), 379–383.

Hermeling, S. et al. (2006) Antibody response to aggregated human interferon alpha2b in wild-type and transgenic immune tolerant mice depends on type and level of aggregation. *Journal of pharmaceutical sciences*. [Online] 95 (5), 1084–1096.

Holliger, P. & Hudson, P. J. (2005) *Engineered antibody fragments and the rise of single domains.* [Online] 23 (9), 1126–1136.

Holliger, P. & Riechmann, L. (1997) A conserved infection pathway for filamentous bacteriophages is suggested by the structure of the membrane penetration

domain of the minor coat protein g3p from phage fd. *Structure (London, England : 1993)*. 5 (2), 265–275.

Holliger, P. et al. (1999) Crystal structure of the two N-terminal domains of g3p from filamentous phage fd at 1.9 A: evidence for conformational lability. *Journal of molecular biology*. [Online] 288 (4), 649–657.

Holmberg, A. et al. (2005) The biotin-streptavidin interaction can be reversibly broken using water at elevated temperatures. *Electrophoresis*. [Online] 26 (3), 501–510.

Holmberg, C. G. & Laurell, C. B. (1946) *Investigations in serum copper; nature of serum copper and its relation to the iron-binding protein in human serum.* Acta Chemica Scandinavica.

Holt, D. W. et al. (1995) Sandimmun neoral pharmacokinetics: impact of the new oral formulation. *Transplantation proceedings*. 27 (1), 1434–1437.

Huang, R.-Q. et al. (2007) Efficient gene delivery targeted to the brain using a transferrin-conjugated polyethyleneglycol-modified polyamidoamine dendrimer. *FASEB journal : official publication of the Federation of American Societies for Experimental Biology*. [Online] 21 (4), 1117–1125.

Hultqvist, G. et al. (2017) Bivalent Brain Shuttle Increases Antibody Uptake by Monovalent Binding to the Transferrin Receptor. *Theranostics*. [Online] 7 (2), 308–318.

Hung, M. E. & Leonard, J. N. (2015) Stabilization of exosome-targeting peptides via engineered glycosylation. *The Journal of biological chemistry*. [Online] 290 (13), 8166–8172.

Irani, Y. et al. (2016) Species Cross-Reactivity of Antibodies Used to Treat Ophthalmic ConditionsSpecies Cross-Reactivity of Antibodies. *Investigative ophthalmology & visual science*. [Online] 57 (2), 586–591.

Ireson, C. R. & Kelland, L. R. (2006) Discovery and development of anticancer aptamers. *Molecular cancer therapeutics*. [Online] 5 (12), 2957–2962.

Jandl, J. H. et al. (1959) Transfer of iron from serum iron-binding protein to human reticulocytes. *The Journal of clinical investigation*. [Online] 38 (1, Part 1), 161–185.

Jefferies, W. A. et al. (1984) Transferrin receptor on endothelium of brain capillaries. *Nature*. 312 (5990), 162–163.

Ji, B. et al. (2006) Pharmacokinetics and brain uptake of lactoferrin in rats. *Life sciences*. [Online] 78 (8), 851–855.

Jijakli, K. et al. (2016) The in vitro selection world. *Methods (San Diego, Calif.)*. [Online] 1063–13.

Jing, S. Q. & Trowbridge, I. S. (1987) Identification of the intermolecular disulfide bonds of the human transferrin receptor and its lipid-attachment site. *The EMBO journal*. 6 (2), 327–331.

Jing, S. Q. & Trowbridge, I. S. (1990) Nonacylated human transferrin receptors are rapidly internalized and mediate iron uptake. *The Journal of biological chemistry*. 265 (20), 11555–11559.

John-White, M. et al. (2017) Crystal structure of a β-aminopeptidase from an Australian Burkholderia sp. *Acta crystallographica. Section F, Structural biology communications*. [Online] 73 (Pt 7), 386–392.

Johnsen, K. B. et al. (2017) Targeting transferrin receptors at the blood-brain barrier improves the uptake of immunoliposomes and subsequent cargo transport into the brain parenchyma. *Scientific Reports*. [Online] 7 (1), 10396.

Joliot, A. et al. (1991) Antennapedia homeobox peptide regulates neural morphogenesis. *Proceedings of the National Academy of Sciences*. 88 (5), 1864–1868.

Joo, S. H. (2012) Cyclic peptides as therapeutic agents and biochemical tools. *Biomolecules & therapeutics*. [Online] 20 (1), 19–26.

Joo, S. H. et al. (2006) High-throughput sequence determination of cyclic peptide library members by partial Edman degradation/mass spectrometry. *Journal of the American Chemical Society*. [Online] 128 (39), 13000–13009.

Joubert, M. K. et al. (2012) Highly aggregated antibody therapeutics can enhance the in vitro innate and late-stage T-cell immune responses. *The Journal of biological chemistry*. [Online] 287 (30), 25266–25279.

Julien, M. et al. (2012) In vitro and in vivo stability and pharmacokinetic profile of unacylated ghrelin (UAG) analogues. *European journal of pharmaceutical sciences : official journal of the European Federation for Pharmaceutical Sciences*. [Online] 47 (4), 625–635.

Kafa, H. et al. (2016) Translocation of LRP1 targeted carbon nanotubes of different diameters across the blood-brain barrier in vitro and in vivo. *Journal of controlled release : official journal of the Controlled Release Society*. [Online] 225217–229.

Kalaidzidis, I. et al. (2015) APPL endosomes are not obligatory endocytic intermediates but act as stable cargo-sorting compartments. *The Journal of cell biology*. [Online] 211 (1), 123–144.

Kamat, V. & Rafique, A. (2017) Extending the throughput of Biacore 4000 biosensor to accelerate kinetic analysis of antibody-antigen interaction. *Analytical biochemistry*. [Online] 53075–86.

Kamouchi, M. et al. (2011) Brain pericytes: emerging concepts and functional roles in brain homeostasis. *Cellular and molecular neurobiology*. [Online] 31 (2), 175–193.

Kamps, J. A. & van Berkel, T. J. (1992) Complete down-regulation of low-density-lipoprotein-receptor activity in the human hepatoma cell line Hep G2 by beta-migrating very-low-density lipoprotein and non-lipoprotein cholesterol. Different cellular regulatory pools of cholesterol. *European journal of biochemistry / FEBS*. 206 (3), 973–978.

Kane, J. F. (1995) Effects of rare codon clusters on high-level expression of heterologous proteins in Escherichia coli. *Current opinion in biotechnology*. 6 (5), 494–500.

Kang, H.-J. et al. (2017) Optimal expression of a Fab-effector fusion protein in Escherichia coli by removing the cysteine residues responsible for an interchain disulfide bond of a Fab molecule. *Immunology letters*. [Online] 18434–42.

Kang, T. et al. (2015) Enhancing Glioblastoma-Specific Penetration by Functionalization of Nanoparticles with an Iron-Mimic Peptide Targeting Transferrin/Transferrin Receptor Complex. *Molecular Pharmaceutics*. [Online] 12 (8), 2947–2961.

Kang, Y.-S. et al. (2016) Use of PEGylated Immunoliposomes to Deliver Dopamine Across the Blood-Brain Barrier in a Rat Model of Parkinson's Disease. *CNS neuroscience & therapeutics*. [Online] 22 (10), 817–823.

Kanwar, J. R. et al. (2011) Chimeric aptamers in cancer cell-targeted drug delivery. *Critical reviews in biochemistry and molecular biology*. [Online] 46 (6), 459–477.

Kaspar, A. A. & Reichert, J. M. (2013) Future directions for peptide therapeutics development. *Drug discovery today*. [Online] 18 (17-18), 807–817.

Katsu, M. et al. (2010) Hemoglobin-induced oxidative stress contributes to matrix metalloproteinase activation and blood-brain barrier dysfunction in vivo. *Journal of cerebral blood flow and metabolism : official journal of the International Society of Cerebral Blood Flow and Metabolism*. [Online] 30 (12), 1939–1950.

Katz, B. A. (1995) Binding to protein targets of peptidic leads discovered by phage display: crystal structures of streptavidin-bound linear and cyclic peptide ligands containing the HPQ sequence. *Biochemistry*. 34 (47), 15421–15429.

Kaup, M. et al. (2002) Processing of the human transferrin receptor at distinct positions within the stalk region by neutrophil elastase and cathepsin G. *Biological chemistry*. [Online] 383 (6), 1011–1020.

Kehoe, J. W. et al. (2006) Using phage display to select antibodies recognizing post-translational modifications independently of sequence context. *Molecular & cellular proteomics : MCP*. [Online] 5 (12), 2350–2363.

Kim, Y. S. et al. (2013) Isolation and characterization of DNA aptamers against Escherichia coli using a bacterial cell-systematic evolution of ligands by exponential enrichment approach. *Analytical biochemistry*. [Online] 436 (1), 22–28.

Kissel, K. et al. (1998) Immunohistochemical localization of the murine transferrin receptor (TfR) on blood-tissue barriers using a novel anti-TfR monoclonal antibody. *Histochemistry and cell biology*. 110 (1), 63–72.

Klausner, R. D. et al. (1984) Failure to release iron from transferrin in a Chinese hamster ovary cell mutant pleiotropically defective in endocytosis. *The Journal of cell biology*. 98 (3), 1098–1101.

Kleber-Janke, T. & Becker, W. M. (2000) Use of modified BL21(DE3) Escherichia coli cells for high-level expression of recombinant peanut allergens affected by poor codon usage. *Protein expression and purification*. [Online] 19 (3), 419–424.

Kogot, J. M. et al. (2012) Increased affinity and solubility of peptides used for direct peptide ELISA on polystyrene surfaces through fusion with a polystyrene-binding peptide tag. *BioTechniques*. [Online] 52 (2), 95–102.

Kohn, W. D. et al. (2007) pI-shifted insulin analogs with extended in vivo time action and favorable receptor selectivity. *Peptides*. [Online] 28 (4), 935–948.

Koide, A. et al. (2009) Accelerating phage-display library selection by reversible and site-specific biotinylation. *Protein engineering, design & selection : PEDS*. [Online] 22 (11), 685–690.

Kordower, J. H. et al. (1994) Intravenous administration of a transferrin receptor antibody-nerve growth factor conjugate prevents the degeneration of cholinergic striatal neurons in a model of Huntington disease. *Proceedings of the National Academy of Sciences*. 91 (19), 9077–9080.

Kozlowski, L. P. (2016) IPC - Isoelectric Point Calculator. *Biology direct*. [Online] 11 (1), 55.

Kreuter, J. (2015) Influence of chronobiology on the nanoparticle-mediated drug uptake into the brain. *Pharmaceutics*. [Online] 7 (1), 3–9.

Kreuter, J. et al. (2002) Apolipoprotein-mediated transport of nanoparticle-bound drugs across the blood-brain barrier. *Journal of drug targeting*. [Online] 10 (4), 317–325.

Kukulski, W. et al. (2016) Clathrin modulates vesicle scission, but not invagination shape, in yeast endocytosis. *eLife*. [Online] 51369.

Kumar, S. et al. (2012) Characterization of glyceraldehyde-3-phosphate dehydrogenase as a novel transferrin receptor. *The international journal of biochemistry & cell biology*. [Online] 44 (1), 189–199.

Kuo, Y.-C. & Shih-Huang, C.-Y. (2013) Solid lipid nanoparticles carrying chemotherapeutic drug across the blood-brain barrier through insulin receptor-mediated pathway. *Journal of drug targeting*. [Online] 21 (8), 730–738.

Kurgonaite, K. et al. (2015) Essential role of endocytosis for interleukin-4-receptor-mediated JAK/STAT signalling. *Journal of cell science*. [Online] 128 (20), 3781–3795.

Lajoie, J. M. & Shusta, E. V. (2015) Targeting receptor-mediated transport for delivery of biologics across the blood-brain barrier. *Annual review of pharmacology and toxicology*. [Online] 55613–631.

Lakhin, A. V. et al. (2013) Aptamers: problems, solutions and prospects. *Acta naturae*. 5 (4), 34–43.

Lakshmipriya, T. et al. (2016) Biotin-Streptavidin Competition Mediates Sensitive Detection of Biomolecules in Enzyme Linked Immunosorbent Assay. Sabato D'Auria (ed.). *PloS one*. [Online] 11 (3), e0151153.

Lane-Donovan, C. & Herz, J. (2017) The ApoE receptors Vldlr and Apoer2 in central nervous system function and disease. *Journal of lipid research*. [Online] 58 (6), 1036–1043.

Lawrence, C. M. et al. (1999) Crystal structure of the ectodomain of human transferrin receptor. *Science (New York, N.Y.)*. 286 (5440), 779–782.

Lebendiker, M. & Danieli, T. (2014) *Production of prone-to-aggregate proteins.* [Online] 588 (2), 236–246.

Lee et al. (2000) Targeting rat anti-mouse transferrin receptor monoclonal antibodies through blood-brain barrier in mouse. *The Journal of pharmacology and experimental therapeutics*. 292 (3), 1048–1052.

Lee, C. V. et al. (2004) High-affinity human antibodies from phage-displayed synthetic Fab libraries with a single framework scaffold. *Journal of molecular biology*. [Online] 340 (5), 1073–1093.

Lee, J. H. et al. (2001) Receptor mediated uptake of peptides that bind the human transferrin receptor. *European journal of biochemistry / FEBS*. 268 (7), 2004–2012. [online]. Available from: http://eutils.ncbi.nlm.nih.gov/entrez/eutils/elink.fcgi?dbfrom=pubmed&id=11277922&retmode=ref&cmd=prlinks.

Lee, J. L. & Streuli, C. H. (2014) Integrins and epithelial cell polarity. *Journal of cell science*. [Online] 127 (Pt 15), 3217–3225.

Leggas, M. et al. (2004) Mrp4 confers resistance to topotecan and protects the brain from chemotherapy. *Molecular and cellular biology*. [Online] 24 (17), 7612–7621.

Lesley, J. et al. (1984) Expression of transferrin receptor on murine hematopoietic progenitors. *Cellular immunology*. 83 (1), 14–25.

LeVine, S. M. & Macklin, W. B. (1990) Iron-enriched oligodendrocytes: a reexamination of their spatial distribution. *Journal of neuroscience research*. [Online] 26 (4), 508–512.

Levy, J. E. et al. (1999) *Transferrin receptor is necessary for development of erythrocytes and the nervous system.* [Online] 21 (4), 396–399.

Li, J. et al. (2011) Identification of peptide sequences that target to the brain using in vivo phage display. *Amino Acids*. [Online] 42 (6), 2373–2381.

Li, J. Y. et al. (2009) Scara5 is a ferritin receptor mediating non-transferrin iron delivery. *Developmental cell*. [Online] 16 (1), 35–46.

Li, T. et al. (2016) Camelid single-domain antibodies: A versatile tool for in vivo imaging of extracellular and intracellular brain targets. *Journal of controlled release : official journal of the Controlled Release Society*. [Online] 2431–10.

Lichota, J. et al. (2010) Macromolecular drug transport into the brain using targeted therapy. *Journal of neurochemistry*. [Online] 113 (1), 1–13.

Lim, J. P. & Gleeson, P. A. (2011) Macropinocytosis: an endocytic pathway for internalising large gulps. *Immunology and cell biology*. [Online] 89 (8), 836–843.

Lindhout, D. A. et al. (2003) High-yield expression of isotopically labeled peptides for use in NMR studies. *Protein science : a publication of the Protein Society*. [Online] 12 (8), 1786–1791.

Liu, J. et al. (2012) Matrix metalloproteinase-2-mediated occludin degradation and caveolin-1-mediated claudin-5 redistribution contribute to blood-brain barrier damage in early ischemic stroke stage. *The Journal of neuroscience : the official journal of the Society for Neuroscience*. [Online] 32 (9), 3044–3057.

Liu, Z. et al. (2015) Effect of Baicalin-loaded PEGylated cationic solid lipid nanoparticles modified by OX26 antibody on regulating the levels of baicalin and amino acids during cerebral ischemia-reperfusion in rats. *International journal of pharmaceutics*. [Online] 489 (1-2), 131–138.

Lorey, S. et al. (2014) Novel ubiquitin-derived high affinity binding proteins with tumor targeting properties. *The Journal of biological chemistry*. [Online] 289 (12), 8493–8507.

Loureiro, J. A. et al. (2016) Cellular uptake of PLGA nanoparticles targeted with anti-amyloid and anti-transferrin receptor antibodies for Alzheimer's disease treatment. *Colloids and Surfaces B: Biointerfaces*. [Online] 1458–13.

Loureiro, J. A. et al. (2015) Immunoliposomes doubly targeted to transferrin receptor and to α-synuclein. *Future science OA*. [Online] 1 (4), FSO71.

Lu, F. et al. (2017) Angiopep-2-conjugated poly(ethylene glycol)-co- poly(ε-caprolactone) polymersomes for dual-targeting drug delivery to glioma in rats. *International journal of nanomedicine*. [Online] 122117–2127.

Lu, J. et al. (1995) Expression and upregulation of transferrin receptors and iron uptake in the epiplexus cells of different aged rats injected with lipopolysaccharide and interferon-gamma. *Journal of anatomy*. 187 (Pt 3)603–611.

Lu, J. Z. et al. (2011) Expression in CHO cells and pharmacokinetics and brain uptake in the Rhesus monkey of an IgG-iduronate-2-sulfatase fusion protein. *Biotechnology and bioengineering*. [Online] 108 (8), 1954–1964.

Lu, M. et al. (2015) A novel molecular marker of breast cancer stem cells identified by cell-SELEX method. *Cancer biomarkers : section A of Disease markers*. [Online] 15 (2), 163–170.

Luissint, A.-C. et al. (2012) Tight junctions at the blood brain barrier: physiological architecture and disease-associated dysregulation. *Fluids and barriers of the CNS*. [Online] 9 (1), 23–1. [online]. Available from: http://eutils.ncbi.nlm.nih.gov/entrez/eutils/elink.fcgi?dbfrom=pubmed&id=23140302&retmode=ref&cmd=prlinks.

Luo, Q. et al. (2011) Chemical modifications in therapeutic protein aggregates generated under different stress conditions. *The Journal of biological chemistry*. [Online] 286 (28), 25134–25144.

Luo, Z. et al. (2017) Precise glioblastoma targeting by AS1411 aptamer-functionalized poly (l-γ-glutamylglutamine)-paclitaxel nanoconjugates. *Journal of colloid and interface science*. [Online] 490783–796.

Ma, L. et al. (2016) Transient Fcho1/2·Eps15/R·AP-2 Nanoclusters Prime the AP-2 Clathrin Adaptor for Cargo Binding. *Developmental cell*. [Online] 37 (5), 428–443.

Macdonald, J., Henri, J., et al. (2016) Development of a bi-functional aptamer targeting the transferrin receptor and EpCAM for the treatment of brain cancer metastases. *ACS chemical neuroscience*. [Online] acschemneuro.6b00369.

Macdonald, J., Houghton, P., et al. (2016) Truncation and Mutation of a Transferrin Receptor Aptamer Enhances Binding Affinity. *Nucleic acid therapeutics*. [Online] 26 (6), 348–354.

Mahar Doan, K. M. et al. (2002) Passive permeability and P-glycoprotein-mediated efflux differentiate central nervous system (CNS) and non-CNS marketed drugs. *The Journal of pharmacology and experimental therapeutics*. [Online] 303 (3), 1029–1037.

Malcor, J.-D. et al. (2012) Chemical optimization of new ligands of the low-density lipoprotein receptor as potential vectors for central nervous system targeting. *Journal of medicinal chemistry*. [Online] 55 (5), 2227–2241.

Malik, A. (2016) Protein fusion tags for efficient expression and purification of recombinant proteins in the periplasmic space of E. coli. *3 Biotech*. [Online] 6 (1), 44.

Mallikaratchy, P. (2017) Evolution of Complex Target SELEX to Identify Aptamers against Mammalian Cell-Surface Antigens. *Molecules (Basel, Switzerland)*. [Online] 22 (2), 215.

Malmberg, A. B. & Basbaum, A. I. (1998) Partial sciatic nerve injury in the mouse as a model of neuropathic pain: behavioral and neuroanatomical correlates. *Pain*. 76 (1-2), 215–222.

Manich, G. et al. (2013) Study of the transcytosis of an anti-transferrin receptor antibody with a Fab′ cargo across the blood–brain barrier in mice. *European Journal of Pharmaceutical Sciences*. [Online] 49 (4), 556–564.

Mariati et al. (2014) Toward stable gene expression in CHO cells. *Bioengineered*. [Online] 5 (5), 340–345.

Markoutsa, E. et al. (2014) Mono and dually decorated nanoliposomes for brain targeting, in vitro and in vivo studies. *Pharmaceutical research*. [Online] 31 (5), 1275–1289.

Marlatt, N. M. et al. (2010) Codon optimization for enhanced Escherichia coli expression of human S100A11 and S100A1 proteins. *Protein expression and purification*. [Online] 73 (1), 58–64.

Maruta, F. et al. (2003) Use of a phage display library to identify oligopeptides binding to the lumenal surface of polarized endothelium by ex vivo perfusion of human umbilical veins. *Journal of drug targeting*. [Online] 11 (1), 53–59.

Masella, A. P. et al. (2012) PANDAseq: paired-end assembler for illumina sequences. *BMC Bioinformatics*. [Online] 13 (1), 31.

Mason, A. B. et al. (2009) A loop in the N-lobe of human serum transferrin is critical for binding to the transferrin receptor as revealed by mutagenesis, isothermal titration calorimetry, and epitope mapping. *Journal of molecular recognition : JMR*. [Online] 22 (6), 521–529.

Mattice, C. M. C. & DeRosa, M. C. (2015) Status and Prospects of Aptamers as Drug Components. *BioDrugs*. [Online] 29 (3), 151–165.

McBride, H. M. et al. (1999) Oligomeric complexes link Rab5 effectors with NSF and drive membrane fusion via interactions between EEA1 and syntaxin 13. *Cell*. 98 (3), 377–386.

McCafferty, J. & Johnson, K. S. (1996) *Construction and screening of antibody display libraries*.

McDonald, P. et al. (2009) Selective antibody precipitation using polyelectrolytes: a novel approach to the purification of monoclonal antibodies. *Biotechnology and bioengineering*. [Online] 102 (4), 1141–1151.

McGonigle, P. (2014) Animal models of CNS disorders. *Biochemical pharmacology*. [Online] 87 (1), 140–149.

McGraw, T. E. et al. (1987) Functional expression of the human transferrin receptor cDNA in Chinese hamster ovary cells deficient in endogenous transferrin receptor. *The Journal of cell biology*. 105 (1), 207–214.

McGraw, T. E. et al. (1988) Phorbol ester treatment increases the exocytic rate of the transferrin receptor recycling pathway independent of serine-24 phosphorylation. *The Journal of cell biology*. 106 (4), 1061–1066.

McKeague, M. & DeRosa, M. C. (2014) Aptamers and SELEX: tools for the development of transformative molecular recognition technology. *Aptamers Synth Antibodies*.

McMahon, H. T. & Boucrot, E. (2011) Molecular mechanism and physiological functions of clathrin-mediated endocytosis. *Nature reviews Molecular cell biology*. [Online] 12 (8), 517.

Mehta, K. et al. (2015) Characterisation of hepcidin response to holotransferrin treatment in CHO TRVb-1 cells. *Blood Cells, Molecules, and Diseases*. [Online] 55 (2), 110–118.

Meibohm, B. & Zhou, H. (2012) Characterizing the impact of renal impairment on the clinical pharmacology of biologics. *Journal of clinical pharmacology*. [Online] 52 (1 Suppl), 54S–62S.

Menendez, A. & Scott, J. K. (2005) The nature of target-unrelated peptides recovered in the screening of phage-displayed random peptide libraries with antibodies. *Analytical biochemistry*. [Online] 336 (2), 145–157.

Meng, L. et al. (2010) Using live cells to generate aptamers for cancer study. *Methods in molecular biology (Clifton, N.J.)*. [Online] 629 (Chapter 23), 355–367.

Meyer, S. C. et al. (2006) Highly selective cyclic peptide ligands for NeutrAvidin and avidin identified by phage display. *Chemical biology & drug design*. [Online] 68 (1), 3–10.

Mills, E. et al. (2010) *Mechanisms of brain iron transport: insight into neurodegeneration and CNS disorders.* 2 (1), 51–64.

Mishra, A. et al. (2010) Structural basis for Rab GTPase recognition and endosome tethering by the C2H2 zinc finger of Early Endosomal Autoantigen 1 (EEA1). *Proceedings of the National Academy of Sciences of the United States of America*. [Online] 107 (24), 10866–10871.

Modh, H. B. et al. (2016) Specific detection of tetanus toxoid using an aptamer-based matrix. *Journal of biotechnology*. [Online] 23815–21.

Modi, M. E. et al. (2016) Peripheral Administration of a Long-Acting Peptide Oxytocin Receptor Agonist Inhibits Fear-Induced Freezing. *The Journal of pharmacology and experimental therapeutics*. [Online] 358 (2), 164–172.

Molino, Y. et al. (2017) Use of LDL receptor-targeting peptide vectors forin vitroandin vivocargo transport across the blood-brain barrier. *FASEB journal : official publication of the Federation of American Societies for Experimental Biology*. [Online] 31 (5), 1807–1827.

Montesano, R. et al. (1990) Increased proteolytic activity is responsible for the aberrant morphogenetic behavior of endothelial cells expressing the middle T oncogene. *Cell*. 62 (3), 435–445.

Moos, T. & Morgan, E. H. (2001) *Restricted transport of anti-transferrin receptor antibody (OX26) through the blood-brain barrier in the rat.* 79 (1), 119–129.

Moos, T. & Morgan, E. H. (2000) Transferrin and transferrin receptor function in brain barrier systems. *Cellular and molecular neurobiology*. 20 (1), 77–95.

Moos, T. et al. (2006) Brain capillary endothelial cells mediate iron transport into the brain by segregating iron from transferrin without the involvement of divalent metal transporter 1. *Journal of neurochemistry*. [Online] 98 (6), 1946–1958.

Moos, T. et al. (2007) Iron trafficking inside the brain. *Journal of neurochemistry*. [Online] 103 (5), 1730–1740.

Moreland, J. L. et al. (2005) The Molecular Biology Toolkit (MBT): a modular platform for developing molecular visualization applications. *BMC Bioinformatics*. [Online] 6 (1), 21.

Morgan, E. H. & Moos, T. (2002) Mechanism and developmental changes in iron transport across the blood-brain barrier. *Developmental neuroscience*. 24 (2-3), 106–113.

Morgan, J. R. et al. (2013) A role for an Hsp70 nucleotide exchange factor in the regulation of synaptic vesicle endocytosis. *The Journal of neuroscience : the official journal of the Society for Neuroscience*. [Online] 33 (18), 8009–8021.

Morita, K. et al. (2003) Expression of claudin-5 in dermal vascular endothelia. *Experimental dermatology*. 12 (3), 289–295.

Motley, A. et al. (2003) Clathrin-mediated endocytosis in AP-2-depleted cells. *The Journal of cell biology*. [Online] 162 (5), 909–918.

Moussa, E. M. et al. (2016) Immunogenicity of Therapeutic Protein Aggregates. *Journal of pharmaceutical sciences*. [Online] 105 (2), 417–430.

Murase, S.-I. et al. (2017) Neuropeptide Y Y5 receptor localization in mouse central nervous system. *Brain research*. [Online] 1655216–232.

Murphy, M. B. et al. (2003) An improved method for the in vitro evolution of aptamers and applications in protein detection and purification. *Nucleic acids research*. [Online] 31 (18), e110–e110.

Murray, C. J. L. et al. (2012) Disability-adjusted life years (DALYs) for 291 diseases and injuries in 21 regions, 1990-2010: a systematic analysis for the Global Burden of Disease Study 2010. *Lancet (London, England)*. [Online] 380 (9859), 2197–2223.

Muruganandam, A. et al. (2002) Selection of phage-displayed llama single-domain antibodies that transmigrate across human blood-brain barrier endothelium. *FASEB journal : official publication of the Federation of American Societies for Experimental Biology*. [Online] 16 (2), 240–242.

Müller-Greven, G. et al. (2017) Macropinocytosis of Bevacizumab by Glioblastoma Cells in the Perivascular Niche Affects their Survival. *Clinical cancer research : an official journal of the American Association for Cancer Research*. [Online] 23 (22), 7059–7071.

Myzithras, M. et al. (2016) Utility of immunodeficient mouse models for characterizing the preclinical pharmacokinetics of immunogenic antibody therapeutics. *mAbs*. [Online] 8 (8), 1606–1611.

Naskar, P. & Puri, N. (2017) Phosphorylation of SNAP-23 regulates its dynamic membrane association during mast cell exocytosis. *Biology open*. [Online] 6 (9), 1257–1269.

Nazer, B. et al. (2008) LRP promotes endocytosis and degradation, but not transcytosis, of the amyloid-β peptide in a blood–brain barrier in vitro model. *Neurobiology of Disease*. [Online] 30 (1), 94–102.

Neutra, M. R. et al. (1985) Intracellular transport of transferrin- and asialoorosomucoid-colloidal gold conjugates to lysosomes after receptor-mediated endocytosis. *The journal of histochemistry and cytochemistry : official journal of the Histochemistry Society*. [Online] 33 (11), 1134–1144.

Ng, E. W. M. et al. (2006) Pegaptanib, a targeted anti-VEGF aptamer for ocular vascular disease. *Nature reviews. Drug discovery*. [Online] 5 (2), 123–132.

Nguyen et al. (2014) Mfsd2a is a transporter for the essential omega-3 fatty acid docosahexaenoic acid. *Nature*. [Online] 509 (7501), 503–506.

Nguyen Quang, N. et al. (2016) Applications of High-Throughput Sequencing for In Vitro Selection and Characterization of Aptamers. *Pharmaceuticals (Basel, Switzerland)*. [Online] 9 (4), 76.

Nguyen, H. H. et al. (2015) Surface plasmon resonance: a versatile technique for biosensor applications. *Sensors (Basel, Switzerland)*. [Online] 15 (5), 10481–10510.

Nieba, L. et al. (1997) BIACORE analysis of histidine-tagged proteins using a chelating NTA sensor chip. *Analytical biochemistry*. [Online] 252 (2), 217–228.

Niewoehner, J. et al. (2014) Increased Brain Penetration and Potency of a Therapeutic Antibody Using a Monovalent Molecular Shuttle. *Neuron*. [Online] 81 (1), 49–60.

Noren, K. A. & Noren, C. J. (2001) Construction of high-complexity combinatorial phage display peptide libraries. *Methods (San Diego, Calif.)*. [Online] 23 (2), 169–178.

Nouri, H. R. et al. (2016) Expression of a Chimeric Allergen with High Rare Codons Content in Codon Bias-Adjusted Escherichia coli: Escherichia coli BL21 (DE3)-Codon Plus RIL as an Efficient Host. *Current microbiology*. [Online] 73 (1), 91–98.

O'Neil, K. T. et al. (1992) Identification of novel peptide antagonists for GPIIb/IIIa from a conformationally constrained phage peptide library. *Proteins*. [Online] 14 (4), 509–515.

Oganesyan, V. et al. (2013) Fibronectin type III domains engineered to bind CD40L: cloning, expression, purification, crystallization and preliminary X-ray diffraction analysis of two complexes. *Acta crystallographica. Section F, Structural biology and crystallization communications*. [Online] 69 (Pt 9), 1045–1048.

Ohshima-Hosoyama, S. et al. (2012) A monoclonal antibody-GDNF fusion protein is not neuroprotective and is associated with proliferative pancreatic lesions in parkinsonian monkeys. R Lee Mosley (ed.). *PloS one*. [Online] 7 (6), e39036. [online]. Available from: http://dx.plos.org/10.1371/journal.pone.0039036.

Ohtsuki, S. & Terasaki, T. (2007) Contribution of Carrier-Mediated Transport Systems to the Blood–Brain Barrier as a Supporting and Protecting Interface for the Brain; Importance for CNS Drug Discovery and Development. *Pharmaceutical research*. [Online] 24 (9), 1745–1758.

Ohtsuki, S. et al. (2013) Quantitative targeted absolute proteomic analysis of transporters, receptors and junction proteins for validation of human cerebral microvascular endothelial cell line hCMEC/D3 as a human blood-brain barrier model. *Molecular Pharmaceutics*. [Online] 10 (1), 289–296.

Ohuchi, S. (2012) *Cell-SELEX Technology.* [Online] 1 (6), 265–272.

Oller-Salvia, B. et al. (2016) Blood-brain barrier shuttle peptides: an emerging paradigm for brain delivery. *Chemical Society reviews*. [Online] 45 (17), 4690–4707.

Oller-Salvia, B. et al. (2013) From venoms to BBB shuttles: Synthesis and blood-brain barrier transport assessment of apamin and a nontoxic analog. Lila Gierasch et al. (eds.). *Biopolymers*. [Online] 100 (6), 675–686.

Omidfar, K. & Daneshpour, M. (2015) Advances in phage display technology for drug discovery. *Expert opinion on drug discovery*. [Online] 10 (6), 651–669.

Orlandi, A. et al. (2015) Brain natriuretic peptide modulates calcium homeostasis and epidermal growth factor receptor gene signalling in asthmatic airways smooth muscle cells. *Pulmonary pharmacology & therapeutics*. [Online] 3151–54.

Ouellet, E. et al. (2015) Hi-Fi SELEX: A high-fidelity digital-PCR based therapeutic aptamer discovery platform. *Biotechnology and bioengineering*. [Online] 112 (8), 1506–1522.

Owen, D. J. & Evans, P. R. (1998) A structural explanation for the recognition of tyrosine-based endocytotic signals. *Science (New York, N.Y.)*. 282 (5392), 1327–1332.

Pang, Z. et al. (2011) Brain delivery and cellular internalization mechanisms for transferrin conjugated biodegradable polymersomes. *International journal of pharmaceutics*. [Online] 415 (1-2), 284–292.

Panzenboeck, U. et al. (2006) … effects of synthetic liver X receptor-and peroxisome-proliferator activated receptor agonists on sterol transport pathways in polarized cerebrovascular endothelial cells. *… of biochemistry & cell …*.

Pardridge, W. M. (2015) Blood-brain barrier drug delivery of IgG fusion proteins with a transferrin receptor monoclonal antibody. *Expert opinion on drug delivery*. [Online] 12 (2), 207–222.

Pardridge, W. M. (2007) Blood–brain barrier delivery. *Drug discovery today*.

Pardridge, W. M. (2002) Drug and gene targeting to the brain with molecular trojan horses. *Nature reviews. Drug discovery*. [Online] 1 (2), 131–139.

Pardridge, W. M. et al. (1995) Human insulin receptor monoclonal antibody undergoes high affinity binding to human brain capillaries in vitro and rapid transcytosis through the blood-brain barrier in vivo in the primate. *Pharmaceutical research*. [Online] 12 (6), 807–816. [online]. Available from: http://eutils.ncbi.nlm.nih.gov/entrez/eutils/elink.fcgi?dbfrom=pubmed&id=7667183&retmode=ref&cmd=prlinks.

Pardridge, W. M. et al. (1991) Selective transport of an anti-transferrin receptor antibody through the blood-brain barrier in vivo. *The Journal of pharmacology and experimental therapeutics*. 259 (1), 66–70.

Paris-Robidas, S. et al. (2011) *In vivo labeling of brain capillary endothelial cells after intravenous injection of monoclonal antibodies targeting the transferrin receptor.* [Online] 80 (1), 32–39.

Park, H. et al. (2017) Antitumor activity, pharmacokinetics, tumor-homing effect, and hepatotoxicity of a species cross-reactive c-Met antibody. *Biochemical and biophysical research communications*. [Online] 494 (1-2), 409–415.

Park, S. W. et al. (2014) Rab11, but not Rab4, facilitates cyclic AMP- and tauroursodeoxycholate-induced MRP2 translocation to the plasma membrane. *American journal of physiology. Gastrointestinal and liver physiology*. [Online] 307 (8), G863–G870.

Pasqualini, R. & Ruoslahti, E. (1996) Organ targeting in vivo using phage display peptide libraries. *Nature*. [Online] 380 (6572), 364–366.

Patabendige, A. et al. (2013) Establishment of a simplified in vitro porcine blood–brain barrier model with high transendothelial electrical resistance. *Brain research*. [Online] 15211–15.

Patel, P. K. et al. (2015) Biologics and biosimilars. *The Journal of dermatological treatment*. [Online] 26 (4), 299–302.

Persidsky, Y. et al. (2006) Blood-brain barrier: structural components and function under physiologic and pathologic conditions. *Journal of neuroimmune pharmacology : the official journal of the Society on NeuroImmune Pharmacology*. [Online] 1 (3), 223–236.

Pinzón-Daza, M. et al. (2012) The association of statins plus LDL receptor-targeted liposome-encapsulated doxorubicin increases in vitro drug delivery across blood-brain barrier cells. *British journal of pharmacology*. [Online] 167 (7), 1431–1447.

Plum, A. et al. (2013) In vitro protein binding of liraglutide in human plasma determined by reiterated stepwise equilibrium dialysis. *Journal of pharmaceutical sciences*. [Online] 102 (8), 2882–2888.

Pool, J. (2015) *Alzheimer's Society guide to the dementia care environment*. Alzheimer's Society.

Pope, A. et al. (1996) In vitro selection of a high affinity antibody to oestradiol using a phage display human antibody library. *Immunotechnology : an international journal of immunological engineering*. 2 (3), 209–217.

Popkov, M. et al. (2004) Human/mouse cross-reactive anti-VEGF receptor 2 recombinant antibodies selected from an immune b9 allotype rabbit antibody library. *Journal of Immunological Methods*. [Online] 288 (1-2), 149–164.

Porciani, D. et al. (2014) Two interconvertible folds modulate the activity of a DNA aptamer against transferrin receptor. *Molecular therapy. Nucleic acids*. [Online] 3e144.

Portioli, C. et al. (2017) Novel functionalization strategies of polymeric nanoparticles as carriers for brain medications. *Journal of biomedical materials research. Part A*. [Online] 105 (3), 847–858.

Prades, R. & Salvia, B. O. (2015) Applying the Retro-Enantio Approach To Obtain a Peptide Capable of Overcoming the Blood–Brain Barrier. *Angewandte Chemie …*. [Online]

Prades, R. et al. (2012) Delivery of gold nanoparticles to the brain by conjugation with a peptide that recognizes the transferrin receptor. *Biomaterials*. [Online] 33 (29), 7194–7205.

Preston, J. E. et al. (2014) Transcytosis of macromolecules at the blood-brain barrier. *Advances in pharmacology (San Diego, Calif.)*. [Online] 71147–163.

Qi, H. et al. (2012) Phagemid Vectors for Phage Display: Properties, Characteristics and Construction. *Journal of molecular biology*. [Online] 417 (3), 129–143.

QIAGEN (2001) *Ni-NTA Magnetic Agarose Beads Handbook*. 1–88.

Qian, Z. M. et al. (2002) Targeted drug delivery via the transferrin receptor-mediated endocytosis pathway. *Pharmacological reviews*. 54 (4), 561–587. [online]. Available from: http://eutils.ncbi.nlm.nih.gov/entrez/eutils/elink.fcgi?dbfrom=pubmed&id=12429868&retmode=ref&cmd=prlinks.

Rader, R. A. (2008) *(Re)defining biopharmaceutical.* [Online] 26 (7), 743–751.

Raje, C. I. et al. (2007) The macrophage cell surface glyceraldehyde-3-phosphate dehydrogenase is a novel transferrin receptor. *The Journal of biological chemistry*. [Online] 282 (5), 3252–3261.

Ramge, P. et al. (1999) Circadian phase-dependent antinociceptive reaction in mice determined by the hot-plate test and the tail-flick test after intravenous injection of dalargin-loaded nanoparticles. *Chronobiology international*. 16 (6), 767–777.

Rapoport, I. et al. (1997) Regulatory interactions in the recognition of endocytic sorting signals by AP-2 complexes. *The EMBO journal*. [Online] 16 (9), 2240–2250.

Raub, T. J. & Newton, C. R. (1991) Recycling kinetics and transcytosis of transferrin in primary cultures of bovine brain microvessel endothelial cells. *Journal of cellular physiology*. [Online] 149 (1), 141–151.

Reese, T. S. & Karnovsky, M. J. (1967) Fine structural localization of a blood-brain barrier to exogenous peroxidase. *The Journal of cell biology*. 34 (1), 207–217.

Remuzgo, C. et al. (2014) Chemical synthesis, structure-activity relationship, and properties of shepherin I: a fungicidal peptide enriched in glycine-glycine-histidine motifs. *Amino Acids*. [Online] 46 (11), 2573–2586.

Renders, M. et al. (2017) Whole cell-SELEX of aptamers with a tyrosine-like side chain against live bacteria. *Organic & biomolecular chemistry*. [Online] 15 (9), 1980–1989.

Rink, J. et al. (2005) Rab conversion as a mechanism of progression from early to late endosomes. *Cell*. [Online] 122 (5), 735–749.

Rolland, Y. et al. (2009) Inhibition of melanoma brain metastasis by targeting melanotransferrin at the cell surface. *Pigment cell & melanoma research*. [Online] 22 (1), 86–98.

Romero, I. A. et al. (2000) Interactions between brain endothelial cells and human T-cell leukemia virus type 1-infected lymphocytes: mechanisms of viral entry into the central nervous system. *Journal of virology*. 74 (13), 6021–6030.

Roque, A. et al. (2004) Antibodies and genetically engineered related molecules: production and purification. *Biotechnology progress*. [Online]

Rosano, G. L. & Ceccarelli, E. A. (2014) Recombinant protein expression in Escherichia coli: advances and challenges. *Frontiers in microbiology*. [Online] 5 (631607), 172. [online]. Available from: http://journal.frontiersin.org/article/10.3389/fmicb.2014.00172/abstract.

Rothenberger, S. et al. (1996) Coincident expression and distribution of melanotransferrin and transferrin receptor in human brain capillary endothelium. *Brain research*. 712 (1), 117–121.

Rouault, T. A. & Cooperman, S. (1995) Quantification of different transferrin receptor pools in primary cultures of porcine blood-brain barrier endothelial cells. *Journal of neurochemistry*. [Online] 64 (6), 2708–2715.

Rouet, R. et al. (2012) Expression of high-affinity human antibody fragments in bacteria. *Nature protocols*. [Online] 7 (2), 364–373.

Ru, B. et al. (2014) PhD7Faster: predicting clones propagating faster from the Ph.D.-7 phage display peptide library. *Journal of bioinformatics and computational biology*. [Online] 12 (1), 1450005.

Ruscito, A. et al. (2017) In Vitro Selection and Characterization of DNA Aptamers to a Small Molecule Target. *Current protocols in chemical biology*. [Online] 9 (4), 233–268.

Rutgers, K. S. et al. (2011) Transmigration of beta amyloid specific heavy chain antibody fragments across the in vitro blood-brain barrier. *Neuroscience*. [Online] 19037–42.

Rutledge, E. A. & Enns, C. A. (1996) Cleavage of the transferrin receptor is influenced by the composition of the O-linked carbohydrate at position 104. *Journal of cellular physiology*. [Online] 168 (2), 284–293.

Rutledge, E. A. et al. (1994) Elimination of the O-linked glycosylation site at Thr 104 results in the generation of a soluble human-transferrin receptor. *Blood*. 83 (2), 580–586.

Rutledge, E. A. et al. (1998) The transferrin receptor cytoplasmic domain determines its rate of transport through the biosynthetic pathway and its susceptibility to cleavage early in the pathway. *The Journal of biological chemistry*. 273 (20), 12169–12175.

Sabet, F. S. et al. (2017) FRET-based aptamer biosensor for selective and sensitive detection of aflatoxin B1 in peanut and rice. *Food chemistry*. [Online] 220527–532.

Sade, H. et al. (2014) A Human Blood-Brain Barrier Transcytosis Assay Reveals Antibody Transcytosis Influenced by pH-Dependent Receptor Binding Felix Schlachetzki (ed.). *PloS one*. [Online] 9 (4), e96340.

Saïda, F. (2007) Overview on the expression of toxic gene products in Escherichia coli. *Current protocols in protein science*. [Online] Chapter 5Unit5.19–5.19.13.

Santos do Carmo, F. et al. (2017) Anti-MUC1 nano-aptamers for triple-negative breast cancer imaging by single-photon emission computed tomography in inducted animals: initial considerations. *International journal of nanomedicine*. [Online] 1253–60.

Savio, A. S. et al. (2012) Enhancement of the inhibitory effect of an IL-15 antagonist peptide by alanine scanning. *Journal of peptide science : an official publication of the European Peptide Society*. [Online] 18 (1), 25–29.

Schielke, G. P. et al. (1990) Potassium activation of the Na,K-pump in isolated brain microvessels and synaptosomes. *Brain research*. 524 (2), 291–296.

Schlachetzki, F. et al. (2002) *Expression of the neonatal Fc receptor (FcRn) at the blood–brain barrier*. [Online] 81 (1), 203–206. [online]. Available from: http://onlinelibrary.wiley.com.libezproxy.open.ac.uk/doi/10.1046/j.1471-4159.2002.00840.x/full.

Schlageter, K. E. et al. (1999) Microvessel organization and structure in experimental brain tumors: microvessel populations with distinctive structural and functional properties. *Microvascular research*. [Online] 58 (3), 312–328.

Schmidt, M. & Wittrup, K. D. (2009) A modeling analysis of the effects of molecular size and binding affinity on tumor targeting. *Molecular cancer therapeutics*. [Online] 8 (10), 2861–2871.

Schmidt, T. et al. (1996) Molecular interaction between the Strep-tag affinity peptide and its cognate target, streptavidin. *Journal of molecular biology*. [Online] 255 (5), 753–766.

Schnabel, M. et al. (2002) Dedifferentiation-associated changes in morphology and gene expression in primary human articular chondrocytes in cell culture. *Osteoarthritis and cartilage*. [Online] 10 (1), 62–70.

Schnittler, H. J. et al. (1990) Role of actin and myosin in the control of paracellular permeability in pig, rat and human vascular endothelium. *The Journal of physiology*. 431379–401.

Scholle, M. D. et al. (2004) In vivo biotinylated proteins as targets for phage-display selection experiments. *Protein expression and purification*. [Online] 37 (1), 243–252.

Schroers, R. et al. (2003) Identification of MHC class II-restricted T-cell epitopes in prostate-specific membrane antigen. *Clinical cancer research : an official journal of the American Association for Cancer Research*. 9 (9), 3260–3271.

Schröder, M. et al. (2002) Induction of protein aggregation in an early secretory compartment by elevation of expression level. *Biotechnology and bioengineering*. 78 (2), 131–140.

Schütze, T. et al. (2011) Probing the SELEX Process with Next-Generation Sequencing Jörg D Hoheisel (ed.). *PloS one*. [Online] 6 (12), e29604.

Sefah, K. et al. (2010) Development of DNA aptamers using Cell-SELEX. *Nature protocols*. [Online] 5 (6), 1169–1185.

Seltzer, Z. et al. (1990) *A novel behavioral model of neuropathic pain disorders produced in rats by partial sciatic nerve injury*. [Online] 43 (2), 205–218. [online]. Available from: http://content.wkhealth.com/linkback/openurl?sid=WKPTLP:landingpage&an=00006396-199011000-00010.

Selvais, C. et al. (2011) Cell cholesterol modulates metalloproteinase-dependent shedding of low-density lipoprotein receptor-related protein-1 (LRP-1) and clearance function. *FASEB journal : official publication of the Federation of American Societies for Experimental Biology*. [Online] 25 (8), 2770–2781.

Seo, J.-K. et al. (2016) Hemerythrin-related antimicrobial peptide, msHemerycin, purified from the body of the Lugworm, Marphysa sanguinea. *Fish & shellfish immunology*. [Online] 5749–59.

Serlin, Y. et al. (2015) Anatomy and physiology of the blood–brain barrier. *Seminars in Cell & Developmental Biology*. [Online] 382–6.

Shan, L. et al. (2016) Generation and Characterization of an IgG4 Monomeric Fc Platform. Sergey Korolev (ed.). *PloS one*. [Online] 11 (8), e0160345.

Sharma, G. et al. (2016) The Role of Cell-Penetrating Peptide and Transferrin on Enhanced Delivery of Drug to Brain. *International journal of molecular sciences*. [Online] 17 (6), 806.

Shawahna, R. et al. (2013) Hurdles with Using In Vitro Models to Predict Human Blood-brain Barrier Drug Permeability: A Special Focus on Transporters and Metabolizing Enzymes. *Current Drug Metabolism*. [Online] 14 (1), 120–136.

Sheff, D. R. et al. (1999) The receptor recycling pathway contains two distinct populations of early endosomes with different sorting functions. *The Journal of cell biology*. 145 (1), 123–139.

Shen, J. et al. (2017) Ginsenoside Rg1 nanoparticle penetrating the blood-brain barrier to improve the cerebral function of diabetic rats complicated with cerebral infarction. *International journal of nanomedicine*. [Online] 126477–6486.

Shih, Y. J. et al. (1990) Serum transferrin receptor is a truncated form of tissue receptor. *The Journal of biological chemistry*. 265 (31), 19077–19081.

Siddappa, A. J. M. et al. (2002) Developmental changes in the expression of iron regulatory proteins and iron transport proteins in the perinatal rat brain. *Journal of neuroscience research*. [Online] 68 (6), 761–775.

Silverberg, G. D. et al. (2010) Amyloid efflux transporter expression at the blood-brain barrier declines in normal aging. *Journal of neuropathology and experimental neurology*. [Online] 69 (10), 1034–1043.

Simionescu, M. et al. (1988) The cerebral microvasculature of the rat: structure and luminal surface properties during early development. *Journal of submicroscopic cytology and pathology*. 20 (2), 243–261.

Simmons, S. C. et al. (2012) Development of novel single-stranded nucleic acid aptamers against the pro-angiogenic and metastatic enzyme heparanase (HPSE1). Maxim Antopolsky (ed.). *PloS one*. [Online] 7 (6), e37938.

Simpson, I. A. et al. (2015) A novel model for brain iron uptake: introducing the concept of regulation. *Journal of cerebral blood flow and metabolism : official journal of the International Society of Cerebral Blood Flow and Metabolism*. [Online] 35 (1), 48–57.

Sipos, R. et al. (2007) Effect of primer mismatch, annealing temperature and PCR cycle number on 16S rRNA gene-targetting bacterial community analysis. *FEMS microbiology ecology*. [Online] 60 (2), 341–350.

Skerra, A. (2007) *Alternative non-antibody scaffolds for molecular recognition*. [Online] 18 (4), 295–304. [online]. Available from: http://linkinghub.elsevier.com/retrieve/pii/S0958166907000808.

Smith, D. B. & Johnson, K. S. (1988) Single-step purification of polypeptides expressed in Escherichia coli as fusions with glutathione S-transferase. *Gene*. 67 (1), 31–40.

Smith, G. P. (1985) Filamentous fusion phage: novel expression vectors that display cloned antigens on the virion surface. *Science (New York, N.Y.)*. 228 (4705), 1315–1317.

Smith, G. P. (1988) Filamentous phage assembly: morphogenetically defective mutants that do not kill the host. *Virology*. 167 (1), 156–165.

Soares, E. S. et al. (2016) Caveolae as a target for Phoneutria nigriventer spider venom. *Neurotoxicology*. [Online] 54111–118. [online]. Available from: http://linkinghub.elsevier.com/retrieve/pii/S0161813X1630050X.

Sofic, E. et al. (1988) Increased iron (III) and total iron content in post mortem substantia nigra of parkinsonian brain. *Journal of neural transmission (Vienna, Austria : 1996)*. 74 (3), 199–205.

Soldevilla, M. M. et al. (2017) Identification of LAG3 high affinity aptamers by HT-SELEX and Conserved Motif Accumulation (CMA). Francis Miller (ed.). *PloS one*. [Online] 12 (9), e0185169.

Song, L. et al. (2009) Broadly neutralizing anti-HIV-1 antibodies disrupt a hinge-related function of gp41 at the membrane interface. *Proceedings of the National Academy of Sciences of the United States of America*. [Online] 106 (22), 9057–9062.

Soundararajan, S. et al. (2009) *Plasma Membrane Nucleolin Is a Receptor for the Anticancer Aptamer AS1411 in MV4-11 Leukemia Cells*. [Online] 76 (5), 984–991.

Soundararajan, S. et al. (2008) The nucleolin targeting aptamer AS1411 destabilizes Bcl-2 messenger RNA in human breast cancer cells. *Cancer research*. [Online] 68 (7), 2358–2365.

Spiess, C. et al. (2015) Alternative molecular formats and therapeutic applications for bispecific antibodies. *Molecular immunology*. [Online] 67 (2 Pt A), 95–106.

Srila, W. & Yamabhai, M. (2013) Identification of Amino Acid Residues Responsible for the Binding to Anti-FLAG™ M2 Antibody Using a Phage Display Combinatorial Peptide Library. *Applied Biochemistry and Biotechnology*. [Online] 171 (3), 583–589.

Stanimirovic, D. B. et al. (2015) Blood-brain barrier models: in vitro to in vivo translation in preclinical development of CNS-targeting biotherapeutics. *Expert opinion on drug discovery*. [Online] 10 (2), 141–155.

Stanislaus, S. et al. (2017) A Novel Fc-FGF21 With Improved Resistance to Proteolysis, Increased Affinity Toward β-Klotho, and Enhanced Efficacy in Mice and Cynomolgus Monkeys. *Endocrinology*. [Online] 158 (5), 1314–1327.

Staquicini, F. I. et al. (2011) Systemic combinatorial peptide selection yields a non-canonical iron-mimicry mechanism for targeting tumors in a mouse model of human glioblastoma. *The Journal of clinical investigation*. [Online] 121 (1), 161–173. [online]. Available from: http://www.jci.org/articles/view/44798.

Stefan, N. et al. (2011) DARPins recognizing the tumor-associated antigen EpCAM selected by phage and ribosome display and engineered for multivalency. *Journal of molecular biology*. [Online] 413 (4), 826–843. [online]. Available from: http://linkinghub.elsevier.com/retrieve/pii/S0022283611010229.

Stoltenburg, R. et al. (2005) FluMag-SELEX as an advantageous method for DNA aptamer selection. *Analytical and bioanalytical chemistry*. [Online] 383 (1), 83–91.

Storck, S. E. et al. (2016) Endothelial LRP1 transports amyloid-β(1-42) across the blood-brain barrier. *The Journal of clinical investigation*. [Online] 126 (1), 123–136.

Strand, J. et al. (2013) Characterization of Fc-fusion protein aggregates derived from extracellular domain disulfide bond rearrangements. *Journal of pharmaceutical sciences*. [Online] 102 (2), 441–453.

Strohl, W. R. (2015) Fusion Proteins for Half-Life Extension of Biologics as a Strategy to Make Biobetters. *BioDrugs*. [Online] 29 (4), 215–239.

Sullenger, B. A. et al. (1990) Overexpression of TAR sequences renders cells resistant to human immunodeficiency virus replication. *Cell*. 63 (3), 601–608.

Škrlec, K. et al. (2015) Non-immunoglobulin scaffolds: a focus on their targets. *Trends in biotechnology*. [Online] 33 (7), 408–418.

Tacheva-Grigorova, S. K. et al. (2013) Clathrin-mediated endocytosis persists during unperturbed mitosis. *Cell reports*. [Online] 4 (4), 659–668.

Tamaki, C. et al. (2007) *Insulin facilitates the hepatic clearance of plasma amyloid beta-peptide (1 40) by intracellular translocation of low-density lipoprotein receptor-related protein 1 (LRP-1) to the plasma membrane in hepatocytes.* [Online] 72 (4), 850–855.

Tan, D. et al. (2013) Improvements in observed and relative survival in follicular grade 1-2 lymphoma during 4 decades: the Stanford University experience. *Blood*. [Online] 122 (6), 981–987.

Tanaka, Y. et al. (2009) In vitro selection and characterization of DNA aptamers specific for phospholamban. *The Journal of pharmacology and experimental therapeutics*. [Online] 329 (1), 57–63.

Tang, Q. et al. (2017) Characterization of Byproducts from Chemical Syntheses of Oligonucleotides Containing 1-Methyladenine and 3-Methylcytosine. *ACS omega*. [Online] 2 (11), 8205–8212.

Tao, Y. et al. (2005) Biotinylation of heat shock protein 70 induces RANTES production in HEK293 cells in a CD40-independent pathway. *Biochemical and biophysical research communications*. [Online] 338 (2), 700–709.

Tegel, H. et al. (2011) Enhancing the protein production levels in Escherichia coli with a strong promoter. *The FEBS journal*. [Online] 278 (5), 729–739.

Terpe, K. (2003) Overview of tag protein fusions: from molecular and biochemical fundamentals to commercial systems. *Applied microbiology and biotechnology*. [Online] 60 (5), 523–533.

ThermoFisher Scientific (2016) *EZ-Link Sulfo-NHS-Biotin Datasheet (Cat. No. 21326)*. [online]. Available from: https://www.thermofisher.com/order/catalog/product/21217.

Thom, G. & Hatcher, J. (2016) *(unpublished data) CNS uptake of Pep1-Fc/IL1RA using a mouse neuropathic pain model*.

Thomas, W. D. et al. (2010) Corruption of phage display libraries by target-unrelated clones: diagnosis and countermeasures. *Analytical biochemistry*. [Online] 407 (2), 237–240.

Thomsen, L. B. et al. (2012) Brain delivery systems via mechanism independent of receptor-mediated endocytosis and adsorptive-mediated endocytosis. *Current pharmaceutical biotechnology*. 13 (12), 2349–2354.

Thomsen, M. S. et al. (2017) Synthesis and deposition of basement membrane proteins by primary brain capillary endothelial cells in a murine model of the blood-brain barrier. *Journal of neurochemistry*. [Online] 140 (5), 741–754.

Tian, X. et al. (2015) LRP-1-mediated intracellular antibody delivery to the Central Nervous System. *Scientific Reports*. [Online] 511990.

Tiede, C. et al. (2014) Adhiron: a stable and versatile peptide display scaffold for molecular recognition applications. *Protein engineering, design & selection : PEDS*. [Online] 27 (5), 145–155.

Tiede, C. et al. (2017) Affimer proteins are versatile and renewable affinity reagents. *eLife*. [Online] 6515.

Tiwari, A. et al. (2010) Enhanced periplasmic expression of high affinity humanized scFv against Hepatitis B surface antigen by codon optimization. *Protein expression and purification*. [Online] 74 (2), 272–279.

Todorich, B. et al. (2008) Tim-2 is the receptor for H-ferritin on oligodendrocytes. *Journal of neurochemistry*. [Online] 107 (6), 1495–1505.

Tolle, F. et al. (2014) By-product formation in repetitive PCR amplification of DNA libraries during SELEX. Mark Isalan (ed.). *PloS one*. [Online] 9 (12), e114693.

Tong, X. et al. (2002) Iron deficiency can upregulate expression of transferrin receptor at both the mRNA and protein level. *British journal of haematology*. 116 (2), 458–464.

Traub, L. M. & Bonifacino, J. S. (2013) Cargo recognition in clathrin-mediated endocytosis. *Cold Spring Harbor perspectives in biology*. [Online] 5 (11), a016790–a016790.

Tuerk, C. & Gold, L. (1990) Systematic evolution of ligands by exponential enrichment: RNA ligands to bacteriophage T4 DNA polymerase. *Science (New York, N.Y.)*. 249 (4968), 505–510.

Turkewitz, A. P., Amatruda, J. F., et al. (1988) A high yield purification of the human transferrin receptor and properties of its major extracellular fragment. *The Journal of biological chemistry*. 263 (17), 8318–8325.

Turkewitz, A. P., Schwartz, A. L., et al. (1988) A pH-dependent reversible conformational transition of the human transferrin receptor leads to self-association. *The Journal of biological chemistry*. 263 (31), 16309–16315.

Uchida, Y. et al. (2011) Quantitative targeted absolute proteomics of human blood-brain barrier transporters and receptors. *Journal of neurochemistry*. [Online] 117 (2), 333–345.

Ueno, M. et al. (2010) The expression of LDL receptor in vessels with blood-brain barrier impairment in a stroke-prone hypertensive model. *Histochemistry and cell biology*. [Online] 133 (6), 669–676.

Uhl, P. et al. (2017) Oral delivery of vancomycin by tetraether lipid liposomes. *European journal of pharmaceutical sciences : official journal of the European Federation for Pharmaceutical Sciences*. [Online] 108111–118.

Uhlig, T. et al. (2014) The emergence of peptides in the pharmaceutical business: From exploration to exploitation. *EuPA Open Proteomics*. 458–69.

Ulbrich, K. et al. (2009) Transferrin- and transferrin-receptor-antibody-modified nanoparticles enable drug delivery across the blood-brain barrier (BBB). *European journal of pharmaceutics and biopharmaceutics : official journal of Arbeitsgemeinschaft fur Pharmazeutische Verfahrenstechnik e.V*. [Online] 71 (2), 251–256. [online]. Available from: http://linkinghub.elsevier.com/retrieve/pii/S0939641108003378.

Underwood, P. A. (1993) Problems and pitfalls with measurement of antibody affinity using solid phase binding in the ELISA. *Journal of Immunological Methods*. 164 (1), 119–130.

Unger, E. L. et al. (2009) Diurnal cycle influences peripheral and brain iron levels in mice. *Journal of applied physiology (Bethesda, Md. : 1985)*. [Online] 106 (1), 187–193.

Urquhart, B. L. & Kim, R. B. (2009) Blood-brain barrier transporters and response to CNS-active drugs. *European journal of clinical pharmacology*. [Online] 65 (11), 1063–1070.

van Breevoort, D. et al. (2014) STXBP1 promotes Weibel-Palade body exocytosis through its interaction with the Rab27A effector Slp4-a. *Blood*. [Online] 123 (20), 3185–3194.

van der Bliek, A. M. et al. (1993) Mutations in human dynamin block an intermediate stage in coated vesicle formation. *The Journal of cell biology*. 122 (3), 553–563.

van Gelder, W. et al. (1995) Quantification of different transferrin receptor pools in primary cultures of porcine blood-brain barrier endothelial cells. *Journal of neurochemistry*. [Online] 64 (6), 2708–2715. [online]. Available from: http://eutils.ncbi.nlm.nih.gov/entrez/eutils/elink.fcgi?dbfrom=pubmed&id=7760051&retmode=ref&cmd=prlinks.

van Horssen, J. et al. (2005) Basement membrane proteins in multiple sclerosis-associated inflammatory cuffs: potential role in influx and transport of leukocytes. *Journal of neuropathology and experimental neurology*. 64 (8), 722–729.

van Horssen, J. et al. (2006) Extensive extracellular matrix depositions in active multiple sclerosis lesions. *Neurobiology of Disease*. [Online] 24 (3), 484–491.

van Rooy, I. et al. (2010) Identification of peptide ligands for targeting to the blood-brain barrier. *Pharmaceutical research*. [Online] 27 (4), 673–682.

Vauquelin, G. & Charlton, S. J. (2013) Exploring avidity: understanding the potential gains in functional affinity and target residence time of bivalent and heterobivalent ligands. *British journal of pharmacology*. [Online] 168 (8), 1771–1785.

Vazquez-Lombardi, R. et al. (2015) Challenges and opportunities for non-antibody scaffold drugs. *Drug discovery today*. [Online] 20 (10), 1271–1283.

Velasco-Aguirre, C. et al. (2017) Improving gold nanorod delivery to the central nervous system by conjugation to the shuttle Angiopep-2. *Nanomedicine (London, England)*. [Online] 12 (20), 2503–2517.

Vigo, D. et al. (2016) Estimating the true global burden of mental illness. *The lancet. Psychiatry*. [Online] 3 (2), 171–178.

Vinores, S. A. (2006) Pegaptanib in the treatment of wet, age-related macular degeneration. *International journal of nanomedicine*. 1 (3), 263–268.

Vlieghe, P. et al. (2010) Synthetic therapeutic peptides: science and market. *Drug discovery today*. [Online] 15 (1-2), 40–56.

Vykhodtseva, N. et al. (2008) Progress and problems in the application of focused ultrasound for blood–brain barrier disruption. *Ultrasonics*. [Online] 48 (4), 279–296.

Wachs, F.-P. et al. (2003) High efficacy of clonal growth and expansion of adult neural stem cells. *Laboratory investigation; a journal of technical methods and pathology*. 83 (7), 949–962.

Wada, A. (2013) Development of Next-Generation Peptide Binders Using In vitro Display Technologies and Their Potential Applications. *Frontiers in immunology*. [Online] 4224.

Wagner, S. et al. (2012) Uptake mechanism of ApoE-modified nanoparticles on brain capillary endothelial cells as a blood-brain barrier model. Mária A Deli (ed.). *PloS one*. [Online] 7 (3), e32568.

Walsh, G. (2014) *Biopharmaceutical benchmarks 2014.* [Online] 32 (10), 992–1000.

Walus, L. R. et al. (1996) Enhanced uptake of rsCD4 across the rodent and primate blood-brain barrier after conjugation to anti-transferrin receptor antibodies. *The Journal of pharmacology and experimental therapeutics*. 277 (2), 1067–1075.

Wan, W. et al. (2015) Aβ(1-42) oligomer-induced leakage in an in vitro blood-brain barrier model is associated with up-regulation of RAGE and metalloproteinases, and down-regulation of tight junction scaffold proteins. *Journal of neurochemistry*. [Online] 134 (2), 382–393.

Wang et al. (2016) Mfsd2a-based pharmacological strategies for drug delivery across the blood-brain barrier. *Pharmacological research*. [Online] 104, 124–131.

Wang, Daren et al. (2013) Engineering a lysosomal enzyme with a derivative of receptor-binding domain of apoE enables delivery across the blood-brain barrier. *Proceedings of the National Academy of Sciences of the United States of America*. [Online] 110 (8), 2999–3004.

Wang, H H et al. (2016) Rab3A, Rab27A, and Rab35 regulate different events during mouse oocyte meiotic maturation and activation. *Histochemistry and cell biology*. [Online] 145 (6), 647–657.

Wang, Lei et al. (2016) Eps15 membrane-binding and -bending activity acts redundantly with Fcho1 during clathrin-mediated endocytosis. *Molecular biology of the cell*. [Online] 27 (17), 2675–2687.

Wang, Lin et al. (2005) Locked nucleic acid molecular beacons. *Journal of the American Chemical Society*. [Online] 127 (45), 15664–15665.

Wang, Ping et al. (2010) Diphtheria toxin mutant CRM197-mediated transcytosis across blood-brain barrier in vitro. *Cellular and molecular neurobiology*. [Online] 30 (5), 717–725.

Wang, Qingqing et al. (2017) LAMP1 expression is associated with poor prognosis in breast cancer. *Oncology letters*. [Online] 14 (4), 4729–4735.

Wang, Wei & Roberts, C. J. (2010) *Aggregation of Therapeutic Proteins*. John Wiley & Sons.

Watkins, J. D. et al. (1997) Determination of the Relative Affinities of Antibody Fragments Expressed inEscherichia coliby Enzyme-Linked Immunosorbent Assay. *Analytical biochemistry*. [Online] 253 (1), 37–45.

Weber, P. C. et al. (1992) Crystal structure and ligand-binding studies of a screened peptide complexed with streptavidin. *Biochemistry*. 31 (39), 9350–9354.

Webster, C. I. et al. (2017) Enhanced delivery of IL-1 receptor antagonist to the central nervous system as a novel anti-transferrin receptor-IL-1RA fusion reverses neuropathic mechanical hypersensitivity. *Pain*. [Online] 1.

Weikert, C. et al. (2003) Cellular engineering of ventricular adult rat cardiomyocytes. *Cardiovascular research*. 59 (4), 874–882.

Weksler, B. et al. (2013) The hCMEC/D3 cell line as a model of the human blood brain barrier. *Fluids and barriers of the CNS*. [Online] 10 (1), 16. [online]. Available from: http://fluidsbarrierscns.biomedcentral.com/articles/10.1186/2045-8118-10-16.

Wenzel, M. et al. (2016) Influence of lipidation on the mode of action of a small RW-rich antimicrobial peptide. *Biochimica et biophysica acta*. [Online] 1858 (5), 1004–1011.

Wiley, D. T. et al. (2013) Transcytosis and brain uptake of transferrin-containing nanoparticles by tuning avidity to transferrin receptor. *Proceedings of the National Academy of Sciences of the United States of America*. [Online] 110 (21), 8662–8667.

Wilkins, M. R. et al. (1999) Protein identification and analysis tools in the ExPASy server. *Methods in molecular biology (Clifton, N.J.)*. 112531–552.

Williams, A. M. & Enns, C. A. (1991) A mutated transferrin receptor lacking asparagine-linked glycosylation sites shows reduced functionality and an association with binding immunoglobulin protein. *The Journal of biological chemistry*. 266 (26), 17648–17654.

Williams, A. M. & Enns, C. A. (1993) A region of the C-terminal portion of the human transferrin receptor contains an asparagine-linked glycosylation site critical for receptor structure and function. *The Journal of biological chemistry*. 268 (17), 12780–12786.

Williams, R. et al. (2006) Amplification of complex gene libraries by emulsion PCR. *Nature methods*. [Online] 3 (7), 545–550.

Willis, C. L. et al. (2004) Focal astrocyte loss is followed by microvascular damage, with subsequent repair of the blood-brain barrier in the apparent absence of direct astrocytic contact. *Glia*. [Online] 45 (4), 325–337.

Willrich, M. A. V. et al. (2015) Tumor necrosis factor inhibitors: clinical utility in autoimmune diseases. *Translational Research*. [Online] 165 (2), 270–282.

Wilner, S. E. et al. (2012) An RNA alternative to human transferrin: a new tool for targeting human cells. *Molecular therapy. Nucleic acids*. [Online] 1e21.

Wilson, J. M. et al. (2000) EEA1, a tethering protein of the early sorting endosome, shows a polarized distribution in hippocampal neurons, epithelial cells, and fibroblasts. *Molecular biology of the cell*. 11 (8), 2657–2671.

Wong, A. D. et al. (2013) The blood-brain barrier: an engineering perspective. *Frontiers in neuroengineering*. [Online] 67.

Wu, B. et al. (2009) RAGE, LDL receptor, and LRP1 expression in the brains of SAMP8. *Neuroscience letters*. [Online] 461 (2), 100–105.

Wu, D. & Pardridge, W. M. (1996) Central nervous system pharmacologic effect in conscious rats after intravenous injection of a biotinylated vasoactive intestinal peptide analog coupled to a blood-brain barrier drug delivery system. *The Journal of pharmacology and experimental therapeutics*. 279 (1), 77–83.

Wu, Y. et al. (2010) *Therapeutic antibody targeting of individual Notch receptors.* [Online] 464 (7291), 1052–1057. [online]. Available from: http://www.nature.com/doifinder/10.1038/nature08878.

Xia, H. et al. (2000) *Recombinant human adenovirus: targeting to the human transferrin receptor improves gene transfer to brain microcapillary endothelium.* 74 (23), 11359–11366. [online]. Available from: http://eutils.ncbi.nlm.nih.gov/entrez/eutils/elink.fcgi?dbfrom=pubmed&id=11070036&retmode=ref&cmd=prlinks.

Xiang, D. et al. (2015) Superior Performance of Aptamer in Tumor Penetration over Antibody: Implication of Aptamer-Based Theranostics in Solid Tumors. *Theranostics*. [Online] 5 (10), 1083–1097.

Xu, F. et al. (2017) Bioactivity of a modified human Glucagon-like peptide-1. Michael Bader (ed.). *PloS one*. [Online] 12 (2), e0171601.

Xu, Y. et al. (2017) Endocytosis and membrane receptor internalization: implication of F-BAR protein Carom. *Frontiers in bioscience (Landmark edition)*. 221439–1457.

Yamamoto, M. et al. (2008) Phosphorylation of claudin-5 and occludin by rho kinase in brain endothelial cells. *The American journal of pathology*. [Online] 172 (2), 521–533.

Yang, D. C. et al. (2001) Expression of transferrin receptor and ferritin H-chain mRNA are associated with clinical and histopathological prognostic indicators in breast cancer. *Anticancer research*. 21 (1B), 541–549.

Yang, D. et al. (2017) Determination of High-affinity Antibody-antigen Binding Kinetics Using Four Biosensor Platforms. *Journal of visualized experiments : JoVE*. [Online] (122).

Yang, L. et al. (2012) Secretory vesicles are preferentially targeted to areas of low molecular SNARE density. Ludger Johannes (ed.). *PloS one*. [Online] 7 (11), e49514.

Yang, W. M. et al. (2011) Transient expression of iron transport proteins in the capillary of the developing rat brain. *Cellular and molecular neurobiology*. [Online] 31 (1), 93–99.

Yang, X. et al. (2002) Construction and selection of bead-bound combinatorial oligonucleoside phosphorothioate and phosphorodithioate aptamer libraries designed for rapid PCR-based sequencing. *Nucleic acids research*. 30 (23), e132.

Yang, Z.-H. & Liu, X.-D. (2008) P-glycoprotein-mediated efflux of phenobarbital at the blood-brain barrier evidence from transport experiments in vitro. *Epilepsy research*. [Online] 78 (1), 40–49.

Yau, Y. H. & Shochat, S. G. (2014) Analysis of affinity of dengue virus protein interaction using Biacore. *Methods in molecular biology (Clifton, N.J.)*. [Online] 1138 (Chapter 17), 271–284.

Ye, D. et al. (2014) A TEM protocol for quality assurance of in vitro cellular barrier models and its application to the assessment of nanoparticle transport mechanisms across barriers. *Analyst*. [Online] 140 (1), 83–97.

Ye, Q. et al. (2012) Generation and functional characterization of the anti-transferrin receptor single-chain antibody-GAL4 (TfRscFv-GAL4) fusion protein. *BMC biotechnology*. [Online] 12 (1), 1.

Yim, Y.-I. et al. (2010) Endocytosis and clathrin-uncoating defects at synapses of auxilin knockout mice. *Proceedings of the National Academy of Sciences of the United States of America*. [Online] 107 (9), 4412–4417.

Young, S. P. et al. (1984) The effect of the iron saturation of transferrin on its binding and uptake by rabbit reticulocytes. *The Biochemical journal*. 219 (2), 505–510.

Yu, Y. J. & Watts, R. J. (2013) Developing Therapeutic Antibodies for Neurodegenerative Disease. *Neurotherapeutics : the journal of the American Society for Experimental NeuroTherapeutics*. [Online] 10 (3), 459–472.

Yu, Y. J. et al. (2011) Boosting brain uptake of a therapeutic antibody by reducing its affinity for a transcytosis target. *Science translational medicine*. [Online] 3 (84), 84ra44–84ra44.

Yu, Y. J. et al. (2014) Therapeutic bispecific antibodies cross the blood-brain barrier in nonhuman primates. *Science translational medicine*. [Online] 6 (261), 261ra154–261ra154.

Yue, P.-J. et al. (2014) OX26/CTX-conjugated PEGylated liposome as a dual-targeting gene delivery system for brain glioma. *Molecular cancer*. [Online] 13 (1), 191.

Zavyalova, E. et al. (2013) Module-Activity Relationship of G-quadruplex Based DNA Aptamers for Human Thrombin. *Current medicinal chemistry*. 20 (38), 4836–4843.

Zecca, L. et al. (2004) Iron, brain ageing and neurodegenerative disorders. *Nature Reviews Neuroscience*. [Online] 5 (11), 863–873.

Zeigerer, A. et al. (2012) Rab5 is necessary for the biogenesis of the endolysosomal system in vivo. *Nature*. [Online] 485 (7399), 465–470.

Zensi, A., Begley, D., Pontikis, C., Legros, C., Mihoreanu, L., Wagner, S., Büchel, C., Briesen, von, H. & Kreuter, J. (2009a) Albumin nanoparticles targeted with Apo E enter the CNS by transcytosis and are delivered to neurones. *Journal of controlled release : official journal of the Controlled Release Society*. [Online] 137 (1), 78–86.

Zensi, A., Begley, D., Pontikis, C., Legros, C., Mihoreanu, L., Wagner, S., Büchel, C., Briesen, von, H. & Kreuter, J. (2009b) Albumin nanoparticles targeted with Apo E enter the CNS by transcytosis and are delivered to neurones. *Journal of controlled release : official journal of the Controlled Release Society*. [Online] 137 (1), 78–86.

Zhang, Deshui et al. (2012) Characterization of transferrin receptor-mediated endocytosis and cellular iron delivery of recombinant human serum transferrin from rice (Oryza sativa L.). *BMC biotechnology*. [Online] 12 (1), 92.

Zhang, Ling et al. (2013) *Nanoporous gold based optical sensor for sub-ppt detection of mercury ions.* [Online] 7 (5), 4595–4600.

Zhang, Yue et al. (2017) Dual-modified liposome codelivery of doxorubicin and vincristine improve targeting and therapeutic efficacy of glioma. *… drug delivery*. [Online] 24 (1), 1045–1055.

Zhang, Yun & Pardridge, W. M. (2006) Blood-brain barrier targeting of BDNF improves motor function in rats with middle cerebral artery occlusion. *Brain research*. [Online] 1111 (1), 227–229.

Zhao, Z. et al. (2015) Central role for PICALM in amyloid-β blood-brain barrier transcytosis and clearance. *Nature neuroscience*. [Online] 18 (7), 978–987.

Zhou, J. & Rossi, J. (2017) Aptamers as targeted therapeutics: current potential and challenges. *Nature reviews. Drug discovery*. [Online] 16 (3), 181–202.

Zhu, D. et al. (2018) Magnesium Reduces Blood-Brain Barrier Permeability and Regulates Amyloid-β Transcytosis. *Molecular neurobiology*. [Online] 24 (3), S115.

Zhu, G. et al. (2004) Structural basis of Rab5-Rabaptin5 interaction in endocytosis. *Nature structural & molecular biology*. [Online] 11 (10), 975–983.

Zhu, J. et al. (2017) Glycocalyx degradation leads to blood-brain barrier dysfunction and brain edema after asphyxia cardiac arrest in rats. *Journal of cerebral blood flow and metabolism : official journal of the International Society of Cerebral Blood Flow and Metabolism*. [Online] 271678X17726062.

Zhu, Q. M. et al. (2015) SNAP23 Regulates Endothelial Exocytosis of von Willebrand Factor. Nanette H Bishopric (ed.). *PloS one*. [Online] 10 (8), e0118737.

Zuchero, Y. J. Y. et al. (2016) Discovery of Novel Blood-Brain Barrier Targets to Enhance Brain Uptake of Therapeutic Antibodies. *Neuron*. [Online] 89 (1), 70–82.

Zwick, M. B. et al. (2001) Broadly neutralizing antibodies targeted to the membrane-proximal external region of human immunodeficiency virus type 1 glycoprotein gp41. *Journal of virology*. [Online] 75 (22), 10892–10905.

Zwolak, A. et al. (2017) Modulation of protein A binding allows single-step purification of mouse bispecific antibodies that retain FcRn binding. *mAbs*. [Online] 9 (8), 1306–1316.

Appendix

Figure S1: PeptideCutter (ExPASy) analysis summary of predicted trypsin cleavage sites on the TfR sequence.

In total, 83 potential trypsin cleavage sites were identified for the 760 amino acid sequence of human TfR. The position of cleavage, resulting peptide sequence, as well as peptide length and mass are shown.

Position of cleavage site	Name of cleaving enzyme(s)	Resulting peptide sequence	Peptide length [aa]	Peptide mass [Da]	Cleavage probability (%)
6	Trypsin	MMDQAR	6	750.886	100 %
22	Trypsin	SAFSNLFGGEPLSYTR	16	1745.909	100 %
27	Trypsin	FSLAR	5	592.696	100 %
39	Trypsin	QVDGDNSHVEMK	12	1358.446	100 %
53	Trypsin	LAVDEEENADNNTK	14	1561.579	100 %
58	Trypsin	ANVTK	5	531.610	19.4 %
60	Trypsin	PK	2	243.306	90.7 %
61	Trypsin	R	1	174.203	100 %
90	Trypsin	CSGSICYGTIAVIVFFLIGFMIGYLGYCK	29	3139.837	82.8 %
95	Trypsin	GVEPK	5	528.606	100 %
100	Trypsin	TECER	5	636.678	100 %
109	Trypsin	LAGTESPVR	9	929.041	100 %
120	Trypsin	EEPGEDFPAAR	11	1217.257	90.4 %
121	Trypsin	R	1	174.203	100 %
128	Trypsin	LYWDDLK	7	952.075	91.8 %
129	Trypsin	R	1	174.203	89.7 %
130	Trypsin	K	1	146.189	83.7 %
134	Trypsin	LSEK	4	475.542	94.7 %
145	Trypsin	LDSTDFTGTIK	11	1197.307	100 %
155	Trypsin	LLNENSYVPR	10	1204.348	100 %
161	Trypsin	EAGSQK	6	618.644	100 %
174	Trypsin	DENLALYVENQFR	13	1610.743	69.6 %
177	Trypsin	EFK	3	422.481	100 %
180	Trypsin	LSK	3	346.427	100 %
183	Trypsin	VWR	3	459.549	100 %
189	Trypsin	DQHFVK	6	772.859	100 %
193	Trypsin	IQVK	4	486.612	100 %
205	Trypsin	DSAQNSVIIVDK	12	1288.420	63.1 %
208	Trypsin	NGR	3	345.358	100 %
224	Trypsin	LVYLVENPGGYVAYSK	16	1772.031	100 %
231	Trypsin	AATVTGK	7	646.742	100 %
240	Trypsin	LVHANFGTK	9	986.139	84.4 %
241	Trypsin	K	1	146.189	84.6 %
258	Trypsin	DFEDLYTPVNGSIVIVR	17	1937.180	100 %
261	Trypsin	AGK	3	274.320	100 %
267	Trypsin	ITFAEK	6	707.825	95.7 %
287	Trypsin	VANAESLNAIGVLIYMDQTK	20	2150.475	100 %

325	Trypsin	FPIVNAELSFFGHAHLGTGDPYTPGFP SFNHTQFPPSR	38	4188.630	100 %
339	Trypsin	SSGLPNIPVQTISR	14	1468.673	91.9 %
344	Trypsin	AAAEK	5	488.541	94.7 %
358	Trypsin	LFGNMEGDCPSDWK	14	1598.765	100 %
364	Trypsin	TDSTCR	6	681.719	100 %
371	Trypsin	MVTSESK	7	780.892	100 %
374	Trypsin	NVK	3	359.426	100 %
382	Trypsin	LTVSNVLK	8	873.060	92.8 %
385	Trypsin	EIK	3	388.464	100 %
394	Trypsin	ILNIFGVIK	9	1016.292	100 %
409	Trypsin	GFVEPDHYVVVGAQR	15	1672.861	100 %
418	Trypsin	DAWGPGAAK	9	871.948	100 %
428	Trypsin	SGVGTALLLK	10	958.166	100 %
439	Trypsin	LAQMFSDMVLK	11	1282.579	86.4 %
446	Trypsin	DGFQPSR	7	805.845	100 %
477	Trypsin	SIIFASWSAGDFGSVGATEWLEGYLSS LHLK	31	3329.713	100 %
486	Trypsin	AFTYINLDK	9	1084.237	92.8 %
495	Trypsin	AVLGTSNFK	9	936.076	89.5 %
508	Trypsin	VSASPLLYTLIEK	13	1433.708	100 %
514	Trypsin	TMQNVK	6	719.854	100 %
531	Trypsin	HPVTGQFLYQDSNWASK	17	1978.151	100 %
534	Trypsin	VEK	3	374.437	94.7 %
574	Trypsin	LTLDNAAFPFLAYSGIPAVSFCFCEDTD YPYLGTTMDTYK	40	4463.024	88.9 %
579	Trypsin	ELIER	5	658.753	75.6 %
585	Trypsin	IPELNK	6	712.844	100 %
588	Trypsin	VAR	3	344.414	100 %
600	Trypsin	AAAEVAGQFVIK	12	1203.404	100 %
613	Trypsin	LTHDVELNLDYER	13	1616.748	100 %
623	Trypsin	YNSQLLSFVR	10	1226.398	100 %
629	Trypsin	DLNQYR	6	807.861	100 %
633	Trypsin	ADIK	4	445.516	93.1 %
646	Trypsin	EMGLSLQWLYSAR	13	1553.796	100 %
651	Trypsin	GDFFR	5	640.696	100 %
655	Trypsin	ATSR	4	433.465	100 %
665	Trypsin	LTTDFGNAEK	10	1095.174	100 %
668	Trypsin	TDR	3	390.396	100 %
672	Trypsin	FVMK	4	523.691	78.5 %
673	Trypsin	K	1	146.189	82 %
677	Trypsin	LNDR	4	516.555	100 %
680	Trypsin	VMR	3	404.528	100 %
693	Trypsin	VEYHFLSPYVSPK	13	1565.789	90.7 %
698	Trypsin	ESPFR	5	634.690	100 %
717	Trypsin	HVFWGSGSHTLPALLENLK	19	2106.412	100 %
719	Trypsin	LR	2	287.362	100 %
720	Trypsin	K	1	146.189	83.1 %
732	Trypsin	QNNGAFNETLFR	12	1410.509	100 %
760	**end of sequence**	NQLALATWTIQGAANALSGDVWDID NEF	28	3034.288	-

Figure S2: Plate transfer summary of screened phage ELISA clones.

Figure showing the series of transfers firstly from source selection plates to deep-well plates (**B**) and subsequently to the phage ELISA screening plates. Plate barcoding was used to avoid mislabeling of plates and plate IDs are shown for each plate.

A

Selection ID	Description	Source plate	Destination (Deep well)
29 (plate 1)	R3 CPEP1 h → m	ZZ1I0I	00658B
29 (plate 2)	R3 CPEP1 h → m	ZZ1I0J	006588
30 (plate 1)	R3 CPEP2 h → m	ZZ1JTV	00659N
30 (plate 2)	R3 CPEP2 h → m	ZZ1JTW	006585
31 (plate 1)	R3 CPEP3 h → m	ZZ1I0G	006582
31 (plate 2)	R3 CPEP3 h → m	ZZ1I0H	00657Z
32 (plate 1)	R4 CPEP1 non-cross to bEnd.3	ZZ1K3W	0064YK
32 (plate 2)	R4 CPEP1 non-cross to bEnd.3	ZZ1K3V	0064YN
33 (plate 1)	R4 CPEP2 non-cross to bEnd.3	ZZ1K3U	0064YQ
33 (plate 2)	R4 CPEP2 non-cross to bEnd.3	ZZ1K3Z	00657K
34 (plate 1)	R4 CPEP3 non-cross to bEnd.3	ZZ1K3Y	00657N
34 (plate 2)	R4 CPEP3 non-cross to bEnd.3	ZZ1K3X	00657Q
35 (plate 1)	R4 CPEP1 cross to bEnd.3	ZZ1IY1	00659E
35 (plate 2)	R4 CPEP1 cross to bEnd.3	ZZ1IY0	00659H
36 (plate 1)	R4 CPEP2 cross to bEnd.3	ZZ1IXZ	00659K
36 (plate 2)	R4 CPEP2 cross to bEnd.3	ZZ1IXY	006598
37 (plate 1)	R4 CPEP3 cross to bEnd.3	ZZ1IXX	00659B
37 (plate 2)	R4 CPEP3 cross to bEnd.3	ZZ1IXW	00657W

B

	Selection ID	mTfR - biotin	hTfR - biotin	insulin - biotin
Round 3 CPEP human to mouse TfR cross selection screen	29 (plate 1)	Y01668	Y02066	Y02153
	29 (plate 2)	Y02263	Y01704	Y01740
	30 (plate 1)	Y01536	Y01776	Y01516
	30 (plate 2)	Y01978	Y01518	Y02371
	31 (plate 1)	Y01878	Y01968	Y01847
	31 (plate 2)	Y01896	Y01903	Y01749
Round 4 CPEP cross selected to b.End 3 cell selection screen	35 (plate 1)	Y02229	Y02481	Y02339
	35 (plate 2)	Y02232	Y02019	Y01586
	36 (plate 1)	Y02311	Y01583	Y01876
	36 (plate 2)	Y02374	Y01529	Y02036
	37 (plate 1)	Y01730	Y01675	Y01868
	37 (plate 2)	Y02306	Y02020	Y02477
Round 4 CPEP non-cross selected to b.End 3 cell selection screen	32 (plate 1)	Y01760	Y02443	Y02447
	32 (plate 2)	Y01698	Y02491	Y02497
	33 (plate 1)	Y01541	Y02116	Y01827
	33 (plate 2)	Y02412	Y03036	Y01761
	34 (plate 1)	Y02411	Y03498	Y02079
	34 (plate 2)	Y02998	Y01963	Y03386

Figure S3: Plate layout and Phage ELISA screening reports

Figure showing the well layout for 96-well plates used throughout the phage ELISA colony screening (**A**). Screening reports highlighting the weak (green) and strong (yellow) phage hits towards biotinylated insulin (control), human TfR and mouse TfR, from round 3 cross-selection cascade (**B**), Round 4 cross-selection to bEnd.3 cell selection cascade (**C**), and Round 4 mTfR to bEnd.3 cell selection cascade (**D**).

A

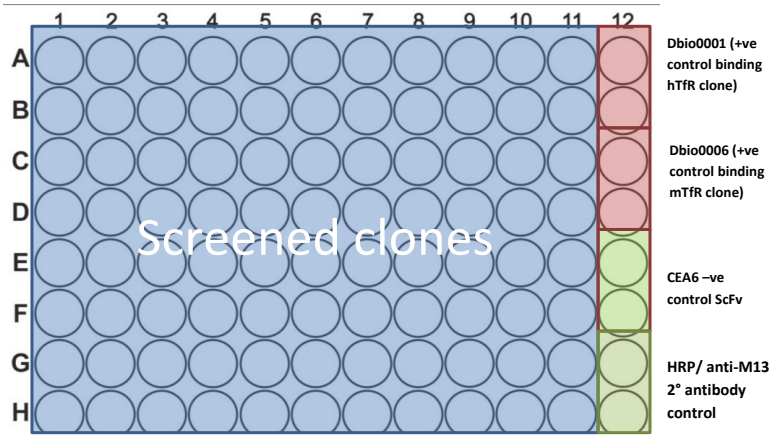

B

Screening Report

Copyright 1998-2014 Cambridge Antibody Technology

Summary of Screen	Round3 cross-selection
Screen Name	
Analysis Name	first pass ELISA
Project	OU Studentship

Summary of Screen

-	Screening Plate b/c	Screening Plate	Source Plate b/c	Quad	Analysis Category	Cut-off	Sample Mean	Sample SD	Sum None	% None	Sum Weak	% Weak	Sum Strong	% Strong
	Y01740	Plate 1	ZZ1IOJ	96:96	Insulin	0.5,0.2	0.12	0.06	79	90	9	10	0	0
	Y01704	Plate 2	ZZ1IOJ	96:96	Human TfR	0.5,0.2	0.58	0.36	16	18	26	30	46	52
	Y02263	Plate 3	ZZ1IOJ	96:96	Mouse TfR	0.5,0.2	0.32	0.33	52	59	17	19	19	22
	Y02153	Plate 4	ZZ1IOI	96:96	Insulin	0.5,0.2	0.13	0.09	76	86	12	14	0	0
	Y02066	Plate 5	ZZ1IOI	96:96	Human TfR	0.5,0.2	0.66	0.38	12	14	25	28	51	58
	Y01668	Plate 6	ZZ1IOI	96:96	Mouse TfR	0.5,0.2	0.34	0.36	49	56	15	17	24	27
	Y02371	Plate 7	ZZ1JTW	96:96	Insulin	0.5,0.2	0.08	0.02	88	100	0	0	0	0
	Y01518	Plate 8	ZZ1JTW	96:96	Human TfR	0.5,0.2	0.41	0.31	34	39	23	26	31	35
	Y01978	Plate 9	ZZ1JTW	96:96	Mouse TfR	0.5,0.2	0.10	0.11	86	98	1	1	1	1
	Y01516	Plate 10	ZZ1JTV	96:96	Insulin	0.5,0.2	0.09	0.07	85	97	3	3	0	0
	Y01776	Plate 11	ZZ1JTV	96:96	Human TfR	0.5,0.2	0.42	0.32	33	38	28	32	27	31
	Y01536	Plate 12	ZZ1JTV	96:96	Mouse TfR	0.5,0.2	0.12	0.18	84	95	0	0	4	5
	Y01749	Plate 13	ZZ1IOH	96:96	Insulin	0.5,0.2	0.24	0.12	28	32	59	67	1	1
	Y01903	Plate 14	ZZ1IOH	96:96	Human TfR	0.5,0.2	0.43	0.17	8	9	48	55	32	36
	Y01896	Plate 15	ZZ1IOH	96:96	Mouse TfR	0.5,0.2	0.34	0.19	27	31	45	51	16	18
	Y01847	Plate 16	ZZ1IOG	96:96	Insulin	0.5,0.2	0.25	0.10	25	28	63	72	0	0
	Y01968	Plate 17	ZZ1IOG	96:96	Human TfR	0.5,0.2	0.44	0.21	13	15	49	56	26	30
	Y01878	Plate 18	ZZ1IOG	96:96	Transferrin receptor	0.5,0.2	0.35	0.19	21	24	51	58	16	18
Mean							0.30	0.20	45	52	26	30	16	19
SD							0.17	0.12	30	34	21	24	17	19

Appendix

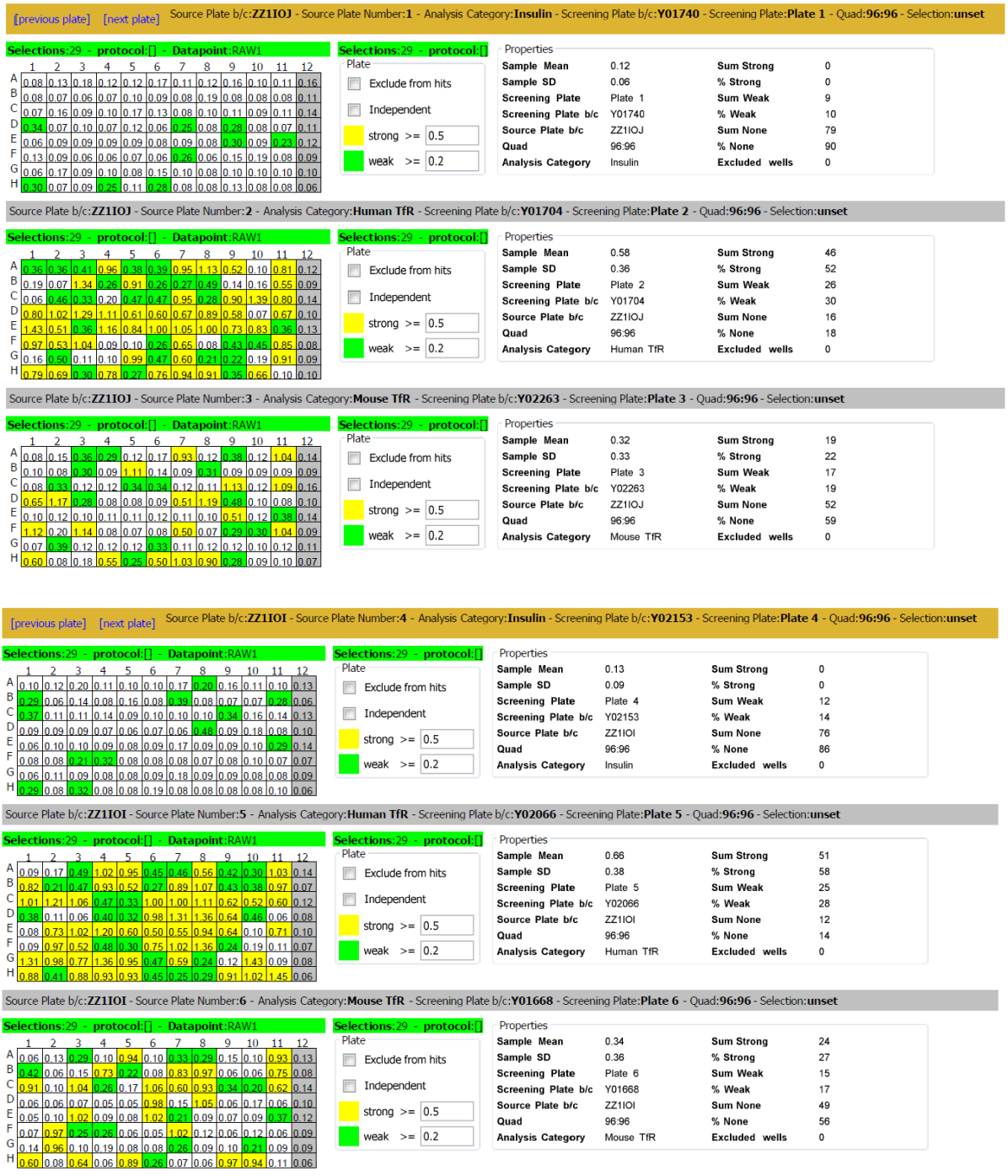
[previous plate] [next plate] Source Plate b/c:ZZ1IOJ - Source Plate Number:1 - Analysis Category:Insulin - Screening Plate b/c:Y01740 - Screening Plate:Plate 1 - Quad:96:96 - Selection:unset
Selections:29 - protocol:[] - Datapoint:RAW1
Selections:29 - protocol:[]
Plate
Exclude from hits
Independent
strong >= 0.5
weak >= 0.2
Properties
Sample Mean 0.12
Sample SD 0.06
Screening Plate Plate 1
Screening Plate b/c Y01740
Source Plate b/c ZZ1IOJ
Quad 96:96
Analysis Category Insulin
Sum Strong 0
% Strong 0
Sum Weak 9
% Weak 10
Sum None 79
% None 90
Excluded wells 0
Source Plate b/c:ZZ1IOJ - Source Plate Number:2 - Analysis Category:Human TfR - Screening Plate b/c:Y01704 - Screening Plate:Plate 2 - Quad:96:96 - Selection:unset
Selections:29 - protocol:[] - Datapoint:RAW1
Selections:29 - protocol:[]
Plate
Exclude from hits
Independent
strong >= 0.5
weak >= 0.2
Properties
Sample Mean 0.58
Sample SD 0.36
Screening Plate Plate 2
Screening Plate b/c Y01704
Source Plate b/c ZZ1IOJ
Quad 96:96
Analysis Category Human TfR
Sum Strong 46
% Strong 52
Sum Weak 26
% Weak 30
Sum None 16
% None 18
Excluded wells 0
Source Plate b/c:ZZ1IOJ - Source Plate Number:3 - Analysis Category:Mouse TfR - Screening Plate b/c:Y02263 - Screening Plate:Plate 3 - Quad:96:96 - Selection:unset
Selections:29 - protocol:[] - Datapoint:RAW1
Selections:29 - protocol:[]
Plate
Exclude from hits
Independent
strong >= 0.5
weak >= 0.2
Properties
Sample Mean 0.32
Sample SD 0.33
Screening Plate Plate 3
Screening Plate b/c Y02263
Source Plate b/c ZZ1IOJ
Quad 96:96
Analysis Category Mouse TfR
Sum Strong 19
% Strong 22
Sum Weak 17
% Weak 19
Sum None 52
% None 59
Excluded wells 0
[previous plate] [next plate] Source Plate b/c:ZZ1IOI - Source Plate Number:4 - Analysis Category:Insulin - Screening Plate b/c:Y02153 - Screening Plate:Plate 4 - Quad:96:96 - Selection:unset
Selections:29 - protocol:[] - Datapoint:RAW1
Selections:29 - protocol:[]
Plate
Exclude from hits
Independent
strong >= 0.5
weak >= 0.2
Properties
Sample Mean 0.13
Sample SD 0.09
Screening Plate Plate 4
Screening Plate b/c Y02153
Source Plate b/c ZZ1IOI
Quad 96:96
Analysis Category Insulin
Sum Strong 0
% Strong 0
Sum Weak 12
% Weak 14
Sum None 76
% None 86
Excluded wells 0
Source Plate b/c:ZZ1IOI - Source Plate Number:5 - Analysis Category:Human TfR - Screening Plate b/c:Y02066 - Screening Plate:Plate 5 - Quad:96:96 - Selection:unset
Selections:29 - protocol:[] - Datapoint:RAW1
Selections:29 - protocol:[]
Plate
Exclude from hits
Independent
strong >= 0.5
weak >= 0.2
Properties
Sample Mean 0.66
Sample SD 0.38
Screening Plate Plate 5
Screening Plate b/c Y02066
Source Plate b/c ZZ1IOI
Quad 96:96
Analysis Category Human TfR
Sum Strong 51
% Strong 58
Sum Weak 25
% Weak 28
Sum None 12
% None 14
Excluded wells 0
Source Plate b/c:ZZ1IOI - Source Plate Number:6 - Analysis Category:Mouse TfR - Screening Plate b/c:Y01668 - Screening Plate:Plate 6 - Quad:96:96 - Selection:unset
Selections:29 - protocol:[] - Datapoint:RAW1
Selections:29 - protocol:[]
Plate
Exclude from hits
Independent
strong >= 0.5
weak >= 0.2
Properties
Sample Mean 0.34
Sample SD 0.36
Screening Plate Plate 6
Screening Plate b/c Y01668
Source Plate b/c ZZ1IOI
Quad 96:96
Analysis Category Mouse TfR
Sum Strong 24
% Strong 27
Sum Weak 15
% Weak 17
Sum None 49
% None 56
Excluded wells 0

Appendix

[previous plate] [next plate] Source Plate b/c:**ZZ1JTW** - Source Plate Number:**7** - Analysis Category:**Insulin** - Screening Plate b/c:**Y02371** - Screening Plate:**Plate 7** - Quad:**96:96** - Selection:**unset**

Selections:30 - **protocol**:[] - **Datapoint**:RAW1

	1	2	3	4	5	6	7	8	9	10	11	12
A	0.09	0.13	0.10	0.11	0.11	0.10	0.10	0.09	0.09	0.09	0.08	0.11
B	0.10	0.09	0.07	0.08	0.07	0.07	0.07	0.06	0.06	0.06	0.07	0.06
C	0.06	0.10	0.11	0.10	0.10	0.10	0.10	0.08	0.08	0.09	0.10	0.11
D	0.09	0.08	0.07	0.08	0.07	0.08	0.06	0.08	0.07	0.07	0.08	0.07
E	0.05	0.09	0.09	0.09	0.08	0.09	0.08	0.09	0.08	0.09	0.09	0.10
F	0.07	0.06	0.06	0.07	0.06	0.06	0.06	0.06	0.06	0.06	0.06	0.06
G	0.06	0.10	0.10	0.09	0.09	0.09	0.08	0.09	0.08	0.07	0.09	0.08
H	0.07	0.07	0.13	0.06	0.06	0.06	0.07	0.07	0.06	0.07	0.08	0.04

Selections:30 - **protocol**:[]

Plate
- Exclude from hits
- Independent
- strong >= 0.5
- weak >= 0.2

Properties

Sample Mean	0.08	**Sum Strong**	0
Sample SD	0.02	**% Strong**	0
Screening Plate	Plate 7	**Sum Weak**	0
Screening Plate b/c	Y02371	**% Weak**	0
Source Plate b/c	ZZ1JTW	**Sum None**	88
Quad	96:96	**% None**	100
Analysis Category	Insulin	**Excluded wells**	0

Source Plate b/c:**ZZ1JTW** - Source Plate Number:**8** - Analysis Category:**Human TfR** - Screening Plate b/c:**Y01518** - Screening Plate:**Plate 8** - Quad:**96:96** - Selection:**unset**

Selections:30 - **protocol**:[] - **Datapoint**:RAW1

	1	2	3	4	5	6	7	8	9	10	11	12
A	0.27	0.80	0.13	0.15	0.14	0.12	0.41	0.08	0.10	0.54	0.30	0.11
B	0.90	0.12	0.11	0.11	0.74	0.51	0.70	0.38	0.58	0.70	0.57	0.07
C	0.06	0.15	0.61	0.54	0.60	0.84	0.72	0.12	0.96	0.34	0.19	0.12
D	0.54	0.69	0.16	0.91	0.68	0.74	0.23	0.12	0.36	0.74	0.12	0.08
E	1.31	0.24	1.04	0.24	0.58	1.11	0.10	0.97	0.08	0.40	0.39	0.11
F	0.89	0.18	0.34	0.44	0.29	1.04	0.09	0.41	0.08	0.06	0.06	0.08
G	0.22	0.45	0.10	0.11	0.09	0.16	0.13	0.11	0.47	0.13	0.35	0.10
H	0.12	0.71	0.07	0.07	1.15	0.38	0.13	0.44	0.48	0.52	0.30	0.05

Selections:30 - **protocol**:[]

Plate
- Exclude from hits
- Independent
- strong >= 0.5
- weak >= 0.2

Properties

Sample Mean	0.41	**Sum Strong**	31
Sample SD	0.31	**% Strong**	35
Screening Plate	Plate 8	**Sum Weak**	23
Screening Plate b/c	Y01518	**% Weak**	26
Source Plate b/c	ZZ1JTW	**Sum None**	34
Quad	96:96	**% None**	39
Analysis Category	Human TfR	**Excluded wells**	0

Source Plate b/c:**ZZ1JTW** - Source Plate Number:**9** - Analysis Category:**Mouse TfR** - Screening Plate b/c:**Y01978** - Screening Plate:**Plate 9** - Quad:**96:96** - Selection:**unset**

Selections:30 - **protocol**:[] - **Datapoint**:RAW1

	1	2	3	4	5	6	7	8	9	10	11	12
A	0.08	0.12	0.10	0.10	0.09	0.10	0.10	0.12	0.10	0.10	0.09	0.12
B	0.08	0.05	0.06	0.08	0.09	0.07	0.20	0.08	0.15	0.08	0.08	0.07
C	0.05	0.09	0.09	0.08	0.09	0.10	0.09	0.08	0.10	0.10	0.09	0.12
D	0.13	0.12	0.09	0.11	0.07	0.09	0.10	0.11	0.09	0.11	0.12	0.10
E	0.06	0.09	0.08	0.09	0.08	0.08	0.08	0.09	0.11	0.19	0.09	0.10
F	0.07	0.13	0.06	0.06	0.06	0.06	0.06	0.09	0.08	0.08	0.07	0.08
G	0.05	0.09	0.10	0.08	0.09	0.09	1.05	0.09	0.09	0.08	0.10	0.08
H	0.07	0.44	0.06	0.06	0.06	0.06	0.07	0.09	0.07	0.08	0.09	0.05

Selections:30 - **protocol**:[]

Plate
- Exclude from hits
- Independent
- strong >= 0.5
- weak >= 0.2

Properties

Sample Mean	0.10	**Sum Strong**	1
Sample SD	0.11	**% Strong**	1
Screening Plate	Plate 9	**Sum Weak**	1
Screening Plate b/c	Y01978	**% Weak**	1
Source Plate b/c	ZZ1JTW	**Sum None**	86
Quad	96:96	**% None**	98
Analysis Category	Mouse TfR	**Excluded wells**	0

[previous plate] [next plate] Source Plate b/c:**ZZ1JTV** - Source Plate Number:**10** - Analysis Category:**Insulin** - Screening Plate b/c:**Y01516** - Screening Plate:**Plate 10** - Quad:**96:96** - Selection:**unset**

Selections:30 - **protocol**:[] - **Datapoint**:RAW1

	1	2	3	4	5	6	7	8	9	10	11	12
A	0.08	0.12	0.11	0.13	0.10	0.13	0.10	0.09	0.10	0.11	0.10	0.13
B	0.08	0.07	0.47	0.08	0.09	0.48	0.09	0.08	0.08	0.07	0.07	0.09
C	0.08	0.09	0.39	0.11	0.09	0.09	0.12	0.10	0.09	0.09	0.09	0.15
D	0.06	0.06	0.05	0.05	0.06	0.05	0.05	0.06	0.06	0.06	0.06	0.11
E	0.05	0.09	0.08	0.09	0.08	0.08	0.08	0.08	0.07	0.09	0.08	0.13
F	0.06	0.06	0.05	0.05	0.05	0.05	0.05	0.05	0.06	0.06	0.06	0.08
G	0.06	0.09	0.09	0.08	0.08	0.08	0.08	0.09	0.08	0.07	0.09	0.12
H	0.09	0.07	0.06	0.06	0.06	0.06	0.07	0.06	0.06	0.06	0.08	0.09

Selections:30 - **protocol**:[]

Plate
- Exclude from hits
- Independent
- strong >= 0.5
- weak >= 0.2

Properties

Sample Mean	0.09	**Sum Strong**	0
Sample SD	0.07	**% Strong**	0
Screening Plate	Plate 10	**Sum Weak**	3
Screening Plate b/c	Y01516	**% Weak**	3
Source Plate b/c	ZZ1JTV	**Sum None**	85
Quad	96:96	**% None**	97
Analysis Category	Insulin	**Excluded wells**	0

Source Plate b/c:**ZZ1JTV** - Source Plate Number:**11** - Analysis Category:**Human TfR** - Screening Plate b/c:**Y01776** - Screening Plate:**Plate 11** - Quad:**96:96** - Selection:**unset**

Selections:30 - **protocol**:[] - **Datapoint**:RAW1

	1	2	3	4	5	6	7	8	9	10	11	12
A	0.15	0.49	0.56	0.33	0.16	0.93	0.51	0.97	0.35	0.13	1.22	0.13
B	0.14	0.19	0.10	1.16	0.50	0.16	0.17	0.15	0.67	1.00	0.61	0.09
C	0.55	0.16	0.29	0.48	0.96	0.13	0.98	0.41	0.27	0.14	1.06	0.19
D	0.13	0.12	0.05	0.14	0.10	0.09	0.73	0.11	0.06	0.08	0.35	0.11
E	0.19	0.39	0.53	0.11	0.76	0.40	1.12	0.12	0.18	0.14	0.44	0.12
F	1.14	0.40	0.97	0.12	0.52	0.74	0.49	0.08	0.34	0.23	0.21	0.08
G	0.16	0.44	0.59	0.43	0.58	0.71	0.36	0.50	0.85	0.12	0.36	0.10
H	0.25	1.20	0.36	0.15	0.09	0.62	0.29	0.41	0.38	0.45	0.18	0.07

Selections:30 - **protocol**:[]

Plate
- Exclude from hits
- Independent
- strong >= 0.5
- weak >= 0.2

Properties

Sample Mean	0.42	**Sum Strong**	27
Sample SD	0.32	**% Strong**	31
Screening Plate	Plate 11	**Sum Weak**	28
Screening Plate b/c	Y01776	**% Weak**	32
Source Plate b/c	ZZ1JTV	**Sum None**	33
Quad	96:96	**% None**	38
Analysis Category	Human TfR	**Excluded wells**	0

Source Plate b/c:**ZZ1JTV** - Source Plate Number:**12** - Analysis Category:**Mouse TfR** - Screening Plate b/c:**Y01536** - Screening Plate:**Plate 12** - Quad:**96:96** - Selection:**unset**

Selections:30 - **protocol**:[] - **Datapoint**:RAW1

	1	2	3	4	5	6	7	8	9	10	11	12
A	0.07	0.12	0.11	0.12	0.10	0.10	0.10	0.09	0.10	0.10	0.10	0.12
B	0.08	0.06	0.06	0.07	0.06	1.01	0.07	0.06	0.08	0.06	0.06	0.06
C	0.06	0.12	0.10	0.09	0.10	0.10	0.09	0.09	0.08	0.09	0.09	0.11
D	0.07	0.06	0.05	0.06	0.05	0.06	0.06	0.07	0.06	0.06	0.09	0.08
E	0.07	0.09	0.08	0.85	0.09	0.08	0.08	1.04	0.09	0.10	0.09	0.10
F	0.08	0.06	0.05	0.06	0.06	0.06	0.06	0.06	0.06	0.06	0.06	0.08
G	0.06	0.10	0.10	0.08	0.09	0.09	0.08	0.10	0.09	0.85	0.10	0.10
H	0.08	0.07	0.07	0.07	0.06	0.08	0.08	0.08	0.07	0.07	0.08	0.08

Selections:30 - **protocol**:[]

Plate
- Exclude from hits
- Independent
- strong >= 0.5
- weak >= 0.2

Properties

Sample Mean	0.12	**Sum Strong**	4
Sample SD	0.18	**% Strong**	5
Screening Plate	Plate 12	**Sum Weak**	0
Screening Plate b/c	Y01536	**% Weak**	0
Source Plate b/c	ZZ1JTV	**Sum None**	84
Quad	96:96	**% None**	95
Analysis Category	Mouse TfR	**Excluded wells**	0

Appendix

[previous plate] [next plate] Source Plate b/c:**ZZ1IOH** - Source Plate Number:**13** - Analysis Category:**Insulin** - Screening Plate b/c:**Y01749** - Screening Plate:**Plate 13** - Quad:**96:96** - Selection:**unset**

Selections:31 - **protocol**:[] - **Datapoint**:RAW1

	1	2	3	4	5	6	7	8	9	10	11	12
A	0.31	0.44	0.11	0.34	0.28	0.25	0.10	0.10	0.26	0.20	0.20	0.14
B	0.57	0.33	0.27	0.21	0.28	0.35	0.09	0.09	0.24	0.09	0.17	0.08
C	0.31	0.20	0.45	0.31	0.34	0.13	0.12	0.37	0.39	0.28	0.34	0.13
D	0.13	0.22	0.33	0.28	0.06	0.06	0.32	0.10	0.08	0.29	0.34	0.08
E	0.33	0.37	0.31	0.26	0.38	0.17	0.08	0.26	0.36	0.09	0.38	0.10
F	0.25	0.31	0.06	0.35	0.28	0.41	0.31	0.28	0.35	0.27	0.36	0.07
G	0.05	0.09	0.10	0.08	0.21	0.08	0.28	0.09	0.09	0.30	0.37	0.08
H	0.27	0.07	0.27	0.23	0.26	0.06	0.34	0.06	0.26	0.24	0.31	0.05

Selections:31 - **protocol**:[]

Plate
- Exclude from hits
- Independent
- strong >= 0.5
- weak >= 0.2

Properties

Sample Mean	0.24	**Sum Strong**	1
Sample SD	0.12	**% Strong**	1
Screening Plate	Plate 13	**Sum Weak**	59
Screening Plate b/c	Y01749	**% Weak**	67
Source Plate b/c	ZZ1IOH	**Sum None**	28
Quad	96:96	**% None**	32
Analysis Category	Insulin	**Excluded wells**	0

Source Plate b/c:**ZZ1IOH** - Source Plate Number:**14** - Analysis Category:**Human TfR** - Screening Plate b/c:**Y01903** - Screening Plate:**Plate 14** - Quad:**96:96** - Selection:**unset**

Selections:31 - **protocol**:[] - **Datapoint**:RAW1

	1	2	3	4	5	6	7	8	9	10	11	12
A	0.41	0.60	0.74	0.43	0.41	0.28	0.50	0.63	0.35	0.27	0.23	0.14
B	0.33	0.33	0.35	0.35	0.50	0.54	0.14	0.58	0.36	0.69	0.22	0.09
C	0.35	0.24	0.64	0.44	0.21	0.66	0.57	0.51	0.61	0.44	0.45	0.14
D	0.84	0.37	0.33	0.31	0.72	0.11	0.34	0.20	0.19	0.48	0.46	0.09
E	0.24	0.42	0.38	0.66	0.64	0.34	0.56	0.45	0.55	0.68	0.38	0.11
F	0.29	0.37	0.07	0.54	0.35	0.50	0.38	0.36	0.54	0.39	0.37	0.09
G	0.70	0.66	0.75	0.78	0.29	0.54	0.18	0.17	0.09	0.31	0.47	0.08
H	0.46	0.18	0.58	0.44	0.42	0.53	0.35	0.66	0.33	0.31	0.60	0.06

Selections:31 - **protocol**:[]

Plate
- Exclude from hits
- Independent
- strong >= 0.5
- weak >= 0.2

Properties

Sample Mean	0.43	**Sum Strong**	32
Sample SD	0.17	**% Strong**	36
Screening Plate	Plate 14	**Sum Weak**	48
Screening Plate b/c	Y01903	**% Weak**	55
Source Plate b/c	ZZ1IOH	**Sum None**	8
Quad	96:96	**% None**	9
Analysis Category	Human TfR	**Excluded wells**	0

Source Plate b/c:**ZZ1IOH** - Source Plate Number:**15** - Analysis Category:**Mouse TfR** - Screening Plate b/c:**Y01896** - Screening Plate:**Plate 15** - Quad:**96:96** - Selection:**unset**

Selections:31 - **protocol**:[] - **Datapoint**:RAW1

	1	2	3	4	5	6	7	8	9	10	11	12
A	0.40	0.63	0.22	0.40	0.42	0.22	0.17	0.10	0.33	0.20	0.17	0.13
B	0.43	0.43	0.40	0.39	0.60	0.74	0.15	0.08	0.39	0.07	0.14	0.08
C	0.47	0.21	0.70	0.46	0.41	0.10	0.19	0.68	0.63	0.42	0.50	0.13
D	0.09	0.32	0.37	0.37	0.11	0.06	0.42	0.12	0.08	0.46	0.51	0.08
E	0.72	0.42	0.40	0.65	0.62	0.33	0.16	0.40	0.64	0.09	0.33	0.10
F	0.37	0.40	0.06	0.66	0.38	0.64	0.39	0.43	0.66	0.35	0.33	0.07
G	0.09	0.09	0.09	0.08	0.31	0.08	0.42	0.09	0.08	0.36	0.58	0.08
H	0.37	0.08	0.52	0.37	0.34	0.07	0.36	0.10	0.34	0.32	0.49	0.05

Selections:31 - **protocol**:[]

Plate
- Exclude from hits
- Independent
- strong >= 0.5
- weak >= 0.2

Properties

Sample Mean	0.34	**Sum Strong**	16
Sample SD	0.19	**% Strong**	18
Screening Plate	Plate 15	**Sum Weak**	45
Screening Plate b/c	Y01896	**% Weak**	51
Source Plate b/c	ZZ1IOH	**Sum None**	27
Quad	96:96	**% None**	31
Analysis Category	Mouse TfR	**Excluded wells**	0

[previous plate] [next plate] Source Plate b/c:**ZZ1IOG** - Source Plate Number:**16** - Analysis Category:**Insulin** - Screening Plate b/c:**Y01847** - Screening Plate:**Plate 16** - Quad:**96:96** - Selection:**unset**

Selections:31 - **protocol**:[] - **Datapoint**:RAW1

	1	2	3	4	5	6	7	8	9	10	11	12
A	0.06	0.43	0.36	0.41	0.29	0.13	0.35	0.24	0.11	0.28	0.30	0.19
B	0.10	0.22	0.11	0.23	0.18	0.13	0.31	0.28	0.24	0.33	0.29	0.21
C	0.30	0.12	0.12	0.11	0.38	0.32	0.36	0.30	0.31	0.09	0.11	0.36
D	0.33	0.33	0.36	0.26	0.10	0.11	0.34	0.30	0.27	0.34	0.28	0.32
E	0.30	0.38	0.26	0.37	0.16	0.13	0.13	0.22	0.22	0.32	0.12	0.30
F	0.24	0.08	0.11	0.35	0.11	0.26	0.23	0.10	0.28	0.32	0.28	0.25
G	0.29	0.27	0.47	0.30	0.30	0.35	0.36	0.14	0.12	0.29	0.31	0.08
H	0.33	0.27	0.15	0.35	0.30	0.30	0.26	0.27	0.33	0.27	0.28	0.04

Selections:31 - **protocol**:[]

Plate
- Exclude from hits
- Independent
- strong >= 0.5
- weak >= 0.2

Properties

Sample Mean	0.25	**Sum Strong**	0
Sample SD	0.10	**% Strong**	0
Screening Plate	Plate 16	**Sum Weak**	63
Screening Plate b/c	Y01847	**% Weak**	72
Source Plate b/c	ZZ1IOG	**Sum None**	25
Quad	96:96	**% None**	28
Analysis Category	Insulin	**Excluded wells**	0

Source Plate b/c:**ZZ1IOG** - Source Plate Number:**17** - Analysis Category:**Human TfR** - Screening Plate b/c:**Y01968** - Screening Plate:**Plate 17** - Quad:**96:96** - Selection:**unset**

Selections:31 - **protocol**:[] - **Datapoint**:RAW1

	1	2	3	4	5	6	7	8	9	10	11	12
A	0.91	0.63	0.55	0.70	0.44	0.44	0.47	0.35	0.11	0.36	0.37	0.13
B	0.08	0.32	0.06	0.25	0.40	0.06	0.43	0.44	0.33	0.77	0.37	0.12
C	0.38	0.75	0.10	0.09	0.82	0.48	0.42	0.46	0.42	0.63	0.50	0.16
D	0.54	0.40	0.37	0.48	0.05	0.42	0.78	0.74	0.42	0.67	0.43	0.12
E	0.36	0.49	0.39	0.50	0.54	0.08	0.11	0.36	0.37	0.46	0.53	0.12
F	0.22	0.11	0.56	0.70	0.43	0.52	0.35	0.06	0.42	0.75	0.43	0.10
G	0.38	0.22	0.74	0.47	0.49	0.43	0.75	0.48	0.12	0.58	0.46	0.08
H	0.52	0.37	1.01	0.74	0.54	0.11	0.38	0.44	0.43	0.48	0.39	0.05

Selections:31 - **protocol**:[]

Plate
- Exclude from hits
- Independent
- strong >= 0.5
- weak >= 0.2

Properties

Sample Mean	0.44	**Sum Strong**	26
Sample SD	0.21	**% Strong**	30
Screening Plate	Plate 17	**Sum Weak**	49
Screening Plate b/c	Y01968	**% Weak**	56
Source Plate b/c	ZZ1IOG	**Sum None**	13
Quad	96:96	**% None**	15
Analysis Category	Human TfR	**Excluded wells**	0

Source Plate b/c:**ZZ1IOG** - Source Plate Number:**18** - Analysis Category:**Transferrin receptor** - Screening Plate b/c:**Y01878** - Screening Plate:**Plate 18** - Quad:**96:96** - Selection:**unset**

Selections:31 - **protocol**:[] - **Datapoint**:RAW1

	1	2	3	4	5	6	7	8	9	10	11	12
A	0.57	0.74	0.43	0.64	0.47	0.09	0.44	0.28	0.10	0.35	0.35	0.13
B	0.08	0.31	0.07	0.16	0.42	0.06	0.41	0.38	0.39	0.64	0.35	0.08
C	0.38	0.12	0.10	0.08	0.74	0.39	0.44	0.41	0.42	0.09	0.08	0.12
D	0.50	0.38	0.37	0.40	0.06	0.14	0.66	0.64	0.40	0.63	0.37	0.08
E	0.39	0.41	0.32	0.46	0.27	0.08	0.11	0.32	0.30	0.42	0.09	0.10
F	0.20	0.06	0.23	0.65	0.25	0.40	0.27	0.06	0.36	0.57	0.38	0.06
G	0.35	0.28	0.72	0.40	0.44	0.31	0.70	0.21	0.09	0.38	0.47	0.09
H	0.54	0.36	0.06	0.64	0.61	0.34	0.33	0.29	0.37	0.28	0.38	0.06

Selections:31 - **protocol**:[]

Plate
- Exclude from hits
- Independent
- strong >= 0.5
- weak >= 0.2

Properties

Sample Mean	0.35	**Sum Strong**	16
Sample SD	0.19	**% Strong**	18
Screening Plate	Plate 18	**Sum Weak**	51
Screening Plate b/c	Y01878	**% Weak**	58
Source Plate b/c	ZZ1IOG	**Sum None**	21
Quad	96:96	**% None**	24
Analysis Category	Transferrin receptor	**Excluded wells**	0

c

Screening Report

Summary of Screen

Screen Name	**Round 4 cross-selection to bEnd.3 cell selection**
Analysis Name	lower plate absorbance definitions
Project	OU Studentship

Summary of Screen

-	Screening Plate b/c	Screening Plate	Source Plate b/c	Quad	Analysis Category	Cut-off	Sample Mean	Sample SD	Sum None	% None	Sum Weak	% Weak	Sum Strong	% Strong
	Y02477	Plate 1	ZZ1IXW	96:96	Insulin	0.5,0.2	0.18	0.27	71	81	6	7	11	12
	Y01868	Plate 2	ZZ1IXX	96:96	Insulin	0.5,0.2	0.18	0.28	73	83	2	2	13	15
	Y02036	Plate 3	ZZ1IXY	96:96	Insulin	0.5,0.2	0.07	0.02	88	100	0	0	0	0
	Y01876	Plate 4	ZZ1IXZ	96:96	Insulin	0.5,0.2	0.07	0.02	88	100	0	0	0	0
	Y01586	Plate 5	ZZ1IY0	96:96	Insulin	0.5,0.2	0.12	0.16	77	88	7	8	4	5
	Y02339	Plate 6	ZZ1IY1	96:96	Insulin	0.5,0.2	0.24	0.19	54	61	26	30	8	9
	Y02020	Plate 7	ZZ1IXW	96:96	Human TfR	0.5,0.2	0.34	0.26	19	22	56	64	13	15
	Y01675	Plate 8	ZZ1IXX	96:96	Human TfR	0.5,0.2	0.39	0.29	17	19	53	60	18	20
	Y01529	Plate 9	ZZ1IXY	96:96	Human TfR	0.5,0.2	0.16	0.16	69	78	14	16	5	6
	Y01583	Plate 10	ZZ1IXZ	96:96	Human TfR	0.5,0.2	0.16	0.17	71	81	10	11	7	8
	Y02019	Plate 11	ZZ1IY0	96:96	Human TfR	0.5,0.2	0.26	0.21	42	48	34	39	12	14
	Y02481	Plate 12	ZZ1IY1	96:96	Human TfR	0.5,0.2	0.30	0.26	45	51	26	30	17	19
	Y02306	Plate 13	ZZ1IXW	96:96	Mouse TfR	0.5,0.2	0.22	0.18	66	75	12	14	10	11
	Y01730	Plate 14	ZZ1IXX	96:96	Mouse TfR	0.5,0.2	0.24	0.28	73	83	0	0	15	17
	Y02374	Plate 15	ZZ1IXY	96:96	Mouse TfR	0.5,0.2	0.07	0.06	85	97	3	3	0	0
	Y02311	Plate 16	ZZ1IXZ	96:96	Mouse TfR	0.5,0.2	0.10	0.12	81	92	3	3	4	5
	Y02232	Plate 17	ZZ1IY0	96:96	Mouse TfR	0.5,0.2	0.24	0.25	60	68	11	12	17	19
	Y02229	Plate 18	ZZ1IY1	96:96	Mouse TfR	0.5,0.2	0.25	0.24	59	67	13	15	16	18
Mean							0.20	0.19	63	72	15	17	9	11
SD							0.09	0.09	21	24	17	20	6	7

[previous plate] [next plate] Source Plate b/c:**ZZ1IXW** - Source Plate Number:**1** - Analysis Category:**Insulin** - Screening Plate b/c:**Y02477** - Screening Plate:**Plate 1** - Quad:**96:96** - Selection:**unset**

protocol:[] - **Datapoint:**RAW1

	1	2	3	4	5	6	7	8	9	10	11	12
A	0.11	0.61	0.08	0.08	0.08	0.07	0.07	0.20	0.31	0.07	0.07	0.10
B	0.09	0.06	1.06	0.06	0.46	0.06	0.07	1.04	0.07	0.05	0.06	0.09
C	0.06	0.06	0.07	0.07	0.05	0.06	0.70	0.06	0.06	0.07	0.06	0.09
D	0.06	1.03	0.06	0.05	0.06	0.07	0.06	0.35	0.60	0.07	0.06	0.10
E	0.07	1.17	0.06	0.06	0.08	0.70	0.06	0.06	0.06	0.06	0.24	0.09
F	0.07	0.06	0.06	0.90	0.07	0.06	0.05	0.05	0.07	0.06	0.05	0.09
G	0.07	0.06	0.06	0.07	0.34	0.06	0.07	0.06	0.07	0.06	0.94	0.07
H	0.52	0.08	0.06	0.18	0.07	0.06	0.06	0.06	0.06	0.07	0.08	0.06

protocol:[]

Plate

Exclude from hits

Independent

strong >= 0.5

weak >= 0.2

Properties

Sample Mean	0.18	**Sum Strong**	11
Sample SD	0.27	**% Strong**	12
Screening Plate	Plate 1	**Sum Weak**	6
Screening Plate b/c	Y02477	**% Weak**	7
Source Plate b/c	ZZ1IXW	**Sum None**	71
Quad	96:96	**% None**	81
Analysis Category	Insulin	**Excluded wells**	0

Source Plate b/c:**ZZ1IXW** - Source Plate Number:**7** - Analysis Category:**Human TfR** - Screening Plate b/c:**Y02020** - Screening Plate:**Plate 7** - Quad:**96:96** - Selection:**unset**

protocol:[] - **Datapoint:**RAW1

	1	2	3	4	5	6	7	8	9	10	11	12
A	0.28	0.82	0.27	0.29	0.32	0.29	0.25	0.20	0.55	0.28	0.37	1.47
B	0.30	0.21	0.97	0.23	0.65	0.22	0.22	1.03	0.16	0.16	0.29	1.35
C	0.31	0.11	0.24	0.24	0.15	0.06	1.08	0.24	0.07	0.32	0.21	0.78
D	0.35	1.04	0.21	0.20	0.19	0.06	0.24	0.39	0.97	0.22	0.27	0.90
E	0.28	1.05	0.20	0.23	0.19	0.92	0.26	0.08	0.20	0.38	0.37	0.10
F	0.34	0.24	0.25	1.08	0.24	0.21	0.24	0.26	0.20	0.25	0.17	0.07
G	0.36	0.24	0.24	0.22	0.36	0.25	0.23	0.07	0.12	0.30	0.91	0.05
H	0.66	0.36	0.34	0.46	0.32	0.06	0.06	0.28	0.06	0.42	0.35	0.05

protocol:[]

Plate

Exclude from hits

Independent

strong >= 0.5

weak >= 0.2

Properties

Sample Mean	0.34	**Sum Strong**	13
Sample SD	0.26	**% Strong**	15
Screening Plate	Plate 7	**Sum Weak**	56
Screening Plate b/c	Y02020	**% Weak**	64
Source Plate b/c	ZZ1IXW	**Sum None**	19
Quad	96:96	**% None**	22
Analysis Category	Human TfR	**Excluded wells**	0

Source Plate b/c:**ZZ1IXW** - Source Plate Number:**13** - Analysis Category:**Mouse TfR** - Screening Plate b/c:**Y02306** - Screening Plate:**Plate 13** - Quad:**96:96** - Selection:**unset**

protocol:[] - **Datapoint:**RAW1

	1	2	3	4	5	6	7	8	9	10	11	12
A	0.20	0.53	0.17	0.14	0.17	0.17	0.18	0.35	0.37	0.20	0.08	0.09
B	0.14	0.15	0.75	0.16	0.36	0.16	0.14	0.16	0.16	0.12	0.22	0.08
C	0.16	0.09	0.20	0.17	0.13	0.07	0.67	0.10	0.08	0.19	0.19	0.09
D	0.16	0.73	0.15	0.16	0.13	0.08	0.13	0.78	0.67	0.17	0.16	0.08
E	0.16	0.73	0.15	0.16	0.14	0.74	0.14	0.14	0.14	0.13	0.24	1.19
F	0.13	0.13	0.18	0.69	0.14	0.16	0.15	0.15	0.14	0.16	0.11	1.10
G	0.17	0.15	0.16	0.17	0.23	0.16	0.17	0.17	0.20	0.20	0.56	0.06
H	0.38	0.20	0.23	0.26	0.19	0.07	0.07	0.07	0.06	0.09	0.18	0.06

protocol:[]

Plate

Exclude from hits

Independent

strong >= 0.5

weak >= 0.2

Properties

Sample Mean	0.22	**Sum Strong**	10
Sample SD	0.18	**% Strong**	11
Screening Plate	Plate 13	**Sum Weak**	12
Screening Plate b/c	Y02306	**% Weak**	14
Source Plate b/c	ZZ1IXW	**Sum None**	66
Quad	96:96	**% None**	75
Analysis Category	Mouse TfR	**Excluded wells**	0

Appendix

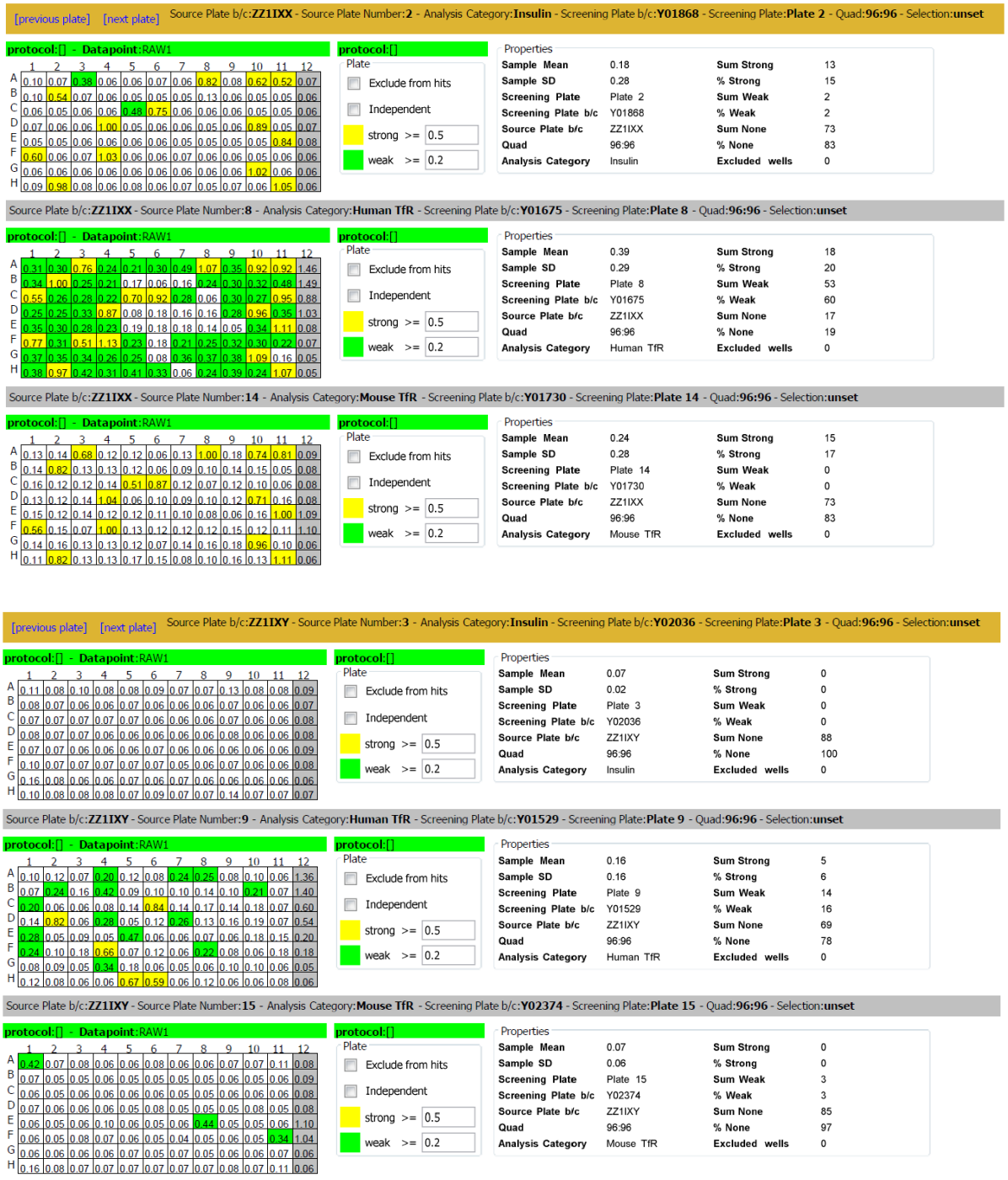
[previous plate] [next plate] Source Plate b/c:ZZ1IXX - Source Plate Number:2 - Analysis Category:Insulin - Screening Plate b/c:Y01868 - Screening Plate:Plate 2 - Quad:96:96 - Selection:unset
protocol:[] - Datapoint:RAW1
protocol:[]
Plate
Exclude from hits
Independent
strong >= 0.5
weak >= 0.2
Properties
Sample Mean 0.18
Sample SD 0.28
Screening Plate Plate 2
Screening Plate b/c Y01868
Source Plate b/c ZZ1IXX
Quad 96:96
Analysis Category Insulin
Sum Strong 13
% Strong 15
Sum Weak 2
% Weak 2
Sum None 73
% None 83
Excluded wells 0
Source Plate b/c:ZZ1IXX - Source Plate Number:8 - Analysis Category:Human TfR - Screening Plate b/c:Y01675 - Screening Plate:Plate 8 - Quad:96:96 - Selection:unset
protocol:[] - Datapoint:RAW1
protocol:[]
Plate
Exclude from hits
Independent
strong >= 0.5
weak >= 0.2
Properties
Sample Mean 0.39
Sample SD 0.29
Screening Plate Plate 8
Screening Plate b/c Y01675
Source Plate b/c ZZ1IXX
Quad 96:96
Analysis Category Human TfR
Sum Strong 18
% Strong 20
Sum Weak 53
% Weak 60
Sum None 17
% None 19
Excluded wells 0
Source Plate b/c:ZZ1IXX - Source Plate Number:14 - Analysis Category:Mouse TfR - Screening Plate b/c:Y01730 - Screening Plate:Plate 14 - Quad:96:96 - Selection:unset
protocol:[] - Datapoint:RAW1
protocol:[]
Plate
Exclude from hits
Independent
strong >= 0.5
weak >= 0.2
Properties
Sample Mean 0.24
Sample SD 0.28
Screening Plate Plate 14
Screening Plate b/c Y01730
Source Plate b/c ZZ1IXX
Quad 96:96
Analysis Category Mouse TfR
Sum Strong 15
% Strong 17
Sum Weak 0
% Weak 0
Sum None 73
% None 83
Excluded wells 0
[previous plate] [next plate] Source Plate b/c:ZZ1IXY - Source Plate Number:3 - Analysis Category:Insulin - Screening Plate b/c:Y02036 - Screening Plate:Plate 3 - Quad:96:96 - Selection:unset
protocol:[] - Datapoint:RAW1
protocol:[]
Plate
Exclude from hits
Independent
strong >= 0.5
weak >= 0.2
Properties
Sample Mean 0.07
Sample SD 0.02
Screening Plate Plate 3
Screening Plate b/c Y02036
Source Plate b/c ZZ1IXY
Quad 96:96
Analysis Category Insulin
Sum Strong 0
% Strong 0
Sum Weak 0
% Weak 0
Sum None 88
% None 100
Excluded wells 0
Source Plate b/c:ZZ1IXY - Source Plate Number:9 - Analysis Category:Human TfR - Screening Plate b/c:Y01529 - Screening Plate:Plate 9 - Quad:96:96 - Selection:unset
protocol:[] - Datapoint:RAW1
protocol:[]
Plate
Exclude from hits
Independent
strong >= 0.5
weak >= 0.2
Properties
Sample Mean 0.16
Sample SD 0.16
Screening Plate Plate 9
Screening Plate b/c Y01529
Source Plate b/c ZZ1IXY
Quad 96:96
Analysis Category Human TfR
Sum Strong 5
% Strong 6
Sum Weak 14
% Weak 16
Sum None 69
% None 78
Excluded wells 0
Source Plate b/c:ZZ1IXY - Source Plate Number:15 - Analysis Category:Mouse TfR - Screening Plate b/c:Y02374 - Screening Plate:Plate 15 - Quad:96:96 - Selection:unset
protocol:[] - Datapoint:RAW1
protocol:[]
Plate
Exclude from hits
Independent
strong >= 0.5
weak >= 0.2
Properties
Sample Mean 0.07
Sample SD 0.06
Screening Plate Plate 15
Screening Plate b/c Y02374
Source Plate b/c ZZ1IXY
Quad 96:96
Analysis Category Mouse TfR
Sum Strong 0
% Strong 0
Sum Weak 3
% Weak 3
Sum None 85
% None 97
Excluded wells 0

Appendix

[previous plate] [next plate] Source Plate b/c:**ZZ1IXZ** - Source Plate Number:**4** - Analysis Category:**Insulin** - Screening Plate b/c:**Y01876** - Screening Plate:**Plate 4** - Quad:**96:96** - Selection:**unset**

protocol:[] - **Datapoint:RAW1**

	1	2	3	4	5	6	7	8	9	10	11	12
A	0.12	0.12	0.10	0.08	0.09	0.09	0.09	0.09	0.07	0.09	0.11	0.22
B	0.12	0.07	0.06	0.06	0.06	0.06	0.05	0.06	0.06	0.05	0.08	0.15
C	0.08	0.07	0.06	0.05	0.06	0.06	0.07	0.06	0.06	0.06	0.06	0.11
D	0.10	0.07	0.07	0.06	0.06	0.06	0.06	0.07	0.05	0.06	0.05	0.17
E	0.08	0.07	0.06	0.06	0.07	0.05	0.06	0.05	0.06	0.05	0.06	0.17
F	0.12	0.06	0.06	0.06	0.06	0.06	0.07	0.06	0.08	0.06	0.06	0.12
G	0.08	0.08	0.08	0.07	0.06	0.06	0.07	0.07	0.07	0.07	0.06	0.06
H	0.10	0.11	0.10	0.10	0.09	0.08	0.09	0.09	0.11	0.08	0.07	0.05

protocol:[]

Plate

Exclude from hits

Independent

strong >= 0.5

weak >= 0.2

Properties

Sample Mean	0.07	**Sum Strong**	0
Sample SD	0.02	**% Strong**	0
Screening Plate	Plate 4	**Sum Weak**	0
Screening Plate b/c	Y01876	**% Weak**	0
Source Plate b/c	ZZ1IXZ	**Sum None**	88
Quad	96:96	**% None**	100
Analysis Category	Insulin	**Excluded wells**	0

Source Plate b/c:**ZZ1IXZ** - Source Plate Number:**10** - Analysis Category:**Human TfR** - Screening Plate b/c:**Y01583** - Screening Plate:**Plate 10** - Quad:**96:96** - Selection:**unset**

protocol:[] - **Datapoint:RAW1**

	1	2	3	4	5	6	7	8	9	10	11	12
A	0.17	0.11	0.52	0.08	0.12	0.16	0.15	0.13	0.08	0.11	0.12	1.44
B	0.08	0.44	0.08	0.08	0.36	0.36	0.82	0.06	0.07	0.06	0.19	1.44
C	0.05	0.17	0.05	0.06	0.14	0.05	0.08	0.43	0.10	0.06	0.84	0.58
D	0.18	0.06	0.06	0.08	0.07	0.11	0.06	0.11	0.07	0.06	0.24	0.65
E	0.07	0.16	0.13	0.06	0.53	0.13	0.11	0.32	0.12	0.23	0.10	0.22
F	0.15	0.10	0.56	0.06	0.07	0.51	0.15	0.05	0.06	0.05	0.05	0.18
G	0.18	0.07	0.16	0.06	0.31	0.06	0.08	0.64	0.14	0.06	0.08	0.05
H	0.15	0.06	0.08	0.08	0.06	0.06	0.07	0.05	0.26	0.12	0.23	0.04

protocol:[]

Plate

Exclude from hits

Independent

strong >= 0.5

weak >= 0.2

Properties

Sample Mean	0.16	**Sum Strong**	7
Sample SD	0.17	**% Strong**	8
Screening Plate	Plate 10	**Sum Weak**	10
Screening Plate b/c	Y01583	**% Weak**	11
Source Plate b/c	ZZ1IXZ	**Sum None**	71
Quad	96:96	**% None**	81
Analysis Category	Human TfR	**Excluded wells**	0

Source Plate b/c:**ZZ1IXZ** - Source Plate Number:**16** - Analysis Category:**Mouse TfR** - Screening Plate b/c:**Y02311** - Screening Plate:**Plate 16** - Quad:**96:96** - Selection:**unset**

protocol:[] - **Datapoint:RAW1**

	1	2	3	4	5	6	7	8	9	10	11	12
A	0.17	0.50	0.07	0.08	0.06	0.08	0.08	0.08	0.06	0.08	0.08	0.09
B	0.08	0.06	0.59	0.09	0.06	0.06	0.06	0.06	0.07	0.36	0.08	0.09
C	0.07	0.06	0.07	0.07	0.06	0.06	0.06	0.06	0.07	0.08	0.09	0.09
D	0.08	0.06	0.10	0.07	0.07	0.06	0.06	0.10	0.08	0.08	0.08	0.10
E	0.06	0.06	0.06	0.06	0.08	0.06	0.06	0.06	0.06	0.06	0.06	1.12
F	0.09	0.06	0.06	0.06	0.07	0.05	0.06	0.06	0.06	0.06	0.06	0.99
G	0.40	0.07	0.06	0.06	0.06	0.07	0.07	0.06	0.06	0.06	0.57	0.06
H	0.08	0.07	0.07	0.08	0.08	0.08	0.08	0.07	0.09	0.62	0.34	0.06

protocol:[]

Plate

Exclude from hits

Independent

strong >= 0.5

weak >= 0.2

Properties

Sample Mean	0.10	**Sum Strong**	4
Sample SD	0.12	**% Strong**	5
Screening Plate	Plate 16	**Sum Weak**	3
Screening Plate b/c	Y02311	**% Weak**	3
Source Plate b/c	ZZ1IXZ	**Sum None**	81
Quad	96:96	**% None**	92
Analysis Category	Mouse TfR	**Excluded wells**	0

[previous plate] [next plate] Source Plate b/c:**ZZ1IY0** - Source Plate Number:**5** - Analysis Category:**Insulin** - Screening Plate b/c:**Y01586** - Screening Plate:**Plate 5** - Quad:**96:96** - Selection:**unset**

protocol:[] - **Datapoint:RAW1**

	1	2	3	4	5	6	7	8	9	10	11	12
A	0.09	0.30	0.07	0.06	0.06	0.06	0.08	0.06	0.09	0.10	0.17	0.17
B	0.17	0.10	0.06	0.05	0.05	0.08	0.10	0.06	0.11	0.05	0.10	0.11
C	0.06	0.06	0.05	0.06	0.08	0.05	0.07	0.30	0.06	0.06	0.06	0.10
D	0.08	0.06	0.09	0.06	0.08	0.07	0.32	0.05	0.09	0.34	0.06	0.11
E	0.07	0.06	0.06	0.06	0.09	0.07	0.06	0.05	0.05	0.06	0.99	0.13
F	0.07	0.08	0.19	0.06	0.08	0.09	0.09	0.07	0.05	0.12	0.06	0.12
G	0.07	0.76	0.06	0.12	0.06	0.73	0.06	0.31	0.06	0.10	0.07	0.06
H	0.11	0.06	0.21	0.05	0.21	0.08	0.09	0.06	0.09	0.54	0.11	0.06

protocol:[]

Plate

Exclude from hits

Independent

strong >= 0.5

weak >= 0.2

Properties

Sample Mean	0.12	**Sum Strong**	4
Sample SD	0.16	**% Strong**	5
Screening Plate	Plate 5	**Sum Weak**	7
Screening Plate b/c	Y01586	**% Weak**	8
Source Plate b/c	ZZ1IY0	**Sum None**	77
Quad	96:96	**% None**	88
Analysis Category	Insulin	**Excluded wells**	0

Source Plate b/c:**ZZ1IY0** - Source Plate Number:**11** - Analysis Category:**Human TfR** - Screening Plate b/c:**Y02019** - Screening Plate:**Plate 11** - Quad:**96:96** - Selection:**unset**

protocol:[] - **Datapoint:RAW1**

	1	2	3	4	5	6	7	8	9	10	11	12
A	0.24	0.30	0.07	0.07	0.08	0.20	0.23	0.36	0.12	0.09	0.29	1.15
B	0.24	0.20	0.30	0.43	0.08	0.06	0.05	0.06	0.07	0.06	0.08	1.33
C	0.09	0.10	0.08	0.08	0.07	0.25	0.10	0.42	0.47	0.26	0.08	0.83
D	0.27	0.52	0.44	0.34	0.06	0.28	0.38	0.06	0.41	0.39	0.07	0.87
E	0.48	0.20	0.18	0.25	0.50	0.06	0.61	0.07	0.24	0.56	1.15	0.11
F	0.43	0.06	0.45	0.04	0.07	0.11	0.23	0.51	0.06	0.06	0.65	0.13
G	0.17	0.74	0.25	0.04	0.41	0.82	0.38	0.44	0.49	0.48	0.54	0.05
H	0.14	0.07	0.32	0.04	0.39	0.12	0.06	0.09	0.07	0.62	0.51	0.05

protocol:[]

Plate

Exclude from hits

Independent

strong >= 0.5

weak >= 0.2

Properties

Sample Mean	0.26	**Sum Strong**	12
Sample SD	0.21	**% Strong**	14
Screening Plate	Plate 11	**Sum Weak**	34
Screening Plate b/c	Y02019	**% Weak**	39
Source Plate b/c	ZZ1IY0	**Sum None**	42
Quad	96:96	**% None**	48
Analysis Category	Human TfR	**Excluded wells**	0

Source Plate b/c:**ZZ1IY0** - Source Plate Number:**17** - Analysis Category:**Mouse TfR** - Screening Plate b/c:**Y02232** - Screening Plate:**Plate 17** - Quad:**96:96** - Selection:**unset**

protocol:[] - **Datapoint:RAW1**

	1	2	3	4	5	6	7	8	9	10	11	12
A	0.09	0.42	0.12	0.07	0.08	0.11	0.09	0.09	0.12	0.12	0.23	0.19
B	0.28	0.55	0.08	0.08	0.07	0.06	0.08	0.11	0.13	0.06	0.10	0.19
C	0.09	0.09	0.07	0.10	0.11	0.08	0.09	0.42	0.66	0.07	0.08	0.18
D	0.15	0.08	0.75	0.58	0.08	0.17	0.34	0.08	0.73	0.35	0.09	0.15
E	0.10	0.09	0.08	0.63	0.38	0.08	0.07	0.07	0.06	0.08	1.01	1.01
F	0.36	0.08	0.75	0.07	0.11	0.06	0.07	0.80	0.07	0.06	0.06	1.03
G	0.09	0.73	0.09	0.07	0.08	0.82	0.68	0.41	0.64	0.68	0.75	0.06
H	0.18	0.12	0.26	0.07	0.26	0.11	0.08	0.10	0.11	0.68	0.73	0.06

protocol:[]

Plate

Exclude from hits

Independent

strong >= 0.5

weak >= 0.2

Properties

Sample Mean	0.24	**Sum Strong**	17
Sample SD	0.25	**% Strong**	19
Screening Plate	Plate 17	**Sum Weak**	11
Screening Plate b/c	Y02232	**% Weak**	12
Source Plate b/c	ZZ1IY0	**Sum None**	60
Quad	96:96	**% None**	68
Analysis Category	Mouse TfR	**Excluded wells**	0

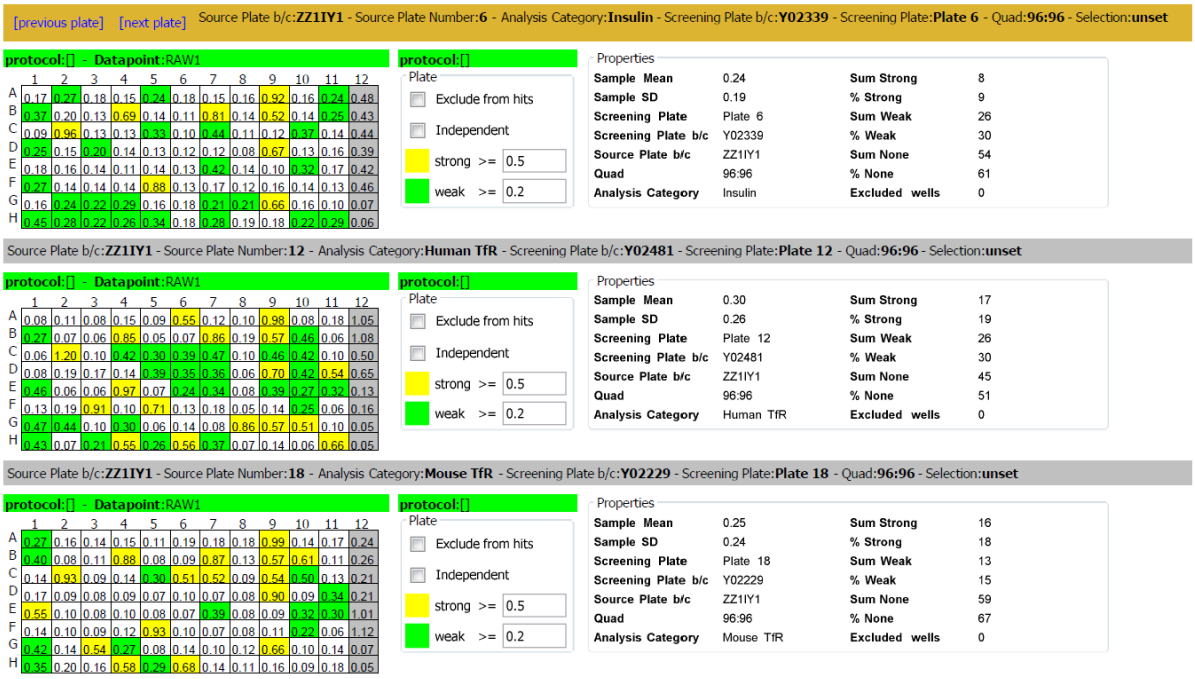

D

Screening Report

Copyright 1998-2014 Cambridge Antibody Technology

Summary of Screen	**Round 4 mTfR Selection to bEnd.3 cell selection**
Screen Name	
Analysis Name	Corrected
Project	OU Studentship

Summary of Screen

-	Screening Plate b/c	Screening Plate	Source Plate b/c	Quad	Analysis Category	Cut-off	Sample Mean	Sample SD	Sum None	% None	Sum Weak	% Weak	Sum Strong	% Strong	Positive1 Mean	Positive1 SD	Positive2 Mean	Positive2 SD	Negative1 Mean	Negative1 SD
	Y03386	Plate 1	ZZ1K3X	96:96	Insulin	0.5,0.2	0.17	0.04	71	81	17	19	0	0	0.06	0.01	0.06	0.00	0.08	0.01
	Y01963	Plate 2	ZZ1K3X	96:96	Human TfR	0.5,0.2	0.13	0.07	74	84	14	16	0	0	0.09	0.01	0.06	0.01	0.11	0.03
	Y02998	Plate 3	ZZ1K3X	96:96	Mouse TfR	0.5,0.2	0.47	0.15	6	7	38	43	44	50	0.08	0.02	0.06	0.01	0.09	0.01
	Y02079	Plate 4	ZZ1K3Y	96:96	Insulin	0.5,0.2	0.10	0.03	88	100	0	0	0	0	0.34	0.10	0.32	0.02	0.13	0.01
	Y03498	Plate 5	ZZ1K3Y	96:96	Human TfR	0.5,0.2	0.12	0.05	83	94	5	6	0	0	0.41	0.02	0.25	0.03	0.07	0.01
	Y02411	Plate 6	ZZ1K3Y	96:96	Mouse TfR	0.5,0.2	0.77	0.25	3	3	12	14	73	83	0.25	0.04	0.36	0.05	0.12	0.02
	Y01761	Plate 7	ZZ1K3Z	96:96	Insulin	0.5,0.2	0.17	0.32	80	91	2	2	6	7	0.27	0.00	0.18	0.02	0.11	0.01
	Y03036	Plate 8	ZZ1K3Z	96:96	Human TfR	0.5,0.2	0.73	0.37	15	17	5	6	68	77	0.36	0.05	0.20	0.05	0.08	0.00
	Y02412	Plate 9	ZZ1K3Z	96:96	Mouse TfR	0.5,0.2	1.22	0.34	4	5	2	2	82	93	0.32	0.01	0.53	0.06	0.11	0.05
	Y01827	Plate 10	ZZ1K3U	96:96	Insulin	0.5,0.2	0.14	0.28	82	93	2	2	4	5	0.22	0.02	0.18	0.02	0.08	0.01
	Y02116	Plate 11	ZZ1K3U	96:96	Human TfR	0.5,0.2	1.32	0.48	5	6	9	10	74	84	0.46	0.08	0.35	0.05	0.13	0.07
	Y01541	Plate 12	ZZ1K3U	96:96	Mouse TfR	0.5,0.2	1.51	0.36	4	5	0	0	84	95	0.25	0.11	0.54	0.01	0.17	0.01
	Y02497	Plate 13	ZZ1K3V	96:96	Insulin	0.5,0.2	0.07	0.02	88	100	0	0	0	0	0.18	0.06	0.10	0.00	0.08	0.01
	Y02491	Plate 14	ZZ1K3V	96:96	Human TfR	0.5,0.2	0.12	0.04	82	93	6	7	0	0	0.27	0.13	0.12	0.01	0.10	0.00
	Y01698	Plate 15	ZZ1K3V	96:96	Mouse TfR	0.5,0.2	0.89	0.26	4	5	2	2	82	93	0.27	0.04	0.86	0.00	0.20	0.02
	Y02447	Plate 16	ZZ1K3W	96:96	Insulin	0.5,0.2	0.08	0.03	88	100	0	0	0	0	0.15	0.09	0.08	0.01	0.09	0.03
	Y02443	Plate 17	ZZ1K3W	96:96	Human TfR	0.5,0.2	0.12	0.07	77	88	11	12	0	0	0.36	0.02	0.12	0.01	0.13	0.04
	Y01760	Plate 18	ZZ1K3W	96:96	Mouse TfR	0.5,0.2	0.48	0.16	7	8	30	34	51	58	0.14	0.06	0.37	0.01	0.06	0.00
Mean							0.48	0.19	48	54	9	10	32	36	0.25	0.05	0.26	0.02	0.11	0.02
SD							0.48	0.15	39	44	11	12	36	41	0.11	0.04	0.21	0.02	0.03	0.02

Appendix

[previous plate] [next plate] Source Plate b/c:**ZZ1K3X** - Source Plate Number:**1** - Analysis Category:**Insulin** - Screening Plate b/c:**Y03386** - Screening Plate:**Plate 1** - Quad:**96:96** - Selection:**unset**

protocol:[] - **Datapoint**:RAW1

	1	2	3	4	5	6	7	8	9	10	11	12
A	0.14	0.11	0.08	0.19	0.08	0.20	0.19	0.13	0.19	0.15	0.19	0.07
B	0.28	0.14	0.24	0.22	0.16	0.16	0.17	0.17	0.17	0.14	0.18	0.06
C	0.26	0.22	0.17	0.22	0.15	0.15	0.10	0.15	0.13	0.15	0.11	0.06
D	0.24	0.13	0.20	0.07	0.17	0.13	0.10	0.13	0.14	0.16	0.19	0.05
E	0.15	0.16	0.20	0.20	0.11	0.16	0.12	0.16	0.13	0.13	0.20	0.08
F	0.22	0.15	0.19	0.16	0.18	0.14	0.10	0.12	0.13	0.14	0.19	0.08
G	0.19	0.20	0.22	0.17	0.19	0.18	0.13	0.15	0.14	0.18	0.17	0.05
H	0.20	0.17	0.20	0.25	0.17	0.17	0.16	0.16	0.22	0.18	0.31	0.04

protocol:[]

Plate

Exclude from hits

Independent

strong >= 0.5

weak >= 0.2

Properties

Sample Mean	0.17	**Source Plate b/c**	ZZ1K3X
Sample SD	0.04	**Quad**	96:96
Positive1 Mean	0.06	**Analysis Category**	Insulin
Positive1 SD	0.01	**Sum Strong**	0
Positive2 Mean	0.06	**% Strong**	0
Positive2 SD	0.00	**Sum Weak**	17
Negative1 Mean	0.08	**% Weak**	19
Negative1 SD	0.01	**Sum None**	71
Z'	3.75	**% None**	81
Screening Plate	Plate 1	**Excluded wells**	0
Screening Plate b/c	Y03386	**Cut-off**	0.5,0.2

Source Plate b/c:**ZZ1K3X** - Source Plate Number:**2** - Analysis Category:**Human TfR** - Screening Plate b/c:**Y01963** - Screening Plate:**Plate 2** - Quad:**96:96** - Selection:**unset**

protocol:[] - **Datapoint**:RAW1

	1	2	3	4	5	6	7	8	9	10	11	12
A	0.30	0.27	0.18	0.25	0.13	0.32	0.28	0.29	0.31	0.15	0.22	0.09
B	0.10	0.07	0.07	0.24	0.17	0.10	0.09	0.06	0.08	0.19	0.08	0.10
C	0.10	0.14	0.10	0.07	0.09	0.10	0.12	0.12	0.08	0.18	0.10	0.07
D	0.11	0.08	0.07	0.08	0.08	0.09	0.08	0.07	0.07	0.12	0.07	0.06
E	0.07	0.08	0.08	0.07	0.10	0.08	0.06	0.13	0.20	0.06	0.08	0.09
F	0.12	0.08	0.09	0.12	0.09	0.08	0.07	0.14	0.08	0.07	0.08	0.13
G	0.12	0.08	0.10	0.27	0.11	0.09	0.06	0.06	0.07	0.08	0.07	0.05
H	0.17	0.14	0.14	0.13	0.12	0.28	0.13	0.10	0.25	0.14	0.32	0.04

protocol:[]

Plate

Exclude from hits

Independent

strong >= 0.5

weak >= 0.2

Properties

Sample Mean	0.13	**Source Plate b/c**	ZZ1K3X
Sample SD	0.07	**Quad**	96:96
Positive1 Mean	0.09	**Analysis Category**	Human TfR
Positive1 SD	0.01	**Sum Strong**	0
Positive2 Mean	0.06	**% Strong**	0
Positive2 SD	0.01	**Sum Weak**	14
Negative1 Mean	0.11	**% Weak**	16
Negative1 SD	0.03	**Sum None**	74
Z'	8.07	**% None**	84
Screening Plate	Plate 2	**Excluded wells**	0
Screening Plate b/c	Y01963	**Cut-off**	0.5,0.2

Source Plate b/c:**ZZ1K3X** - Source Plate Number:**3** - Analysis Category:**Mouse TfR** - Screening Plate b/c:**Y02998** - Screening Plate:**Plate 3** - Quad:**96:96** - Selection:**unset**

protocol:[] - **Datapoint**:RAW1

	1	2	3	4	5	6	7	8	9	10	11	12
A	0.42	0.64	0.67	0.60	0.28	0.54	0.46	0.64	0.67	0.45	0.66	0.09
B	0.67	0.52	0.67	0.44	0.67	0.60	0.50	0.18	0.52	0.52	0.59	0.06
C	0.24	0.56	0.60	0.34	0.54	0.41	0.38	0.51	0.32	0.31	0.43	0.06
D	0.47	0.44	0.68	0.41	0.53	0.36	0.37	0.45	0.11	0.49	0.16	0.06
E	0.58	0.65	0.64	0.42	0.64	0.61	0.53	0.45	0.35	0.16	0.57	0.09
F	0.45	0.55	0.58	0.42	0.57	0.41	0.36	0.56	0.33	0.44	0.54	0.08
G	0.73	0.62	0.64	0.64	0.56	0.56	0.07	0.24	0.40	0.14	0.25	0.05
H	0.58	0.49	0.58	0.53	0.27	0.39	0.32	0.33	0.35	0.37	0.60	0.04

protocol:[]

Plate

Exclude from hits

Independent

strong >= 0.5

weak >= 0.2

Properties

Sample Mean	0.47	**Source Plate b/c**	ZZ1K3X
Sample SD	0.15	**Quad**	96:96
Positive1 Mean	0.08	**Analysis Category**	Mouse TfR
Positive1 SD	0.02	**Sum Strong**	44
Positive2 Mean	0.06	**% Strong**	50
Positive2 SD	0.01	**Sum Weak**	38
Negative1 Mean	0.09	**% Weak**	43
Negative1 SD	0.01	**Sum None**	6
Z'	5.90	**% None**	7
Screening Plate	Plate 3	**Excluded wells**	0
Screening Plate b/c	Y02998	**Cut-off**	0.5,0.2

[previous plate] [next plate] Source Plate b/c:**ZZ1K3Y** - Source Plate Number:**4** - Analysis Category:**Insulin** - Screening Plate b/c:**Y02079** - Screening Plate:**Plate 4** - Quad:**96:96** - Selection:**unset**

protocol:[] - **Datapoint**:RAW1

	1	2	3	4	5	6	7	8	9	10	11	12
A	0.14	0.15	0.14	0.13	0.14	0.15	0.16	0.14	0.16	0.17	0.13	0.41
B	0.13	0.10	0.08	0.08	0.08	0.08	0.09	0.08	0.08	0.10	0.09	0.28
C	0.12	0.09	0.07	0.07	0.08	0.08	0.08	0.07	0.07	0.08	0.08	0.30
D	0.11	0.08	0.07	0.07	0.07	0.07	0.07	0.07	0.07	0.08	0.08	0.33
E	0.10	0.08	0.07	0.07	0.08	0.08	0.08	0.08	0.08	0.07	0.08	0.14
F	0.12	0.08	0.07	0.08	0.08	0.07	0.08	0.07	0.07	0.07	0.07	0.12
G	0.14	0.08	0.09	0.08	0.08	0.07	0.08	0.07	0.08	0.08	0.07	0.05
H	0.19	0.16	0.15	0.15	0.13	0.14	0.15	0.16	0.13	0.13	0.17	0.04

protocol:[]

Plate

Exclude from hits

Independent

strong >= 0.5

weak >= 0.2

Properties

Sample Mean	0.10	**Source Plate b/c**	ZZ1K3Y
Sample SD	0.03	**Quad**	96:96
Positive1 Mean	0.34	**Analysis Category**	Insulin
Positive1 SD	0.10	**Sum Strong**	0
Positive2 Mean	0.32	**% Strong**	0
Positive2 SD	0.02	**Sum Weak**	0
Negative1 Mean	0.13	**% Weak**	0
Negative1 SD	0.01	**Sum None**	88
Z'	-0.55	**% None**	100
Screening Plate	Plate 4	**Excluded wells**	0
Screening Plate b/c	Y02079	**Cut-off**	0.5,0.2

Source Plate b/c:**ZZ1K3Y** - Source Plate Number:**5** - Analysis Category:**Human TfR** - Screening Plate b/c:**Y03498** - Screening Plate:**Plate 5** - Quad:**96:96** - Selection:**unset**

protocol:[] - **Datapoint**:RAW1

	1	2	3	4	5	6	7	8	9	10	11	12
A	0.10	0.15	0.12	0.13	0.13	0.12	0.14	0.24	0.12	0.16	0.16	0.40
B	0.12	0.08	0.11	0.23	0.07	0.07	0.09	0.10	0.11	0.09	0.17	0.42
C	0.10	0.09	0.07	0.08	0.10	0.06	0.06	0.20	0.11	0.07	0.08	0.27
D	0.09	0.06	0.09	0.10	0.08	0.06	0.08	0.09	0.10	0.18	0.17	0.22
E	0.09	0.10	0.09	0.07	0.10	0.07	0.08	0.17	0.09	0.06	0.08	0.08
F	0.11	0.17	0.08	0.09	0.18	0.09	0.13	0.06	0.08	0.18	0.06	0.06
G	0.12	0.09	0.11	0.11	0.23	0.10	0.09	0.08	0.09	0.08	0.06	0.05
H	0.21	0.12	0.16	0.19	0.26	0.15	0.17	0.14	0.17	0.10	0.15	0.04

protocol:[]

Plate

Exclude from hits

Independent

strong >= 0.5

weak >= 0.2

Properties

Sample Mean	0.12	**Source Plate b/c**	ZZ1K3Y
Sample SD	0.05	**Quad**	96:96
Positive1 Mean	0.41	**Analysis Category**	Human TfR
Positive1 SD	0.02	**Sum Strong**	0
Positive2 Mean	0.25	**% Strong**	0
Positive2 SD	0.03	**Sum Weak**	5
Negative1 Mean	0.07	**% Weak**	6
Negative1 SD	0.01	**Sum None**	83
Z'	0.72	**% None**	94
Screening Plate	Plate 5	**Excluded wells**	0
Screening Plate b/c	Y03498	**Cut-off**	0.5,0.2

Source Plate b/c:**ZZ1K3Y** - Source Plate Number:**6** - Analysis Category:**Mouse TfR** - Screening Plate b/c:**Y02411** - Screening Plate:**Plate 6** - Quad:**96:96** - Selection:**unset**

protocol:[] - **Datapoint**:RAW1

	1	2	3	4	5	6	7	8	9	10	11	12
A	0.51	0.96	0.46	1.02	1.06	0.97	0.99	1.15	0.53	0.73	0.76	0.28
B	0.21	1.00	0.82	1.06	1.03	0.52	0.83	1.04	0.94	0.94	0.79	0.22
C	0.62	0.45	0.59	0.85	0.90	0.48	0.77	1.03	0.79	0.39	0.68	0.40
D	0.18	0.40	0.81	0.81	0.95	0.86	0.85	0.87	0.71	0.82	0.84	0.33
E	0.30	0.97	0.96	0.55	0.92	0.92	0.90	1.03	0.82	0.55	0.66	0.14
F	0.34	0.98	0.57	0.99	0.96	0.80	0.88	0.67	0.51	0.94	0.20	0.11
G	0.24	0.56	1.00	0.96	1.18	1.02	0.84	0.63	0.89	0.88	0.48	0.05
H	0.83	0.11	0.43	0.99	1.12	0.92	1.01	1.05	0.86	0.47	0.84	0.04

protocol:[]

Plate

Exclude from hits

Independent

strong >= 0.5

weak >= 0.2

Properties

Sample Mean	0.77	**Source Plate b/c**	ZZ1K3Y
Sample SD	0.25	**Quad**	96:96
Positive1 Mean	0.25	**Analysis Category**	Mouse TfR
Positive1 SD	0.04	**Sum Strong**	73
Positive2 Mean	0.36	**% Strong**	83
Positive2 SD	0.05	**Sum Weak**	12
Negative1 Mean	0.12	**% Weak**	14
Negative1 SD	0.02	**Sum None**	3
Z'	-0.49	**% None**	3
Screening Plate	Plate 6	**Excluded wells**	0
Screening Plate b/c	Y02411	**Cut-off**	0.5,0.2

Appendix

[previous plate] [next plate] Source Plate b/c:**ZZ1K3Z** - Source Plate Number:**7** - Analysis Category:**Insulin** - Screening Plate b/c:**Y01761** - Screening Plate:**Plate 7** - Quad:**96:96** - Selection:**unset**

protocol:[] - **Datapoint:**RAW1

	1	2	3	4	5	6	7	8	9	10	11	12
A	0.12	0.10	0.11	0.10	0.10	0.10	0.12	0.12	0.10	0.12	0.12	0.27
B	0.11	0.09	0.07	0.09	0.06	0.07	0.10	0.07	0.07	0.06	0.07	0.27
C	1.40	0.07	0.06	0.06	0.06	0.06	0.06	0.46	0.09	0.06	0.06	0.19
D	0.09	0.06	0.06	0.06	0.06	0.06	0.06	0.06	0.05	0.06	0.06	0.17
E	0.08	0.08	0.06	0.06	0.06	0.06	0.06	0.06	0.06	1.19	0.06	0.10
F	0.09	0.47	1.28	0.07	0.06	0.06	0.06	0.06	1.13	0.07	0.06	0.12
G	1.57	0.07	0.07	0.06	1.41	0.07	0.06	0.07	0.06	0.06	0.06	0.05
H	0.14	0.11	0.10	0.09	0.09	0.10	0.08	0.09	0.08	0.09	0.08	0.04

protocol:[]

Plate

Exclude from hits

Independent

strong >= 0.5

weak >= 0.2

Properties

Sample Mean	0.17	**Source Plate b/c**	ZZ1K3Z
Sample SD	0.32	**Quad**	96:96
Positive1 Mean	0.27	**Analysis Category**	Insulin
Positive1 SD	0.00	**Sum Strong**	6
Positive2 Mean	0.18	**% Strong**	7
Positive2 SD	0.02	**Sum Weak**	2
Negative1 Mean	0.11	**% Weak**	2
Negative1 SD	0.01	**Sum None**	80
Z'	0.72	**% None**	91
Screening Plate	Plate 7	**Excluded wells**	0
Screening Plate b/c	Y01761	**Cut-off**	0.5,0.2

Source Plate b/c:**ZZ1K3Z** - Source Plate Number:**8** - Analysis Category:**Human TfR** - Screening Plate b/c:**Y03036** - Screening Plate:**Plate 8** - Quad:**96:96** - Selection:**unset**

protocol:[] - **Datapoint:**RAW1

	1	2	3	4	5	6	7	8	9	10	11	12
A	0.76	0.20	0.83	0.50	0.68	0.21	0.76	0.91	1.03	0.62	0.83	0.39
B	0.96	0.07	0.70	0.98	0.78	0.98	0.92	1.06	1.09	0.97	0.76	0.32
C	1.37	0.09	0.06	0.06	0.98	0.70	0.16	0.58	0.63	0.92	0.07	0.23
D	0.96	0.85	0.24	1.05	0.18	0.97	0.79	1.04	1.03	0.16	0.60	0.16
E	0.28	0.19	1.00	1.04	0.18	0.80	0.96	0.27	1.04	1.43	0.89	0.08
F	0.89	0.72	1.19	0.93	0.83	0.09	0.80	1.01	1.31	0.79	0.92	0.08
G	1.68	0.87	1.00	0.92	1.39	0.92	0.87	0.51	1.01	0.15	0.20	0.05
H	0.88	0.82	0.72	0.89	0.70	0.85	0.12	0.84	0.80	0.68	0.16	0.04

protocol:[]

Plate

Exclude from hits

Independent

strong >= 0.5

weak >= 0.2

Properties

Sample Mean	0.73	**Source Plate b/c**	ZZ1K3Z
Sample SD	0.37	**Quad**	96:96
Positive1 Mean	0.36	**Analysis Category**	Human TfR
Positive1 SD	0.05	**Sum Strong**	68
Positive2 Mean	0.20	**% Strong**	77
Positive2 SD	0.05	**Sum Weak**	5
Negative1 Mean	0.08	**% Weak**	6
Negative1 SD	0.00	**Sum None**	15
Z'	0.46	**% None**	17
Screening Plate	Plate 8	**Excluded wells**	0
Screening Plate b/c	Y03036	**Cut-off**	0.5,0.2

Source Plate b/c:**ZZ1K3Z** - Source Plate Number:**9** - Analysis Category:**Mouse TfR** - Screening Plate b/c:**Y02412** - Screening Plate:**Plate 9** - Quad:**96:96** - Selection:**unset**

protocol:[] - **Datapoint:**RAW1

	1	2	3	4	5	6	7	8	9	10	11	12
A	1.51	0.82	1.50	1.12	1.32	0.85	1.71	1.60	1.32	1.16	1.46	0.33
B	1.46	0.10	1.06	1.27	1.52	1.40	1.63	1.52	1.45	1.39	1.30	0.31
C	1.37	0.09	0.09	0.08	1.48	1.39	1.06	0.40	1.16	1.39	0.73	0.57
D	1.36	1.32	0.84	1.29	1.07	1.33	1.58	1.39	1.20	0.90	1.08	0.48
E	0.86	0.97	1.27	1.47	1.10	1.37	1.57	0.92	1.36	1.23	1.40	0.15
F	1.33	1.24	1.30	1.47	1.34	0.45	1.53	1.40	1.26	1.44	1.37	0.08
G	1.63	1.37	1.48	1.43	1.32	1.39	1.50	1.06	1.08	1.07	1.22	0.05
H	1.40	1.29	1.30	1.38	1.46	1.34	1.15	1.29	1.25	1.37	1.04	0.04

protocol:[]

Plate

Exclude from hits

Independent

strong >= 0.5

weak >= 0.2

Properties

Sample Mean	1.22	**Source Plate b/c**	ZZ1K3Z
Sample SD	0.34	**Quad**	96:96
Positive1 Mean	0.32	**Analysis Category**	Mouse TfR
Positive1 SD	0.01	**Sum Strong**	82
Positive2 Mean	0.53	**% Strong**	93
Positive2 SD	0.06	**Sum Weak**	2
Negative1 Mean	0.11	**% Weak**	2
Negative1 SD	0.05	**Sum None**	4
Z'	0.13	**% None**	5
Screening Plate	Plate 9	**Excluded wells**	0
Screening Plate b/c	Y02412	**Cut-off**	0.5,0.2

[previous plate] [next plate] Source Plate b/c:**ZZ1K3U** - Source Plate Number:**10** - Analysis Category:**Insulin** - Screening Plate b/c:**Y01827** - Screening Plate:**Plate 10** - Quad:**96:96** - Selection:**unset**

protocol:[] - **Datapoint:**RAW1

	1	2	3	4	5	6	7	8	9	10	11	12
A	0.12	0.13	0.09	0.12	0.12	0.12	0.12	0.14	0.11	0.11	0.12	0.24
B	0.11	0.08	0.06	0.07	0.07	0.06	0.06	0.07	0.06	0.07	1.33	0.21
C	0.08	0.07	0.35	0.06	0.07	0.06	0.06	0.06	0.06	0.07	0.06	0.16
D	0.08	0.09	0.05	0.06	0.06	0.05	0.06	0.05	0.06	0.06	0.06	0.19
E	0.08	0.06	0.35	0.06	0.06	0.06	0.06	0.06	0.06	0.06	0.06	0.08
F	0.09	0.07	0.05	0.06	0.06	0.06	0.05	0.05	0.06	0.05	0.05	0.08
G	0.09	0.07	0.06	0.06	0.06	0.06	0.06	1.41	0.06	1.40	0.07	0.05
H	0.12	0.12	0.07	0.13	0.09	1.36	0.08	0.08	0.10	0.10	0.11	0.04

protocol:[]

Plate

Exclude from hits

Independent

strong >= 0.5

weak >= 0.2

Properties

Sample Mean	0.14	**Source Plate b/c**	ZZ1K3U
Sample SD	0.28	**Quad**	96:96
Positive1 Mean	0.22	**Analysis Category**	Insulin
Positive1 SD	0.02	**Sum Strong**	4
Positive2 Mean	0.18	**% Strong**	5
Positive2 SD	0.02	**Sum Weak**	2
Negative1 Mean	0.08	**% Weak**	2
Negative1 SD	0.01	**Sum None**	82
Z'	0.42	**% None**	93
Screening Plate	Plate 10	**Excluded wells**	0
Screening Plate b/c	Y01827	**Cut-off**	0.5,0.2

Source Plate b/c:**ZZ1K3U** - Source Plate Number:**11** - Analysis Category:**Human TfR** - Screening Plate b/c:**Y02116** - Screening Plate:**Plate 11** - Quad:**96:96** - Selection:**unset**

protocol:[] - **Datapoint:**RAW1

	1	2	3	4	5	6	7	8	9	10	11	12
A	1.59	1.50	0.11	1.24	1.26	1.50	1.62	1.70	1.35	1.04	1.51	0.41
B	1.57	1.17	1.68	0.40	1.61	1.39	1.64	1.66	1.45	1.56	1.57	0.52
C	1.46	1.68	1.66	1.74	0.74	1.70	1.67	1.28	1.41	1.20	1.53	0.32
D	1.42	1.72	1.60	1.52	1.68	1.75	1.26	1.77	1.69	0.39	0.44	0.39
E	0.32	1.70	1.76	1.52	1.64	1.42	1.31	1.38	1.60	1.31	1.57	0.08
F	1.08	1.42	1.66	0.41	1.71	0.42	1.30	1.57	1.26	1.71	0.11	0.18
G	0.45	1.60	1.70	0.44	1.74	0.40	1.57	1.60	1.67	1.56	1.68	0.05
H	1.34	1.55	0.09	1.41	0.09	1.52	0.10	1.56	1.41	1.50	1.41	0.04

protocol:[]

Plate

Exclude from hits

Independent

strong >= 0.5

weak >= 0.2

Properties

Sample Mean	1.32	**Source Plate b/c**	ZZ1K3U
Sample SD	0.48	**Quad**	96:96
Positive1 Mean	0.46	**Analysis Category**	Human TfR
Positive1 SD	0.08	**Sum Strong**	74
Positive2 Mean	0.35	**% Strong**	84
Positive2 SD	0.05	**Sum Weak**	9
Negative1 Mean	0.13	**% Weak**	10
Negative1 SD	0.07	**Sum None**	5
Z'	-0.33	**% None**	6
Screening Plate	Plate 11	**Excluded wells**	0
Screening Plate b/c	Y02116	**Cut-off**	0.5,0.2

Source Plate b/c:**ZZ1K3U** - Source Plate Number:**12** - Analysis Category:**Mouse TfR** - Screening Plate b/c:**Y01541** - Screening Plate:**Plate 12** - Quad:**96:96** - Selection:**unset**

protocol:[] - **Datapoint:**RAW1

	1	2	3	4	5	6	7	8	9	10	11	12
A	1.85	1.81	0.14	1.46	1.57	1.76	1.77	1.71	1.68	1.49	1.68	0.34
B	1.71	1.58	1.71	1.35	1.64	1.63	1.79	1.64	1.76	1.70	1.62	0.17
C	1.60	1.39	1.75	1.45	1.35	1.73	1.49	1.23	1.27	1.58	1.56	0.53
D	1.55	1.69	1.72	1.58	1.63	1.78	1.47	1.71	1.68	1.15	1.37	0.54
E	1.18	1.73	1.76	1.66	1.72	1.56	1.38	1.50	1.67	1.27	1.62	0.17
F	1.45	1.37	1.76	1.22	1.70	1.34	1.54	1.70	1.31	1.72	0.60	0.16
G	1.40	1.65	1.86	1.32	1.70	1.44	1.76	1.46	1.44	1.85	1.70	0.05
H	1.77	1.82	0.14	1.80	0.12	1.57	0.12	1.69	1.66	1.72	1.75	0.04

protocol:[]

Plate

Exclude from hits

Independent

strong >= 0.5

weak >= 0.2

Properties

Sample Mean	1.51	**Source Plate b/c**	ZZ1K3U
Sample SD	0.36	**Quad**	96:96
Positive1 Mean	0.25	**Analysis Category**	Mouse TfR
Positive1 SD	0.11	**Sum Strong**	84
Positive2 Mean	0.54	**% Strong**	95
Positive2 SD	0.01	**Sum Weak**	0
Negative1 Mean	0.17	**% Weak**	0
Negative1 SD	0.01	**Sum None**	4
Z'	-3.15	**% None**	5
Screening Plate	Plate 12	**Excluded wells**	0
Screening Plate b/c	Y01541	**Cut-off**	0.5,0.2

Appendix

[previous plate] [next plate] Source Plate b/c:**ZZ1K3V** - Source Plate Number:**13** - Analysis Category:**Insulin** - Screening Plate b/c:**Y02497** - Screening Plate:**Plate 13** - Quad:**96:96** - Selection:**unset**

protocol:[] - **Datapoint:**RAW1

	1	2	3	4	5	6	7	8	9	10	11	12
A	0.09	0.08	0.08	0.13	0.10	0.10	0.10	0.11	0.09	0.09	0.09	0.22
B	0.09	0.07	0.13	0.08	0.06	0.07	0.08	0.06	0.07	0.06	0.09	0.14
C	0.08	0.06	0.08	0.05	0.06	0.06	0.05	0.05	0.06	0.05	0.05	0.10
D	0.08	0.05	0.06	0.05	0.05	0.05	0.06	0.08	0.10	0.05	0.06	0.10
E	0.08	0.07	0.05	0.05	0.05	0.05	0.06	0.09	0.06	0.09	0.07	0.07
F	0.12	0.08	0.06	0.06	0.06	0.06	0.06	0.07	0.05	0.05	0.07	0.10
G	0.11	0.10	0.06	0.06	0.06	0.06	0.06	0.06	0.06	0.06	0.06	0.05
H	0.11	0.10	0.08	0.09	0.09	0.09	0.06	0.08	0.09	0.07	0.09	0.04

protocol:[]

Plate

Exclude from hits

Independent

strong >= 0.5

weak >= 0.2

Properties

Sample Mean	0.07	**Source Plate b/c**	ZZ1K3V
Sample SD	0.02	**Quad**	96:96
Positive1 Mean	0.18	**Analysis Category**	Insulin
Positive1 SD	0.06	**Sum Strong**	0
Positive2 Mean	0.10	**% Strong**	0
Positive2 SD	0.00	**Sum Weak**	0
Negative1 Mean	0.08	**% Weak**	0
Negative1 SD	0.01	**Sum None**	88
Z'	-1.26	**% None**	100
Screening Plate	Plate 13	**Excluded wells**	0
Screening Plate b/c	Y02497	**Cut-off**	0.5,0.2

Source Plate b/c:**ZZ1K3V** - Source Plate Number:**14** - Analysis Category:**Human TfR** - Screening Plate b/c:**Y02491** - Screening Plate:**Plate 14** - Quad:**96:96** - Selection:**unset**

protocol:[] - **Datapoint:**RAW1

	1	2	3	4	5	6	7	8	9	10	11	12
A	0.13	0.11	0.10	0.16	0.19	0.12	0.12	0.20	0.14	0.18	0.13	0.36
B	0.13	0.11	0.19	0.14	0.10	0.10	0.17	0.10	0.15	0.10	0.16	0.17
C	0.12	0.10	0.19	0.09	0.13	0.08	0.11	0.08	0.08	0.08	0.08	0.13
D	0.11	0.08	0.13	0.08	0.08	0.07	0.08	0.07	0.14	0.15	0.08	0.12
E	0.23	0.08	0.08	0.07	0.08	0.12	0.15	0.11	0.10	0.15	0.07	0.10
F	0.13	0.08	0.07	0.10	0.07	0.07	0.07	0.07	0.07	0.06	0.07	0.11
G	0.21	0.20	0.08	0.07	0.08	0.10	0.15	0.12	0.08	0.13	0.06	0.05
H	0.15	0.21	0.11	0.18	0.11	0.21	0.10	0.11	0.18	0.10	0.08	0.04

protocol:[]

Plate

Exclude from hits

Independent

strong >= 0.5

weak >= 0.2

Properties

Sample Mean	0.12	**Source Plate b/c**	ZZ1K3V
Sample SD	0.04	**Quad**	96:96
Positive1 Mean	0.27	**Analysis Category**	Human TfR
Positive1 SD	0.13	**Sum Strong**	0
Positive2 Mean	0.12	**% Strong**	0
Positive2 SD	0.01	**Sum Weak**	6
Negative1 Mean	0.10	**% Weak**	7
Negative1 SD	0.00	**Sum None**	82
Z'	-1.47	**% None**	93
Screening Plate	Plate 14	**Excluded wells**	0
Screening Plate b/c	Y02491	**Cut-off**	0.5,0.2

Source Plate b/c:**ZZ1K3V** - Source Plate Number:**15** - Analysis Category:**Mouse TfR** - Screening Plate b/c:**Y01698** - Screening Plate:**Plate 15** - Quad:**96:96** - Selection:**unset**

protocol:[] - **Datapoint:**RAW1

	1	2	3	4	5	6	7	8	9	10	11	12
A	1.09	0.87	0.13	1.10	0.71	0.77	0.15	0.78	1.01	0.94	0.68	0.30
B	1.10	1.25	1.13	1.02	0.99	1.09	0.92	1.12	1.00	0.91	0.81	0.24
C	1.16	1.11	1.06	1.07	0.79	1.03	0.55	0.94	0.83	1.03	0.54	0.86
D	1.17	0.97	0.75	0.94	1.00	1.21	1.02	0.94	0.88	1.05	0.30	0.85
E	1.22	0.11	1.06	0.10	0.89	0.84	0.95	0.68	0.53	0.98	0.69	0.18
F	1.02	1.05	1.04	0.66	1.00	1.20	1.10	0.74	1.10	1.12	0.82	0.21
G	1.13	0.91	0.98	1.03	1.20	0.90	0.99	0.64	1.14	0.68	0.64	0.05
H	0.85	0.58	0.79	1.07	1.07	1.06	0.33	1.17	0.77	0.86	0.95	0.04

protocol:[]

Plate

Exclude from hits

Independent

strong >= 0.5

weak >= 0.2

Properties

Sample Mean	0.89	**Source Plate b/c**	ZZ1K3V
Sample SD	0.26	**Quad**	96:96
Positive1 Mean	0.27	**Analysis Category**	Mouse TfR
Positive1 SD	0.04	**Sum Strong**	82
Positive2 Mean	0.86	**% Strong**	93
Positive2 SD	0.00	**Sum Weak**	2
Negative1 Mean	0.20	**% Weak**	2
Negative1 SD	0.02	**Sum None**	4
Z'	-1.55	**% None**	5
Screening Plate	Plate 15	**Excluded wells**	0
Screening Plate b/c	Y01698	**Cut-off**	0.5,0.2

[previous plate] [next plate] Source Plate b/c:**ZZ1K3W** - Source Plate Number:**16** - Analysis Category:**Insulin** - Screening Plate b/c:**Y02447** - Screening Plate:**Plate 16** - Quad:**96:96** - Selection:**unset**

protocol:[] - **Datapoint:**RAW1

	1	2	3	4	5	6	7	8	9	10	11	12
A	0.14	0.12	0.14	0.11	0.13	0.13	0.11	0.13	0.10	0.10	0.13	0.22
B	0.15	0.07	0.08	0.10	0.10	0.08	0.08	0.11	0.07	0.07	0.07	0.09
C	0.10	0.08	0.07	0.08	0.07	0.07	0.06	0.07	0.07	0.06	0.06	0.09
D	0.10	0.07	0.10	0.07	0.06	0.06	0.07	0.07	0.07	0.06	0.06	0.07
E	0.08	0.06	0.07	0.06	0.06	0.06	0.06	0.06	0.06	0.06	0.06	0.12
F	0.10	0.06	0.06	0.07	0.06	0.06	0.07	0.06	0.06	0.05	0.07	0.07
G	0.11	0.09	0.12	0.08	0.07	0.07	0.06	0.09	0.10	0.06	0.06	0.05
H	0.14	0.10	0.10	0.10	0.09	0.09	0.10	0.14	0.08	0.08	0.09	0.04

protocol:[]

Plate

Exclude from hits

Independent

strong >= 0.5

weak >= 0.2

Properties

Sample Mean	0.08	**Source Plate b/c**	ZZ1K3W
Sample SD	0.03	**Quad**	96:96
Positive1 Mean	0.15	**Analysis Category**	Insulin
Positive1 SD	0.09	**Sum Strong**	0
Positive2 Mean	0.08	**% Strong**	0
Positive2 SD	0.01	**Sum Weak**	0
Negative1 Mean	0.09	**% Weak**	0
Negative1 SD	0.03	**Sum None**	88
Z'	-4.80	**% None**	100
Screening Plate	Plate 16	**Excluded wells**	0
Screening Plate b/c	Y02447	**Cut-off**	0.5,0.2

Source Plate b/c:**ZZ1K3W** - Source Plate Number:**17** - Analysis Category:**Human TfR** - Screening Plate b/c:**Y02443** - Screening Plate:**Plate 17** - Quad:**96:96** - Selection:**unset**

protocol:[] - **Datapoint:**RAW1

	1	2	3	4	5	6	7	8	9	10	11	12
A	0.15	0.17	0.23	0.12	0.13	0.12	0.14	0.34	0.11	0.12	0.13	0.37
B	0.33	0.07	0.08	0.08	0.16	0.08	0.14	0.33	0.08	0.07	0.06	0.34
C	0.11	0.08	0.07	0.08	0.07	0.08	0.17	0.12	0.07	0.10	0.08	0.13
D	0.12	0.18	0.15	0.16	0.06	0.06	0.18	0.13	0.15	0.06	0.06	0.12
E	0.09	0.07	0.20	0.06	0.07	0.06	0.07	0.06	0.10	0.06	0.06	0.16
F	0.12	0.15	0.07	0.13	0.06	0.10	0.15	0.06	0.07	0.06	0.05	0.10
G	0.25	0.21	0.19	0.13	0.06	0.06	0.06	0.22	0.11	0.06	0.06	0.05
H	0.21	0.11	0.12	0.10	0.28	0.10	0.21	0.30	0.10	0.10	0.10	0.04

protocol:[]

Plate

Exclude from hits

Independent

strong >= 0.5

weak >= 0.2

Properties

Sample Mean	0.12	**Source Plate b/c**	ZZ1K3W
Sample SD	0.07	**Quad**	96:96
Positive1 Mean	0.36	**Analysis Category**	Human TfR
Positive1 SD	0.02	**Sum Strong**	0
Positive2 Mean	0.12	**% Strong**	0
Positive2 SD	0.01	**Sum Weak**	11
Negative1 Mean	0.13	**% Weak**	12
Negative1 SD	0.04	**Sum None**	77
Z'	0.12	**% None**	88
Screening Plate	Plate 17	**Excluded wells**	0
Screening Plate b/c	Y02443	**Cut-off**	0.5,0.2

Source Plate b/c:**ZZ1K3W** - Source Plate Number:**18** - Analysis Category:**Mouse TfR** - Screening Plate b/c:**Y01760** - Screening Plate:**Plate 18** - Quad:**96:96** - Selection:**unset**

protocol:[] - **Datapoint:**RAW1

	1	2	3	4	5	6	7	8	9	10	11	12
A	0.71	0.39	0.57	0.57	0.65	0.56	0.70	0.69	0.50	0.58	0.22	0.18
B	0.56	0.05	0.58	0.63	0.46	0.65	0.39	0.57	0.71	0.49	0.06	0.10
C	0.13	0.49	0.57	0.65	0.51	0.57	0.55	0.58	0.51	0.52	0.38	0.36
D	0.55	0.52	0.53	0.59	0.67	0.39	0.50	0.46	0.56	0.46	0.56	0.38
E	0.06	0.50	0.52	0.61	0.55	0.36	0.57	0.05	0.26	0.41	0.46	0.07
F	0.70	0.34	0.05	0.45	0.62	0.26	0.44	0.53	0.51	0.05	0.44	0.06
G	0.37	0.60	0.60	0.52	0.54	0.45	0.37	0.67	0.37	0.51	0.37	0.05
H	0.29	0.56	0.63	0.31	0.62	0.58	0.47	0.57	0.56	0.58	0.43	0.04

protocol:[]

Plate

Exclude from hits

Independent

strong >= 0.5

weak >= 0.2

Properties

Sample Mean	0.48	**Source Plate b/c**	ZZ1K3W
Sample SD	0.16	**Quad**	96:96
Positive1 Mean	0.14	**Analysis Category**	Mouse TfR
Positive1 SD	0.06	**Sum Strong**	51
Positive2 Mean	0.37	**% Strong**	58
Positive2 SD	0.01	**Sum Weak**	30
Negative1 Mean	0.06	**% Weak**	34
Negative1 SD	0.00	**Sum None**	7
Z'	-1.27	**% None**	8
Screening Plate	Plate 18	**Excluded wells**	0
Screening Plate b/c	Y01760	**Cut-off**	0.5,0.2

Figure S4: Phage ELISA positive hits sequence alignment.

The 197 TfR species cross-reactive hits identified from initial phage ELISA screening were sequenced and analysed using Blaze 2.0 (Continuity software package, MedImmune, Cambridge). Sequences were assembled as fdDOG sequences and aligned according to the peptide insert region. Yellow highlights indicate the position of the cysteine residues which form the disulphide bond of the cyclic peptide.

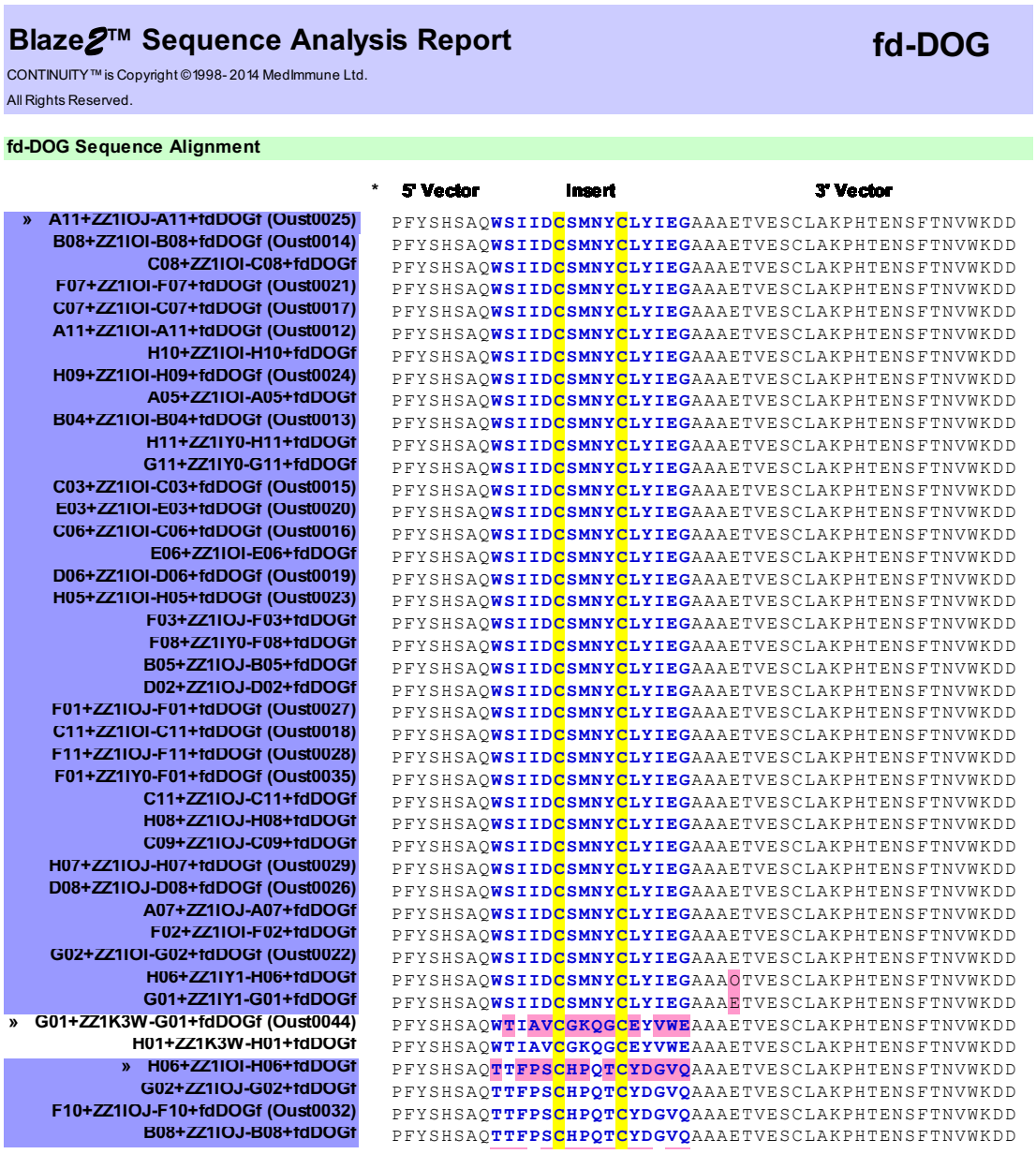

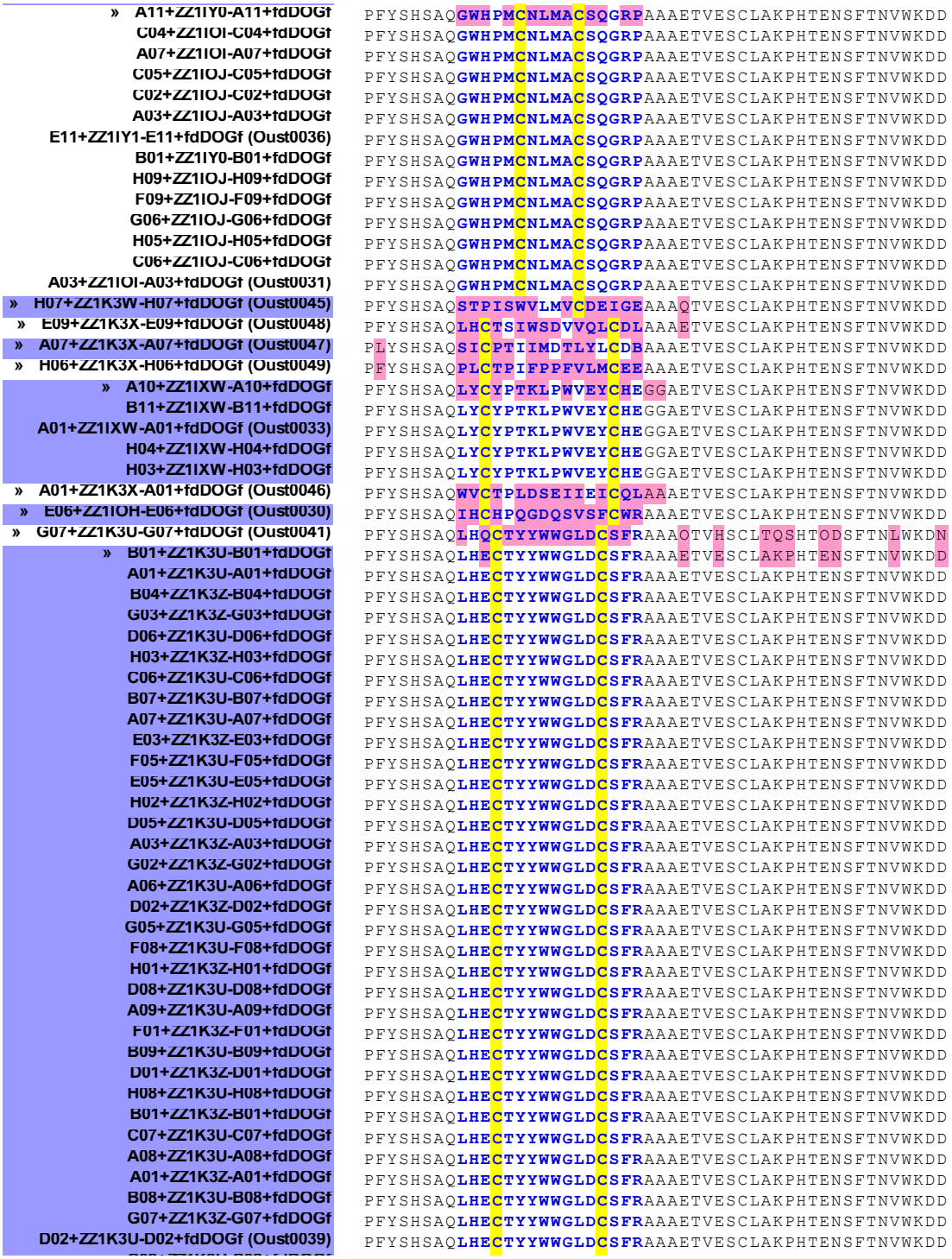
» A11+ZZ1IY0-A11+fdDOGf PFYSHSAQGWHPMCNLMACSQGRPAAAETVESCLAKPHTENSFTNVWKDD
C04+ZZ1IOI-C04+fdDOGf PFYSHSAQGWHPMCNLMACSQGRPAAAETVESCLAKPHTENSFTNVWKDD
A07+ZZ1IOI-A07+fdDOGf PFYSHSAQGWHPMCNLMACSQGRPAAAETVESCLAKPHTENSFTNVWKDD
C05+ZZ1IOJ-C05+fdDOGf PFYSHSAQGWHPMCNLMACSQGRPAAAETVESCLAKPHTENSFTNVWKDD
C02+ZZ1IOJ-C02+fdDOGf PFYSHSAQGWHPMCNLMACSQGRPAAAETVESCLAKPHTENSFTNVWKDD
A03+ZZ1IOJ-A03+fdDOGf PFYSHSAQGWHPMCNLMACSQGRPAAAETVESCLAKPHTENSFTNVWKDD
E11+ZZ1IY1-E11+fdDOGf (Oust0036) PFYSHSAQGWHPMCNLMACSQGRPAAAETVESCLAKPHTENSFTNVWKDD
B01+ZZ1IY0-B01+fdDOGf PFYSHSAQGWHPMCNLMACSQGRPAAAETVESCLAKPHTENSFTNVWKDD
H09+ZZ1IOJ-H09+fdDOGf PFYSHSAQGWHPMCNLMACSQGRPAAAETVESCLAKPHTENSFTNVWKDD
F09+ZZ1IOJ-F09+fdDOGf PFYSHSAQGWHPMCNLMACSQGRPAAAETVESCLAKPHTENSFTNVWKDD
G06+ZZ1IOJ-G06+fdDOGf PFYSHSAQGWHPMCNLMACSQGRPAAAETVESCLAKPHTENSFTNVWKDD
H05+ZZ1IOJ-H05+fdDOGf PFYSHSAQGWHPMCNLMACSQGRPAAAETVESCLAKPHTENSFTNVWKDD
C06+ZZ1IOJ-C06+fdDOGf PFYSHSAQGWHPMCNLMACSQGRPAAAETVESCLAKPHTENSFTNVWKDD
A03+ZZ1IOI-A03+fdDOGf (Oust0031) PFYSHSAQGWHPMCNLMACSQGRPAAAETVESCLAKPHTENSFTNVWKDD
» H07+ZZ1K3W-H07+fdDOGf (Oust0045) PFYSHSAQSTPISWVLMVCDEIGEAAAQTVESCLAKPHTENSFTNVWKDD
» E09+ZZ1K3X-E09+fdDOGf (Oust0048) PFYSHSAQLHCTSIWSDVVQLCDLAAAETVESCLAKPHTENSFTNVWKDD
» A07+ZZ1K3X-A07+fdDOGf (Oust0047) PLYSHSAQSICPTIIMDTLYLCDBAAAETVESCLAKPHTENSFTNVWKDD
» H06+ZZ1K3X-H06+fdDOGf (Oust0049) PFYSHSAQPLCTPIFPPFVLMCEEAAAETVESCLAKPHTENSFTNVWKDD
» A10+ZZ1IXW-A10+fdDOGf PFYSHSAQLYCYPTKLPWVEYCHEGGAETVESCLAKPHTENSFTNVWKDD
B11+ZZ1IXW-B11+fdDOGf PFYSHSAQLYCYPTKLPWVEYCHEGGAETVESCLAKPHTENSFTNVWKDD
A01+ZZ1IXW-A01+fdDOGf (Oust0033) PFYSHSAQLYCYPTKLPWVEYCHEGGAETVESCLAKPHTENSFTNVWKDD
H04+ZZ1IXW-H04+fdDOGf PFYSHSAQLYCYPTKLPWVEYCHEGGAETVESCLAKPHTENSFTNVWKDD
H03+ZZ1IXW-H03+fdDOGf PFYSHSAQLYCYPTKLPWVEYCHEGGAETVESCLAKPHTENSFTNVWKDD
» A01+ZZ1K3X-A01+fdDOGf (Oust0046) PFYSHSAQWVCTPLDSEIIEICQLAAAETVESCLAKPHTENSFTNVWKDD
» E06+ZZ1IOH-E06+fdDOGf (Oust0030) PFYSHSAQIHCHPQGDQSVSFCWRAAAETVESCLAKPHTENSFTNVWKDD
» G07+ZZ1K3U-G07+fdDOGf (Oust0041) PFYSHSAQLHQCTYYWWGLDCSFRAAAQTVHSCLTQSHTODSFTNLWKDN
» B01+ZZ1K3U-B01+fdDOGf PFYSHSAQLHECTYYWWGLDCSFRAAAETVESCLAKPHTENSFTNVWKDD
A01+ZZ1K3U-A01+fdDOGf PFYSHSAQLHECTYYWWGLDCSFRAAAETVESCLAKPHTENSFTNVWKDD
B04+ZZ1K3Z-B04+fdDOGf PFYSHSAQLHECTYYWWGLDCSFRAAAETVESCLAKPHTENSFTNVWKDD
G03+ZZ1K3Z-G03+fdDOGf PFYSHSAQLHECTYYWWGLDCSFRAAAETVESCLAKPHTENSFTNVWKDD
D06+ZZ1K3U-D06+fdDOGf PFYSHSAQLHECTYYWWGLDCSFRAAAETVESCLAKPHTENSFTNVWKDD
H03+ZZ1K3Z-H03+fdDOGf PFYSHSAQLHECTYYWWGLDCSFRAAAETVESCLAKPHTENSFTNVWKDD
C06+ZZ1K3U-C06+fdDOGf PFYSHSAQLHECTYYWWGLDCSFRAAAETVESCLAKPHTENSFTNVWKDD
B07+ZZ1K3U-B07+fdDOGf PFYSHSAQLHECTYYWWGLDCSFRAAAETVESCLAKPHTENSFTNVWKDD
A07+ZZ1K3U-A07+fdDOGf PFYSHSAQLHECTYYWWGLDCSFRAAAETVESCLAKPHTENSFTNVWKDD
E03+ZZ1K3Z-E03+fdDOGf PFYSHSAQLHECTYYWWGLDCSFRAAAETVESCLAKPHTENSFTNVWKDD
F05+ZZ1K3U-F05+fdDOGf PFYSHSAQLHECTYYWWGLDCSFRAAAETVESCLAKPHTENSFTNVWKDD
E05+ZZ1K3U-E05+fdDOGf PFYSHSAQLHECTYYWWGLDCSFRAAAETVESCLAKPHTENSFTNVWKDD
H02+ZZ1K3Z-H02+fdDOGf PFYSHSAQLHECTYYWWGLDCSFRAAAETVESCLAKPHTENSFTNVWKDD
D05+ZZ1K3U-D05+fdDOGf PFYSHSAQLHECTYYWWGLDCSFRAAAETVESCLAKPHTENSFTNVWKDD
A03+ZZ1K3Z-A03+fdDOGf PFYSHSAQLHECTYYWWGLDCSFRAAAETVESCLAKPHTENSFTNVWKDD
G02+ZZ1K3Z-G02+fdDOGf PFYSHSAQLHECTYYWWGLDCSFRAAAETVESCLAKPHTENSFTNVWKDD
A06+ZZ1K3U-A06+fdDOGf PFYSHSAQLHECTYYWWGLDCSFRAAAETVESCLAKPHTENSFTNVWKDD
D02+ZZ1K3Z-D02+fdDOGf PFYSHSAQLHECTYYWWGLDCSFRAAAETVESCLAKPHTENSFTNVWKDD
G05+ZZ1K3U-G05+fdDOGf PFYSHSAQLHECTYYWWGLDCSFRAAAETVESCLAKPHTENSFTNVWKDD
F08+ZZ1K3U-F08+fdDOGf PFYSHSAQLHECTYYWWGLDCSFRAAAETVESCLAKPHTENSFTNVWKDD
H01+ZZ1K3Z-H01+fdDOGf PFYSHSAQLHECTYYWWGLDCSFRAAAETVESCLAKPHTENSFTNVWKDD
D08+ZZ1K3U-D08+fdDOGf PFYSHSAQLHECTYYWWGLDCSFRAAAETVESCLAKPHTENSFTNVWKDD
A09+ZZ1K3U-A09+fdDOGf PFYSHSAQLHECTYYWWGLDCSFRAAAETVESCLAKPHTENSFTNVWKDD
F01+ZZ1K3Z-F01+fdDOGf PFYSHSAQLHECTYYWWGLDCSFRAAAETVESCLAKPHTENSFTNVWKDD
B09+ZZ1K3U-B09+fdDOGf PFYSHSAQLHECTYYWWGLDCSFRAAAETVESCLAKPHTENSFTNVWKDD
D01+ZZ1K3Z-D01+fdDOGf PFYSHSAQLHECTYYWWGLDCSFRAAAETVESCLAKPHTENSFTNVWKDD
H08+ZZ1K3U-H08+fdDOGf PFYSHSAQLHECTYYWWGLDCSFRAAAETVESCLAKPHTENSFTNVWKDD
B01+ZZ1K3Z-B01+fdDOGf PFYSHSAQLHECTYYWWGLDCSFRAAAETVESCLAKPHTENSFTNVWKDD
C07+ZZ1K3U-C07+fdDOGf PFYSHSAQLHECTYYWWGLDCSFRAAAETVESCLAKPHTENSFTNVWKDD
A08+ZZ1K3U-A08+fdDOGf PFYSHSAQLHECTYYWWGLDCSFRAAAETVESCLAKPHTENSFTNVWKDD
A01+ZZ1K3Z-A01+fdDOGf PFYSHSAQLHECTYYWWGLDCSFRAAAETVESCLAKPHTENSFTNVWKDD
B08+ZZ1K3U-B08+fdDOGf PFYSHSAQLHECTYYWWGLDCSFRAAAETVESCLAKPHTENSFTNVWKDD
G07+ZZ1K3Z-G07+fdDOGf PFYSHSAQLHECTYYWWGLDCSFRAAAETVESCLAKPHTENSFTNVWKDD
D02+ZZ1K3U-D02+fdDOGf (Oust0039) PFYSHSAQLHECTYYWWGLDCSFRAAAETVESCLAKPHTENSFTNVWKDD

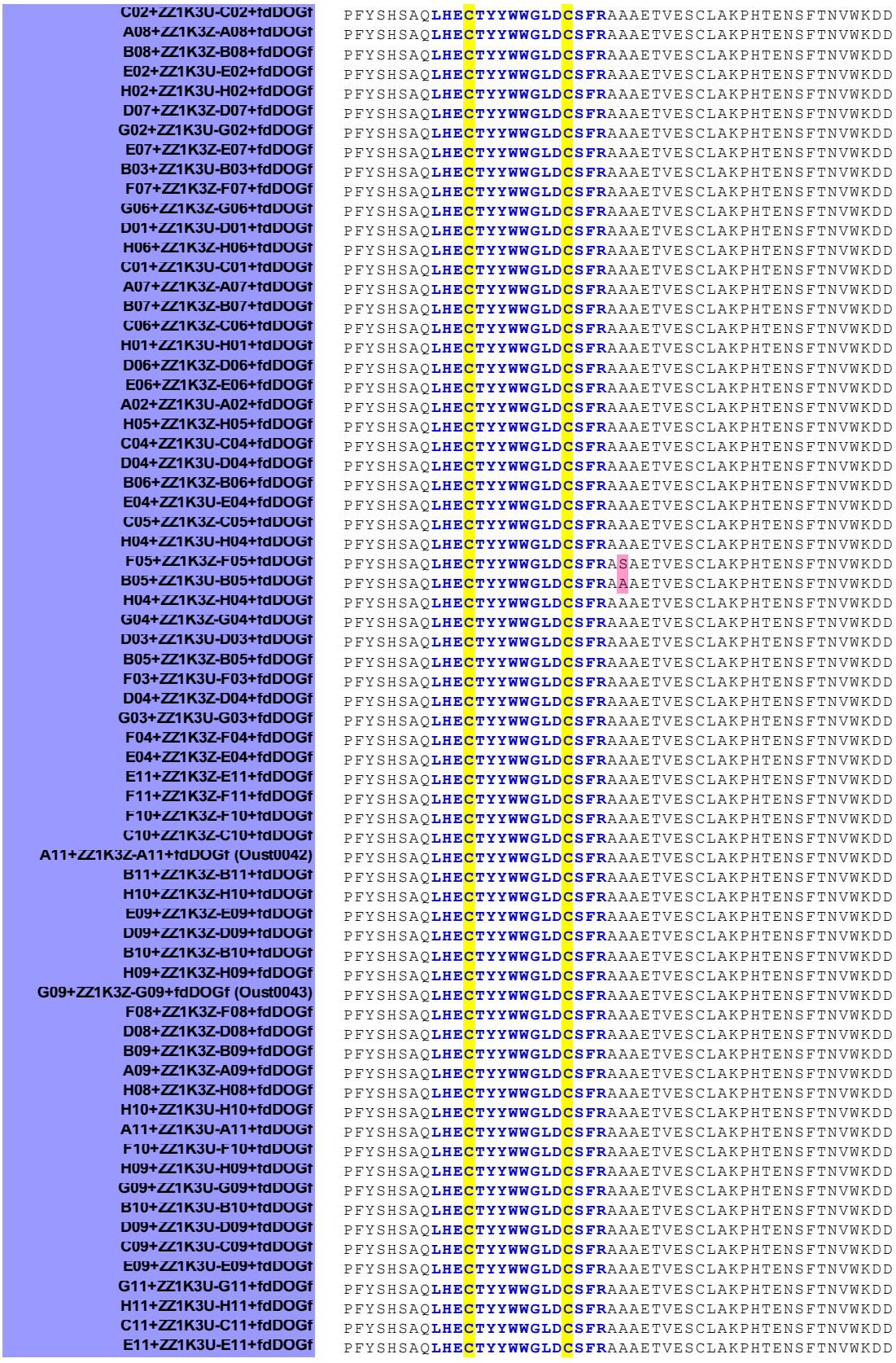
C02+ZZ1K3U-C02+fdDOGf PFYSHSAQLHECTYYWWGLDCSFRAAAETVESCLAKPHTENSFTNVWKDD
A08+ZZ1K3Z-A08+fdDOGf PFYSHSAQLHECTYYWWGLDCSFRAAAETVESCLAKPHTENSFTNVWKDD
B08+ZZ1K3Z-B08+fdDOGf PFYSHSAQLHECTYYWWGLDCSFRAAAETVESCLAKPHTENSFTNVWKDD
E02+ZZ1K3U-E02+fdDOGf PFYSHSAQLHECTYYWWGLDCSFRAAAETVESCLAKPHTENSFTNVWKDD
H02+ZZ1K3U-H02+fdDOGf PFYSHSAQLHECTYYWWGLDCSFRAAAETVESCLAKPHTENSFTNVWKDD
D07+ZZ1K3Z-D07+fdDOGf PFYSHSAQLHECTYYWWGLDCSFRAAAETVESCLAKPHTENSFTNVWKDD
G02+ZZ1K3U-G02+fdDOGf PFYSHSAQLHECTYYWWGLDCSFRAAAETVESCLAKPHTENSFTNVWKDD
E07+ZZ1K3Z-E07+fdDOGf PFYSHSAQLHECTYYWWGLDCSFRAAAETVESCLAKPHTENSFTNVWKDD
B03+ZZ1K3U-B03+fdDOGf PFYSHSAQLHECTYYWWGLDCSFRAAAETVESCLAKPHTENSFTNVWKDD
F07+ZZ1K3Z-F07+fdDOGf PFYSHSAQLHECTYYWWGLDCSFRAAAETVESCLAKPHTENSFTNVWKDD
G06+ZZ1K3Z-G06+fdDOGf PFYSHSAQLHECTYYWWGLDCSFRAAAETVESCLAKPHTENSFTNVWKDD
D01+ZZ1K3U-D01+fdDOGf PFYSHSAQLHECTYYWWGLDCSFRAAAETVESCLAKPHTENSFTNVWKDD
H06+ZZ1K3Z-H06+fdDOGf PFYSHSAQLHECTYYWWGLDCSFRAAAETVESCLAKPHTENSFTNVWKDD
C01+ZZ1K3U-C01+fdDOGf PFYSHSAQLHECTYYWWGLDCSFRAAAETVESCLAKPHTENSFTNVWKDD
A07+ZZ1K3Z-A07+fdDOGf PFYSHSAQLHECTYYWWGLDCSFRAAAETVESCLAKPHTENSFTNVWKDD
B07+ZZ1K3Z-B07+fdDOGf PFYSHSAQLHECTYYWWGLDCSFRAAAETVESCLAKPHTENSFTNVWKDD
C06+ZZ1K3Z-C06+fdDOGf PFYSHSAQLHECTYYWWGLDCSFRAAAETVESCLAKPHTENSFTNVWKDD
H01+ZZ1K3U-H01+fdDOGf PFYSHSAQLHECTYYWWGLDCSFRAAAETVESCLAKPHTENSFTNVWKDD
D06+ZZ1K3Z-D06+fdDOGf PFYSHSAQLHECTYYWWGLDCSFRAAAETVESCLAKPHTENSFTNVWKDD
E06+ZZ1K3Z-E06+fdDOGf PFYSHSAQLHECTYYWWGLDCSFRAAAETVESCLAKPHTENSFTNVWKDD
A02+ZZ1K3U-A02+fdDOGf PFYSHSAQLHECTYYWWGLDCSFRAAAETVESCLAKPHTENSFTNVWKDD
H05+ZZ1K3Z-H05+fdDOGf PFYSHSAQLHECTYYWWGLDCSFRAAAETVESCLAKPHTENSFTNVWKDD
C04+ZZ1K3U-C04+fdDOGf PFYSHSAQLHECTYYWWGLDCSFRAAAETVESCLAKPHTENSFTNVWKDD
D04+ZZ1K3U-D04+fdDOGf PFYSHSAQLHECTYYWWGLDCSFRAAAETVESCLAKPHTENSFTNVWKDD
B06+ZZ1K3Z-B06+fdDOGf PFYSHSAQLHECTYYWWGLDCSFRAAAETVESCLAKPHTENSFTNVWKDD
E04+ZZ1K3U-E04+fdDOGf PFYSHSAQLHECTYYWWGLDCSFRAAAETVESCLAKPHTENSFTNVWKDD
C05+ZZ1K3Z-C05+fdDOGf PFYSHSAQLHECTYYWWGLDCSFRAAAETVESCLAKPHTENSFTNVWKDD
H04+ZZ1K3U-H04+fdDOGf PFYSHSAQLHECTYYWWGLDCSFRAAAETVESCLAKPHTENSFTNVWKDD
F05+ZZ1K3Z-F05+fdDOGf PFYSHSAQLHECTYYWWGLDCSFRASAETVESCLAKPHTENSFTNVWKDD
B05+ZZ1K3U-B05+fdDOGf PFYSHSAQLHECTYYWWGLDCSFRAAAETVESCLAKPHTENSFTNVWKDD
H04+ZZ1K3Z-H04+fdDOGf PFYSHSAQLHECTYYWWGLDCSFRAAAETVESCLAKPHTENSFTNVWKDD
G04+ZZ1K3Z-G04+fdDOGf PFYSHSAQLHECTYYWWGLDCSFRAAAETVESCLAKPHTENSFTNVWKDD
D03+ZZ1K3U-D03+fdDOGf PFYSHSAQLHECTYYWWGLDCSFRAAAETVESCLAKPHTENSFTNVWKDD
B05+ZZ1K3Z-B05+fdDOGf PFYSHSAQLHECTYYWWGLDCSFRAAAETVESCLAKPHTENSFTNVWKDD
F03+ZZ1K3U-F03+fdDOGf PFYSHSAQLHECTYYWWGLDCSFRAAAETVESCLAKPHTENSFTNVWKDD
D04+ZZ1K3Z-D04+fdDOGf PFYSHSAQLHECTYYWWGLDCSFRAAAETVESCLAKPHTENSFTNVWKDD
G03+ZZ1K3U-G03+fdDOGf PFYSHSAQLHECTYYWWGLDCSFRAAAETVESCLAKPHTENSFTNVWKDD
F04+ZZ1K3Z-F04+fdDOGf PFYSHSAQLHECTYYWWGLDCSFRAAAETVESCLAKPHTENSFTNVWKDD
E04+ZZ1K3Z-E04+fdDOGf PFYSHSAQLHECTYYWWGLDCSFRAAAETVESCLAKPHTENSFTNVWKDD
E11+ZZ1K3Z-E11+fdDOGf PFYSHSAQLHECTYYWWGLDCSFRAAAETVESCLAKPHTENSFTNVWKDD
F11+ZZ1K3Z-F11+fdDOGf PFYSHSAQLHECTYYWWGLDCSFRAAAETVESCLAKPHTENSFTNVWKDD
F10+ZZ1K3Z-F10+fdDOGf PFYSHSAQLHECTYYWWGLDCSFRAAAETVESCLAKPHTENSFTNVWKDD
C10+ZZ1K3Z-C10+fdDOGf PFYSHSAQLHECTYYWWGLDCSFRAAAETVESCLAKPHTENSFTNVWKDD
A11+ZZ1K3Z-A11+fdDOGf (Oust0042) PFYSHSAQLHECTYYWWGLDCSFRAAAETVESCLAKPHTENSFTNVWKDD
B11+ZZ1K3Z-B11+fdDOGf PFYSHSAQLHECTYYWWGLDCSFRAAAETVESCLAKPHTENSFTNVWKDD
H10+ZZ1K3Z-H10+fdDOGf PFYSHSAQLHECTYYWWGLDCSFRAAAETVESCLAKPHTENSFTNVWKDD
E09+ZZ1K3Z-E09+fdDOGf PFYSHSAQLHECTYYWWGLDCSFRAAAETVESCLAKPHTENSFTNVWKDD
D09+ZZ1K3Z-D09+fdDOGf PFYSHSAQLHECTYYWWGLDCSFRAAAETVESCLAKPHTENSFTNVWKDD
B10+ZZ1K3Z-B10+fdDOGf PFYSHSAQLHECTYYWWGLDCSFRAAAETVESCLAKPHTENSFTNVWKDD
H09+ZZ1K3Z-H09+fdDOGf PFYSHSAQLHECTYYWWGLDCSFRAAAETVESCLAKPHTENSFTNVWKDD
G09+ZZ1K3Z-G09+fdDOGf (Oust0043) PFYSHSAQLHECTYYWWGLDCSFRAAAETVESCLAKPHTENSFTNVWKDD
F08+ZZ1K3Z-F08+fdDOGf PFYSHSAQLHECTYYWWGLDCSFRAAAETVESCLAKPHTENSFTNVWKDD
D08+ZZ1K3Z-D08+fdDOGf PFYSHSAQLHECTYYWWGLDCSFRAAAETVESCLAKPHTENSFTNVWKDD
B09+ZZ1K3Z-B09+fdDOGf PFYSHSAQLHECTYYWWGLDCSFRAAAETVESCLAKPHTENSFTNVWKDD
A09+ZZ1K3Z-A09+fdDOGf PFYSHSAQLHECTYYWWGLDCSFRAAAETVESCLAKPHTENSFTNVWKDD
H08+ZZ1K3Z-H08+fdDOGf PFYSHSAQLHECTYYWWGLDCSFRAAAETVESCLAKPHTENSFTNVWKDD
H10+ZZ1K3U-H10+fdDOGf PFYSHSAQLHECTYYWWGLDCSFRAAAETVESCLAKPHTENSFTNVWKDD
A11+ZZ1K3U-A11+fdDOGf PFYSHSAQLHECTYYWWGLDCSFRAAAETVESCLAKPHTENSFTNVWKDD
F10+ZZ1K3U-F10+fdDOGf PFYSHSAQLHECTYYWWGLDCSFRAAAETVESCLAKPHTENSFTNVWKDD
H09+ZZ1K3U-H09+fdDOGf PFYSHSAQLHECTYYWWGLDCSFRAAAETVESCLAKPHTENSFTNVWKDD
G09+ZZ1K3U-G09+fdDOGf PFYSHSAQLHECTYYWWGLDCSFRAAAETVESCLAKPHTENSFTNVWKDD
B10+ZZ1K3U-B10+fdDOGf PFYSHSAQLHECTYYWWGLDCSFRAAAETVESCLAKPHTENSFTNVWKDD
D09+ZZ1K3U-D09+fdDOGf PFYSHSAQLHECTYYWWGLDCSFRAAAETVESCLAKPHTENSFTNVWKDD
C09+ZZ1K3U-C09+fdDOGf PFYSHSAQLHECTYYWWGLDCSFRAAAETVESCLAKPHTENSFTNVWKDD
E09+ZZ1K3U-E09+fdDOGf PFYSHSAQLHECTYYWWGLDCSFRAAAETVESCLAKPHTENSFTNVWKDD
G11+ZZ1K3U-G11+fdDOGf PFYSHSAQLHECTYYWWGLDCSFRAAAETVESCLAKPHTENSFTNVWKDD
H11+ZZ1K3U-H11+fdDOGf PFYSHSAQLHECTYYWWGLDCSFRAAAETVESCLAKPHTENSFTNVWKDD
C11+ZZ1K3U-C11+fdDOGf PFYSHSAQLHECTYYWWGLDCSFRAAAETVESCLAKPHTENSFTNVWKDD
E11+ZZ1K3U-E11+fdDOGf PFYSHSAQLHECTYYWWGLDCSFRAAAETVESCLAKPHTENSFTNVWKDD

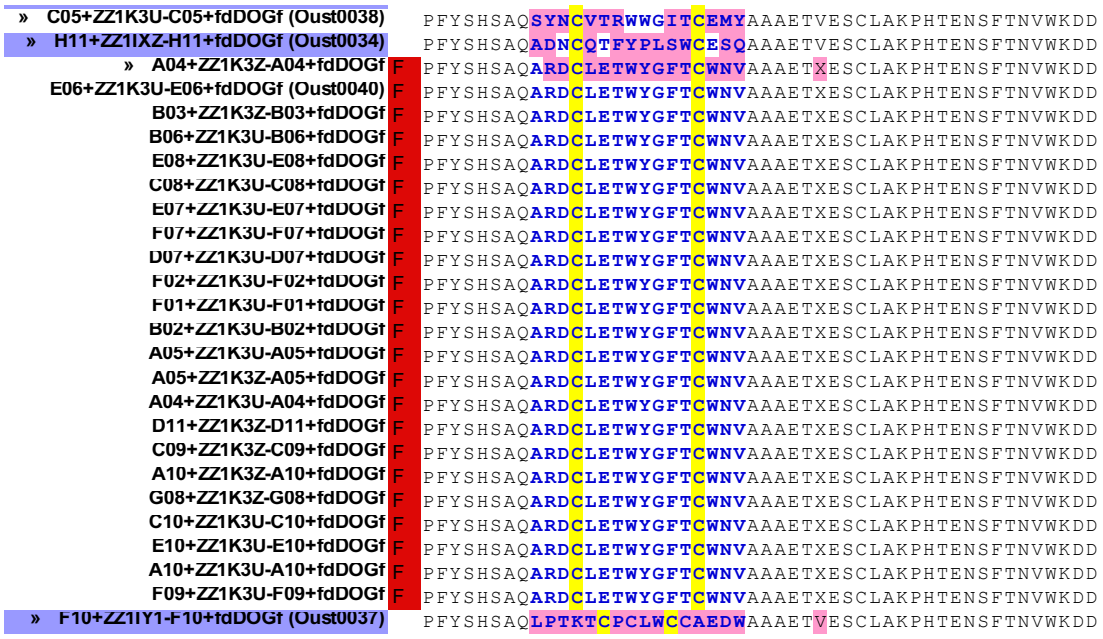
» C05+ZZ1K3U-C05+fdDOGf (Oust0038) PFYSHSAQSYNCVTRWWGITCEMYAAAETVESCLAKPHTENSFTNVWKDD
» H11+ZZ1IXZ-H11+fdDOGf (Oust0034) PFYSHSAQADNCQTFYPLSWCESQAAAETVESCLAKPHTENSFTNVWKDD
» A04+ZZ1K3Z-A04+fdDOGf F PFYSHSAQARDCLETWYGFTCWNVAAAETXESCLAKPHTENSFTNVWKDD
E06+ZZ1K3U-E06+fdDOGf (Oust0040) F PFYSHSAQARDCLETWYGFTCWNVAAAETXESCLAKPHTENSFTNVWKDD
B03+ZZ1K3Z-B03+fdDOGf F PFYSHSAQARDCLETWYGFTCWNVAAAETXESCLAKPHTENSFTNVWKDD
B06+ZZ1K3U-B06+fdDOGf F PFYSHSAQARDCLETWYGFTCWNVAAAETXESCLAKPHTENSFTNVWKDD
E08+ZZ1K3U-E08+fdDOGf F PFYSHSAQARDCLETWYGFTCWNVAAAETXESCLAKPHTENSFTNVWKDD
C08+ZZ1K3U-C08+fdDOGf F PFYSHSAQARDCLETWYGFTCWNVAAAETXESCLAKPHTENSFTNVWKDD
E07+ZZ1K3U-E07+fdDOGf F PFYSHSAQARDCLETWYGFTCWNVAAAETXESCLAKPHTENSFTNVWKDD
F07+ZZ1K3U-F07+fdDOGf F PFYSHSAQARDCLETWYGFTCWNVAAAETXESCLAKPHTENSFTNVWKDD
D07+ZZ1K3U-D07+fdDOGf F PFYSHSAQARDCLETWYGFTCWNVAAAETXESCLAKPHTENSFTNVWKDD
F02+ZZ1K3U-F02+fdDOGf F PFYSHSAQARDCLETWYGFTCWNVAAAETXESCLAKPHTENSFTNVWKDD
F01+ZZ1K3U-F01+fdDOGf F PFYSHSAQARDCLETWYGFTCWNVAAAETXESCLAKPHTENSFTNVWKDD
B02+ZZ1K3U-B02+fdDOGf F PFYSHSAQARDCLETWYGFTCWNVAAAETXESCLAKPHTENSFTNVWKDD
A05+ZZ1K3U-A05+fdDOGf F PFYSHSAQARDCLETWYGFTCWNVAAAETXESCLAKPHTENSFTNVWKDD
A05+ZZ1K3Z-A05+fdDOGf F PFYSHSAQARDCLETWYGFTCWNVAAAETXESCLAKPHTENSFTNVWKDD
A04+ZZ1K3U-A04+fdDOGf F PFYSHSAQARDCLETWYGFTCWNVAAAETXESCLAKPHTENSFTNVWKDD
D11+ZZ1K3Z-D11+fdDOGf F PFYSHSAQARDCLETWYGFTCWNVAAAETXESCLAKPHTENSFTNVWKDD
C09+ZZ1K3Z-C09+fdDOGf F PFYSHSAQARDCLETWYGFTCWNVAAAETXESCLAKPHTENSFTNVWKDD
A10+ZZ1K3Z-A10+fdDOGf F PFYSHSAQARDCLETWYGFTCWNVAAAETXESCLAKPHTENSFTNVWKDD
G08+ZZ1K3Z-G08+fdDOGf F PFYSHSAQARDCLETWYGFTCWNVAAAETXESCLAKPHTENSFTNVWKDD
C10+ZZ1K3U-C10+fdDOGf F PFYSHSAQARDCLETWYGFTCWNVAAAETXESCLAKPHTENSFTNVWKDD
E10+ZZ1K3U-E10+fdDOGf F PFYSHSAQARDCLETWYGFTCWNVAAAETXESCLAKPHTENSFTNVWKDD
A10+ZZ1K3U-A10+fdDOGf F PFYSHSAQARDCLETWYGFTCWNVAAAETXESCLAKPHTENSFTNVWKDD
F09+ZZ1K3U-F09+fdDOGf F PFYSHSAQARDCLETWYGFTCWNVAAAETXESCLAKPHTENSFTNVWKDD
» F10+ZZ1IY1-F10+fdDOGf (Oust0037) PFYSHSAQLPTKTCPCLWCCAEDWAAAETVESCLAKPHTENSFTNVWKDD

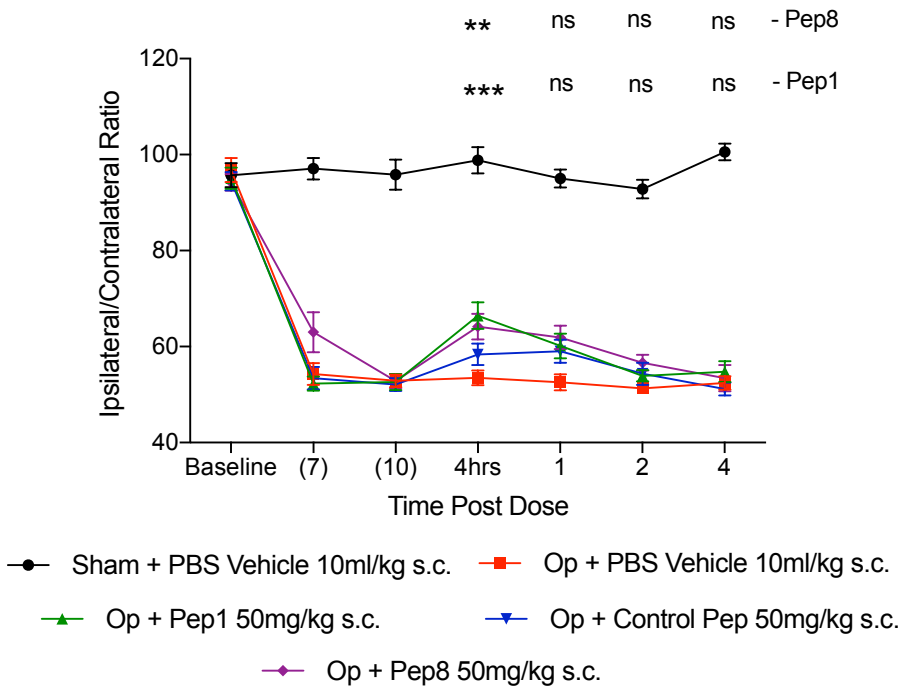

Figure S5: Effect of Pep1- and Pep8-Fc/IL1RA on the reversal of partial nerve ligation induced mechanical hyperalgesia - Ipsi/Contra Ratio

Partial nerve ligation (PNL) of operated mice was conducted at the baseline time point. Mice were administered control or CPep-Fc/IL1RA on day 10 and were re-tested for changes in mechanical hyperalgesia at 4hrs post dose and also on 1, 2 and 4 days post dose. Ipsilateral to contralateral ratios for Sham + PBS Vehicle control (Black), Operated (Op) + PBS Vehicle control (red), Op + Pep1-FcIL1RA (green), Op + Pep8-Fc/IL1RA, and Op + control CPep-FcIL1RA (blue) are shown. Data analysed using 2 way ANOVA with time and treatment as dependant factors. Subsequent statistical significance obtained using Tukey's Post Hoc test. Individual comparisons as shown ** P<0.01 Op + PBS vs Pep8; *** P<0.001 Op + PBS vs Pep1, n= 9-10 per group